

Two-Field Models of Inflationary and Bouncing Scenarios

By

Rathul Nath Raveendran

PHYS10201304003

The Institute of Mathematical Sciences, Chennai

A thesis submitted to the

Board of Studies in Physical Sciences

In partial fulfillment of requirements

For the Degree of

DOCTOR OF PHILOSOPHY

of

HOMI BHABHA NATIONAL INSTITUTE



December 2018

Homi Bhabha National Institute

Recommendations of the Viva Voce Committee

As members of the Viva Voce Committee, we certify that we have read the dissertation prepared by Rathul Nath Raveendran entitled "Two-field models of inflationary and bouncing scenarios" and recommend that it may be accepted as fulfilling the dissertation requirement for the Degree of Doctor of Philosophy.

Chair - S. Kalyana Rama **Date:**

Guide/Convener - Balachandran Sathiapalan **Date:**

Co-guide - L. Sriramkumar **Date:**

Examiner - **Date:**

Member 1 - Shrihari Gopalakrishna **Date:**

Member 2 - R. Ganesh **Date:**

Member 3 - Sibasish Ghosh **Date:**

Final approval and acceptance of this dissertation is contingent upon the candidate's submission of the final copies of the dissertation to HBNI.

We hereby certify that we have read this dissertation prepared under our direction and recommend that it may be accepted as fulfilling the dissertation requirement.

Date: _____ **Guide:** Balachandran Sathiapalan

Place: _____ **Co-guide:** L. Sriramkumar

STATEMENT BY AUTHOR

This dissertation has been submitted in partial fulfillment of requirements for an advanced degree at Homi Bhabha National Institute (HBNI) and is deposited in the Library to be made available to borrowers under rules of the HBNI.

Brief quotations from this dissertation are allowable without special permission, provided that accurate acknowledgement of source is made. Requests for permission for extended quotation from or reproduction of this manuscript in whole or in part may be granted by the Competent Authority of HBNI when in his or her judgement the proposed use of the material is in the interests of scholarship. In all other instances, however, permission must be obtained from the author.

Rathul Nath Raveendran

DECLARATION

I, hereby declare that the investigation presented in the thesis has been carried out by me. The work is original and has not been submitted earlier as a whole or in part for a degree/diploma at this or any other Institution/University.

Rathul Nath Raveendran

List of publications arising from the thesis

1. **R. N. Raveendran** and L. Sriramkumar, *Numerical evaluation of the tensor bispectrum in two field inflation*, JCAP **1707**, 035 (2017) [arXiv:1611.00473 [astro-ph.CO]].
2. **R. N. Raveendran**, D. Chowdhury and L. Sriramkumar, *Viable tensor-to-scalar ratio in a symmetric matter bounce*, JCAP **1801**, 030 (2018) [arXiv:1703.10061 [gr-qc]].
3. **R. N. Raveendran** and L. Sriramkumar, *Primordial features from ekpyrotic bounces*, Phys. Rev. D **99**, 043527 (2019) [arXiv:1809.03229 [astro-ph.CO]].
4. **R. N. Raveendran** and L. Sriramkumar, *Viable scalar spectral tilt and tensor-to-scalar ratio in near-matter bounces*, arXiv:1812.06803 [astro-ph.CO].
5. **R. N. Raveendran**, K. Parattu and L. Sriramkumar, *Contrasting the quantum-to-classical transition of primordial perturbations in inflationary and bouncing scenarios*, in preparation.

ACKNOWLEDGEMENTS

I would like to express my sincere gratitude to my supervisor Prof. L. Sriramkumar for his valuable guidance, scholarly advice and encouragement, without which I would not have been able to complete this thesis. He showed me proper direction as well as offered help when I was facing difficulty in carrying out my work.

I would like to thank Prof. Ghanashyam Date who has offered me extensive personal and professional guidance and taught me a great deal about both scientific research as well as life in general. I also wish to thank Prof. Bala Sathiapalan for the support and help provided during the last stages of my thesis work. Further, I would like to take this opportunity to thank all the members of my Doctoral Committee. I owe my sincere thanks to the faculty members of The Institute of Mathematical Sciences (IMSc) for the helpful discussions which we had at the time of our course work.

I gratefully acknowledge the support from the Centre for Cosmological Studies, University of Oxford, United Kingdom, to visit and work with Prof. Patrick Peter at the Institut d'Astrophysique de Paris, Paris, France. I would like to express my sincere thanks to Prof. Patrick Peter for the opportunity to work with him. He has always made himself available to clarify my doubts despite his busy schedule and I have greatly benefited from my interactions with him.

I am thankful to Krishnamohan and Debika—my collaborators and erstwhile office mates—for their indispensable help.

I am grateful to my seniors Sreenath and Jaffino who have directed me and provided important inputs during the initial stages of my research career.

I gratefully acknowledge the support I have received at IMSc, where I have spent

more than five years as a Ph.D. student. The institute offered an inspiring atmosphere throughout the course work, during lectures and discussion sessions with faculty members and friends. I am also indebted to my batch mates who have helped me during my entire Ph.D. career. Apart from them, the staff in the Computer Centre at IMSc have also helped me to a great extent to pursue my research. I would like to thank the staff members at the office, library and security of our institution for their support during my time as a Ph.D. student.

I must mention Dr. Ravikrishnan who played the role of a mentor in my life. A reservoir of knowledge is the only adjective apt for him. His inspiring words while I was pursuing B.Sc. became a turning point in my life and motivated me to pursue research.

I am thankful to my family for the constant support and encouragement they have extended to me during all the stages of my Ph.D. work. Most importantly, I wish to thank my loving and supportive wife Anvy. She understands the life of a research scholar perfectly and makes things easier for me. Her constant encouragement and inspiration elevated the level of my work. I would like to thank all my friends for their extensive support during my Ph.D. work.

Contents

Synopsis	1
1 Introduction	17
1.1 The standard model of cosmology	18
1.1.1 Friedmann-Lemaître-Robertson-Walker (FLRW) metric . . .	19
1.1.2 Friedmann equations	20
1.1.3 Problems with the standard big bang model	24
1.2 Inflation and the generation of primordial perturbations	27
1.2.1 Overcoming problems of the big bang model with inflation	27
1.2.2 Scalar field in a FLRW universe	30
1.2.3 Perturbations	34
1.2.4 Generation of primordial fluctuations	38
1.2.5 Quantization and power spectra	40
1.2.6 The Bunch-Davies initial conditions	43
1.2.7 Two-field models	45
1.2.8 Challenges to the inflationary scenario	47
1.3 Bouncing scenario as an alternative paradigm	48
1.3.1 The simple matter bounce scenario and challenges	50
1.3.2 The idea of ekpyrosis	51
1.3.3 Tensor-to-scalar ratio in bounces	52

1.4	Organization of the thesis	52
2	Numerical evaluation of the tensor bispectrum in two-field inflation	55
2.1	Introduction	55
2.2	Background equations	59
2.3	The tensor bispectrum and the corresponding non-Gaussianity parameter	60
2.4	The non-Gaussianity parameter h_{NL} in slow roll inflation	63
2.5	Numerical evaluation	64
2.5.1	Double inflation	66
2.5.2	Hybrid inflation	68
2.5.3	Aligned natural inflation	69
2.6	Consistency relation in the squeezed limit	77
2.7	The contribution during preheating	78
2.8	Discussion	79
3	Viable tensor-to-scalar ratio in a symmetric matter bounce	81
3.1	Introduction	81
3.2	The scale factor describing the matter bounce	86
3.3	The evolution of tensor perturbations and the tensor power spectrum	88
3.3.1	Analytical evaluation of the tensor perturbations	89
3.3.2	E-N-folds and the numerical evaluation of the tensor modes	92
3.3.3	Tensor power spectrum	94
3.4	Modeling the bounce with scalar fields	96
3.5	Equations of motion governing the scalar perturbations	101
3.5.1	The first order Einstein's equations	101
3.5.2	Equations governing the perturbations in the scalar fields	102

3.5.3	Constructing the curvature and isocurvature perturbations .	104
3.5.4	Equations governing the curvature and the isocurvature perturbations	107
3.5.5	Perturbations in a specific gauge	110
3.6	Evolution of the scalar perturbations	111
3.6.1	Equations in terms of e-N-folds	113
3.6.2	Initial conditions and power spectra	114
3.6.3	Evolution of the perturbations	116
3.7	Analytical arguments	118
3.7.1	Solutions in the first domain	118
3.7.2	Solutions in the second domain	120
3.7.3	Comparison with the numerical results	121
3.8	The scalar power spectra and the tensor-to-scalar ratio	123
3.9	Discussion	128

4 Viable scalar spectral tilt and tensor-to-scalar ratio in

near-matter bounces		133
4.1	Introduction	133
4.2	Background and sources	134
4.3	The tensor modes and the resulting power spectrum	138
4.4	Arriving at the equations governing the scalar perturbations	139
4.4.1	The Einstein's equations and the equations describing the perturbations in the scalar fields	140
4.4.2	Equations governing the scalar perturbations, and circumventing the diverging coefficients	142
4.5	Evolution of the perturbations and power spectra	145
4.5.1	Analytical solutions at early times	146
4.5.2	Numerical evolution across the bounce	148

4.5.3	Behavior of the perturbations and the power spectra	149
4.6	Discussion	152
5	Primordial features from ekpyrotic bounces	155
5.1	Introduction	155
5.2	Ekpyrotic attractor	158
5.3	Featureless power spectra in ekpyrosis	161
5.3.1	Equations governing the scalar perturbations	161
5.3.2	The scalar power spectra	163
5.4	Converting the isocurvature perturbations into curvature perturbations	164
5.5	Generating ekpyrotic features	168
5.6	Prospects	170
6	Quantum-to-classical transition of primordial perturbations in inflationary and bouncing scenarios	173
6.1	Introduction	173
6.2	Review of the single field case	175
6.2.1	Action governing the scalar perturbations	176
6.2.2	Schrodinger equation, wave function and variances	177
6.2.3	The Wigner function	180
6.2.4	The squeezing parameter and the squeezing angle	181
6.2.5	Power law inflation and contraction	183
6.3	Two-field models: Essential formalism	187
6.3.1	The action and the equations of motion	187
6.3.2	The Gaussian ansatz for the wave function	189
6.3.3	The Wigner function and the reduced density matrix	193
6.3.4	The squeezing parameters	195
6.4	Application to double inflation and ekpyrotic contraction	197

6.4.1	The case of double inflation	198
6.4.2	The case of ekpyrotic contraction	198
6.4.3	Approach to classicality	200
6.5	Discussion	205
7	Conclusions	207
7.1	Summary of work done	207
7.2	Outlook	210
A	Fixing the coefficients	213
B	Is a diverging curvature perturbation acceptable?	217

Synopsis

Introduction

One of the outstanding problems in cosmology today is understanding the origin of the primordial perturbations. The inflationary and the bouncing scenarios constitute two competing paradigms for the generation of perturbations in the early universe (for instance, see the following texts [1] and reviews [2,3]). While the inflationary scenario has been investigated to a great extent and is, without doubt, the most simple, effective as well as popular paradigm to describe the origin of the perturbations, there has been a persistent effort over the last two decades to construct viable alternatives.

As is well known, the inflationary scenario was invoked to overcome the horizon problem associated with standard hot big bang model [2]. Inflation refers to a brief period of accelerated expansion during the early stages of the conventional radiation dominated era. Such a phase of rapid expansion permits a causal mechanism to generate the primordial perturbations. The epoch of inflation is usually assumed to be driven by scalar fields, which are encountered regularly in high energy physics. These scalar fields contain quantum fluctuations and it is possible to impose well motivated, natural initial conditions on the fluctua-

tions when the modes are well within the causal domain during the early stages of inflation. Later, as the modes leave the causally connected domain due to the accelerated expansion, the quantum fluctuations are converted into classical perturbations that leave their imprints as anisotropies in the Cosmic Microwave Background (CMB) and the large scale structure. Many models consisting of single and multiple scalar fields have been proposed to achieve inflation. The background inflationary dynamics determines the characteristics of these perturbations, which are conveniently described in terms of correlation functions. The pattern of anisotropies in the CMB as observed by the recent Planck mission [4,5], along with other cosmological data, point to a nearly scale-invariant and adiabatic primordial scalar power spectrum as is generated by the simplest models of inflation [6,7].

It turns out to be rather easy to construct an inflationary model that is consistent with the cosmological data. This efficiency of the paradigm has led to a profusion of inflationary models and, despite the increasingly accurate cosmological observations, many of the models continue to remain consistent with the data (for a comprehensive list of single field models, see Ref. [8]). Such a degeneracy has even led to the concern whether, as a paradigm, inflation can be falsified at all. In such a situation, it has become imperative to explore alternatives to inflation. The most investigated alternative to the inflationary paradigm is the classical bouncing scenario (see the recent reviews [3]). In the bouncing scenarios, the universe goes through an initial phase of contraction until the scale factor reaches a minimum value, before it begins to expand. During the early stages of the contracting phase, one can impose well motivated initial conditions on the perturbations, thereby overcoming the horizon problem in a manner similar to inflation. In contrast to inflation which can be easily achieved with a single scalar field, because of the fact that the null energy condition is violated as the scale factor approaches the minimum value, the bouncing scenarios often require more than one scalar

field to drive them. This thesis is aimed at studying certain aspects of inflationary and bouncing scenarios driven by two scalar fields.

Motivation, objective and scope

While inflationary models involving a single scalar field has been studied extensively, it would be fair to say that inflation driven by multi-field models, specifically, two-field models, have not been explored to an equal extent (for early discussions, see, for example, Refs. [9–11]). As far as the background evolution is concerned, two-field models offer a richer dynamics than the single field models due to the possibility of different types of trajectories in the field space. At the level of perturbations, the existence of isocurvature perturbations in two-field models can lead to a non-trivial evolution of the curvature perturbation on super-Hubble scales.

In the context of bounces, as we alluded to above, models involving two scalar fields prove to be a natural choice for achieving the required background evolution. However, when compared to inflation, it turns out to be difficult to construct well motivated sources which can drive bounces (see, for instance, Refs. [12–14]). This difficulty can be largely attributed to the fact that, as we mentioned, the null energy condition may have to be violated in the vicinity of the bounce. It is interesting to note that, in the simplest of bouncing scenarios, the shape of the power spectrum is determined by the behavior of the early contracting phase. It is easy to show that a contracting phase which behaves close to a matter dominated epoch can lead to nearly scale-invariant spectra that can be consistent with the CMB data. Such a scenario is referred to as the matter bounce. Though conceptually simple, matter bounces are plagued by a few difficulties, primarily associated with the instabilities arising due to the rapid growth of anisotropic stress during

the contraction (for a list of difficulties faced, see, for example, Refs. [3, 15–17]). Moreover, some of the earlier analysis suggest that the tensor-to-scalar ratio r can be rather large in these models, beyond the upper bound of $r \lesssim 0.07$ from the recent Planck data [12]. The challenge has been to construct pathology-free near-matter bounces that can lead to nearly scale-invariant scalar power spectra and a small tensor-to-scalar ratio consistent with the current observations.

Though nearly scale-invariant primordial power spectra, as is generated by slow roll inflation, are remarkably consistent with the cosmological data, certain features in the primordial scalar power spectrum are known to provide an improved fit to the CMB data [7, 18–23]. Such features can be easily generated during inflation by introducing brief departures from slow roll [19–22]. Since the inflationary trajectory is largely an attractor, it will restore slow roll after the deviations from it. In contrast, most of the models which have been considered towards achieving bounces, such as, say, the popular matter bounce, require fine tuned initial conditions [24]. This implies that these models will be ruled out if future observations confirm the presence of features in the primordial spectrum. Amongst the bouncing models, it is only the ekpyrotic scenarios that permit attractors (for the original ideas, see Refs. [25]; for more recent discussions, see Refs. [26, 27]). It becomes imperative to examine whether such models can generate features in the primordial spectrum that have been considered in the context of inflation.

As we discussed, in inflation as well as the bouncing models, the primordial perturbations are generated due to quantum fluctuations associated with scalar fields that drive the background. As the universe evolves, the quantum fluctuations are expected to eventually turn classical and eventually leave their imprints as anisotropies in the CMB. This quantum-to-classical transition of the primordial perturbations remains to be satisfactorily understood. While the issue has been investigated to a considerable extent in the context of inflation, there has been

only a very limited effort in this direction in the bouncing scenarios (for discussions in the inflationary context, see Refs. [28–30]; for investigations in bouncing scenarios, see Refs. [31–33]).

This thesis examines specific issues related to the problems described above. It is based on five pieces of work, which investigate the following problems: (1) numerical evaluation of the tensor bispectrum in two-field models of inflation, (2) constructing a symmetric matter bounce model leading to scale-invariant spectra and a small tensor-to-scalar ratio, (3) extending the model to near-matter bounces leading to a spectral tilt that is consistent with the observations, (4) examining the possibility of generating features in ekpyrotic bounces, and (5) comparing the quantum-to-classical transition in two-field inflationary and bouncing models.

Summary of the research work

In this section, we shall briefly describe the five pieces of work that will constitute the thesis.

Numerical evaluation of the tensor bispectrum in two-field inflation

Over the last decade and a half, it has been recognized that observations of primordial non-Gaussianities—in particular, the amplitude of the three-point functions—can help us arrive at a smaller class of viable inflationary models [34–36]. This expectation has been corroborated to a large extent by the strong constraints that have been arrived at by the Planck data on the three non-

Gaussianity parameters that describe the amplitude of the scalar bispectrum [37]. Theoretically, a considerable amount of work has been carried out towards understanding the non-Gaussianities generated in single and multi-field inflationary models (see, for example, Refs. [36, 38]). However, the theoretical understanding of non-Gaussianities generated in inflationary models and the observational constraints that have been arrived at are largely concentrated on the scalar bispectrum and the corresponding non-Gaussianity parameters. In fact, apart from the scalar bispectrum, there arise three other three-point functions when the tensor perturbations are also included [39]. The three-point functions are often evaluated analytically in the slow roll approximation, and one has to resort to numerical efforts to evaluate these three-point functions in a generic situation [40–42]. Also, while numerical procedures have been developed to evaluate the three-point functions in single field models, until recently, there has been little effort towards computing these quantities in multi-field models [43, 44]. Our eventual goal is to arrive at a numerical procedure to evaluate all the three-point functions in two-field and, in general, multi-field models. In contrast to the scalars, the tensor perturbations are simpler to study as they depend only on the evolution of the scale factor. As a first step of the process, our aim is to compute the tensor bispectrum and the corresponding non-Gaussianity parameter in two-field models of inflation.

In this work, we have evaluated the dimensionless non-Gaussianity parameter, say, h_{NL} , that characterizes the amplitude of the tensor bispectrum numerically for a class of two-field inflationary models such as double inflation, hybrid inflation and aligned natural inflation. We have compared the numerical results with the slow roll results which can be obtained analytically and have found that the numerical procedure we have adopted is quite accurate (*cf.* figure 1). In the context of double inflation, we have also investigated the effects on h_{NL} due to curved trajectories in the field space. For instance, we have observed that the

change in the direction of the trajectory produces a bump in the first slow roll parameter, which increases the amplitude of h_{NL} over a certain domain. Moreover, we have explicitly examined the validity of the consistency relation which governs the tensor bispectrum in the squeezed limit. Lastly, we have shown that the contribution to h_{NL} due to the epoch of preheating can be completely neglected, due to the constant amplitude of the tensor modes during this period.

Viable tensor-to-scalar ratio in a symmetric matter bounce

As we mentioned, matter bounces refer to scenarios wherein the universe contracts at early times as in a matter dominated epoch. While such scenarios are known to lead to scale-invariant spectra of primordial perturbations after the bounce, the challenge has been to construct completely symmetric bounces that lead to a tensor-to-scalar ratio which is small enough to be consistent with the recent cosmological data [13].

In this work, we have constructed a viable symmetric matter bounce. We assume that the scale factor describing the bounce is given in terms of the conformal time η as follows:

$$a = a_0 (1 + k_0^2 \eta^2), \quad (1)$$

where a_0 is the scale factor at the bounce and k_0 is a constant. We show that such a background evolution can be driven by two scalar fields, a canonical field, say, ϕ and a non-canonical ghost field, say, χ , that are described by the action

$$S[\phi, \chi] = - \int d^4x \sqrt{-g} \left[\frac{1}{2} \partial_\mu \phi \partial^\mu \phi + V(\phi) + U_0 \left(-\frac{1}{2} \partial_\mu \chi \partial^\mu \chi \right)^q \right], \quad (2)$$

where U_0 is an arbitrary positive constant. We find that, if we set $q = 2$ and choose the potential to be $V(\phi) = 6 M_{\text{Pl}}^2 (k_0/a_0)^2 \text{sech}^6[\phi/(\sqrt{12} M_{\text{Pl}})]$, the model

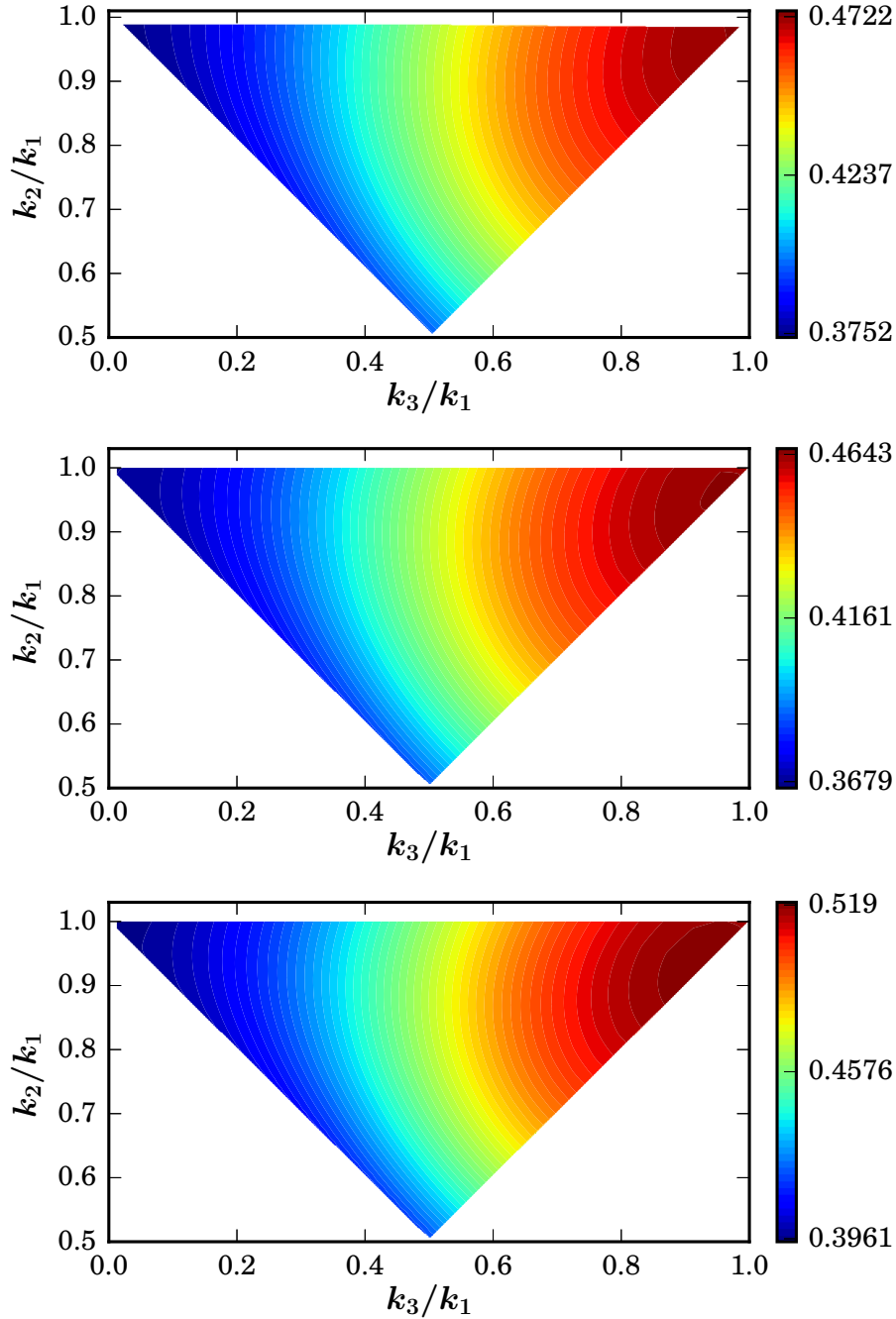


Figure 1: Density plots of the tensor non-Gaussianity parameter h_{NL} for an arbitrary triangular configuration of the wavenumbers evaluated analytically in the case of de Sitter inflation (on the top) and obtained numerically for double inflation with $m_\chi = m_\phi$ (in the middle). It is evident that the analytical and the numerical results match rather well, indicating the accuracy of the numerical procedures that have been adopted. We have also plotted the corresponding results, obtained numerically, for the case of double inflation with $m_\chi = 8 m_\phi$ (at the bottom). The relatively higher values of h_{NL} in the last case arises due to the turn in the trajectory in the field space.

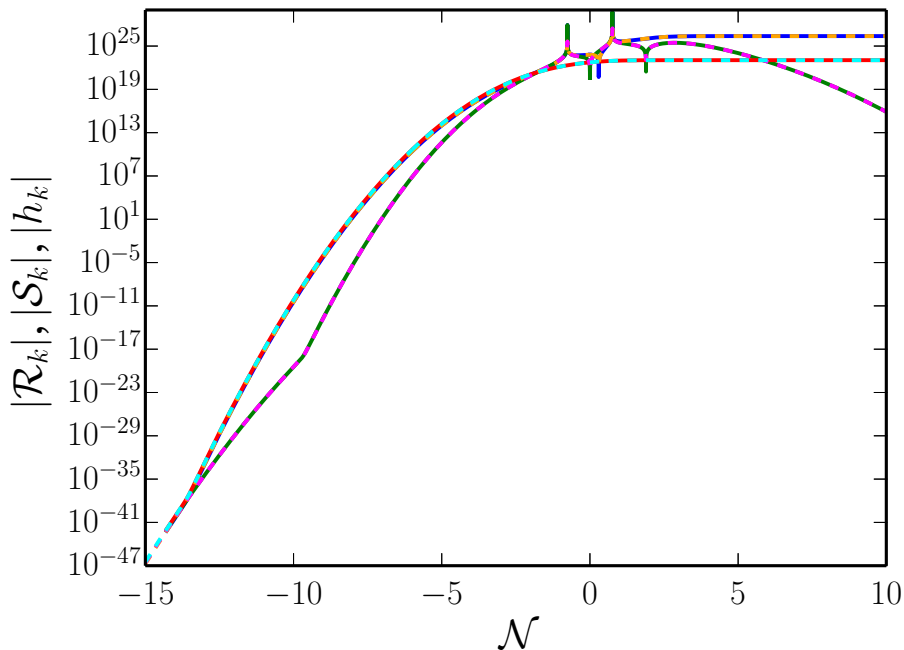


Figure 2: The evolution of the amplitudes of the curvature perturbation \mathcal{R}_k (blue solid line and orange dashed line), the isocurvature perturbation \mathcal{S}_k (green solid line and magenta dashed line) and the tensor mode h_k (red solid line and cyan dashed line) corresponding to the wavenumber $k/k_0 = 10^{-20}$ has been plotted a function of e-N-folds \mathcal{N} in terms of which the scale factor is defined as $a(\mathcal{N}) = a_0 \exp(\mathcal{N}^2/2)$. Evidently, the numerical results (solid lines) match the analytical results (dashed lines) very well. Notice that, around the bounce, the amplitude of the scalar perturbations are enhanced by a few orders of magnitude more than that of the tensor perturbations.

leads to the scalar factor (1). Since the model involves two fields, apart from the curvature perturbations, isocurvature perturbations also arise. We have solved the equations governing the scalar and tensor perturbations numerically and we have also been able to support the numerical results with analytical arguments. In fact, we have been able to evolve the perturbations across the bounce (in this context, see figure 2), and evaluate the power spectra *after* the bounce. We find that the model can be completely described in terms of a single parameter, *viz.* the ratio k_0/a_0 . Importantly, we have been able to show that, while the scalar and tensor perturbation spectra are scale-invariant over scales of cosmological interest [and COBE normalized for $k_0/(a_0 M_{\text{Pl}}) = 3.3 \times 10^{-8}$], the tensor-to-scalar ratio r proves to be of the order of 10^{-6} , which is much smaller than the current upper bound

from Planck [7].

Generating power spectra with a tilt in bouncing scenarios

As is well known, slow roll inflation can generate scalar and tensor power spectra with a red tilt that are consistent with the CMB observations [2]. In a similar manner, near-matter bounces can be expected to generate spectra with a tilt as in slow roll inflation. In this work, we have extended the matter bounce model involving two fields (that we discussed above) to drive bounces described by the following scale factor:

$$a(\eta) = a_0 (1 + k_0^2 \eta^2)^{1+\varepsilon}. \quad (3)$$

Clearly, such a scale factor will correspond to near-matter bounces when $\varepsilon \ll 1$. We have shown that such a scale factor can be achieved with the aid of two scalar fields governed by the action (2) if we set $q = (2 + \varepsilon)/(1 - \varepsilon)$, and choose the potential to be

$$V(\phi) = 2(3 + 4\varepsilon)(1 + \varepsilon) M_{\text{Pl}}^2 \left(\frac{k_0}{a_0}\right)^2 \text{sech}^{2(3+2\varepsilon)} \left[\frac{\phi}{\sqrt{4(1 + \varepsilon)(3 + 2\varepsilon)} M_{\text{Pl}}} \right]. \quad (4)$$

However, unfortunately, the model does not permit analytical evaluation of the scalar perturbations near the bounce. Therefore, with the aid of techniques developed in our earlier work, we have investigated the scalar and tensor power spectra numerically. While roughly the same value of k_0/a_0 that we had mentioned above leads to COBE normalization and a rather small tensor-to-scalar ratio (of $r \simeq 10^{-6}$), the additional parameter ε leads to a tilt in the spectra. We find that one obtains a scalar spectral index of $n_s \simeq 0.96$ if we choose $\varepsilon \simeq 0.01$, perfectly consistent with the current CMB constraints.

Primordial features from ekpyrotic bounces

We had pointed out earlier that, while nearly scale-invariant primordial spectra are remarkably consistent with the cosmological data, it has been repeatedly noticed that specific features in the power spectra lead to a better fit to the data. The features that improve the fit to the CMB data can be broadly classified into the following three types: (1) sharp drop in power at large scales corresponding to the Hubble radius today [19], (2) a burst of oscillations over an intermediate range of scales [20], and (3) persisting oscillations over a wide range of scales [21]. In inflation, due to the attractor nature of the trajectory, such features can be generated with the aid of potentials that permit brief deviations from slow roll. It is the features in the potential and the resulting non-trivial dynamics that translates to features in the power spectra [18, 22]. In complete contrast, bouncing scenarios such as the matter and near-matter bounces we discussed above require extremely fine tuned initial conditions. Therefore, they cannot generate features in the primordial spectra and, in fact, such models will cease to be viable if forthcoming observations confirm the presence of primordial features.

As we had mentioned, amongst the bouncing scenarios, it is only the ekpyrotic models that admit attractors [25, 26]. Ekpyrotic models are designed to smooth and flatten the universe with the aid of a matter component whose energy density grows to dominate all other forms of energy, importantly, anisotropies. However, it is found that ekpyrotic models involving a single field cannot generate nearly scale-invariant curvature perturbation spectra as is required by the observations (in this context, see Refs. [45]). Therefore, one resorts to two-field models wherein the ekpyrotic contracting phase is dominated by isocurvature perturbations with a nearly scale-invariant spectrum. The second field is utilized to convert the isocurvature perturbations to nearly scale-invariant adiabatic pertur-

bations [26,46].

In this work, we have considered a specific ekpyrotic model, which firstly leads to scale-invariant primordial spectra, in the manner described above. The model involves two scalar fields ϕ and χ , which are governed by the following action consisting of the potential $V(\phi, \chi)$ and a function $b(\phi)$ [26]:

$$S[\phi, \chi] = \int d^4x \sqrt{-g} \left[-\frac{1}{2} \partial_\mu \phi \partial^\mu \phi - \frac{e^{2b(\phi)}}{2} \partial_\mu \chi \partial^\mu \chi - V(\phi, \chi) \right]. \quad (5)$$

We have worked with the potential $V(\phi, \chi) = V_{\text{ek}}(\phi) = V_0 e^{\lambda \phi / M_{\text{Pl}}}$ and choose $b(\phi) = \mu \phi / (2 M_{\text{Pl}})$, where λ and μ are positive constants. In such a case, it can be shown that the phase driven by the above ekpyrotic potential permits an attractor provided V_0 is negative (or, equivalently, $\lambda^2 > 6$). The ekpyrotic phase leads to a strongly blue curvature perturbation spectrum. However, one finds that the parameter μ can be chosen suitably to lead to a nearly scale-free isocurvature perturbation spectrum. We have then multiplied the original potential $V_{\text{ek}}(\phi)$ by the term $V_c(\phi, \chi) = 1 + \beta \chi \exp - [(\phi - \phi_c) / \Delta \phi_c]^2$, which leads to a turn in the field space along the χ direction. As the turn occurs, the isocurvature perturbations source the curvature perturbations boosting their amplitude. We find that this process also alters the shape of the curvature perturbation spectrum, which attains the nearly scale-invariant shape of the original isocurvature perturbation spectrum.

Having obtained a nearly scale-invariant curvature perturbation spectrum, we generate features in the spectrum by further multiplying the ekpyrotic potential by suitable terms, say, $V_f(\phi)$, to lead to the three types of features we discussed above. Since the background dynamics in the ekpyrotic scenario is rather distinct from the inflationary case, prior experience with the inflationary features does not necessarily help in constructing ekpyrotic potentials leading to the de-

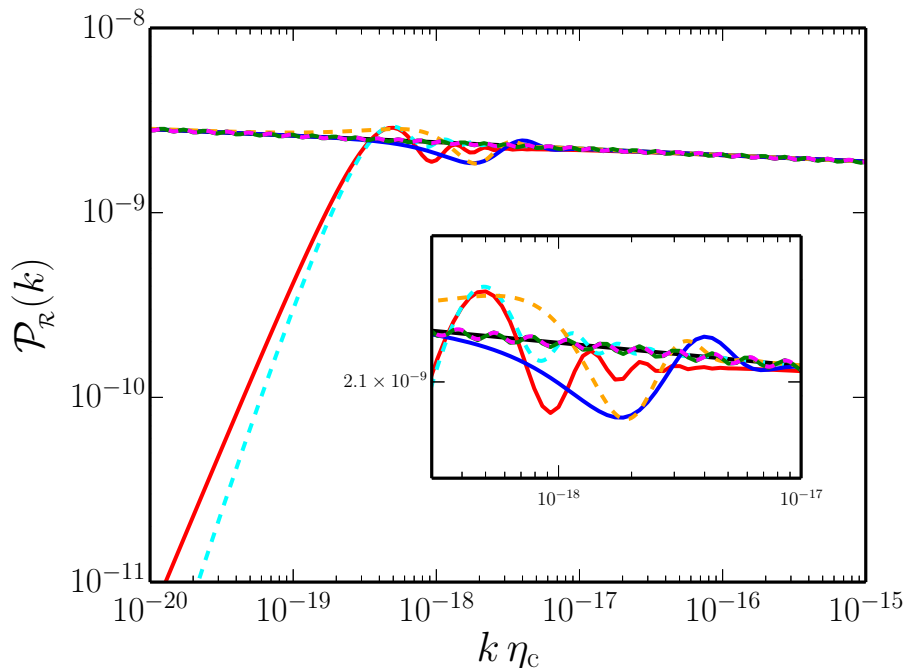


Figure 3: The power spectra of the curvature perturbation with the three types of features (type 1 in red and cyan, type 2 in blue and orange, and type 3 in green and pink) generated in the ekpyrotic (solid lines) and the inflationary (dashed lines) scenarios have been plotted over scales of cosmological interest. The inflationary spectra correspond to those that lead to an improved fit to the CMB data [7]. Clearly, the ekpyrotic spectra closely resemble the inflationary spectra with features.

sired features. We had to experiment with different multiplicative functions $V_f(\phi)$ before arriving at the required forms. The power spectra of the curvature perturbations arising in the different cases has been plotted in figure 3. In the figure, we have also plotted inflationary power spectra with features that lead to a better fit to the most recent Planck data (in this context, see Refs. [4]). It is clear from the figure that the ekpyrotic features match the inflationary features reasonably well.

Quantum-to-classical transition of the primordial perturbations

In this work, we compare and contrast the quantum-to-classical transition of the primordial perturbations in the inflationary and bouncing scenarios [28, 30–32]. Since, as we have seen, the bouncing scenarios are often driven by two scalar

fields, we carry out a comparison between the double inflation model and the ekpyrotic scenario. We examine the transition with the aid of the Wigner function and the behavior of the squeezing parameters describing the curvature perturbation as the universe evolves. In the case of double inflation, we observe that the Wigner ellipse (the locus of the Wigner function in phase space for a given amplitude) generically gets more and more squeezed along the direction of the curvature perturbation (see figure 4). In the ekpyrotic scenario, we initially observe a very fast squeezing of the Wigner ellipse along the direction of the momentum conjugate to the curvature perturbation. At later times, due to the influence of the isocurvature perturbation, the ellipse rotates and is squeezed along the direction of the curvature perturbation (*cf.* figure 4). We find that the highly squeezed Wigner ellipse eventually orients itself along the asymptotic classical trajectory in the phase space. Such a behavior allows us to conclude that the cosmological perturbations starting in an initially quantum state become more and more classical with time. These conclusions are also corroborated by the behavior of the squeezing parameter characterizing the curvature perturbation.

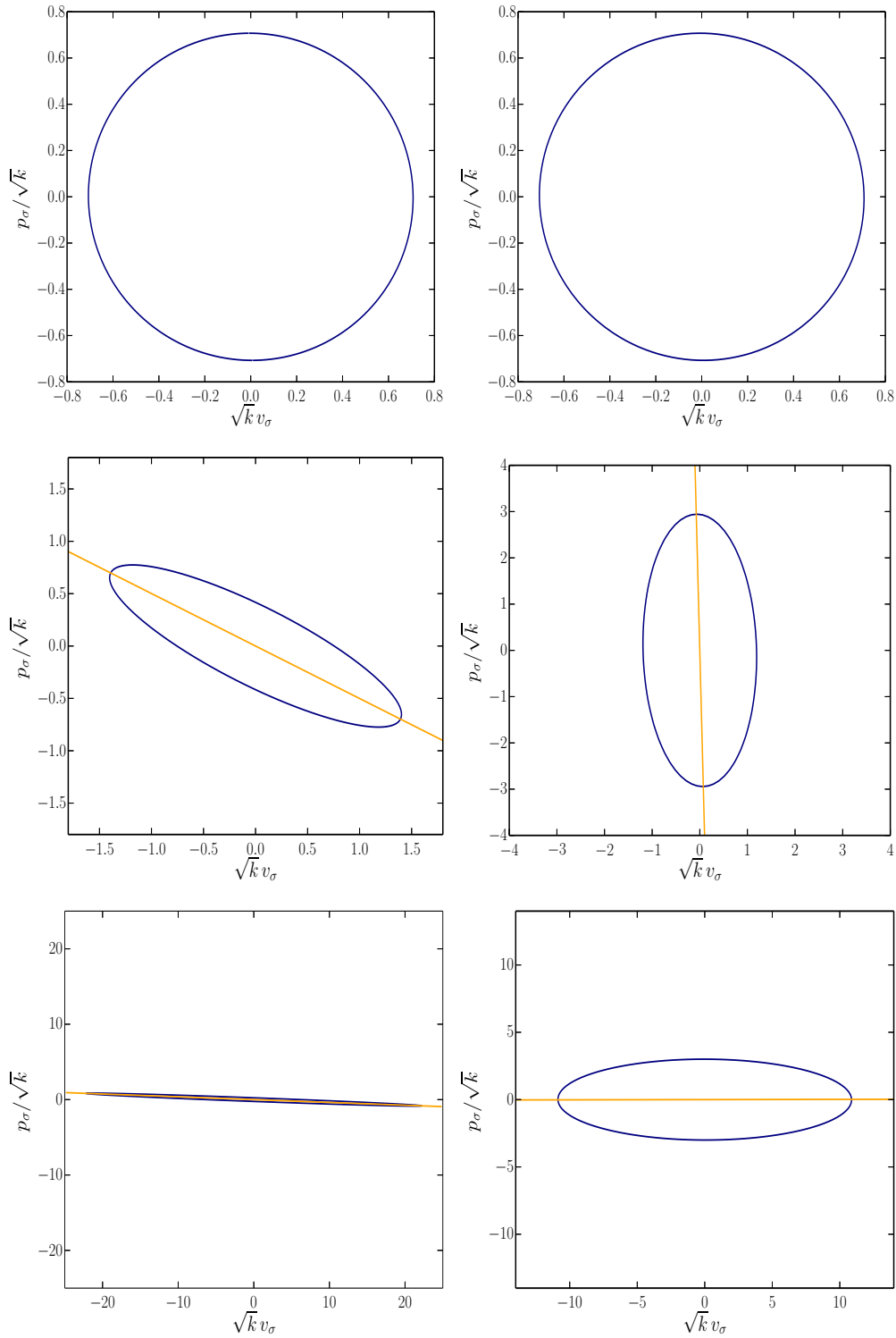


Figure 4: Evolution of the Wigner ellipse describing the curvature perturbation v_σ and its conjugate momentum p_σ (for a typical cosmological scale of interest) in a double inflationary scenario (on the left) and during the ekpyrotic contracting phase (on the right). Note that the original circle gets squeezed into an ellipse, which rotates and eventually orients itself axis of the curvature perturbation.

Chapter 1

Introduction

About two centuries ago, German astronomer Heinrich Olbers argued that, if the universe is eternal and static and filled with stars like the sun, then the night sky would be bright, not dark as we observe it to be. There had been many attempts at explaining this puzzle, but the solution to this problem lies in the fact that the universe is not static but evolving. Interestingly, such an evolving universe arises naturally in Einstein's general theory of relativity. Observations also indicate that our universe is expanding with time. Hence, one can imagine that, in the past, the universe was smaller and denser. Extrapolating Einstein's equations back through this high density regime points to a singularity which observations suggest to have occurred approximately 13.8 billion years ago. This event is referred to as the big bang (see the following texts [1]). Ever since then, light, which travels at finite speed, could have traversed only a finite distance. In turn, this means that observers on Earth today can see only a finite distance away and hence only finitely many stars. Therefore, the total intensity is finite and the night sky is dark, thereby resolving the Olber's paradox.

This thesis is focused on studying issues related to the very early epochs of the

universe often referred to as inflation. Inflation is a paradigm which, as we shall discuss, is considered to be responsible for the generation of the primordial perturbations. A competing paradigm are the bouncing scenarios wherein the big bang is avoided and is replaced by a big bounce. Specifically, this thesis examines inflationary and bouncing scenarios driven by two scalar fields. Before we go on to discuss the contents of the thesis, in this chapter, we shall provide the background that will help in appreciating the issues discussed in this thesis.

A few remarks on our conventions and notations in this thesis are in order at this stage of our discussion. We shall work with natural units such that $\hbar = c = 1$, and set the reduced Planck mass to be $M_{\text{Pl}} = (8\pi G)^{-1/2}$. We shall always work in (3+1) spacetime dimensions and we shall adopt the metric signature of $(-, +, +, +)$. Note that, while Greek indices shall denote the spacetime coordinates, the Latin indices shall represent the spatial coordinates, except for k which shall be reserved for denoting the wavenumber. Moreover, an overdot and an overprime shall denote differentiation with respect to the cosmic and the conformal time coordinates, respectively.

1.1 The standard model of cosmology

The idea of an expanding universe was first proposed by Alexander Friedmann based on the Einstein's general theory of relativity [47]. Soon after, Edwin Hubble provided the comprehensive observational evidence of redshifts of galaxies and he had noticed that the recession speed of the galaxies are proportional to the distance from us [49]. This empirical relation is now called the Hubble-Lemaître law [48]. According to general relativity, this indicates the expansion of spacetime itself. This observational evidence and its theoretical understanding eventually led to the formulation of hot big bang model.

The hot big bang model is the broadly accepted theory for the evolution of our universe. It postulates that a very hot and dense early universe expanded and cooled to its present state. This theory is based on two key ideas: general relativity and the cosmological principle. The cosmological principle is the assumption that the universe is homogeneous and isotropic on the large scales. While the principle was originally motivated theoretically, currently, observations of the large scale structure strongly support this idea. Observations suggest that the universe is homogeneous over the scales of the order of 100 Mpc [50]. Moreover, the big bang model predicts the presence of a relic Cosmic Microwave Background (CMB) with a temperature of around a few degrees Kelvin. The discovery of the CMB (with a temperature 2.73 K today) together with the observed Hubble expansion of the universe established the hot big bang model as the model of our universe [51].

1.1.1 Friedmann-Lemaître-Robertson-Walker (FLRW) metric

As mentioned above, observations suggest that our universe is homogeneous and isotropic at large scales. Homogeneity implies that any one place in space is like any other. Isotropy implies that the universe looks the same in all directions. In general relativity, spacetime is described by the metric tensor. The most general metric satisfying these symmetries is the Friedmann-Lemaître-Robertson-Walker (FLRW) metric, which can be written in terms of the spherical polar coordinates as follows [1]:

$$ds^2 = -dt^2 + a^2(t) \left[\frac{dr^2}{1 - \kappa r^2} + r^2 (d\theta^2 + \sin^2 \theta d\phi^2) \right], \quad (1.1)$$

where t is the cosmic time, *i.e.* the proper time as measured by observers who are comoving with the expansion. In the above metric, κ can be chosen to be $-1, 0,$

or +1 corresponding to spaces of constant negative (open), zero (flat), or positive (closed) spatial curvature, respectively. The quantity a , called the scale factor is, in general, a function of time. Our current understanding of the evolution of the universe is based upon the FLRW metric. However, geometrical considerations alone are not adequate to determine the curvature and the scale factor. The scale factor has to be determined from the Einstein's equations once the matter content of the universe is specified and the spatial curvature κ has to be determined from the observations.

1.1.2 Friedmann equations

According to the general theory of relativity, the spacetime geometry, described in terms of the Einstein tensor G_{ν}^{μ} and stress-energy tensor T_{ν}^{μ} associated with the sources are related via the following Einstein's equations [1]:

$$G_{\nu}^{\mu} = R_{\nu}^{\mu} - \frac{1}{2} \delta_{\nu}^{\mu} R = \frac{1}{M_{\text{Pl}}^2} T_{\nu}^{\mu}. \quad (1.2)$$

In this relation, R_{ν}^{μ} and R are Ricci tensor and Ricci scalar, which can be determined from the metric tensor $g_{\mu\nu}$. The assumption of isotropy and homogeneity implies that T_{ν}^{μ} is diagonal and all the spatial components are equal in the comoving coordinates. In such a case, the stress-energy tensor T_{ν}^{μ} takes the simple form

$$T_{\nu}^{\mu} = \text{diag.} [-\rho(t), p(t), p(t), p(t)], \quad (1.3)$$

where ρ and p denote the energy density and pressure of the sources that drive the scale factor. Under these assumptions, the Einstein's equations (1.2) corresponding to the FLRW line-element (1.1) lead to

$$H^2 + \frac{\kappa}{a^2} = \frac{\rho}{3 M_{\text{Pl}}^2}, \quad (1.4a)$$

$$\frac{\ddot{a}}{a} = -\frac{1}{6 M_{\text{Pl}}^2} (\rho + 3p), \quad (1.4b)$$

where $H = \dot{a}/a$ is the Hubble parameter. These equations are called the Friedmann equations. From these equations one can obtain the continuity equation

$$\dot{\rho} + 3H(\rho + p) = 0, \quad (1.5)$$

which describes the conservation of the stress-energy tensor.

The two Friedmann equations (1.4) contain three unknowns a , ρ and p . In order to obtain solutions to these equations, it is necessary to choose an equation of state, *i.e.* a relationship between pressure p and energy density ρ . Consider an equation of state of the form $p = w\rho$, with a constant w . In such a case, the equation (1.5) leads to $\rho \propto a^{-3(1+w)}$. Observations suggest that our universe contains non-relativistic matter ($w = 0$), radiation ($w = 1/3$) and an unknown form of energy generically referred to as dark energy ($w \simeq -1$). For non-relativistic matter and radiation, we find that $\rho_{\text{m}} \propto a^{-3}$ and $\rho_{\text{r}} \propto a^{-4}$, respectively. For $w = -1$, the energy density remains constant with time. This type of energy density, say, ρ_{Λ} , is referred to as the cosmological constant. When $\kappa = 0$, *i.e.* in a spatially flat universe, we can integrate the Friedmann equations to obtain that

$$a(t) \propto \begin{cases} t^{2/[3(1-w)]}, & \text{when } w \neq -1, \\ e^{Ht}, & \text{when } w = -1, \end{cases} \quad (1.6)$$

where H is constant in the case of $w = -1$.

According to the hot big bang model, our universe has evolved through various epochs. It started as a hot primordial soup of relativistic particles and photons, which is called the radiation dominated epoch. As we have seen above, the radiation density falls faster than the matter density. So, there was a time t_{eq} when

these densities became equal and after that the universe became matter dominated. There was yet another time which is important in the evolution of the universe. This is t_{dec} , when matter ceased to interact with radiation and hence radiation decoupled from matter and continued evolving independently [1]. Thereafter, the decoupled radiation cooled down as the universe expanded, which we observe today as the CMB. The energy content of the present universe has been determined to be dominated by the cosmological constant, which is driving its current accelerated expansion. Using these information, we can rewrite equation (1.4a) as

$$H^2 = \frac{1}{3 M_{\text{Pl}}^2} \left(\rho_\Lambda - \frac{3\kappa}{a^2} + \frac{\rho_m}{a^3} + \frac{\rho_r}{a^4} \right). \quad (1.7)$$

It is useful to define the critical density ρ_c as

$$\rho_c = 3 H^2 M_{\text{Pl}}^2 \quad (1.8)$$

and the time-dependent density parameters Ω_i as

$$\Omega_i = \frac{\rho_i}{\rho_c}. \quad (1.9)$$

In terms of these quantities, equation (1.4a) can be written as

$$\frac{\kappa}{a^2 H^2} = \Omega - 1 = \Omega_\kappa, \quad (1.10)$$

where Ω is the time-dependent density parameter associated with the total energy density. From cosmological observations, the current value of density parameters Ω_i^0 can be estimated to be [5]:

$$\Omega_\Lambda^0 = 0.6889 \pm 0.0056, \quad (1.11a)$$

$$\Omega_\kappa^0 = 0.0007 \pm 0.0019, \quad (1.11b)$$

$$\Omega_m^0 = 0.3111 \pm 0.0056, \quad (1.11c)$$

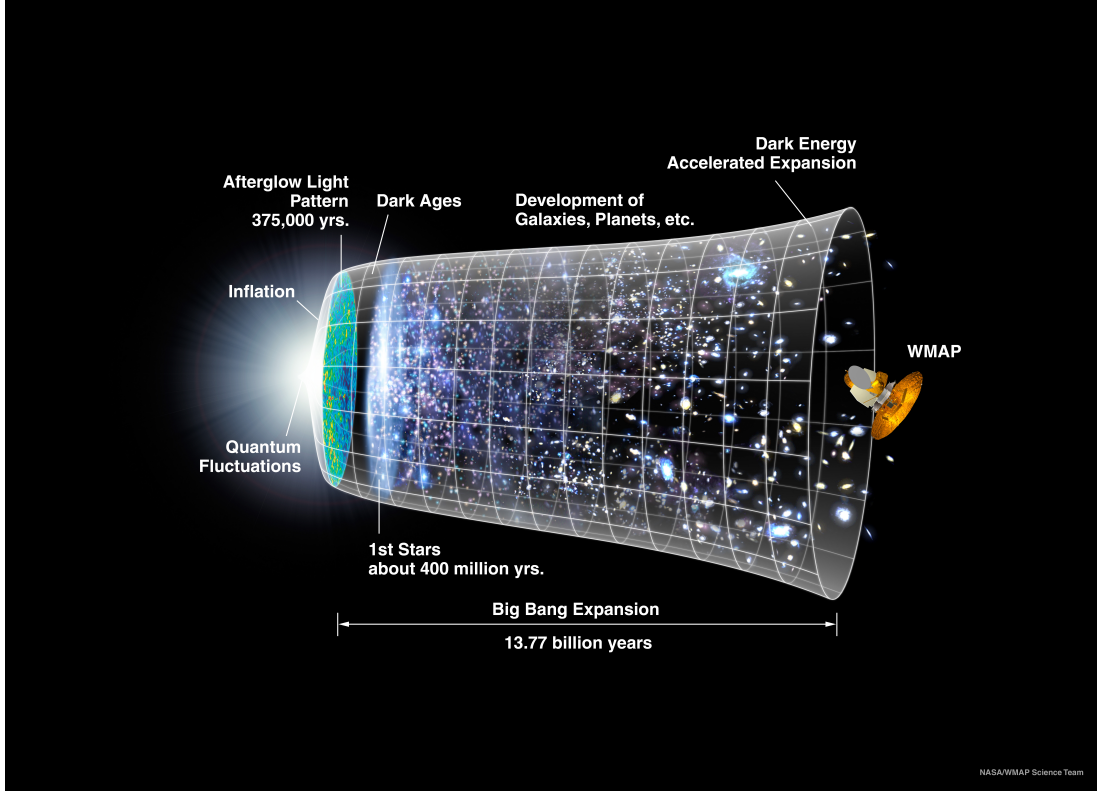


Figure 1.1: A schematic diagram depicting the evolution of the universe, according to the hot big bang model. It also includes the epoch of inflation. (This figure is adapted from Ref. [52].)

$$\Omega_r^0 \simeq \mathcal{O}(10^{-5}). \quad (1.11d)$$

It is clear that the most of the energy density today is contained in matter and cosmological constant. In fact, most of the matter has been determined to be in the form of dark matter which interacts with the rest of the components only through the gravitational force. Hence this kind of parametrization of the hot big bang model is known as the Λ CDM (Λ -Cold Dark Matter) model. Figure 1.1 shows the various epochs of the universe according to the hot big bang model. It also includes the epoch of inflation which will be discussed in section 1.2.

1.1.3 Problems with the standard big bang model

The hot big bang model is unable to explain certain key features of the observed universe. The first such problem is the horizon problem. In this model there is no possible explanation for the extent of observed isotropy of the CMB. Due to the finite speed of light, there is a greatest possible distance—a particle horizon—over which physical information can travel. The maximal distance a photon can travel between an initial time t_i and a later time t in a FLRW universe is defined as

$$h(t) = a(t) \int_{t_i}^t \frac{d\tilde{t}}{a(\tilde{t})}. \quad (1.12)$$

Another relevant time parameter often used in cosmology is the conformal time η which is defined via the relation

$$\eta = \int \frac{dt}{a(t)}. \quad (1.13)$$

In terms of the conformal time, the expression (1.12) can be written as

$$h(t) = a(t) \Delta\eta, \quad (1.14)$$

where $\Delta\eta$ is the amount of conformal time elapsed during the interval $\Delta t = t - t_i$. For a matter dominated universe, the backward horizon at the time of decoupling t_{dec} is

$$\ell_b(t_0, t_{\text{dec}}) = a_{\text{dec}} \int_{t_{\text{dec}}}^{t_0} \frac{d\tilde{t}}{a(\tilde{t})} = a_{\text{dec}} \Delta\eta_b, \quad (1.15)$$

where a_{dec} is the scale factor at decoupling and subscript b denotes the backward horizon. Similarly, the forward horizon at decoupling due to the radiation domi-

nated universe can be expressed as

$$\ell_f(0, t_{\text{dec}}) = a_{\text{dec}} \int_0^{t_{\text{dec}}} \frac{d\tilde{t}}{a(\tilde{t})} = a_{\text{dec}} \Delta\eta_f, \quad (1.16)$$

where f refers to the forward horizon. If we calculate the ratio ℓ_b/ℓ_f of the backward and forward horizons at decoupling, we obtain that

$$\frac{\ell_b}{\ell_f} = \frac{\Delta\eta_b}{\Delta\eta_f} = \frac{3 \left(t_0^{1/3} - t_{\text{dec}}^{1/3} \right)}{2 t_{\text{dec}}^{1/3}} \simeq \frac{3}{2} \left(\frac{t_0}{t_{\text{dec}}} \right)^{1/3}. \quad (1.17)$$

In obtaining this relation, we have used equation (1.6). From observations it is found that $t_{\text{dec}} \simeq 10^5$ years and $t_0 \simeq 10^{10}$ years. Upon using these values, we obtain the ratio $\Delta\eta_b/\Delta\eta_f$ to be 70. This implies that most of the regions at the time of decoupling are not causally connected. Therefore, these regions could have never been able to exchange information. But observations suggest that the CMB is extremely isotropic and it is this difficulty that is referred to as the horizon problem. One can show that the size of the forward horizon ℓ_f subtends an angle of about one degree in the sky, whereas we observe that the temperature is isotropic across the entire sky (see, for instance, Refs. [1]). This is another way of stating the horizon problem.

The second mystery is the observed degree of spatial flatness of the universe. From observations, it is found that the present value of Ω_κ is smaller than 10^{-2} [cf. equation (1.11b)]. In a universe dominated by a fluid with equation of state w , the term $1/(aH)$ evolves as

$$\frac{1}{aH} \propto a^{(1+3w)/2}. \quad (1.18)$$

This implies that, as we go back in time, this term decreases for sources which satisfy the condition $(1+3w) > 0$. Then, from the relation (1.10), we can see that, at much earlier times, Ω_κ must have been extremely close to zero. For instance,

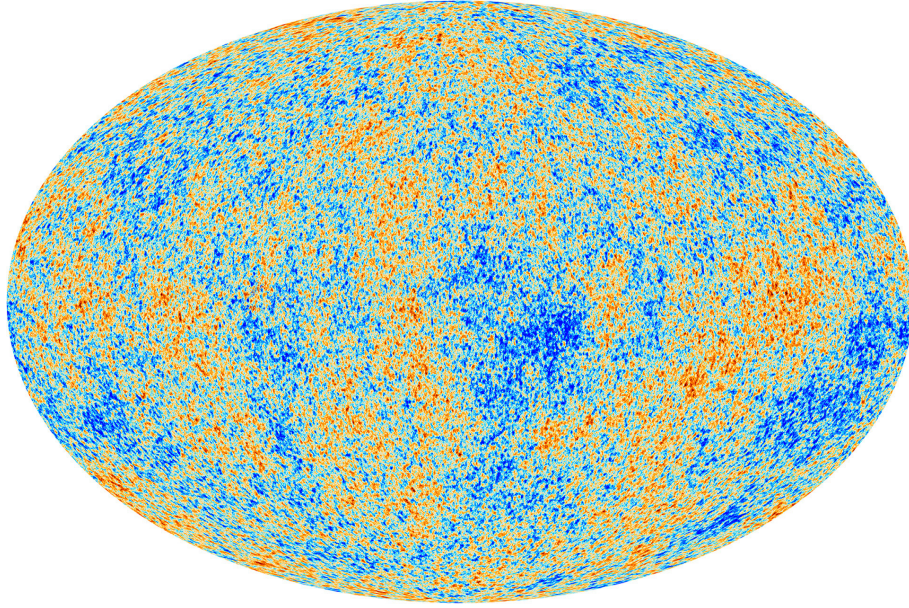


Figure 1.2: The anisotropies in the CMB as observed by Planck (image from Ref. [55]). The blue, yellow and red spots indicate the deviations from the mean value of $T_0 = 2.73$ K. The amplitude of these variations is of the order of $\Delta T/T \simeq 10^{-5}$.

we find that in order for Ω_κ to be nearly close to zero (say, 10^{-2}) today, it must have been about 10^{-50} at the very early stages of the radiation dominated epoch, say, when the temperature was around 10^{14} GeV. Why was Ω_κ so small during the very early epochs? This problem is referred to as the flatness problem.

As we have discussed, the homogeneity of space is one of the assumptions of the standard model but we observe structures such as galaxies and clusters of galaxies in the sky. Moreover, the CMB has been measured to high precision by the various missions such as COBE [53], WMAP [54] and Planck [5]. These observations point to a small variation with direction in the temperature of the order of $\Delta T/T \simeq 10^{-5}$ (see figure 1.2). This temperature fluctuation is due to the variation in the density of matter and radiation contained in the universe at the time of decoupling. These density fluctuations are the seeds of the large scale structures that we observe today. The hot big bang model also cannot explain the origin of the anisotropies in the CMB.

It is important to note that, the general theory of relativity breaks down when the universe becomes very small and as the singularity is approached. One can argue that the hot big bang model is inadequate to explain the first moments of the evolution of the universe. Therefore, it may be worthwhile to also consider scenarios that can avoid the big bang.

When one constructs an early universe scenario beyond the hot big bang model, the above-mentioned problems need to be addressed. Even though various scenarios have been proposed to resolve these difficulties, the theory of inflation is the most widely accepted one. It would be fair to say that, the most popular alternative to inflation are the classical non-singular bouncing scenarios. In the following sections, we shall explain these scenarios and their primary predictions.

1.2 Inflation and the generation of primordial perturbations

Inflation refers to a period of accelerated expansion of the universe during the early stages of the radiation dominated epoch. This idea was postulated to overcome the problems of big bang model, such as the horizon problem and the flatness problems [2,56]. Importantly, in the modern view point, inflation is also able to make other predictions related to the characteristics of the perturbations which can be tested against the cosmological data [1,2,7].

1.2.1 Overcoming problems of the big bang model with inflation

In this section, we shall discuss as to how inflation aids in evading the abovementioned problems of the hot big bang model. The size of the horizon between an

initial time t_i and a later time $t > t_i$ [cf. equation (1.12)] can be written in terms of the Hubble radius $d_H = 1/H$ as follows:

$$h(t) = k a(t) \int_{a(t_i)}^{a(t)} da(\tilde{t}) \left(\frac{d_H(\tilde{t})}{\lambda_p(\tilde{t})} \right), \quad (1.19)$$

where λ_p is the physical distance between two points in the CMB sky which have the same temperature and $k = a/\lambda_p$ is the comoving distance between the points. Consider a λ_p which is outside the horizon at early times in the hot big bang model. Since we observe these points to be at the same temperature in the CMB, the physical length λ_p should be brought inside the horizon, as we go back in time, in the very early stages of the universe so that they are causally connected. From equation (1.19), it can be concluded that the above requirement can be achieved when there is a period wherein

$$\frac{d}{da} \left(\frac{d_H}{\lambda_p} \right) < 0. \quad (1.20)$$

This implies that $\ddot{a} > 0$. We can conclude that, a period of inflation helps in overcoming the horizon problem.

It should be evident from equation (1.10) that whatever the initial value of Ω_{κ} , it will reduce towards zero if we have an epoch of sufficient duration wherein $(aH)^{-1}$ is decreasing with time. In other words, we require

$$\frac{d}{dt} \left(\frac{1}{aH} \right) < 0 \quad (1.21)$$

to overcome the flatness problem as well. This again implies that the universe must be accelerating. In summary, both the horizon and flatness problems can be solved with a period of inflation.

We have so far discussed about how inflation helps in overcoming the above men-

tioned problems. In fact, inflation also has to last for a sufficiently long time in order to solve these puzzles. We need to ensure that at least the forward horizon is as big as backward horizon at the time of decoupling. In order to calculate the minimum amount of inflation needed to solve the horizon problem, for simplicity, let us consider an epoch of inflation described by the exponential expansion of scale factor that starts from a_i at t_i and ends at t_f with the scale factor a_f . In other words, during $t_i < t < t_f$, the scale factor is given by

$$a(t) = a_i \exp [H_1 (t - t_i)], \quad (1.22)$$

where the Hubble parameter $H = H_1$ is constant during the exponential expansion. On denoting $A = a_f/a_i$, assuming $A \gg 1$, and using equation (1.12), the forward horizon can be evaluated to be

$$\ell_1(t_{\text{dec}}, 0) \simeq \frac{A}{H_1} \left(\frac{t_{\text{dec}}}{t_f} \right)^{1/2}. \quad (1.23)$$

In deriving this expression, we have assumed that most of the contribution to the forward horizon at decoupling arises due to inflation. In such a situation, the ratio of the forward and the backward horizons at decoupling can be found to be

$$R_1 = \frac{\ell_1}{\ell_b} \simeq \frac{A}{10^{26}}, \quad (1.24)$$

where we have set $H_1 \simeq 10^{13}$ GeV. This ratio tells us that we need at least $A = 10^{26}$ to overcome the horizon problem. Usually, the extent of inflation from a_i to a given a is expressed in terms of number of e-folds, which is defined as

$$N = \ln \left(\frac{a}{a_i} \right). \quad (1.25)$$

In terms of N , requiring $A \sim 10^{26}$ implies that we need around 60 e-folds of

inflation to solve the horizon problem.

Importantly, in order to obtain the the desired behavior $\ddot{a} > 0$, it is evident from the Friedmann equation (1.4b) that we require a source which obeys the condition $(\rho + 3p) < 0$. In terms of the equation of state parameter w , this condition implies that $w < -1/3$. The amount of conformal time elapsed during the interval $\Delta t = t - t_i$ can be written as

$$\Delta\eta = \int_{a(t_i)}^{a(t)} d \ln a \left(\frac{1}{aH} \right). \quad (1.26)$$

Then, upon using the relation (1.18), we obtain that

$$\Delta\eta = \frac{2}{1+3w} \left[a^{(1+3w)/2} - a_i^{(1+3w)/2} \right]. \quad (1.27)$$

From this equation we can conclude that inflation (with $w < -1/3$) pushes the conformal time to negative values (in this context, see figure 1.3). This ensures that the forward horizon at decoupling can be made at least as big as the backward horizon.

Since inflation resolves the flatness problem and observations too point to a spatially flat universe [4], we shall hereafter work with the case wherein $\kappa = 0$. In such a case, the FLRW line-element (1.1) can be expressed in terms of the Cartesian coordinates as

$$ds^2 = -dt^2 + a^2(t) \delta_{ij} dx^i dx^j. \quad (1.28)$$

1.2.2 Scalar field in a FLRW universe

The simplest way to construct a source with the desired equation of state to drive inflation is to employ a scalar field, say, ϕ . Often one considers a scalar field

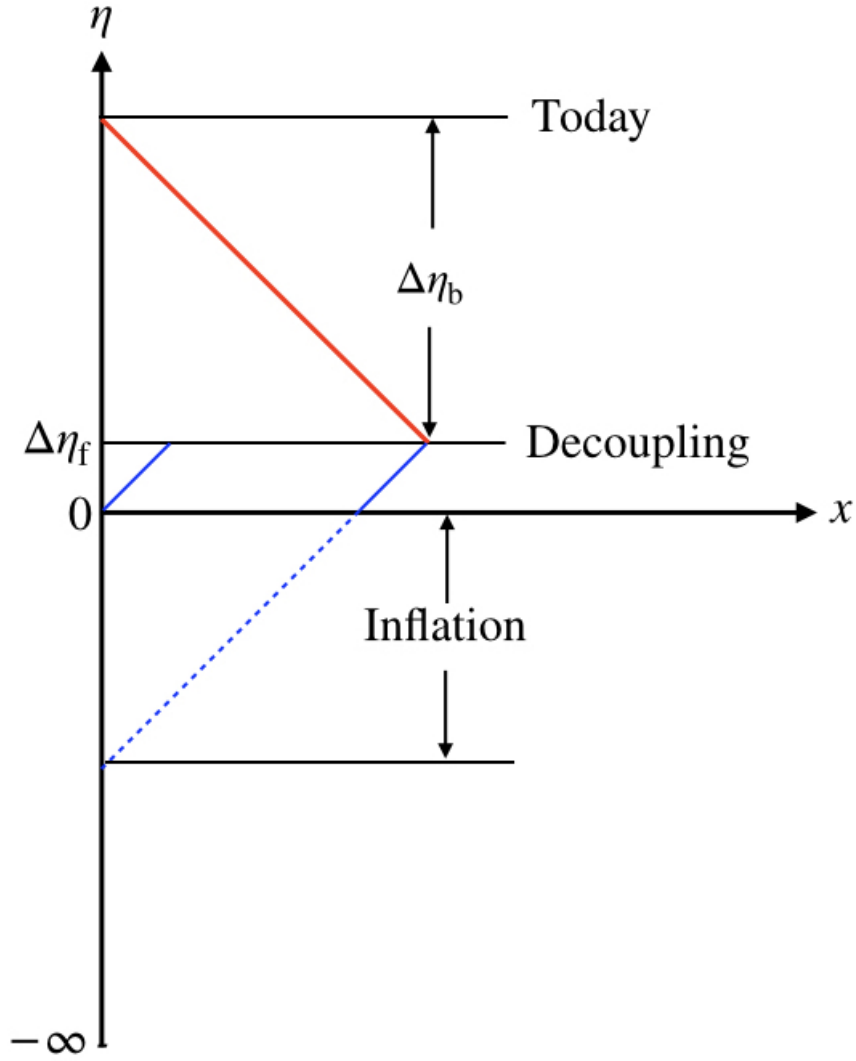


Figure 1.3: An illustration of how inflation resolves the horizon problem. The vertical axis is conformal time and the horizontal axis is comoving distance. The quantity $\Delta\eta_f$ denotes the comoving size of the forward horizon between the end of inflation (or from the big bang, in the absence of inflation) and the time of decoupling. Whereas $\Delta\eta_b$ is the comoving size of the backward horizon between the time of decoupling and today. The figure shows that the forward horizon can be made as big as the backward horizon by extending the conformal time to negative values, which is essentially what inflation achieves.

described by the canonical kinetic energy term and governed by a potential $V(\phi)$. Such a field is described by the action

$$S[\phi] = - \int d^4x \sqrt{-g} \left[-X^{\phi\phi} + V(\phi) \right], \quad (1.29)$$

where the kinetic term $X^{\phi\phi}$ is defined as

$$X^{\phi\phi} = -\frac{1}{2} \partial_\mu \phi \partial^\mu \phi. \quad (1.30)$$

In a spatially flat FLRW universe, the equation of motion governing a homogeneous scalar field is given by

$$\ddot{\phi} + 3H\dot{\phi} + V_\phi = 0, \quad (1.31)$$

where $V_\phi = dV/d\phi$. The stress-energy tensor associated with the scalar field described by the action (1.29) can be obtained to be

$$T_\nu^\mu = \partial^\mu \phi \partial_\nu \phi - \delta_\nu^\mu \left[-X^{\phi\phi} + V(\phi) \right]. \quad (1.32)$$

The energy density ρ_ϕ and the pressure p_ϕ corresponding to the homogeneous scalar field are given by

$$T_{0(\phi)}^0 = -\rho_\phi = -\frac{\dot{\phi}^2}{2} - V(\phi), \quad (1.33a)$$

$$T_{j(\phi)}^i = p_\phi \delta_j^i = \left[\frac{\dot{\phi}^2}{2} - V(\phi) \right] \delta_j^i. \quad (1.33b)$$

In this section, for simplicity, we shall model a scalar field source with a constant equation of state parameter w . Such a source can be achieved with the help of the potential [57]

$$V(\phi) = V_0 e^{\lambda\phi/M_{\text{Pl}}}, \quad (1.34)$$

where $\lambda = \sqrt{3(1+w)}$ and V_0 is a constant. It is easy to establish that this potential leads to a scale factor of the form

$$a = a_1 \left(\frac{\eta}{\eta_1} \right)^{2/(\lambda^2-2)}, \quad (1.35)$$

where a_1 and η_1 are constants. Also, one can show that

$$V_0 = -\frac{2}{(a_1 \eta_1)^2} \frac{\lambda^2 - 6}{(\lambda^2 - 2)^2}. \quad (1.36)$$

For studying the background dynamics, it is convenient to rewrite the background equations in terms of the dimensionless variables

$$(x, y) = \left(\frac{\dot{\phi}}{\sqrt{6} M_{\text{Pl}} H}, \frac{\sqrt{V}}{\sqrt{3} M_{\text{Pl}} H} \right). \quad (1.37)$$

In terms of these variables, the equation governing the scalar field (1.31) and the first Friedmann equation (1.4a) can be written as

$$\frac{dx}{dN} = 3x(x^2 - 1) - \sqrt{\frac{3}{2}} y^2 \lambda, \quad (1.38a)$$

$$x^2 + y^2 = 1. \quad (1.38b)$$

This system of equations admits the following four fixed points:

$$(x_{1\pm}^*, y_{1\pm}^*) = (\pm 1, 0), \quad (1.39a)$$

$$(x_{2\pm}^*, y_{2\pm}^*) = \left(-\frac{\lambda}{\sqrt{6}}, \pm \sqrt{1 - \frac{\lambda^2}{6}} \right). \quad (1.39b)$$

It is easy to show that, in the expanding phase of our interest here, the fixed points $(x_{2\pm}^*, y_{2\pm}^*)$ are stable when $\lambda^2 < 6$. The equation of state parameter corresponding to this fixed point is $w = \lambda^2/3 - 1$. From the above analysis it is evident that the expanding phase with the equation of state $w < 1$, which includes matter domination ($w = 0, \lambda^2 = 3$), radiation domination ($w = 1/3, \lambda^2 = 4$) and power law inflation ($w < -1/3, \lambda^2 < 2$) are all attractors. It is also useful to note that the above points are stable when $\lambda^2 > 6$ in a contracting universe. We shall discuss this point in more detail later in the thesis.

1.2.3 Perturbations

We have so far considered the universe to be homogeneous and isotropic. As we have mentioned earlier, we observe that the large scale structures are distributed inhomogeneously in the universe which are supposed to have evolved from the small anisotropies observed in the CMB. Cosmological perturbation theory studies the evolution of the perturbations in the gravitational and matter degrees of freedom on the cosmological scales. In this thesis, we shall be interested in the primordial fluctuations which are small and hence we shall mostly work with linear perturbation theory. In other words, we shall write all the quantities as a sum of background and linear order terms, and ignore terms which contain product of more than one perturbation. In such a case, the Einstein's equations at the first order in the perturbations can be written as

$$\delta G_{\mu\nu} = \frac{1}{M_{\text{Pl}}^2} \delta T_{\mu\nu}, \quad (1.40)$$

where $\delta G_{\mu\nu}$ and $\delta T_{\mu\nu}$ are quantities that are linear in the perturbations.

Let $\delta g_{\mu\nu}$ denote the perturbed metric at the linear order in the spatially flat Friedmann universe. Such a metric can be written as

$$\delta g_{\mu\nu} = (\delta g_{00}, \delta g_{0i}, \delta g_{ij}). \quad (1.41)$$

It is known that according to the behavior under the rotation of spatial coordinates on hypersurfaces of constant time, the perturbations can be classified as scalars, vectors and tensors (see, for instance, Refs. [1]). Evidently, δg_{00} can be identified as a scalar, say, A . Similarly, δg_{0i} is a vector and δg_{ij} is a symmetric tensor. As is well known, we can decompose a generic vector into the gradient of

a scalar and a divergence free vector. Hence we can write the quantity δg_{0i} as

$$\delta g_{0i} = \nabla_i B + \mathcal{S}_i, \quad (1.42)$$

where B is a scalar and \mathcal{S}_i is a divergence free vector, *i.e.* $\nabla_i \mathcal{S}^i = 0$. In the same manner, the symmetric tensor δg_{ij} can be decomposed as follows:

$$\delta g_{ij} = \psi \delta_{ij} + \left[\frac{1}{2} (\nabla_i \nabla_j + \nabla_j \nabla_i) - \frac{1}{3} \delta_{ij} \nabla^2 \right] E + (\nabla_i \mathcal{F}_j + \nabla_j \mathcal{F}_i) + h_{ij}, \quad (1.43)$$

where ψ and E are scalars, \mathcal{F}_i is another divergence free vector and h_{ij} is a symmetric traceless tensor which satisfies the condition $\nabla_i h^{ij} = 0$. In (3+1) spacetime dimensions of our interest, clearly, the metric perturbation $\delta g_{\mu\nu}$ has ten components. These degrees of freedom are distributed as four scalars A , B , E and ψ (four degrees of freedom), two divergence free vectors \mathcal{F}_i and \mathcal{S}_i (four degrees of freedom), and a symmetric traceless tensor h_{ij} (two degrees of freedom), in the decomposition of the perturbed metric. However, four of them are not physical degrees of freedom, as they correspond to the freedom in choosing the four coordinates (x^μ). So, there are actually only six physical degrees of freedom. (In general relativity, the gravitational sector has only two degrees of freedom, corresponding to the two polarizations of gravitational waves. The additional degrees of freedom arise when sources are present.) Such a decomposition proves to be useful. One can show that the perturbed Einstein's equations for scalars, vectors and tensors do not couple to each other at the linear order and therefore evolve independently.

If we now take into account only the scalar perturbations to the background met-

ric (1.28), then the FLRW line-element, in general, can be written as [1]

$$ds^2 = -(1 + 2A) dt^2 + 2a(t) (\partial_i B) dt dx^i + a^2(t) [(1 - 2\psi) \delta_{ij} + 2(\partial_i \partial_j E)] dx^i dx^j, \quad (1.44)$$

where A , B , ψ and E are four scalar functions that describe the perturbations, which depend on time as well as space. However, recall that, there exist only two independent degrees of freedom describing the scalar perturbations. The two additional degrees of freedom arise due to the following scalar gauge (*i.e.* infinitesimal coordinate) transformations that are permitted [1]:

$$t \rightarrow t + \delta t, \quad (1.45a)$$

$$x_i \rightarrow x_i + \partial_i (\delta x), \quad (1.45b)$$

where δt and δx are scalar quantities that are functions of time and space. Clearly, the metric perturbations will not be invariant under such a change of coordinates and, it is easy to show that, under the gauge transformations (1.45), the functions A , B , ψ and E transform as follows:

$$A \rightarrow A - \dot{\delta t}, \quad (1.46a)$$

$$B \rightarrow B + \frac{\delta t}{a} - a \dot{\delta x}, \quad (1.46b)$$

$$\psi \rightarrow \psi + H \delta t, \quad (1.46c)$$

$$E \rightarrow E - \delta x. \quad (1.46d)$$

For simplicity, one can choose specific forms for the quantities δt and δx , thereby restricting oneself to a particular gauge. Or, one can work with gauge invariant quantities.

The components of the perturbed Einstein's tensor corresponding to the line-

element (1.44) can be obtained to be

$$\delta G_0^0 = 6H(\dot{\psi} + HA) - \frac{2}{a^2} \nabla^2 [\psi - aH(B - a\dot{E})], \quad (1.47a)$$

$$\delta G_i^0 = -2\partial_i(\dot{\psi} + HA), \quad (1.47b)$$

$$\begin{aligned} \delta G_j^i = & \left[2\ddot{\psi} + 2H(3\dot{\psi} + \dot{A}) + 2(2\dot{H} + 3H^2)A \right. \\ & \left. + \frac{1}{a^2} \nabla^2 \left\{ (A - \psi) + \frac{1}{a} [a^2(B - a\dot{E})] \right\} \right] \delta_j^i \\ & - \frac{1}{a^2} \delta^{il} \partial_l \partial_j \left\{ (A - \psi) + \frac{1}{a} [a^2(B - a\dot{E})] \right\}, \end{aligned} \quad (1.47c)$$

where $\nabla^2 = \delta^{ij} \partial_i \partial_j$. It is important to note that, if one considers only scalar field sources, vector perturbations do not arise at all. Also, if there are any vector sources already present, one can show that they will decay in an expanding universe. We shall briefly comment about the evolution of vector perturbations in bouncing universes in due course.

From the decomposition of the FRLW metric [*cf.* equation (1.43)], it should be clear that, when only the tensor perturbations are taken into account, the metric can be written as

$$ds^2 = -dt^2 + a^2(t) (\delta_{ij} + \gamma_{ij}) dx^i dx^j. \quad (1.48)$$

Note that the symmetric, traceless and transverse tensor γ_{ij} represents gravitational waves and it contains two degrees of freedom. These degrees of freedom correspond to the two polarizations of the gravitational waves. The perturbed Einstein tensor corresponding to the above metric can be calculated to be

$$\delta G_0^0 = \delta G_i^i = 0, \quad (1.49a)$$

$$\delta G_j^i = \frac{1}{2} \left(\ddot{\gamma}_{ij} + 3H\dot{\gamma}_{ij} - \frac{1}{a^2} \nabla^2 \gamma_{ij} \right). \quad (1.49b)$$

In the absence of anisotropic stresses, *i.e.* when $\delta T_j^i = 0$, we have $\delta G_j^i = 0$ and

hence we obtain that

$$\gamma''_{ij} + 2\mathcal{H}\gamma'_{ij} - \nabla^2\gamma_{ij} = 0, \quad (1.50)$$

where $\mathcal{H} = a'/a$ is the conformal Hubble parameter. Note that we have written the above equation in terms of the conformal time coordinate. It should be mentioned that gravitational waves can be generated even in the absence of sources.

1.2.4 Generation of primordial fluctuations

In the previous section, we have described the perturbations in the metric. According to the theory of inflation, the primordial fluctuations are generated due to the quantum fluctuations in the matter fields. These fluctuations are stretched to the cosmic scales during inflation. The scalar fluctuations produced in such a fashion are the cause of the anisotropies in the CMB and the large scale structure that we observe. The tensor perturbations also leave their distinct imprints on the CMB. The detection of the direct signatures of primordial gravitational waves in the CMB is a holy grail in observational cosmology today.

In this section, we shall study the behavior of the scalar and tensor perturbations in power law inflation and calculate their resulting power spectra. As we discussed in the earlier sections, inflation is achieved with the aid of scalar fields. Let $\delta\phi$ denote the perturbation in the scalar field. On using the metric (1.44), the perturbed stress-energy tensor associated with the scalar field can be obtained to be

$$\delta T_{0(\phi)}^0 = -\left(\dot{\phi}\dot{\delta\phi} - \dot{\phi}^2 A + V_\phi \delta\phi\right) = -\delta\rho_\phi, \quad (1.51a)$$

$$\delta T_{i(\phi)}^0 = -\partial_i\left(\dot{\phi}\delta\phi\right) = -\partial_i(\delta q_\phi), \quad (1.51b)$$

$$\delta T_{j(\phi)}^i = \left(\dot{\phi}\dot{\delta\phi} - \dot{\phi}^2 A - V_\phi \delta\phi\right)\delta_j^i = \delta p_\phi \delta_j^i. \quad (1.51c)$$

Under the infinitesimal coordinate transformation (1.45), the scalar field transforms as

$$\delta\phi \rightarrow \delta\phi - \dot{\phi} \delta t. \quad (1.52)$$

The primordial scalar perturbation is usually described in terms of comoving curvature perturbation which is defined as [1]

$$\mathcal{R} = \psi - \frac{H}{\rho_\phi + p_\phi} \delta\phi = \psi + \frac{H}{\dot{\phi}} \delta\phi, \quad (1.53)$$

where ρ_ϕ and p_ϕ denote the energy density and pressure associated with the scalar field [*cf.* equations (1.33)]. It is important to mention that, in comoving gauge wherein $\delta q_\phi = 0$, \mathcal{R} is related to the perturbation in the spatial curvature (which can be expressed in terms of ψ) and hence the name comoving curvature perturbation. This quantity is gauge invariant as is evident from equations (1.46) and (1.52) and it can be shown that it is conserved on super-Hubble scales (see, for instance, Refs. [1]).

One can show that, at the quadratic order, the action governing the curvature perturbation \mathcal{R} is given by [1,2]

$$\mathcal{S}_2[\mathcal{R}] = \frac{1}{2} \int d\eta \int d^3\mathbf{x} z^2 \left[\mathcal{R}'^2 - (\partial\mathcal{R})^2 \right], \quad (1.54)$$

where the quantity z is defined as

$$z = \frac{a\dot{\phi}}{H} = \frac{\sqrt{-2\dot{H}}}{H} M_{\text{Pl}} a. \quad (1.55)$$

In a similar fashion, at the quadratic order, the action governing the tensor perturbations can be obtained to be [1,34]

$$\mathcal{S}_2[\gamma_{ij}] = \frac{M_{\text{Pl}}^2}{8} \int d\eta \int d^3\mathbf{x} a^2 \left[\gamma'_{ij}{}^2 - (\partial\gamma_{ij})^2 \right], \quad (1.56)$$

which leads to the linear equation of motion (1.50) that we had arrived at earlier.

1.2.5 Quantization and power spectra

As we have mentioned, the primordial perturbations are generated due to the quantum fluctuations of the scalar field. Upon varying the action (1.54), we can arrive at the following equation governing the curvature perturbation in Fourier space:

$$\mathcal{R}_k'' + 2 \frac{z'}{z} \mathcal{R}_k' + k^2 \mathcal{R}_k = 0. \quad (1.57)$$

Note that, this equation depends on the background through the quantity z which can be, in principle, expressed in terms of a and its derivatives. In quantum field theory, the classical variable \mathcal{R} can be elevated to be a quantum operator and can be expanded in Fourier modes \mathcal{R}_k as follows:

$$\begin{aligned} \hat{\mathcal{R}}(\eta, \mathbf{x}) &= \int \frac{d^3 \mathbf{k}}{(2\pi)^{3/2}} \hat{\mathcal{R}}_{\mathbf{k}}(\eta) e^{i\mathbf{k}\cdot\mathbf{x}} \\ &= \int \frac{d^3 \mathbf{k}}{(2\pi)^{3/2}} \left[\hat{a}_{\mathbf{k}} \mathcal{R}_{\mathbf{k}}(\eta) e^{i\mathbf{k}\cdot\mathbf{x}} + \hat{a}_{\mathbf{k}}^\dagger \mathcal{R}_{\mathbf{k}}^*(\eta) e^{-i\mathbf{k}\cdot\mathbf{x}} \right], \end{aligned} \quad (1.58)$$

where $\hat{a}_{\mathbf{k}}$ and $\hat{a}_{\mathbf{k}}^\dagger$ are the conventional annihilation and creation operators. These operators satisfy the following standard commutation relations:

$$[\hat{a}_{\mathbf{k}}, \hat{a}_{\mathbf{k}'}] = [\hat{a}_{\mathbf{k}}^\dagger, \hat{a}_{\mathbf{k}'}^\dagger] = 0, \quad [\hat{a}_{\mathbf{k}}, \hat{a}_{\mathbf{k}'}^\dagger] = \delta^{(3)}(\mathbf{k} - \mathbf{k}'). \quad (1.59)$$

We define the vacuum state $|0\rangle$ as

$$\hat{a}_{\mathbf{k}} |0\rangle = 0, \quad (1.60)$$

for all k . If we now introduce another variable

$$v_k = z \mathcal{R}_k, \quad (1.61)$$

called the Mukhanov-Sasaki variable, the equation (1.57) governing \mathcal{R}_k reduces to

$$v_k'' + \left(k^2 - \frac{z''}{z} \right) v_k = 0. \quad (1.62)$$

This equation can be treated as the equation of a harmonic oscillator with *time-dependent* frequency. The Mukhanov-Sasaki equation is hard to solve in full generality for a model described by an arbitrary potential. However, it is known that the solutions can be easily obtained for a model described by the exponential potential (1.34).

Since we are dealing with linear perturbation theory, the perturbations are expected to be Gaussian. For a Gaussian perturbation, the complete statistical information is contained in the two-point correlation function. In cosmology, the two-point correlation function in Fourier space is referred to as the power spectrum. The power spectrum of the scalar perturbations $\mathcal{P}_\mathcal{R}(k)$ is defined to be [1]

$$\langle \hat{\mathcal{R}}_{\mathbf{k}} \hat{\mathcal{R}}_{\mathbf{k}'} \rangle = \frac{2\pi^2}{k^3} \mathcal{P}_\mathcal{R}(k) \delta^{(3)}(\mathbf{k} + \mathbf{k}'). \quad (1.63)$$

Using the decomposition (1.58) one can arrive at the relation between the power spectrum and the modes of the curvature perturbation to be

$$\mathcal{P}_\mathcal{R}(k) = \frac{k^3}{2\pi^2} |\mathcal{R}_k|^2 = \frac{k^3}{2\pi^2} \left(\frac{|v_k|}{z} \right)^2. \quad (1.64)$$

Upon variation of the action (1.56), one finds that, the tensor modes in Fourier

space, say, h_k , satisfy the following equation of motion:

$$h_k'' + 2 \frac{a'}{a} h_k' + k^2 h_k = 0. \quad (1.65)$$

On quantization, the quantum operator associated with the tensor perturbation $\hat{\gamma}_{ij}$ can be decomposed in terms of the corresponding Fourier modes h_k as follows:

$$\begin{aligned} \hat{\gamma}_{ij}(\eta, \mathbf{x}) &= \int \frac{d^3 \mathbf{k}}{(2\pi)^{3/2}} \hat{\gamma}_{ij}^{\mathbf{k}}(\eta) e^{i \mathbf{k} \cdot \mathbf{x}} \\ &= \sum_s \int \frac{d^3 \mathbf{k}}{(2\pi)^{3/2}} \left(\hat{b}_{\mathbf{k}}^s \varepsilon_{ij}^s(\mathbf{k}) h_k(\eta) e^{i \mathbf{k} \cdot \mathbf{x}} + \hat{b}_{\mathbf{k}}^{s\dagger} \varepsilon_{ij}^{s*}(\mathbf{k}) h_k^*(\eta) e^{-i \mathbf{k} \cdot \mathbf{x}} \right), \end{aligned} \quad (1.66)$$

where the annihilation and creation operators $\hat{b}_{\mathbf{k}}^s$ and $\hat{b}_{\mathbf{k}}^{s\dagger}$ satisfy the following standard commutation relations:

$$\left[\hat{b}_{\mathbf{k}}^s, \hat{b}_{\mathbf{k}'}^{s'} \right] = \left[\hat{b}_{\mathbf{k}}^{s\dagger}, \hat{b}_{\mathbf{k}'}^{s'\dagger} \right] = 0, \quad \left[\hat{b}_{\mathbf{k}}^s, \hat{b}_{\mathbf{k}'}^{s'\dagger} \right] = \delta^{(3)}(\mathbf{k} - \mathbf{k}') \delta_{ss'}. \quad (1.67)$$

The quantity $\varepsilon_{ij}^s(\mathbf{k})$ represents the polarization tensor of gravitational waves with their helicity being denoted by the index s . The transverse and traceless nature of the gravitational waves lead to the conditions $k_i \varepsilon_{ij}^s(\mathbf{k}) = \varepsilon_{ii}^s(\mathbf{k}) = 0$. We shall choose to work with the following normalization of the polarization tensor: $\varepsilon_{ij}^r(\mathbf{k}) \varepsilon_{ij}^{s*}(\mathbf{k}) = 2 \delta^{rs}$ [34]. If we write $h_k = \sqrt{2} u_k / (M_{\text{Pl}} a)$, then the equation (1.65) simplifies to

$$u_k'' + \left(k^2 - \frac{a''}{a} \right) u_k = 0, \quad (1.68)$$

which is similar to the equation (1.62) for the case of scalars with the quantity z replaced by a . The tensor power spectrum, *viz.* $\mathcal{P}_{\text{T}}(k)$, is defined as

$$\langle \hat{\gamma}_{ij}^{\mathbf{k}} \hat{\gamma}_{mn}^{\mathbf{k}'} \rangle = \frac{(2\pi)^2}{2k^3} \frac{\Pi_{ij,mn}^{\mathbf{k}}}{4} \mathcal{P}_{\text{T}}(k) \delta^{(3)}(\mathbf{k} + \mathbf{k}'), \quad (1.69)$$

where the quantity $\Pi_{ij,mn}^{\mathbf{k}}$ is given by

$$\Pi_{ij,mn}^{\mathbf{k}} = \sum_s \varepsilon_{ij}^s(\mathbf{k}) \varepsilon_{mn}^{s*}(\mathbf{k}). \quad (1.70)$$

On making use of the decomposition (1.66), the inflationary tensor power spectrum evaluated in the vacuum state $|0\rangle$ (such that $\hat{b}_{\mathbf{k}}^s|0\rangle = 0 \forall \mathbf{k}$ and s) can be expressed as

$$\mathcal{P}_{\text{T}}(k) = 4 \frac{k^3}{2\pi^2} |h_k|^2 = 8 \frac{k^3}{2\pi^2 M_{\text{Pl}}^2} \left(\frac{|u_k|}{a} \right)^2. \quad (1.71)$$

The power spectra are calculated in the super-Hubble limit where the amplitude of the perturbations become constant. If the power spectrum is independent of k , one has a scale-invariant spectrum. The deviations from the scale invariance can be quantified in terms of the following spectral indices:

$$n_{\mathcal{R}} = 1 + \frac{d \ln \mathcal{P}_{\mathcal{R}}}{d \ln k}, \quad (1.72a)$$

$$n_{\mathcal{T}} = \frac{d \ln \mathcal{P}_{\mathcal{T}}}{d \ln k}. \quad (1.72b)$$

Note that the scale-invariant power spectra correspond to $n_{\mathcal{R}} = 1$ and $n_{\mathcal{T}} = 0$. Importantly, these quantities can be constrained by observations. Another observable quantity we will be interested in is the tensor-to-scalar ratio which is defined as

$$r(k) = \frac{\mathcal{P}_{\mathcal{T}}(k)}{\mathcal{P}_{\mathcal{R}}(k)}. \quad (1.73)$$

Note that r is often quoted at a specific scale.

1.2.6 The Bunch-Davies initial conditions

The initial conditions have to be chosen in the far past, when all the comoving scales are far inside the Hubble radius, *i.e.* when $k \gg aH$ (in this context, see

figure 1.4). If we consider wavelengths much smaller than the Hubble radius, the effects of spacetime curvature can be ignored and modes can be expected to behave as in Minkowski spacetime. In this limit, the equations governing the scalar and tensor Mukhanov-Sasaki variables [*i.e.* equations (1.62) and (1.68)] reduce to

$$v_k'' + k^2 v_k \simeq 0, \quad (1.74a)$$

$$u_k'' + k^2 u_k \simeq 0. \quad (1.74b)$$

Note that, each of these equations describes a simple harmonic oscillator with a *constant* frequency k . The positive frequency solutions to these modes behave in the following form:

$$\lim_{k/(aH) \rightarrow \infty} [v_k(\eta), u_k(\eta)] \rightarrow \frac{1}{\sqrt{2k}} e^{-ik\eta}. \quad (1.75)$$

It is these initial conditions that we shall impose in the limit wherein $k \gg aH$. The vacuum state corresponding to such mode functions is referred to as the Bunch-Davies vacuum.

Let us now try to solve equations (1.62) and (1.68) corresponding to the initial condition (1.75) analytically. As we have mentioned earlier, the analytical solution can be obtained for a model described by the exponential potential (1.34). In such a model, the equation governing the Mukhanov-Sasaki variable associated with the scalar perturbation v_k is given by

$$v_k'' + \left[k^2 + \frac{2(\lambda^2 - 4)}{\eta^2(\lambda^2 - 2)^2} \right] v_k = 0. \quad (1.76)$$

In power law expansion (1.35), one finds that the Mukhanov-Sasaki variable associated with the tensor perturbation u_k also satisfies the same equation. The solutions to the above differential equation with the Bunch-Davies initial condi-

tions can be obtained as

$$v_k(\eta) = u_k(\eta) = \sqrt{\frac{-\eta\pi}{4}} e^{i(\nu+1/2)\pi/2} H_\nu^{(1)}(-k\eta), \quad (1.77)$$

where $\nu = (\lambda^2 - 6)/[2(\lambda^2 - 2)]$ and $H_\nu^{(1)}(x)$ is the Hankel function of the first kind. In the super-Hubble limit, *i.e.* when $k|\eta| \ll 1$, the scalar and tensor power spectra can be obtained to be

$$\mathcal{P}_\mathcal{R}(k) = \left[\frac{|\Gamma(|\nu|)|/\Gamma(3/2)}{4\pi M_{\text{Pl}}\lambda} \right]^2 \left(\frac{k}{a} \right)^2 \left(\frac{-k\eta}{2} \right)^{1-2|\nu|}, \quad (1.78a)$$

$$\mathcal{P}_\mathcal{T}(k) = 8 \left[\frac{|\Gamma(|\nu|)|/\Gamma(3/2)}{4\pi M_{\text{Pl}}\lambda} \right]^2 \left(\frac{k}{a} \right)^2 \left(\frac{-k\eta}{2} \right)^{1-2|\nu|}. \quad (1.78b)$$

The corresponding tensor-to-scalar ratio is found to be $r = 8\lambda^2$. The spectral indices associated with the perturbations can be calculated to be

$$n_\mathcal{R} = n_\mathcal{T} + 1 = 4 - \left| \frac{\lambda^2 - 6}{\lambda^2 - 2} \right|. \quad (1.79)$$

It is easy to see that nearly scale-invariant spectra arise when $\lambda \simeq 0$, corresponding to near de Sitter inflation.

1.2.7 Two-field models

In the case of inflation, even though the single field model is consistent with the most of the observations, one finds that the models based on high energy physics, in particular ones derived in string theory, usually involve more than one scalar field [9, 11, 58, 59]. As far as the background evolution is concerned, two-field models offer a richer dynamics than the single field models due to the possibility of different types of trajectories in the field space. At the level of perturbations, in two-field models, there are two types of independent scalar perturbations that

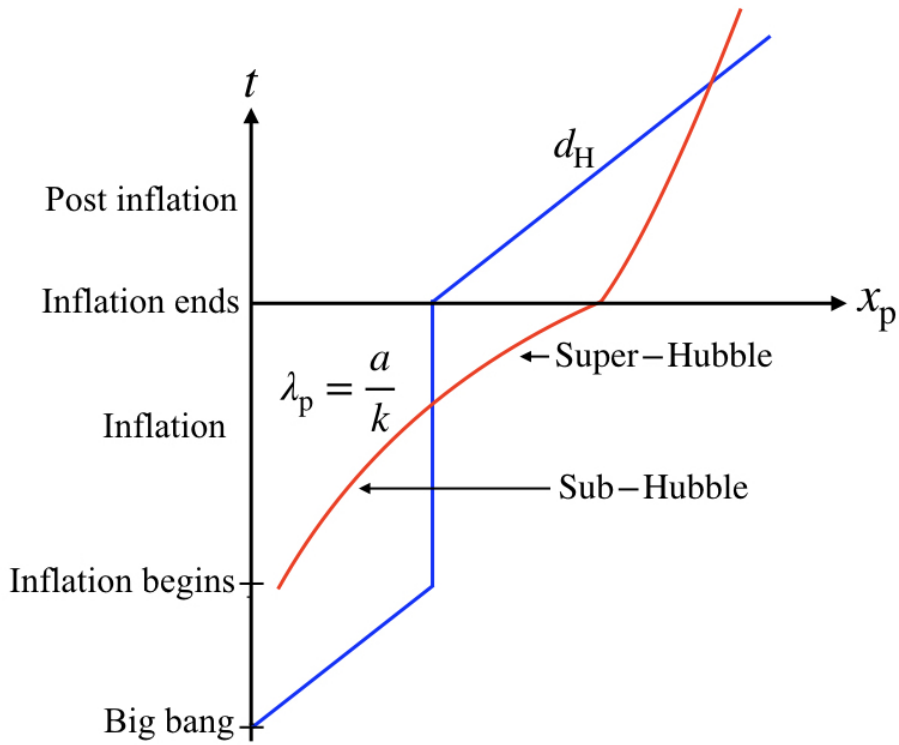


Figure 1.4: Behavior of physical wavelength λ_p associated with a mode of the scalar and tensor perturbations (in red) and the Hubble radius d_H (in blue) in inflationary cosmology. The vertical axis is time, while the horizontal axis is physical distance. The initial conditions are imposed when the modes are well inside the Hubble radius and the power spectra are calculated when the modes are well outside the Hubble radius.

arise. It is conventional to decompose these scalar perturbations along the two directions, parallel and orthogonal to the background trajectory in field space. The perturbation parallel to the trajectory is usually called the adiabatic or curvature perturbation, while the perturbation orthogonal to the trajectory is called the entropy or isocurvature perturbation (see, in this context, figure 1.5). The existence of isocurvature perturbations in multi-field models can lead to a non-trivial evolution of the curvature perturbations on super-Hubble scales, whereas this amplitude is frozen in single field inflation.

The isocurvature perturbation is the relative entropy perturbation between the various scalar fields. It acts as a source term for the evolution equation for the curvature perturbation. The equations governing these two perturbations are in

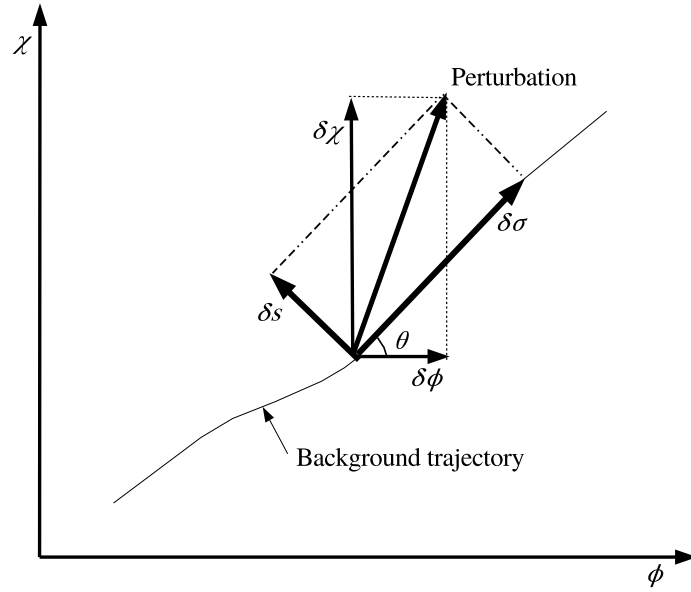


Figure 1.5: An illustration of the decomposition of an arbitrary perturbation into an adiabatic $\delta\sigma$ and entropy δs component in a model containing two scalar fields, say, ϕ and χ (in this context, see Ref. [10]). The perturbations in the scalar fields $\delta\phi$ and $\delta\chi$ are also shown. Evidently, $\delta\sigma$ and δs are linear combinations of $\delta\phi$ and $\delta\chi$. It should be mentioned that $\delta\sigma$ is related to the comoving curvature perturbation \mathcal{R} .

general coupled and the coupling strength is determined by the extent of bending of the background trajectory in the field space. We shall highlight the various aspects of two-field models in due course.

1.2.8 Challenges to the inflationary scenario

Inflation has proved to be a simple, compelling and effective paradigm. It turns out to be rather easy to construct an inflationary model that is consistent with the cosmological data, primarily of the anisotropies in the CMB, as observed by missions such as Planck. This efficiency of the paradigm has led to a profusion of inflationary models and, despite the increasingly accurate cosmological observations, many of these models continue to remain consistent with the data (see, for instance, Ref. [8]). For example, chaotic inflation was touted to have been the

most highly favored model when the original BICEP2 result was announced [60]. Currently, there exist stronger bounds on the tensor-to-scalar ratio and, in fact, the simple quadratic potential is now being increasingly ruled out by the data. Despite such reversals, inflation is continued to be claimed as the most favored paradigm [7,61]. One may consider this is to be the versatility of inflation. However, this has also led to the concern whether, as a paradigm, inflation can be falsified at all (in this context, see, for example, Ref. [62]). Moreover, inflation does not provide a complete history of the universe, and one may enquire what happened prior to inflation or how the inflationary phase began. In such a situation, it becomes important to explore alternatives to inflation.

1.3 Bouncing scenario as an alternative paradigm

Inflation solves the horizon problem due to a rapid expansion of the particle horizon such that a large region of space, which includes the largest observable scale today, is causally connected. But this mechanism is not unique and there is another way of solving the horizon problem. A phase of contracting universe starting from an infinite past will naturally have a large horizon and thereby can help us in overcoming the horizon problem. Moreover, one can show that, during a *non-accelerating* contracting phase, one can impose the Bunch-Davies initial conditions in a manner similar to inflation (in this context, see figure 1.6). The most popular alternative to the inflationary paradigm is the classical bouncing scenario. In such a scenario, the universe goes through an initial phase of contraction until the scale factor reaches a minimum value, before it begins to expand (see the reviews [3]).

While inflation is easy to achieve, it proves to be difficult to construct well motivated sources which can drive bounces. This difficulty can be largely attributed to

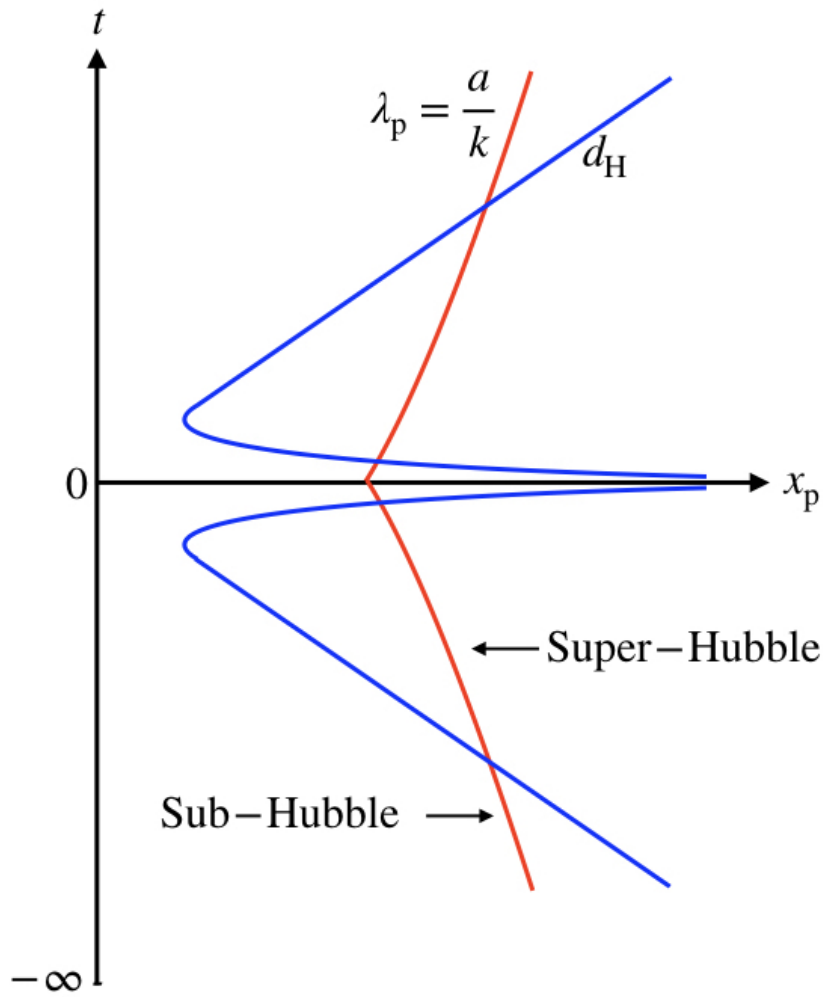


Figure 1.6: A sketch of the evolution of the physical wavelength λ_p (in red) and the Hubble radius d_H (in blue) in a non-singular and symmetric bouncing universe. The vertical axis is time and the horizontal axis is physical distance. Note that, one can impose the Bunch-Davies initial conditions when the modes are well inside the Hubble radius at a suitably early time during the contracting phase. One finds that this is possible if there exists a phase of *non-accelerating* contraction.

the fact that the Null Energy Condition (NEC) has to be violated near the bounce. One of the primary problems confronting contracting universes are their instability to the growth of anisotropic stresses [63]. The energy density associated with the anisotropies in the universe can be shown to scale as a^{-6} . In inflationary universes, they dilute much faster than the other stress-energy components and therefore quickly become negligible. In contracting universes the anisotropies

grow and become dominant rather rapidly. Another problem that is encountered in bouncing universe are the gradient instabilities which seem to be always associated with the violation of the NEC [3].

Note that the discussion we have carried out, as far as the perturbations are concerned, applies to inflation as well as bounces. However, it is important to recognize that there is a significant difference in the behavior of evolution of perturbations between these two paradigms. In the case of inflation, the amplitude of the curvature perturbation becomes constant soon after the modes leave the Hubble radius. In contrast, in a contracting phase, the amplitude of the scalar and tensor perturbations grow as one approaches the bounce. We shall discuss this behavior of perturbations in some detail in the later chapters.

1.3.1 The simple matter bounce scenario and challenges

One of the successes of the inflationary theory is to arrive at a nearly scale-invariant spectrum of primordial fluctuations that can seed the large scale structure. Similarly, one can show that, a contracting phase which behaves as a matter dominated epoch can lead to a scale-invariant spectrum (see, in this context, Ref. [64]). If the scale-invariant spectrum is preserved across the bounce, it can then possibly provide an explanation for the observed fluctuations in the CMB. Such a scenario is referred to as the matter bounce. Even though this model predicts a scale-invariant spectrum, the model is plagued by a variety of issues, such as the anisotropy problem. Moreover, one can show that the contracting matter dominated phase is not an attractor and hence needs very fine tuned initial conditions [24]. In addition, most of the efforts show that the tensor-to-scalar ratio can be very large in these models which can be inconsistent with the observations [12]. One requires more complex matter bounce scenarios to achieve the

suppression of anisotropic instabilities and lead to a tensor-to-scalar ratio that is consistent with the observations (for a recent effort in this direction, see, for instance, Ref. [65]).

1.3.2 The idea of ekpyrosis

As we have discussed earlier, the advantage of inflation is that the background trajectory is an attractor. Similarly, one can show that the contracting phase dominated by super stiff matter (*i.e.* with $w > 1$) is an attractor (see for instance, Refs. [24, 26]). Such a contracting phase is referred to as the ekpyrotic scenario. The original proposal of the ekpyrotic bounce is based on the braneworld picture of the universe [25]. It is interesting to note that the ekpyrotic phase is driven by a negative potential. During this phase (wherein $w > 1$), the energy density grows faster than the anisotropies and hence this scenario is also free from the anisotropy problem.

However, one finds that ekpyrosis involving a single scalar field produces an adiabatic spectrum with a strong blue tilt that is inconsistent with the observations. Therefore, viable ekpyrotic models that produce the observed fluctuations necessarily have to involve two scalar fields [26]. In these examples, the isocurvature perturbations are scale-invariant on super-Hubble scales. Moreover, the amplitude of isocurvature perturbation can be large compared to the amplitude of the curvature perturbation. After the ekpyrotic phase, the isocurvature perturbations source the curvature perturbations, eventually converting them into a scale-invariant spectrum of adiabatic perturbations [26].

1.3.3 Tensor-to-scalar ratio in bounces

As we have discussed, in the case of the matter bounce scenario, both the tensor and the scalar fluctuations have a similar evolution history during the early contracting phase. This implies the the tensor-to-scalar ratio before the bounce can be calculated from the initial conditions. This ratio can be shown to be of the order of $\mathcal{O}(20)$ which is very large compared to the current upper bounds. Hence, in order to obtain a small tensor-to-scalar ratio after the bounce, the curvature perturbation need to be enhanced during the bounce (in this context, see Refs. [3]). In the case of ekpyrotic contracting phase, the amplitude of the tensor perturbation is very small compared to the curvature perturbation, leading to an insignificant tensor-to-scalar ratio.

1.4 Organization of the thesis

In this section, we shall provide a brief, chapterwise outline of the thesis.

In chapter 2, we shall numerically evaluate the dimensionless non-Gaussianity parameter that characterizes the amplitude of the tensor bispectrum for a class of two-field inflationary models such as double inflation, hybrid inflation and aligned natural inflation. We shall compare the numerical results with the slow roll results which can be obtained analytically. In the context of double inflation, we shall also investigate the effects on the non-Gaussianity parameter due to curved trajectories in the field space.

In chapter 3, we shall construct a model involving two scalar fields that drives a symmetric matter bounce and study the evolution of the scalar and tensor perturbations in the model. We shall evolve the perturbations analytically as well as

numerically across the bounce and evaluate the power spectra after the bounce. We shall show that, for a suitable value of the parameter describing the model, while the scalar and tensor perturbation spectra are scale-invariant over scales of cosmological interest, the tensor-to-scalar ratio proves to be much smaller than the current upper bound from the observations of the CMB anisotropies by the Planck mission.

In chapter 4, we shall extend our earlier model to drive near-matter bounces. With the aid of techniques which we had used in the previous chapter, we shall evaluate the scalar and tensor power spectra arising in the model numerically. We find that the new model involves an additional parameter (apart from the scale associated with the bounce) which determines the tilt of the power spectra. We show that a suitable value for the additional parameter leads to red scalar as well as tensor power spectra and a scalar spectral tilt that is consistent with the observations. The value of the original parameter, which is fixed by the COBE normalized value of the scalar power spectrum, leads to a very small tensor-to-scalar ratio that is consistent with the current upper bound from the observations.

While nearly scale-invariant primordial power spectra are remarkably consistent with the cosmological data, it has often been found that certain features in the power spectra lead to an improved fit to the cosmological data. In inflation, the features in the power spectrum can be generated by allowing for deviations from slow roll. This is possible due to the fact that inflation, typically, is an attractor. This aspect allows slow roll inflation to be restored after brief periods of deviation from it. As we have mentioned earlier, the ekpyrotic trajectory is an attractor in the contracting universe. Utilizing the attractive nature of the background, in chapter 5, we shall study the possibility of generating features in the power spectrum in bouncing scenarios. This aspect can, in principle, strongly discriminate between the inflationary and bouncing scenarios.

In the early universe, the primordial perturbations are generated due to quantum fluctuations and, as the universe evolves, they are expected to be converted to classical stochastic perturbations. While such a quantum-to-classical transition of the perturbations has been studied extensively in the inflationary scenario, the corresponding analysis in bouncing scenarios has been rather limited. In two-field models, the effect of the isocurvature perturbations needs to be accounted for while examining the quantum-to-classical transition of the curvature perturbations. In chapter 6, we shall compare and contrast the quantum-to-classical transition of the curvature perturbation in inflationary and bouncing scenarios driven by two scalar fields.

Chapter 2

Numerical evaluation of the tensor bispectrum in two-field inflation

2.1 Introduction

In the absence of equally effective alternatives, the inflationary paradigm continues to remain the most compelling scenario to describe the origin of perturbations in the primordial universe. Inflation—which refers to a period of accelerated expansion during the early stages of the radiation dominated epoch—was initially proposed to explain cosmological observations such as the extent of homogeneity and spatial flatness of the universe. However, soon after the original proposal, it was realized that apart from helping to overcome the drawbacks of the conventional hot big bang model, the inflationary scenario also provides a causal mechanism for the generation of primordial perturbations. According to the inflationary paradigm, the primordial perturbations are generated due to quantum fluctuations, which are rapidly stretched to cosmological scales due to the accelerated expansion. The perturbations generated during inflation lead to

anisotropies in the CMB, which in turn result in the large scale structure of galaxies and clusters of galaxies that we see around us today (see, for instance, any of the following reviews [2]).

As we have discussed in the previous chapter, typically, the period of accelerated expansion is assumed to be driven by scalar fields. Many models consisting of single and multiple scalar fields have been proposed to achieve inflation. The potentials governing the scalar fields, along with the values of the parameters describing them, determine the dynamics during inflation. It is the quantum fluctuations associated with the scalar fields that are responsible for the primordial perturbations. The background inflationary dynamics determines the characteristics of these perturbations, which are conveniently described in terms of correlation functions. The CMB and other cosmological data point to a nearly scale-invariant primordial scalar power spectrum as is generated by the simplest models of slow roll inflation [8, 66, 67]. However, despite the strong constraints that have emerged, there exist many inflationary models that are consistent with the data at the level of two-point functions. In the case of canonical single field models, there has been a comprehensive comparative analysis of a fairly large set of models with the cosmological data [8, 67]. Clearly, in the long run, it would be desirable to carry out a similar comparison of multi-field models and, more specifically, two-field models with the data (see, for instance, Refs. [68]). As far as the background evolution is concerned, two-field models offer a richer dynamics than the single field models due to the possibility of different types of trajectories in the field space. At the level of perturbations, the existence of isocurvature perturbations in multi-field models can lead to a non-trivial evolution of the curvature perturbation on super-Hubble scales (see, for example, the following articles [9, 10] or reviews [69]).

Over the last decade and a half, it has been recognized that observations

of primordial non-Gaussianities—in particular, the amplitude of three-point functions—can help us arrive at a smaller class of viable inflationary models. This expectation has been corroborated to a large extent by the strong constraints that have been arrived at by the Planck data on the three non-Gaussianity parameters that describe the amplitude of the scalar bispectrum [37]. Theoretically, a good amount of work has been carried out towards calculating the non-Gaussianities generated in single and multi-field inflationary models. But, the theoretical understanding of non-Gaussianities generated in the inflationary models and the observational constraints that have been arrived at have largely focused on the scalar bispectrum and the related non-Gaussianity parameters [34–36].

Other than the scalar bispectrum, there arise three other three-point functions when the tensor perturbations are also taken into account [39]. Often, the three-point functions are calculated analytically in the slow roll approximation. In a generic situation, one has to adopt a numerical approach to evaluate these three-point functions (in this context, see, for instance, Refs. [40–43]). Moreover, while numerical procedures have been developed to evaluate the three-point functions in single field models [40–43], until recently, there has been very little effort towards computing these quantities in multi-field models (see, however, Refs. [44]). Though the recent efforts are indeed more comprehensive and focus on the important case of scalars, the approach adopted in these efforts (the so-called transport method) is different from the method we shall work with. Eventually, we would like to arrive at a numerical procedure to evaluate all the three-point functions in two-field and, in general, multi-field models. In contrast to the scalars, the tensor perturbations are simpler to study as they depend only on the evolution of the scale factor. Therefore, as a first step, in this chapter, we shall compute the tensor bispectrum and the corresponding non-Gaussianity parameter in two-field models of inflation. To check the accuracy of the numerical procedure, we shall first consider simple situations leading to slow roll inflation and com-

pare the numerical results with the analytical results available in such cases. We shall then study the effects of the curved trajectory in the field space on the tensor bispectrum and the corresponding non-Gaussianity parameter. We shall also explicitly examine the validity of the consistency relation governing the three-point function in the squeezed limit and discuss the contributions to tensor non-Gaussianities during the epoch of preheating.

This chapter is organized as follows. In the following section, we shall quickly summarize the equations of motion describing the background dynamics of inflationary scenarios driven by two canonical scalar fields. In section 2.3, we shall present the essential expressions governing the tensor bispectrum arrived at using the Maldacena formalism and introduce the dimensionless non-Gaussianity parameter h_{NL} that characterizes the amplitude of the tensor bispectrum. In section 2.4, we shall discuss the analytical results for the tensor bispectrum and the corresponding non-Gaussianity parameter in the de Sitter limit. In section 2.5, we shall describe the numerical procedure that we adopt to calculate the tensor bispectrum and the non-Gaussianity parameter and then go on to evaluate these quantities in three different two-field models, *viz.* double inflation, hybrid inflation and aligned natural inflation. Moreover, in the case of double inflation, we shall study the imprints of turning trajectories on h_{NL} . In section 2.6, using our numerical techniques, we shall also examine the so-called consistency condition relating the tensor bispectrum to the tensor power spectrum in the squeezed limit, wherein one of the wavenumbers involved is much smaller than the other two. In section 2.7, we shall discuss the effects of preheating on the non-Gaussianity parameter h_{NL} . Lastly, in section 2.8, we shall conclude with a brief summary.

2.2 Background equations

We shall consider the background to be described by the spatially flat FLRW line-element (1.28). We shall study inflationary models consisting of two scalar fields, say, ϕ and χ , that are described by the action

$$\mathcal{S}[\phi_I] = - \int d^4x \sqrt{-g} \left[\frac{1}{2} \sum_{I=1}^2 \partial_\mu \phi_I \partial^\mu \phi_I + V(\phi_I) \right], \quad (2.1)$$

where $\phi_I = \{\phi, \chi\}$ and $V(\phi_I)$ is the potential characterizing the scalar fields. The equations of motion that govern the homogeneous components of these scalar fields are given by

$$\ddot{\phi}_I + 3H \dot{\phi}_I + V_I = 0, \quad (2.2)$$

where $V_I = \partial V / \partial \phi_I$. Recall that, the quantity $H = \dot{a}/a$ denotes the Hubble parameter and its evolution is described by the following Friedmann equation:

$$H^2 = \frac{1}{3 M_{\text{Pl}}^2} \left[\frac{1}{2} \sum_{I=1}^2 \dot{\phi}_I^2 + V(\phi_I) \right]. \quad (2.3)$$

It is useful to introduce here the so-called first slow roll parameter ϵ_1 , which is defined as

$$\epsilon_1 = - \frac{\dot{H}}{H^2}. \quad (2.4)$$

Moreover, one finds that the quantity a''/a that governs the evolution of the tensor Mukhanov-Sasaki variable u_k [cf. equation (1.68)] can be expressed in terms of the slow roll parameter ϵ_1 as

$$\frac{a''}{a} = (aH)^2 (2 - \epsilon_1). \quad (2.5)$$

2.3 The tensor bispectrum and the corresponding non-Gaussianity parameter

As we have mentioned earlier, we shall be focusing on the tensor perturbations in this chapter. When the tensor perturbations are taken into account, the FLRW metric can be expressed as [34]

$$ds^2 = a^2(\eta) \left\{ -d\eta^2 + [e^{\gamma(\eta, \mathbf{x})}]_{ij} dx^i dx^j \right\}, \quad (2.6)$$

where γ_{ij} is a symmetric, transverse and traceless tensor. Note that the line-element (1.48) corresponds to the case wherein the tensor perturbation γ_{ij} are retained only up to the linear order.

The dominant signatures of non-Gaussianities are the three-point functions. The tensor bispectrum, *viz.* the three-point correlation function describing the tensor perturbations, that arises in a given inflationary model can be evaluated using the so-called Maldacena formalism [34]. The formalism involves first deriving the cubic order action governing the perturbations. At the cubic order, upon using the line-element (2.6) the action describing the tensor perturbations can be obtained to be [39]

$$S_3[\gamma_{ij}] = \frac{M_{\text{Pl}}^2}{2} \int d\eta \int d^3\mathbf{x} a^2 \left[\frac{1}{2} \gamma_{lj} \gamma_{im} \partial_l \partial_m \gamma_{ij} - \frac{1}{4} \gamma_{ij} \gamma_{lm} \partial_l \partial_m \gamma_{ij} \right]. \quad (2.7)$$

Given this action, the corresponding three-point function can then be arrived at using the standard techniques of quantum field theory. In this section, we shall gather the essential expressions describing the tensor bispectrum. We shall also define the corresponding dimensionless non-Gaussianity parameter that can be introduced for conveniently characterizing the amplitude of the tensor bispec-

trum, as is popularly done in the scalar case [43].

The tensor bispectrum in Fourier space, *viz.* $\mathcal{B}_{\gamma\gamma\gamma}^{m_1 n_1 m_2 n_2 m_3 n_3}(\mathbf{k}_1, \mathbf{k}_2, \mathbf{k}_3)$, evaluated towards the end of inflation at the conformal time, say, η_e , is defined as

$$\begin{aligned} \langle \hat{\gamma}_{m_1 n_1}^{\mathbf{k}_1}(\eta_e) \hat{\gamma}_{m_2 n_2}^{\mathbf{k}_2}(\eta_e) \hat{\gamma}_{m_3 n_3}^{\mathbf{k}_3}(\eta_e) \rangle \\ = (2\pi)^3 \mathcal{B}_{\gamma\gamma\gamma}^{m_1 n_1 m_2 n_2 m_3 n_3}(\mathbf{k}_1, \mathbf{k}_2, \mathbf{k}_3) \delta^{(3)}(\mathbf{k}_1 + \mathbf{k}_2 + \mathbf{k}_3). \end{aligned} \quad (2.8)$$

It should be mentioned that the delta function on the right hand side implies that the wavevectors \mathbf{k}_1 , \mathbf{k}_2 and \mathbf{k}_3 form the edges of a triangle. For convenience, hereafter, we shall set

$$\mathcal{B}_{\gamma\gamma\gamma}^{m_1 n_1 m_2 n_2 m_3 n_3}(\mathbf{k}_1, \mathbf{k}_2, \mathbf{k}_3) = (2\pi)^{-9/2} G_{\gamma\gamma\gamma}^{m_1 n_1 m_2 n_2 m_3 n_3}(\mathbf{k}_1, \mathbf{k}_2, \mathbf{k}_3). \quad (2.9)$$

The quantity $G_{\gamma\gamma\gamma}^{m_1 n_1 m_2 n_2 m_3 n_3}(\mathbf{k}_1, \mathbf{k}_2, \mathbf{k}_3)$, evaluated in the perturbative vacuum, can be obtained to be (see, for instance, Refs. [34, 43])

$$\begin{aligned} G_{\gamma\gamma\gamma}^{m_1 n_1 m_2 n_2 m_3 n_3}(\mathbf{k}_1, \mathbf{k}_2, \mathbf{k}_3) = & M_{\text{Pl}}^2 \left[\left(\Pi_{m_1 n_1, ij}^{\mathbf{k}_1} \Pi_{m_2 n_2, im}^{\mathbf{k}_2} \Pi_{m_3 n_3, lj}^{\mathbf{k}_3} \right. \right. \\ & - \frac{1}{2} \Pi_{m_1 n_1, ij}^{\mathbf{k}_1} \Pi_{m_2 n_2, ml}^{\mathbf{k}_2} \Pi_{m_3 n_3, ij}^{\mathbf{k}_3} \left. \left. k_{1m} k_{1l} \right. \right. \\ & \left. \left. + \text{five permutations} \right] \right. \\ & \times \left[h_{k_1}(\eta_e) h_{k_2}(\eta_e) h_{k_3}(\eta_e) \mathcal{G}_{\gamma\gamma\gamma}(\mathbf{k}_1, \mathbf{k}_2, \mathbf{k}_3) \right. \\ & \left. + \text{complex conjugate} \right], \end{aligned} \quad (2.10)$$

where the quantity $\Pi_{mn, ij}^{\mathbf{k}}$ is defined in equation (1.70). The tensor modes $h_{\mathbf{k}}$ satisfy the differential equation (1.65), while $\mathcal{G}_{\gamma\gamma\gamma}(\mathbf{k}_1, \mathbf{k}_2, \mathbf{k}_3)$ is described by the integral

$$\mathcal{G}_{\gamma\gamma\gamma}(\mathbf{k}_1, \mathbf{k}_2, \mathbf{k}_3) = -\frac{i}{4} \int_{\eta_i}^{\eta_e} d\eta a^2 h_{k_1}^* h_{k_2}^* h_{k_3}^*, \quad (2.11)$$

with η_i denoting the time when the initial conditions are imposed on the pertur-

bations.

As is well known, in the case of the scalars, a dimensionless non-Gaussianity parameter is often introduced (in fact, a set of three parameters are considered) to roughly characterize the amplitude of the scalar bispectrum. A similar dimensionless quantity can be introduced to describe the tensor bispectrum. It can be defined to be the following dimensionless ratio of the tensor bispectrum and the power spectrum [43]:

$$\begin{aligned}
h_{\text{NL}}(\mathbf{k}_1, \mathbf{k}_2, \mathbf{k}_3) &= - \left(\frac{4}{2\pi^2} \right)^2 [k_1^3 k_2^3 k_3^3 G_{\gamma\gamma\gamma}^{m_1 n_1 m_2 n_2 m_3 n_3}(\mathbf{k}_1, \mathbf{k}_2, \mathbf{k}_3)] \\
&\times [\Pi_{m_1 n_1, m_3 n_3}^{k_1} \Pi_{m_2 n_2, \bar{m}\bar{n}}^{k_2} k_3^3 \mathcal{P}_{\text{T}}(k_1) \mathcal{P}_{\text{T}}(k_2) + \text{five permutations}]^{-1},
\end{aligned} \tag{2.12}$$

where the overbars on the indices imply that they need to be summed over all allowed values. Since we shall be focusing here only on the amplitude of the tensor bispectrum, for simplicity, we shall set the polarization tensor to unity. In such a case, the expression (2.10) for the tensor bispectrum reduces to

$$\begin{aligned}
G_{\gamma\gamma\gamma}(\mathbf{k}_1, \mathbf{k}_2, \mathbf{k}_3) &= M_{\text{Pl}}^2 [h_{k_1}(\eta_e) h_{k_2}(\eta_e) h_{k_3}(\eta_e) \bar{\mathcal{G}}_{\gamma\gamma\gamma}(\mathbf{k}_1, \mathbf{k}_2, \mathbf{k}_3) \\
&+ \text{complex conjugate}],
\end{aligned} \tag{2.13}$$

where the quantity $\bar{\mathcal{G}}_{\gamma\gamma\gamma}(\mathbf{k}_1, \mathbf{k}_2, \mathbf{k}_3)$ is described by the integral

$$\bar{\mathcal{G}}_{\gamma\gamma\gamma}(\mathbf{k}_1, \mathbf{k}_2, \mathbf{k}_3) = -\frac{i}{4} (k_1^2 + k_2^2 + k_3^2) \int_{\eta_i}^{\eta_e} d\eta a^2 h_{k_1}^* h_{k_2}^* h_{k_3}^*. \tag{2.14}$$

Also, if we ignore the factors involving the polarization tensor, the non-Gaussianity parameter h_{NL} simplifies to

$$h_{\text{NL}}(\mathbf{k}_1, \mathbf{k}_2, \mathbf{k}_3) = - \left(\frac{4}{2\pi^2} \right)^2 [k_1^3 k_2^3 k_3^3 G_{\gamma\gamma\gamma}(\mathbf{k}_1, \mathbf{k}_2, \mathbf{k}_3)]$$

$$\times \left[2 k_3^3 \mathcal{P}_T(k_1) \mathcal{P}_T(k_2) + \text{two permutations} \right]^{-1}. \quad (2.15)$$

2.4 The non-Gaussianity parameter h_{NL} in slow roll inflation

Evidently, in order to evaluate the tensor bispectrum, we shall first require the modes h_k . Also, using the modes, we need to be able to evaluate the integral (2.14) and the asymptotic forms of the modes to arrive at the tensor bispectrum and the corresponding non-Gaussianity parameter. In slow roll inflation, one often works in the de Sitter approximation wherein the tensor modes h_k are given by

$$h_k(\eta) = \frac{\sqrt{2} i H_1}{M_{\text{Pl}} \sqrt{2} k^3} (1 + i k \eta) e^{-i k \eta}, \quad (2.16)$$

with H_1 being the constant Hubble parameter in de Sitter inflation. These modes can be easily used to arrive at the following well-known, strictly scale-invariant tensor power spectrum (evaluated towards the end of inflation, *i.e.* as $\eta_e \rightarrow 0$):

$$\mathcal{P}_T(k) = \frac{2 H_1^2}{\pi^2 M_{\text{Pl}}^2}. \quad (2.17)$$

Using the modes (2.16), the integral (2.14) can be evaluated to be

$$\bar{\mathcal{G}}_{\gamma\gamma\gamma}(\mathbf{k}_1, \mathbf{k}_2, \mathbf{k}_3) = -\frac{i H_1 (k_1^2 + k_2^2 + k_3^2)}{4 M_{\text{Pl}}^3 (k_1 k_2 k_3)^{3/2}} \left(k_T - \frac{k_1 k_2 + k_1 k_3 + k_2 k_3}{k_T} - \frac{k_1 k_2 k_3}{k_T^2} \right), \quad (2.18)$$

where $k_T = k_1 + k_2 + k_3$. In the limit $\eta_e \rightarrow 0$, the corresponding tensor bispectrum $G_{\gamma\gamma\gamma}(\mathbf{k}_1, \mathbf{k}_2, \mathbf{k}_3)$ and the non-Gaussianity parameter $h_{\text{NL}}(\mathbf{k}_1, \mathbf{k}_2, \mathbf{k}_3)$ can be

obtained to be

$$G_{\gamma\gamma\gamma}(\mathbf{k}_1, \mathbf{k}_2, \mathbf{k}_3) = -\frac{H_0^4 (k_1^2 + k_2^2 + k_3^2)}{2 M_{\text{Pl}}^4 (k_1 k_2 k_3)^3} \left(k_{\text{T}} - \frac{k_1 k_2 + k_1 k_3 + k_2 k_3}{k_{\text{T}}} - \frac{k_1 k_2 k_3}{k_{\text{T}}^2} \right) \quad (2.19)$$

and

$$h_{\text{NL}}(\mathbf{k}_1, \mathbf{k}_2, \mathbf{k}_3) = \frac{1}{4} \left(\frac{k_1^2 + k_2^2 + k_3^2}{k_1^3 + k_2^3 + k_3^3} \right) \left(k_{\text{T}} - \frac{k_1 k_2 + k_2 k_3 + k_3 k_1}{k_{\text{T}}} - \frac{k_1 k_2 k_3}{k_{\text{T}}^2} \right). \quad (2.20)$$

Note that, in the equilateral limit (*i.e.* when $k_1 = k_2 = k_3$), we have $h_{\text{NL}} = 17/36 \simeq 0.472$, while in the squeezed limit (*i.e.* as $k_1 = k_2$ and $k_3 \rightarrow 0$), we have $h_{\text{NL}} = 3/8 = 0.375$. These analytical results prove to be very handy for examining the accuracy of the numerical procedures that we shall adopt to evaluate the tensor modes, the tensor power spectrum and the tensor bispectrum.

2.5 Numerical evaluation

As we have described before, our aim in this chapter is to numerically evaluate the magnitude and shape of the non-Gaussianity parameter h_{NL} in two-field models of inflation. We shall make use of the analytical results available in the slow roll limit (actually, in the de Sitter limit) to check the accuracy of our numerical results. In this section, we shall first quickly describe the numerical procedure that we shall adopt for the evaluation of the non-Gaussianity parameter h_{NL} . Thereafter, we shall consider three specific inflationary models and evaluate the non-Gaussianity parameter h_{NL} in these models.

Evidently, we shall first require the behavior of the background quantities and the tensor modes. Once these are at hand, the tensor bispectrum (2.13) can be arrived at by computing the integral (2.14) and then using the asymptotic forms

of the tensor modes. These quantities can be utilized to finally obtain the non-Gaussianity parameter h_{NL} .

Our numerical procedure is essentially similar to an earlier work in this context which had dealt with single field models of inflation [43]. Once the parameters in the potential and the initial conditions are specified, one can integrate the equations (2.2) that govern the scalar fields and the Friedmann equation (2.3) to arrive at the evolution of the background quantities. Usually the initial value of the fields are chosen to lead to enough number of e-folds (say, 60-70 e-folds of inflation). Once we have the background quantities, we can solve for the tensor perturbations by integrating the governing equation (1.65), along with the Bunch-Davies initial condition (1.75). In this computation, the initial conditions are imposed on the modes when they are sufficiently inside the Hubble radius [we have chosen when $k/(aH) = 10^2$]. The power spectrum is evaluated in the super-Hubble domain, when the amplitude of the modes have reached a constant value [which typically occur when $k/(aH) \simeq 10^{-5}$].

We solve the background and the perturbation equations as functions of the number of e-folds using the fifth order Runge-Kutta algorithm (see, for instance, Ref. [70]). Since the amplitude of the tensor modes are constant during the super-Hubble evolution, we can neglect the contribution of h_{NL} during this period (for more details, see Ref. [43]). This simplifies the numerical integration involved in the calculation of h_{NL} . Note that the modes oscillate strongly in the sub-Hubble domain, leading to oscillating integrands. In order to handle such integrands, an exponential cut-off is included to regulate the integrals in the sub-Hubble domain, as has been implemented earlier in similar contexts (in this context, see Refs. [40, 41, 43, 71]). Such a cut-off can be justified theoretically as it helps in identifying the correct perturbative vacuum [35, 41]. The integration is carried

out using the Bode's rule¹, from the earliest time η_i when the smallest of the three wavenumbers (k_1, k_2, k_3) is well inside the Hubble radius to the final time η_e when the largest of them is sufficiently outside the Hubble radius.

2.5.1 Double inflation

The simplest of two-field inflationary models is the model which is described by the potential [72]

$$V(\phi, \chi) = \frac{1}{2} m_\phi^2 \phi^2 + \frac{1}{2} m_\chi^2 \chi^2. \quad (2.21)$$

This model is often referred to as double inflation, since it can lead to two different epochs of inflation (characterized by different values of the Hubble parameter) if the parameters m_ϕ and m_χ are very different. Even though this model seems to be ruled out by the current observations, it is instructive to work with this model since it is very simple. As we have mentioned earlier, one of our aims is to study the effects of curved trajectories in field space on h_{NL} and, in this model, it is easy to construct different types of curved trajectories.

For numerical analysis, we shall set $m_\phi = 7.12 \times 10^{-6} M_{\text{Pl}}$, and choose m_χ to be a multiple of m_ϕ . We shall choose the initial value of the fields to be $\phi_i = 14.4 M_{\text{Pl}}$ and $\chi_i = 8.5 M_{\text{Pl}}$. The corresponding initial velocities of the fields are chosen such that the first slow roll parameter ϵ_1 is small. In figure 2.1, we have shown the trajectories of the two scalar fields and the evolution of the slow roll parameter ϵ_1 for three different mass ratios m_χ/m_ϕ . For $m_\chi = m_\phi$, the slow roll parameter ϵ_1 is very small throughout inflation, as one would have naively expected. For $m_\chi = 4 m_\phi$, the trajectory in the field space is characterized by a smooth turn from a χ dominated phase to the $\chi = 0$ valley and inflation continues along this valley. In the case of $m_\chi = 8 m_\phi$, the turn is more sharp and the field reaches

¹We should add that there is some confusion concerning whether it is Bode's or Boole's rule [70].

the $\chi = 0$ valley faster than in the former cases. It is important to note the effect of turning on the evolution of the first slow roll parameter ϵ_1 . When the mass ratio increases, the turns become sharper and the slow roll parameter ϵ_1 changes considerably during the turn.

Let us now turn to understand the behavior of the non-Gaussianity parameter in these situations. Since the case of $m_\chi = m_\phi$ leads to nearly de Sitter inflation, the numerical results for h_{NL} from this case can be compared with the analytical results we had discussed earlier. Evidently, this exercise can help us determine the accuracy of our numerical procedure. In figure 2.2, we have illustrated the density plots of h_{NL} for a triangular configuration of the wavenumbers (k_1, k_2, k_3) evaluated analytically in the case of de Sitter inflation and the numerical results for the double inflation model with equal values for the masses for the two fields. To arrive at the density plots of h_{NL} , we have set $k_1 = 5 \times 10^{-2} \text{ Mpc}^{-1}$, and chosen k_2 and k_3 such that $5 \times 10^{-4} \text{ Mpc}^{-1} < (k_2, k_3) < 5 \times 10^{-2} \text{ Mpc}^{-1}$. Note that the non-Gaussianity parameter h_{NL} has an equilateral shape, *i.e.* its value is the largest in the equilateral limit (wherein $k_1 = k_2 = k_3$). The equilateral shape can be attributed to the fact that the non-Gaussianities are essentially generated as the modes leave the Hubble radius and the contributions on the super-Hubble scales are insignificant. This figure clearly illustrates that the numerical and the analytical results match quite well. In fact, we find that the maximum difference between them is less than 2%.

Our next task is to study the effect of the turning of the trajectory in the field space on h_{NL} , and we shall utilize the cases wherein $m_\chi = 4m_\phi$ and $m_\chi = 8m_\phi$ for this purpose. We should mention that, in these cases, the scales of our interest leave the Hubble radius between the e-folds of 16 and 33, and the direction of the trajectory changes exactly in this domain. The change in the trajectory in the field space leads to a deviation from slow roll, as is evident from figure 2.1. This effects the

tensor modes and the associated non-Gaussianities. In figure 2.3, we have plotted the non-Gaussianity parameter h_{NL} that arises in these two cases. While the deviation from slow roll inflation clearly modifies the amplitude of the parameter h_{NL} , the broad equilateral shape is indeed retained. The departure from slow roll boosts the amplitude of h_{NL} to a slight extent from the slow roll values. As we had mentioned, we have considered the double inflation model because of its simplicity. In figure. 2.6, we have plotted the scalar (*i.e.* the adiabatic) and the tensor power spectra that arise in these cases. Even the simpler case of $m_\phi = m_\chi$ will not be favored by the CMB data because of the large tensor-to-scalar ratio that the model leads to. (Recall that, the upper bound on the tensor-to-scalar ratio is $r \lesssim 0.07$, according to the recent Planck data [7].) The other two cases lead to a broad step-like feature in the power spectra. They also result in higher scalar power on large scales and a large tensor-to-scalar ratio. Due to these reasons, these cases are ruled out by the data as well.

In what follows, we shall discuss two more models, *viz.* hybrid inflation and aligned natural inflation. As we shall see, in these models, for the values of the parameters that we work with, the first slow roll parameter evolves smoothly and also remains very small during inflation. As a result, the non-Gaussianity parameter h_{NL} in these models does not differ much from the case of de Sitter inflation.

2.5.2 Hybrid inflation

In most of the models, inflation ends when the scalar field approaches the minimum of the potential. The hybrid model of inflation had been introduced as an alternative way of ending inflation [58,73]. In this model, inflation does not end because the field reaches a minimum, but due to a phase transition which occurs

at a critical point of one of the fields. This model is based on the potential

$$V(\phi, \chi) = \frac{1}{2} m^2 \phi^2 + \frac{\lambda}{4} (\chi^2 - M^2)^2 + \frac{\lambda'}{2} \phi^2 \chi^2, \quad (2.22)$$

where λ and λ' are two positive coupling constants, while m and M represent two mass parameters. One finds that, in this model, a wide variety of trajectories are possible for different initial conditions [74]. When confined to domains of sub-Planckian values for the fields, the initial values which lead to sufficient amount of e-folds are found to be near the $\chi = 0$ valley and as random points in the space of the scalar fields. But, it is observed that the initial conditions which give sufficiently long inflation can be always found in the region of super-Planckian values of the fields [75].

In our analysis, we shall set $m = 2.63 \times 10^{-12} M_{\text{Pl}}$, $M = 4.14 \times 10^{-14} M_{\text{Pl}}$ and $\lambda = \lambda' = 2.75 \times 10^{-13}$. The scalar fields start from the initial values $\phi_i = 10.02 M_{\text{Pl}}$ and $\chi_i = 21.05 M_{\text{Pl}}$. The behavior of the slow roll parameter ϵ_1 in this model is plotted in figure. 2.4, and the resulting tensor bispectrum is plotted in figure. 2.5.

2.5.3 Aligned natural inflation

The next model we shall study is the natural inflation model with a strong alignment [59,76]. The model is described by the potential

$$V(\phi, \chi) = \Lambda^4 \left[1 - \frac{1}{1 + \beta} \cos(c_1 \alpha \phi + c_2 \chi) - \frac{\beta}{1 + \beta} \cos(c_3 \alpha \phi + c_4 \chi) \right]. \quad (2.23)$$

This model also admits different types of trajectories. But, for the values of the parameters $\Lambda = 1.76 \times 10^{-10} M_{\text{Pl}}$, $c_1 = 8.20 M_{\text{Pl}}^{-1}$, $c_2 = 12.12 M_{\text{Pl}}^{-1}$, $c_3 = 8.80 M_{\text{Pl}}^{-1}$, $c_4 = 27.27 M_{\text{Pl}}^{-1}$, $\alpha = 0.01$ and $\beta = 0.41$, the initial conditions $\phi_i = 24.2 M_{\text{Pl}}$ and $\chi_i = -0.1 M_{\text{Pl}}$ lead to a special kind of trajectory in which inflation ends due to

the instability in the direction of the heavy field. This trajectory is interesting due to the fact that it leads to a suppressed value for the tensor-to-scalar ratio. The first slow roll parameter is very small throughout inflation and it undergoes an extremely sharp change in its value to end inflation (*cf.* figure 2.4). We shall make use of this trajectory for evaluating h_{NL} .

From figure 2.4, it is clear that in both the models (*i.e.* the hybrid inflation model and the aligned natural inflation model), the slow roll parameter ϵ_1 remains very small throughout inflation. So, we do not expect much change in the value of h_{NL} from the case of de Sitter inflation and this expectation is confirmed by figure 2.5. For the sake of completeness we have included the plots of the scalar and tensor power spectra that arise in these models in figure 2.6. For the values of the parameters we have worked with, the hybrid inflation model seems to lead to a rather high tensor-to-scalar ratio, and hence it is likely to be ruled out by the data. In contrast, as we had mentioned, the aligned natural inflation model results in a considerably suppressed tensor-to-scalar ratio and, therefore, it can be expected to be consistent with the data.

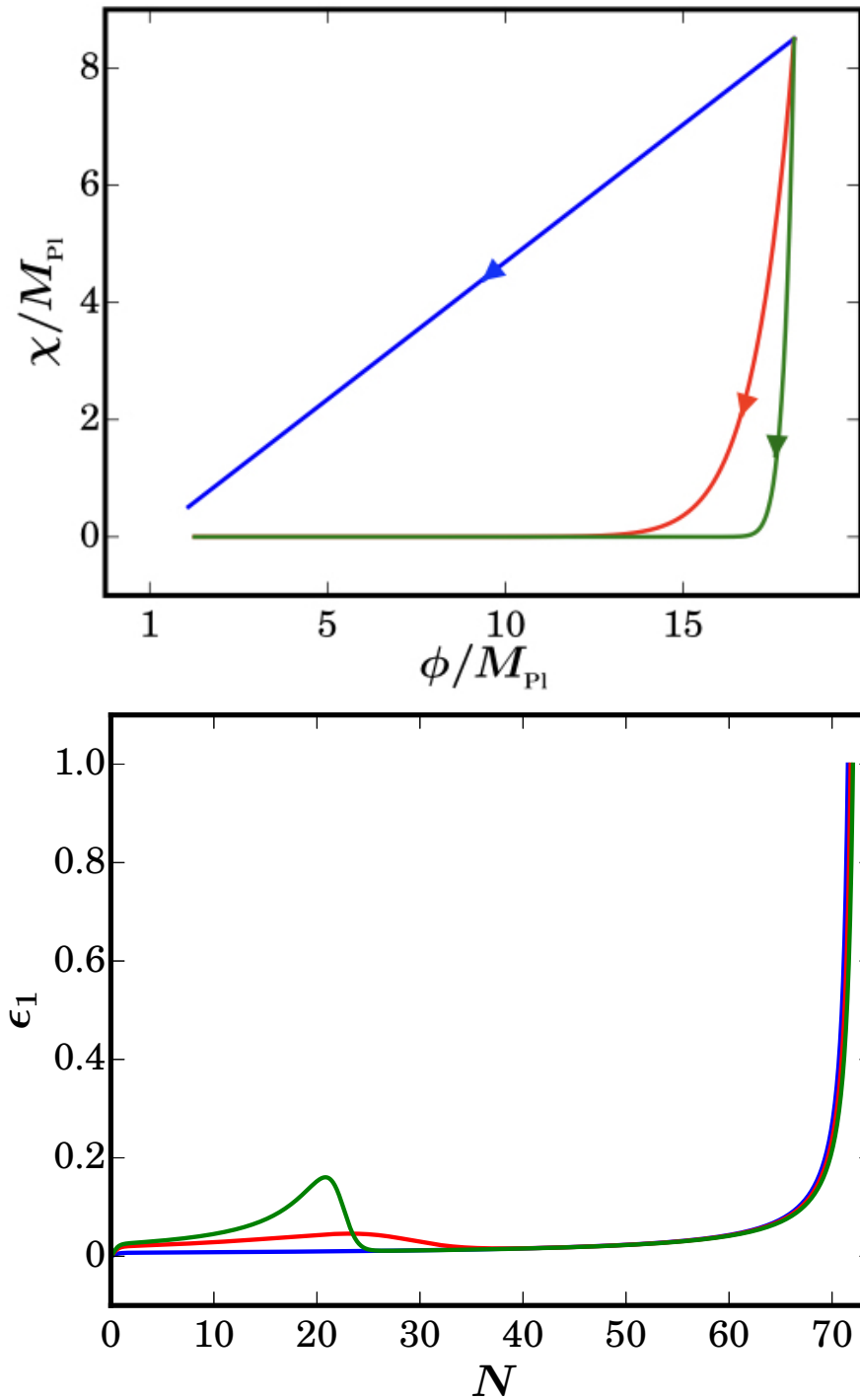


Figure 2.1: The trajectories of the fields ϕ and χ in the field space have been plotted (on top) in the case of double inflation for different mass ratios $m_\chi = m_\phi$ (in blue), $m_\chi = 4m_\phi$ (in red) and $m_\chi = 8m_\phi$ (in green). The corresponding evolution of first slow roll parameter ϵ_1 has been plotted as a function of the number of e-folds N (at the bottom) with the same choices of colors for the different cases (as in the figure on the top).

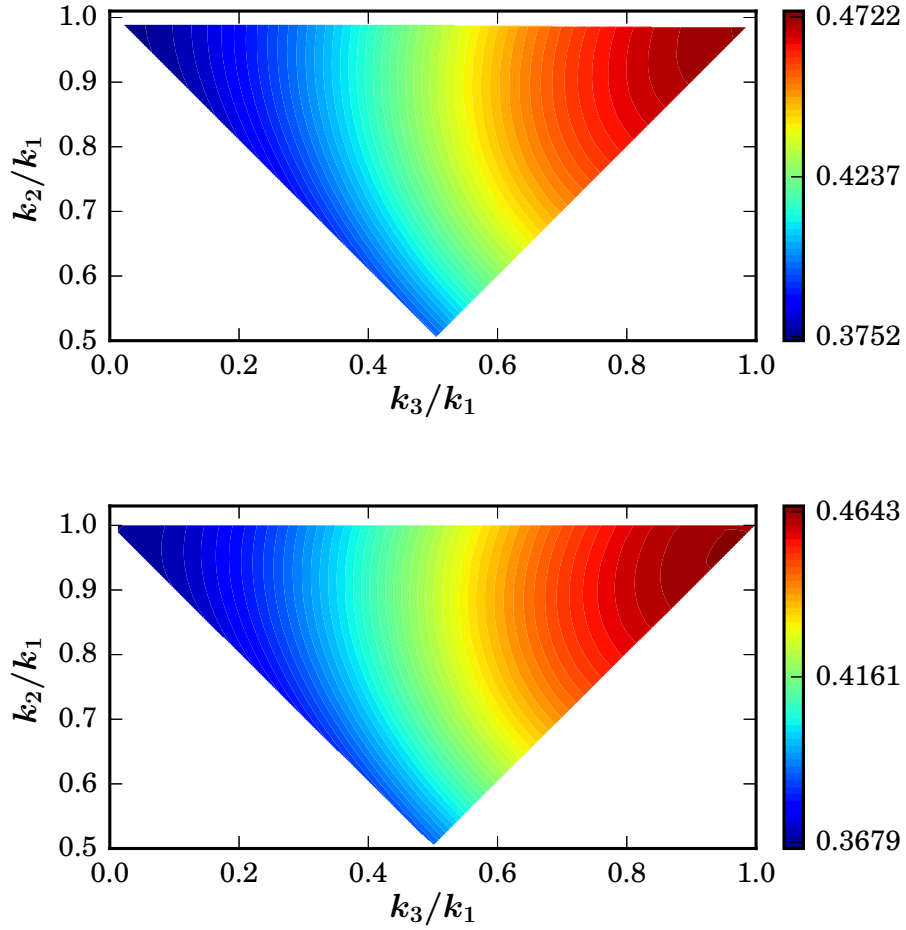


Figure 2.2: Density plots of h_{NL} for an arbitrary triangular configuration of the wavenumbers evaluated analytically in the case of de Sitter inflation (on top) and obtained numerically for double inflation with $m_\chi = m_\phi$ (at the bottom). It is evident that the analytical and the numerical results match quite well, indicating the accuracy of the numerical procedures that have been adopted.

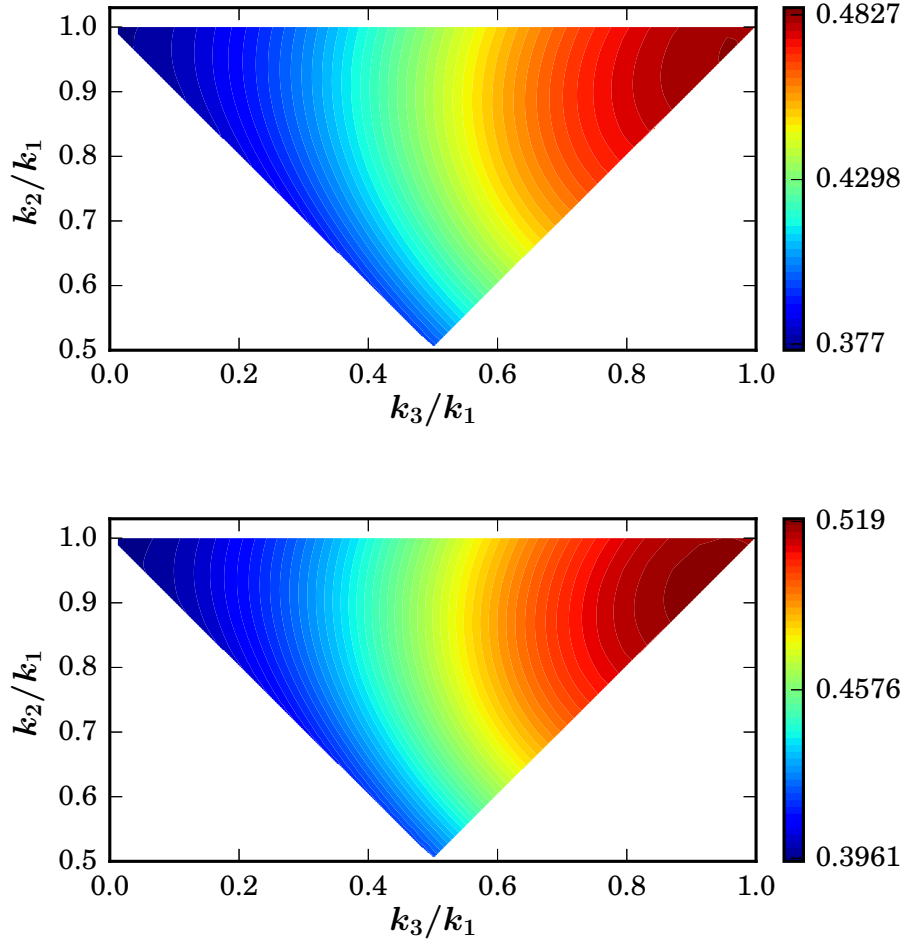


Figure 2.3: Density plots of h_{NL} computed numerically for an arbitrary triangular configuration of the wavenumbers for the case of double inflation with $m_\chi = 4 m_\phi$ (on top) and $m_\chi = 8 m_\phi$ (at the bottom). Note that, in these cases, the departure from slow roll arises due to the turn in the trajectory in the field space. This deviation from slow roll enhances the amplitude of the non-Gaussianity parameter h_{NL} to some extent from the slow roll values.

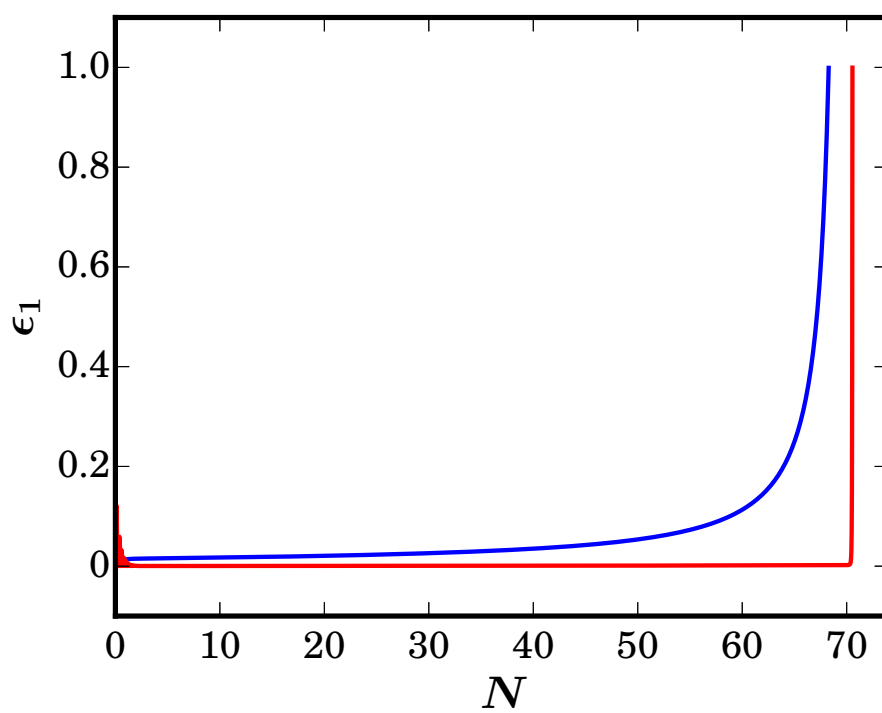


Figure 2.4: The evolution of first slow roll parameter ϵ_1 in the the case of hybrid inflation (in blue) and aligned natural inflation (in red).

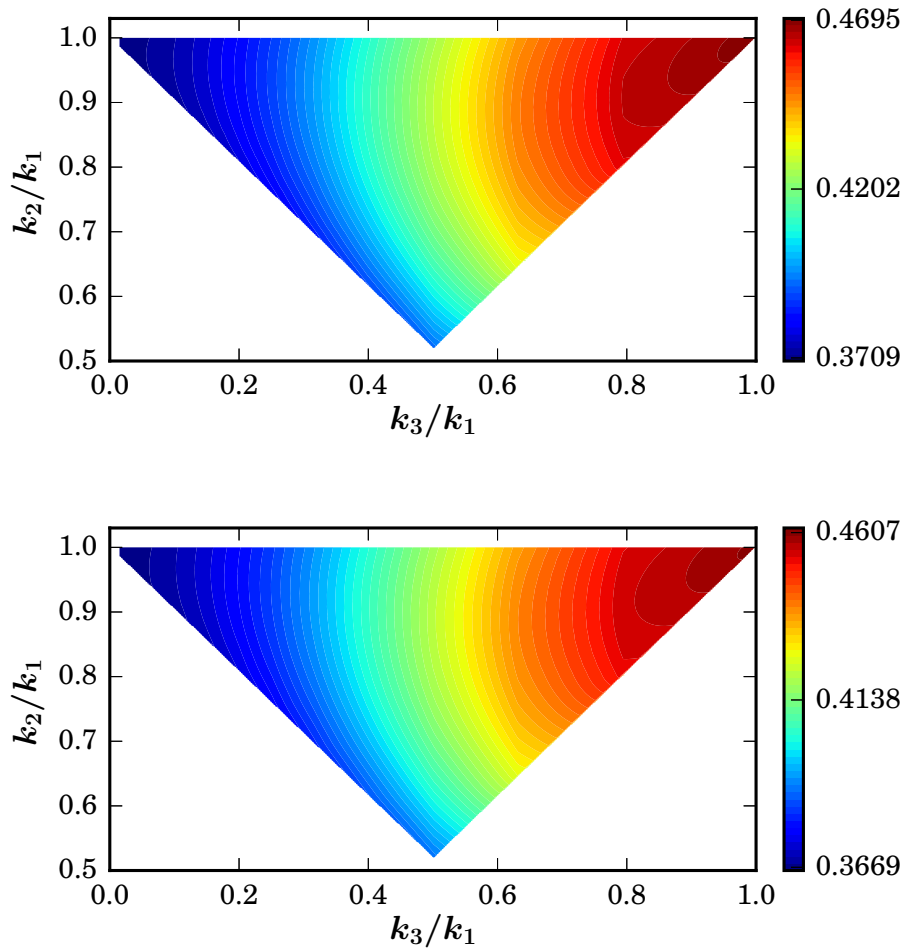


Figure 2.5: Density plots of the non-Gaussianity parameter h_{NL} evaluated numerically for an arbitrary triangular configuration of the wavenumbers for the case of hybrid inflation (on top) and aligned natural inflation (at the bottom).

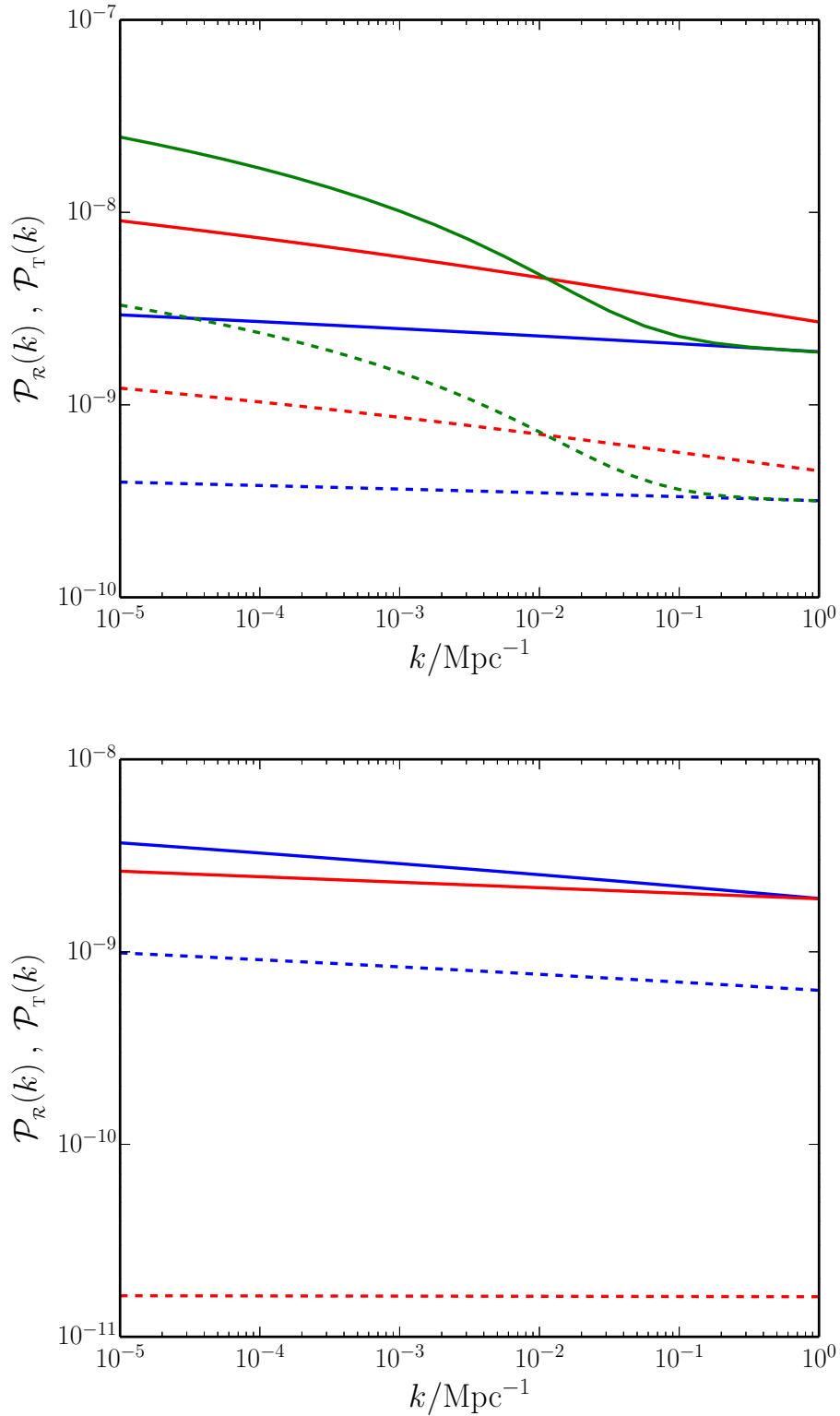


Figure 2.6: The scalar, *i.e.* adiabatic (solid line), and the tensor (dashed line) power spectra have been plotted (on top) for the double inflation model with $m_\chi = m_\phi$ (in blue), $m_\chi = 4 m_\phi$ (in red) and $m_\chi = 8 m_\phi$ (in green). The power spectra (with same choice of lines) have also been plotted (at the bottom) for the cases of the hybrid inflation (in blue) and the aligned natural inflation (in red) models.

2.6 Consistency relation in the squeezed limit

It is well known that the amplitude of the tensor perturbations freeze on super-Hubble scales. Due to this reason, if one considers the long wavelength limit of one of the wavenumbers (often referred to as the squeezed limit), it can be shown that the tensor bispectrum can be completely expressed in terms of the tensor power spectrum. Specifically, if we choose $k_3 \rightarrow 0$ so that $k_2 \simeq k_3 = k$, one finds that the non-Gaussianity parameter h_{NL} can be expressed as follows [71]:

$$\lim_{k_3 \rightarrow 0} h_{\text{NL}}(\mathbf{k}, -\mathbf{k}, \mathbf{k}_3) = \frac{1}{8} [n_{\text{T}}(k) - 3], \quad (2.24)$$

where n_{T} is the tensor spectral index defined as in equation (1.72). Since we have been able to evaluate the non-Gaussianity parameter h_{NL} (and the spectral index n_{T}) for an arbitrary triangular configuration of the wavenumbers, it is interesting to examine if the above consistency is indeed satisfied in the models we have considered. In figure 2.7, we have plotted these two quantities for the double inflation model with $m_{\chi} = 8 m_{\phi}$, which leads to the maximum possible deviation from slow roll. We find that the maximum difference between these quantities evaluated numerically is about 1.2%, which clearly supports the validity of the consistency relation even in situations involving departures from slow roll.

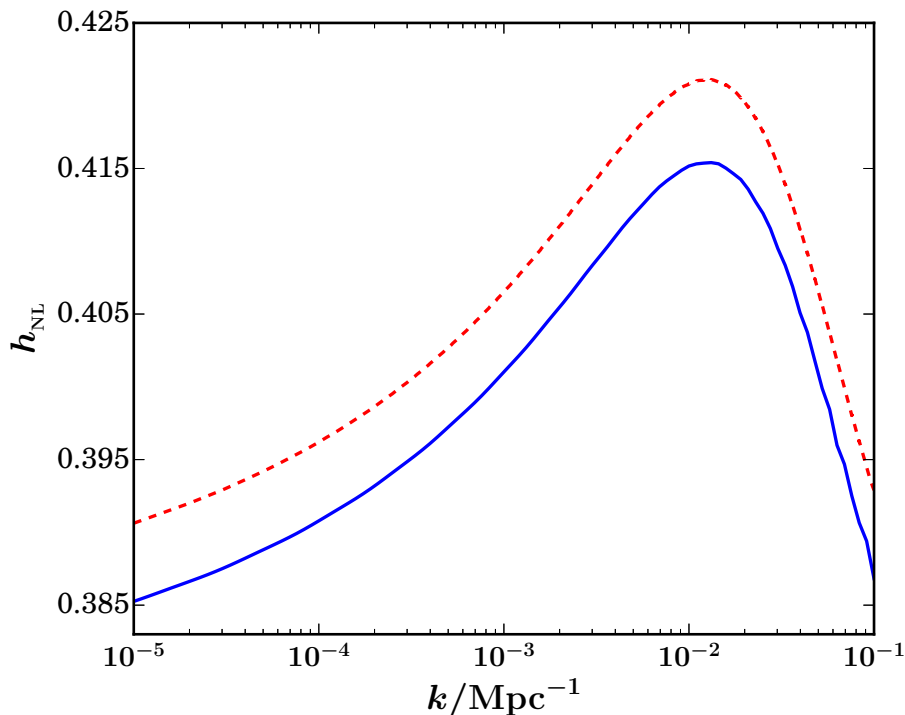


Figure 2.7: The non-Gaussianity parameter h_{NL} evaluated numerically in the squeezed limit (the solid line) and the quantity $(n_{\text{T}} - 3)/8$ obtained from the tensor power spectrum (the dashed line) have been plotted in the case of the double inflation model wherein $m_{\chi} = 8m_{\phi}$. The maximum difference between these quantities is about 1.2% and the difference can be attributed to the level of numerical accuracy that one has worked with. This suggests that the consistency relation is valid even away from slow roll.

2.7 The contribution during preheating

In models such as double inflation, the scalar field rolls down the potential and inflation is terminated when the field is close to the minimum of the potential. After inflation has ended, the scalar field oscillates about the minimum of the potential, a phase which is referred to as preheating. Note that all perturbations of cosmological interest are on super-Hubble scales during the domain of preheating. Due to this reason, the oscillations in the scalar field are not expected to affect the evolution of the amplitude of h_k , which remain constant as in the super-Hubble domain during inflation. We have evolved the tensor perturbations numerically through the epoch of preheating. In figure. 2.8, we have plotted the

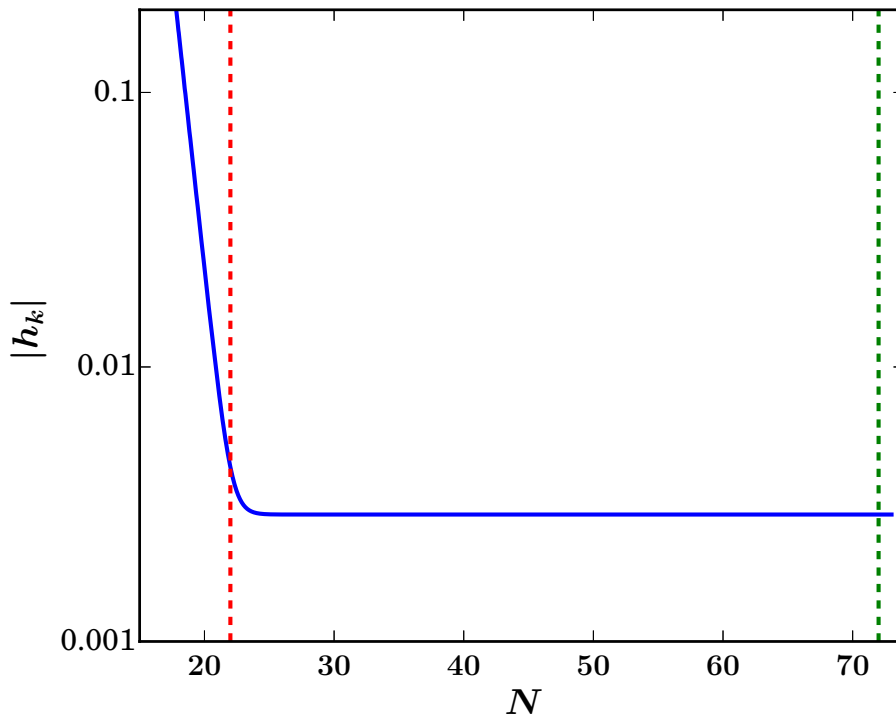


Figure 2.8: Evolution of the absolute value of h_k for $k = 0.05 \text{ Mpc}^{-1}$ during the epochs of inflation and reheating in the case of the double inflation model with $m_\chi = 8 m_\phi$. The vertical lines indicate the time when the mode leaves the Hubble radius during inflation (in red) and the end of inflation (in green), respectively.

evolution of the amplitude of h_k (for a specific mode) in the case of the double inflation model during the epochs of inflation and preheating. Clearly, the figure corroborates the expectation that the amplitude of h_k is constant at suitably late times. Since the amplitude of the tensor modes is constant, the contribution to the non-Gaussianity parameter h_{NL} due to this epoch is identically zero [43].

2.8 Discussion

As we have stressed earlier, primordial non-Gaussianities are expected to provide crucial information to help us arrive at stronger constraints on the physics of the early universe. Apart from the very recent efforts, there has been little work towards the numerical evaluation of non-Gaussianities in multi-field models of

inflation. As a preliminary step, in this chapter, we have evaluated the tensor bispectrum in two-field models of inflation [77]. We have been able to compare the numerical results with the analytical results available in the case of slow roll inflation. This comparison suggests that the numerical procedure we have adopted is quite accurate. The two-field models are interesting because of the curved trajectories that can be generated in the field space in a rather simple manner. One of our aims was to identify the effect of such a turn in the trajectory on the magnitude and the shape of h_{NL} . In double inflation, we have found that the change in the direction of the trajectory produces a bump in the first slow roll parameter, which increases the amplitude of h_{NL} over a certain domain. We have also studied the behavior of h_{NL} in the case of hybrid inflation and aligned natural inflation. Lastly, we have shown that the contribution to h_{NL} due to the epoch of preheating can be completely neglected, due to the constant amplitude of the tensor modes during this period.

Evaluating the tensor bispectrum has proved to be simpler since the evolution of the tensor modes depend only on the behavior of the scale factor. Moreover, the fact the tensor modes freeze on super-Hubble scales makes the computation easier. We are presently extending our code to evaluate the other three-point functions in two-field models. In the case of the three-point functions involving scalars, the presence of isocurvature perturbations provides a challenge, as they can lead to non-trivial evolution of the curvature perturbation on super-Hubble scales. We are currently working on this issue.

Chapter 3

Viable tensor-to-scalar ratio in a symmetric matter bounce

3.1 Introduction

Bouncing models refer to scenarios wherein the universe undergoes a period of contraction until the scale factor attains a minimum value, whereupon it transits to the more standard phase of expansion. As we have discussed in the introductory chapter, such scenarios provide an alternative to the inflationary framework as they can also aid in overcoming the horizon problem associated with the conventional hot big bang model, in a fashion similar to inflation. Importantly, certain bouncing scenarios are also known to lead to nearly scale-invariant spectra of primordial perturbations (see, for instance, the reviews [3,27,78–80]), as required by the cosmological data. It is generally expected that quantum gravitational effects will have a substantial influence on the dynamics of the very early universe, close to the big bang. In this chapter, we shall consider *classical bounces*, which correspond to situations wherein the background energy density and pressure

remain sufficiently lower than the Planckian energy density, even as the universe evolves across the bounce. This enables us to carry out our analysis without having to take into account possible Planck scale effects, which may otherwise play a significant role near the bounce.

Though there may be differences of opinion about the theoretical motivations for specific models, it has to be acknowledged that, as a broad paradigm, inflation has been a tremendous success (see, for example, the following reviews [2]). However, the remarkable effectiveness of the inflationary paradigm also seems to be responsible for its major drawback. Despite the strong observational constraints that have emerged, we still seem far from the desirable goal of arriving at a reasonably small subset of viable inflationary models (for a comprehensive list of single field models and their performance against the cosmological data, see Refs. [8, 67]). Moreover, it is not clear whether the paradigm can be falsified at all (in this context, see Ref. [62])! In sharp contrast, bouncing models have been plagued by various difficulties and constructing a model that is free of pathologies, while being consistent with the observations, seems to pose considerable challenges. At this stage, we believe it is important that we highlight some of the generic issues. Firstly, in a universe which is undergoing accelerated expansion, any classical perturbations that are originally present in the sub-Hubble regime will quickly decay. But, such perturbations will rapidly grow during the contracting phase as one approaches the bounce. This behavior raises the concern if a smooth and homogeneous background that is required as an initial condition at suitably early times is sufficiently probable. It can also bring into question the validity of linear perturbation theory in the proximity of the bounce [3, 81–83]. However, it has been shown that, for a large class of bouncing scenarios, one can work in a specific, well-defined gauge wherein linear perturbation theory is valid near the bounce (in this context, see Refs. [81, 82]). Secondly, small anisotropies are known to grow during the contracting phase, which may lead to the so-called

Belinsky-Khalatnikov-Lifshitz instability [63]. While the above two issues can be alleviated to some extent in specific models such as the ekpyrotic scenario (see, for example, Refs. [25, 26]), generically, they could be overcome only by careful fine tuning of the initial conditions (for a recent discussion on this point, see Ref. [24]). Thirdly, certain gauge invariant quantities are bound to diverge in the vicinity of the bounce (when the NEC is initially violated and later restored) which may pose fundamental difficulties in evolving the perturbations across the bounce. However, as we shall discuss in due course, this difficulty can be circumvented by working in a suitable gauge and evolving the perturbations in that particular gauge (in this context, see, for example, Ref. [12]). Fourthly, vector perturbations, if present, can grow rapidly in a contracting universe [3, 82]. But, this issue can be overcome if one assumes that there are no vector sources at early times. In spite of such issues, bouncing models have attracted a lot of attention in the literature over the last two decades (for an intrinsically incomplete list of efforts in this direction, see Refs. [3, 12, 14, 15, 17, 24–26, 46, 84–96]). These efforts suggest that bouncing scenarios can be regarded as the most popular alternative to the inflationary paradigm. In this chapter, we shall consider a specific model leading to a completely symmetric matter bounce and investigate, both numerically and analytically, the evolution of scalar perturbations in this scenario.

A matter bounce corresponds to a certain class of bouncing scenarios wherein, during the early stages of the contracting phase, the scale factor behaves as in a matter dominated universe. Such models are known to be ‘dual’ to de Sitter inflation, and hence are expected to lead to scale-invariant spectra of primordial perturbations [64, 97]. Before we go on to discuss about the specific model that we shall consider, let us make a few summarizing remarks regarding the existing matter bounce models. One of the primary problems concerning symmetric matter bounce scenarios seems to be the fact that in many of these models [3, 12, 79, 87, 94], the tensor-to-scalar ratio r turns out to be far in excess of the

current upper bound of $r \lesssim 0.07$ from the Planck mission [7]. One possible way of circumventing this difficulty seems to be to model the regular component as a perfect fluid. In particular, a suitably small speed of sound for the scalar perturbations ensures that the tensor-to-scalar ratio r is small enough to be consistent with the data [98]. Due to the small speed of sound, the scalar perturbations leave the Hubble radius at earlier times (when compared with the tensor perturbations) providing them with more time for their amplitude to grow as the bounce is approached. It has been also been shown that, by making a judicious choice of the initial conditions, a small tensor-to-scalar ratio can be obtained in asymmetric bounces [12]. Within the context of Einsteinian gravity, it is well known that the NEC has to be violated in order to obtain a bounce. Moreover, since the Hubble parameter changes sign at the bounce, the total background energy density vanishes at the bounce. The simplest way to drive such a background would be to introduce a ghost field which carries a negative energy density (see, for instance, Refs. [12, 86]). However, there are certain issues associated with ghost fields, mostly pertaining to the absence of a stable quantum vacuum [99]. The so-called ghost-condensate mechanism has been introduced as an improvement upon the typical ghost fields because the perturbative ghost instability can be avoided in this situation (see, for example, Refs. [15, 88]). Nevertheless, it has been shown that it is impossible to embed the ghost condensate Lagrangian into an ultraviolet complete theory [100]. In the matter bounce curvaton scenario [89], which also contains a ghost field in addition to a much lighter second field, the tensor-to-scalar ratio has been shown to be suppressed by ‘kinetic amplification’. Another alternative would be to use the Galileon Lagrangian [15, 17, 90], wherein the gradient instability, which may otherwise lead to an exponential growth of the comoving curvature perturbation, can be avoided. Moreover, these models also permit us to circumvent the instabilities associated with ghosts. In certain single field models which lead to a non-singular bounce, it has been argued that

the scalar perturbations are amplified more during the bounce relative to the tensor perturbations, which may lead to a viable value of r [91,95].

Therefore, the challenge seems to be to construct a *completely* symmetric matter bounce scenario wherein the tensor-to-scalar ratio is small enough to be in agreement with the observations. In an earlier work, we had studied the behavior of the tensor perturbations in a matter bounce scenario described by a specific form of the scale factor and had gone on to evaluate the tensor power spectrum and bispectrum in the model [101]. The most dominant of the primordial perturbations are, of course, the scalar perturbations. While the tensor perturbations are completely determined by the behavior of the scale factor, as is well known, the evolution of the scalar perturbations strongly depends on the nature of the source driving the background. In this chapter, assuming Einsteinian gravity, we shall construct a model that leads to the specific form of the scale factor for which we had previously obtained a scale-invariant spectrum of tensor perturbations. As we shall see, the scale factor of our interest can be driven with the aid of two scalar fields, one of which is a canonical field described by a potential, whereas the other is a purely kinetic ghost field with a negative energy density. We shall show that it is possible to construct exact analytical solutions for the background dynamics of our model. Utilizing the analytical solutions for the background and, working in a specific gauge, we shall numerically evolve the perturbations across the bounce and evaluate the power spectrum of the scalar perturbations after the bounce. Interestingly, we find that the amplitude of the scale-invariant scalar and tensor perturbation spectra (over cosmological scales) are dependent on only one parameter, *viz.* the scale associated with the bounce. Further, we shall illustrate that the tensor-to-scalar ratio is completely independent of even this parameter, and it is in agreement with the constraints from Planck. Lastly, we should mention that, we shall also present analytical arguments to support our numerical results.

This chapter is organized as follows. In the following section, we shall quickly introduce the scale factor characterizing the bouncing scenario of our interest and stress a few basic points. In section 4.3, to illustrate some aspects, we shall revisit the behavior of the tensor perturbations and the evaluation of the tensor power spectrum in the scenario. In section 3.4, we shall construct the source for the bouncing scenario of our interest using two scalar fields. In section 3.5, we shall first arrive at the equations of motion governing the scalar perturbations in a generic gauge. Thereafter, we shall obtain the reduced equations in a specific gauge wherein the perturbations behave well in the vicinity of the bounce. In section 3.6, we shall evolve the scalar perturbations numerically across the bounce. In section 3.7, we shall construct analytical solutions to the equations governing the perturbations under certain approximations and we shall show that the analytical arguments support our numerical results. In section 3.8, we shall evaluate the scalar power spectrum and the tensor-to-scalar ratio after the bounce, both numerically as well as analytically, and illustrate that the resulting spectra are broadly in agreement with the constraints from the Planck data. We shall conclude in section 4.6 with a summary and a brief outlook.

Apart from the cosmic and conformal time coordinates, in this chapter, we shall also work with a new time variable that we have introduced in an earlier work on bouncing scenarios, *viz.* e-N-folds, which we shall denote as \mathcal{N} [101, 102].

3.2 The scale factor describing the matter bounce

In this chapter, we shall consider the background to be the spatially flat FLRW metric that is described by the line-element (1.28). We shall assume that the scale

factor describing the bounce is given in terms of the conformal time as follows:

$$a(\eta) = a_0 (1 + \eta^2/\eta_0^2) = a_0 (1 + k_0^2 \eta^2), \quad (3.1)$$

where a_0 is the value of the scale factor at the bounce (*i.e.* at $\eta = 0$) and $k_0 = 1/\eta_0$ is the scale associated with the bounce. At very early times, *viz.* when $\eta \ll -\eta_0$, the scale factor behaves as $a \propto \eta^2$, which is the behavior in a matter dominated universe. It is for this reason that the above scale factor corresponds to a matter bounce scenario. In the absence of any other scale in the problem, it seems natural to assume that the quantity k_0 is related to the Planck scale. As we shall see later, the source driving the scale factor of our interest as well as the results we obtain depend only on the ratio k_0/a_0 . Specifically, it is the dimensionless ratio $k_0/(a_0 M_{\text{Pl}})$ that shall determine the amplitude of the power spectra. We find that the scales of cosmological interest are about 20-30 orders of magnitude smaller than the wavenumber k_0 (in this context, see Ref. [101]).

Let us now highlight a few points concerning the above scale factor and the nature of the sources that are expected to drive the bounce. To begin with, the scale factor is completely symmetric about the bounce. Also, since the Hubble parameter $H = a'/a^2$ vanishes at the bounce, so does the total energy density, *i.e.* $\rho = 3 H^2 M_{\text{Pl}}^2$, of the sources driving the scale factor. It is straightforward to show that the energy density ρ too is symmetric about the bounce. The energy density initially increases on either side as one moves away from the bounce, reaches the maximum value $\rho_{\text{max}} = 3^4 M_{\text{Pl}}^2 k_0^2/(4^3 a_0^2)$ at $\eta = \pm\eta_*$, where $\eta_* = \eta_0/\sqrt{3}$, and decreases thereafter. Note that ρ_{max} depends only on the combination k_0/a_0 . The fact that k_0/a_0 is the only parameter in the problem will become more evident when we attempt to model the sources that drive the bounce. If we assume $k_0/(a_0 M_{\text{Pl}})$ to be, say, of the order of 10^{-5} or so, then, clearly, the energy density ρ will always remain much smaller than the Planckian density. It is for

this reason that we are able to treat the bounce as completely classical. Interestingly, in the domain $-\eta_* < \eta < \eta_*$, wherein the energy density decreases as one approaches bounce, one finds that $\dot{H} > 0$. Since $\dot{H} = -(\rho + p)/(2 M_{\text{pl}}^2)$, where p is the total pressure, $(\rho + p) < 0$ during this period. In other words, the NEC is violated over this domain. It should be clarified that, while $\eta_* \simeq 1/k_0$, the duration of the bounce in terms of the in terms of cosmic time is actually of the order of a_0/k_0 .

It can be easily shown that the above scale factor can be driven by two fluids, one which is ordinary, pressureless matter and another which behaves exactly as radiation, albeit with a negative energy density [14,103]. In fact, it is this negative energy density (and the associated negative pressure) that leads to the violation of the NEC near the bounce and also ensures that the total energy density of the two fluids vanishes at the bounce. In due course, we shall model these two fluids in terms of scalar fields. We shall achieve the violation of the NEC with the aid of a ghost field. It ought to be stressed here that, in Einsteinian gravity that are working with, it is impossible to achieve bounces in a spatially flat FLRW universe without violating the NEC.

3.3 The evolution of tensor perturbations and the tensor power spectrum

In this section, we shall revisit the evolution of the tensor perturbations and the evaluation of the corresponding power spectrum in the matter bounce scenario of our interest, which we have discussed in an earlier work [101]. We shall study the evolution of the perturbations analytically as well as numerically. This exercise permits us to introduce the concept of e-N-folds and also highlight a few points

concerning the evolution of perturbations in bouncing scenarios. Later, we shall adopt similar methods to obtain analytical solutions for the scalar perturbations. As we have emphasized earlier, the tensor perturbations are simpler to study because of the fact that the equation governing their evolution depends only on the scale factor.

3.3.1 Analytical evaluation of the tensor perturbations

Let us first discuss the analytical evaluation of the tensor modes and the tensor power spectrum.

Recall that, when the tensor perturbations characterized by γ_{ij} are taken into account, the spatially flat FLRW metric can be expressed as in equation (1.48). The Fourier modes h_k corresponding to the tensor perturbations are governed by the differential equation (1.65). Often, it proves to be convenient to introduce the so-called Mukhanov-Sasaki variable u_k , defined through the relation $h_k = \sqrt{2} u_k / (M_{\text{Pl}} a)$, which satisfies the differential equation (1.68). In the context of inflation, one imposes the standard Bunch-Davies initial condition on the modes when they are well inside the Hubble radius. As we shall have discussed in the introductory chapter, in bouncing scenarios, such a condition can be imposed at sufficiently early times during the contracting phase. Also recall that the tensor power spectrum, evaluated at a suitably late time, say, η_e , is defined in equation (1.71). As is common knowledge, in the inflationary scenario, the power spectra are evaluated on super-Hubble scales. In bouncing models, the spectra are typically evaluated some time after the bounce, when the universe is expected to make a transition to the conventional radiation dominated epoch.

From the expression (3.1) for the scale factor, we obtain that

$$\frac{a''}{a} = \frac{2 k_0^2}{1 + k_0^2 \eta^2}. \quad (3.2)$$

Clearly, the quantity a''/a exhibits a maximum at the bounce, with the maximum value being of the order of k_0^2 , and it vanishes as $\eta \rightarrow \pm\infty$. For modes of cosmological interest such that $k \ll k_0$, we find that $k^2 \gg a''/a$ as $\eta \rightarrow -\infty$, *i.e.* at very early times. This behavior permits us to impose the standard Bunch-Davies initial condition on the modes u_k at early times.

As we mentioned, we shall be interested in evaluating the tensor power spectrum after the bounce. Let us assume that, after the bounce, the universe transits to the radiation domination epoch at, say, $\eta = \beta \eta_0$, where we shall set $\beta \simeq 10^2$. We should hasten to clarify that, while this value of β is somewhat arbitrary, we find that the final results do not strongly depend on the choice of β . In order to study the evolution of the tensor modes analytically, let us divide the period $-\infty < \eta \leq \beta \eta_0$ into two domains. The first domain is determined by the condition $-\infty < \eta \leq -\alpha \eta_0$, where α is a very large number, which we shall set to be 10^5 . In other words, this domain corresponds to very early times during the contracting phase before the bounce. The second domain $-\alpha \eta_0 \leq \eta \leq \beta \eta_0$ evidently involves periods prior to as well as immediately after the bounce. We find that, under suitable approximations, we can evaluate the tensor modes analytically in both of these domains.

In the first domain (*i.e.* during $-\infty < \eta \leq -\alpha \eta_0$), the scale factor (3.1) reduces to

$$a(\eta) \simeq a_0 k_0^2 \eta^2, \quad (3.3)$$

so that we have $a''/a \simeq 2/\eta^2$, which is exactly the behavior in de Sitter inflation. Upon imposing the Bunch-Davies initial condition [*cf.* equation (1.75)] at early

times when $k^2 \gg 2/\eta^2$, the mode h_k in the first domain can be easily determined to be [64, 101, 104, 105]

$$h_k \simeq \frac{\sqrt{2}}{M_{\text{Pl}}} \frac{1}{\sqrt{2}k} \frac{1}{a_0 k_0^2 \eta^2} \left(1 - \frac{i}{k\eta}\right) e^{-ik\eta}. \quad (3.4)$$

Let us now consider the behavior of the modes in the second domain, *i.e.* $-\alpha\eta_0 \leq \eta \leq \beta\eta_0$. In this domain, for scales of cosmological interest, which correspond to $k \ll k_0$, the equation governing the tensor mode h_k simplifies to

$$h_k'' + \frac{2a'}{a} h_k' \simeq 0. \quad (3.5)$$

We should clarify that, since we are working in the domain wherein $\eta \geq -\alpha\eta_0$, this equation is actually valid for wavenumbers such that $k \ll k_0/\alpha$. The above equation can be integrated to yield

$$h_k(\eta) \simeq h_k(\eta_1) + h_k'(\eta_1) a^2(\eta_1) \int_{\eta_1}^{\eta} \frac{d\tilde{\eta}}{a^2(\tilde{\eta})}, \quad (3.6)$$

where η_1 is a suitably chosen time, and we have set the constants of integration to be $h_k(\eta_1)$ and $h_k'(\eta_1)$. Upon choosing $\eta_1 = -\alpha\eta_0$ and using the form (3.1) of the scale factor, we find that, in the second domain, the tensor mode can be expressed as

$$h_k = \mathcal{A}_k + \mathcal{B}_k f(k_0\eta), \quad (3.7)$$

where the function $f(x)$ is given by

$$f(x) = \frac{x}{1+x^2} + \tan^{-1}(x). \quad (3.8)$$

The quantities \mathcal{A}_k and \mathcal{B}_k can be determined from the solution (3.4) in the first

domain and are given by

$$\mathcal{A}_k = \frac{\sqrt{2}}{M_{\text{Pl}}} \frac{1}{\sqrt{2k}} \frac{1}{a_0 \alpha^2} \left(1 + \frac{i k_0}{\alpha k}\right) e^{i \alpha k/k_0} + \mathcal{B}_k f(\alpha), \quad (3.9a)$$

$$\mathcal{B}_k = \frac{\sqrt{2}}{M_{\text{Pl}}} \frac{1}{\sqrt{2k}} \frac{1}{2 a_0 \alpha^2} (1 + \alpha^2)^2 \left(\frac{3 i k_0}{\alpha^2 k} + \frac{3}{\alpha} - \frac{i k}{k_0}\right) e^{i \alpha k/k_0}. \quad (3.9b)$$

It is interesting to note here that, after the bounce, the first term in $f(k_0 \eta)$ decays while the second term exhibits a mild growth.

3.3.2 E-N-folds and the numerical evaluation of the tensor modes

To understand the accuracy of the approximations involved, we can compare the above analytical results for the evolution of the tensor modes with the corresponding numerical results. Since the scale factor is specified, it is essentially a matter of numerically integrating the differential equation (1.65) governing the tensor perturbations with known coefficients. However, the conformal time coordinate does not prove to be an efficient time variable for numerical integration, in particular, when a large range in the scale factor needs to be covered. In the context of inflation, one works with e-folds N as the independent time variable, with the scale factor being given by $a(N) \propto e^N$. But, the function e^N is monotonically increasing function, whereas, in a bounce, the scale factor decreases at first before beginning to increase.

In order to describe the completely symmetric bouncing universe of our interest, we shall introduce a new time variable \mathcal{N} , in terms of which the scale factor is given by [101, 102]

$$a(\mathcal{N}) = a_0 e^{\mathcal{N}^2/2}. \quad (3.10)$$

We shall refer to the variable \mathcal{N} as e-N-fold, and we shall perform the numerical

integration using this variable. We shall assume that \mathcal{N} is zero at the bounce, with negative values representing the phase prior to the bounce and positive values after. It is useful to note that the amount of e-N-folds, say, $\Delta\mathcal{N}$, is related to the more conventional number of e-folds, say, ΔN , as $\Delta\mathcal{N} = \sqrt{2\Delta N}$. For instance, $\Delta N \simeq 50\text{--}60$ corresponds to $\Delta\mathcal{N} \simeq 10\text{--}11$.

In terms of e-N-folds, the differential equation (1.65) governing the evolution of the tensor modes can be expressed as

$$\frac{d^2 h_k}{d\mathcal{N}^2} + \left(3\mathcal{N} + \frac{1}{H} \frac{dH}{d\mathcal{N}} - \frac{1}{\mathcal{N}} \right) \frac{dh_k}{d\mathcal{N}} + \left(\frac{k\mathcal{N}}{aH} \right)^2 h_k = 0, \quad (3.11)$$

where H is the Hubble parameter. In order to determine the coefficients of the above equation, we need to express the Hubble parameter in terms of e-N-folds. Upon using the expression for the scale factor (3.1), we obtain that

$$\eta(\mathcal{N}) = \pm k_0^{-1} \left(e^{\mathcal{N}^2/2} - 1 \right)^{1/2}. \quad (3.12)$$

It is important to note that, since the Hubble parameter is negative during the contracting phase and positive during the expanding regime, we shall have to choose the root of $\eta(\mathcal{N})$ accordingly during each phase. We numerically integrate the differential equation (3.11) using a fifth order Runge-Kutta algorithm. We impose the initial conditions at a sufficiently early time, say, \mathcal{N}_i , when $k^2 = 10^4 (a''/a)$. Evidently, the standard Bunch-Davies initial condition on u_k [*cf.* equation (1.75)] can be converted to initial conditions on the mode h_k and its derivative with respect to the e-N-fold [101]. The tensor mode h_k evaluated numerically has been plotted in figure 3.1 for a specific wavenumber. In the same figure, we have also plotted the analytical result we have obtained for the tensor mode. It is clear from the figure that the analytical results match the exact numerical results exceedingly well, which illustrates the extent of accuracy of the

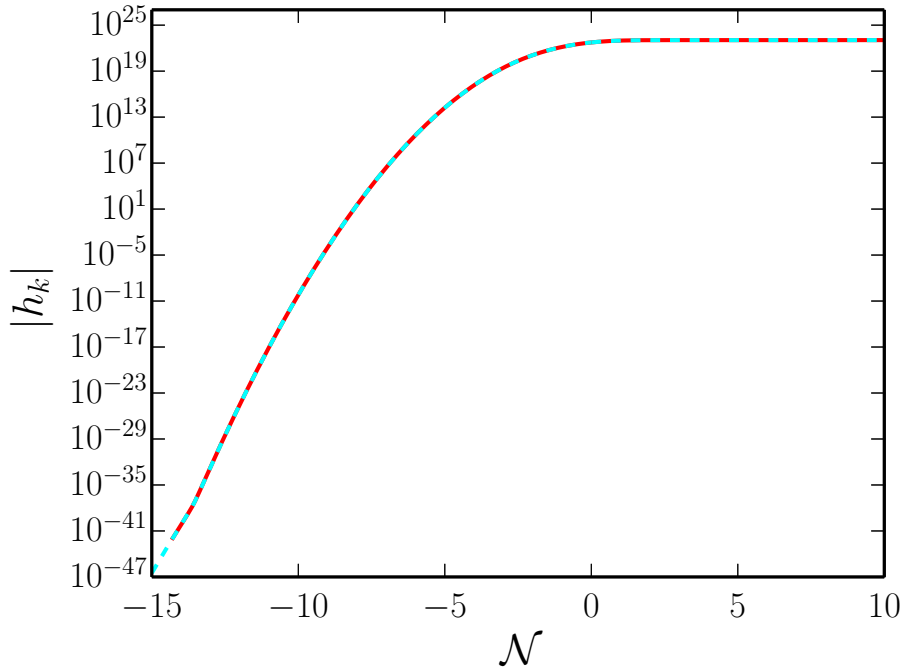


Figure 3.1: The numerical (in red) and the analytical (in cyan) results for the amplitude of the tensor mode h_k corresponding to the wavenumber $k/k_0 = 10^{-20}$ has been plotted as a function of e-N-fold. We have set $k_0/(a_0 M_{\text{Pl}}) = 3.3 \times 10^{-8}$ and, for plotting the analytical results, we have also chosen $\alpha = 10^5$. Note that, to arrive at the plots we have chosen $k_0 = M_{\text{Pl}}$ and $a_0 = 3.0 \times 10^7$, which is consistent with the above mentioned value of $k_0/(a_0 M_{\text{Pl}})$. We have plotted the results from the initial e-N-fold \mathcal{N}_i [when $k^2 = 10^4 (a''/a)$] corresponding to the mode. Clearly, the match between the analytical and numerical results is very good. This indicates that the approximation for determining the modes analytically works quite well.

analytical approximations.

3.3.3 Tensor power spectrum

The tensor power spectrum can now be evaluated using the solutions for the modes that we have obtained. Upon substituting the modes (3.7) in the expression (1.69), we find that the tensor power spectrum after the bounce, evaluated at $\eta = \beta \eta_0$, can be written as

$$\mathcal{P}_{\text{T}}(k) = 4 \frac{k^3}{2\pi^2} |\mathcal{A}_k + \mathcal{B}_k f(\beta)|^2, \quad (3.13)$$

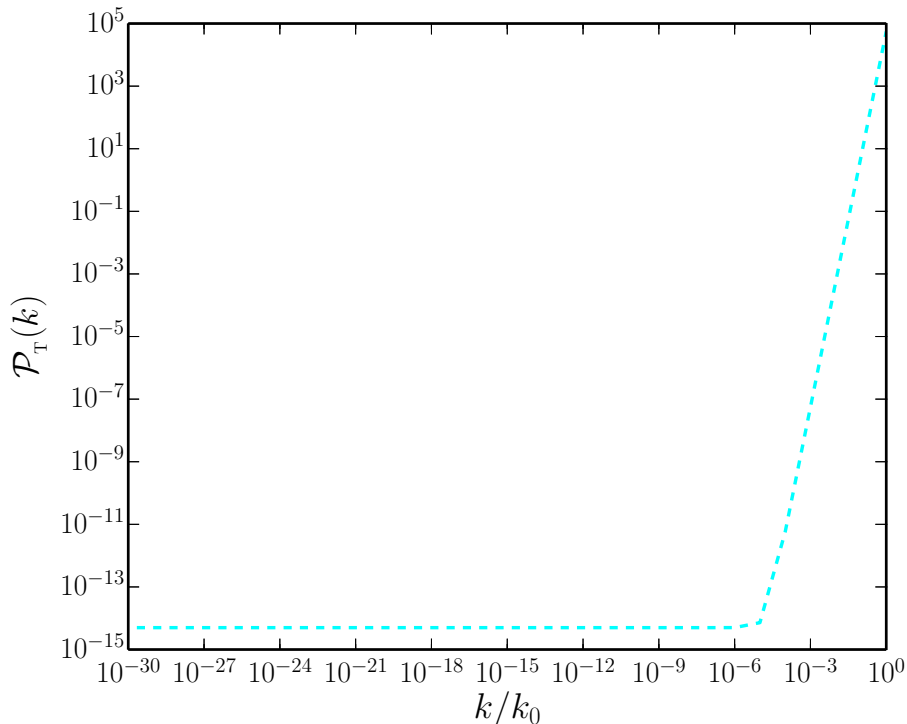


Figure 3.2: The tensor power spectrum $\mathcal{P}_T(k)$, evaluated analytically, has been plotted as a function of k/k_0 for a wide range of wavenumbers. In plotting this figure, we have chosen the same values for k_0/a_0 and α as in the previous figure, and have set $\beta = 10^2$. We should stress that the approximations we have worked with are valid only for wavenumbers such that $k \ll k_0/\alpha$. It is clear from the figure that the power spectrum is scale-invariant over these wavenumbers. Note that, for the values of the parameters mentioned above, at small enough wavenumbers, the tensor power spectrum has the scale-invariant amplitude of $\mathcal{P}_T(k) \simeq 5 \times 10^{-15}$.

with \mathcal{A}_k and \mathcal{B}_k given by equations (3.9), and f by equation (3.8). As we had pointed out, our approximations are valid only for modes such that $k \ll k_0/\alpha$. Also, for reasons discussed earlier, we need to choose β to be reasonably large. We have plotted the resulting tensor power spectrum in figure 3.2 for $k_0/(a_0 M_{\text{Pl}}) = 3.3 \times 10^{-8}$, $\alpha = 10^5$ and $\beta = 10^2$. Clearly, the spectrum is scale-invariant for wavenumbers such that $k \ll k_0/\alpha$. It is straightforward to determine the scale-invariant amplitude of the power spectrum to be [64, 104, 105]

$$\mathcal{P}_T(k) \simeq \frac{9 k_0^2}{2 M_{\text{Pl}}^2 a_0^2}. \quad (3.14)$$

Note that this tensor power spectrum depends only on the parameter k_0/a_0 . As we shall illustrate later (see figure 3.6), the numerical results for the power spectrum (evaluated at $\eta = \beta \eta_0$) matches this scale-invariant amplitude quite well.

3.4 Modeling the bounce with scalar fields

Our aim now is to construct sources involving scalar fields to drive the scale factor (3.1). We had mentioned earlier that the scale factor can be achieved with the aid of two fluids, one of which is pressureless matter and another which behaves as radiation, but with a negative energy density. It is well known that non-canonical scalar fields with a purely kinetic term can act as perfect fluids [106]. However, purely kinetic scalar fields cannot mimic pressureless matter, as a potential term is required to ensure that the pressure always remains zero. We shall model pressureless matter by a canonical scalar field with a potential, and describe radiation with negative energy density in terms of a suitable purely kinetic, non-canonical and ghost scalar field. As we had mentioned in the introductory section, such ghost fields pose certain conceptual difficulties. At this stage, we shall choose to overlook these difficulties and continue with our analysis. We shall make a few remarks about the issue in the concluding section.

Let the canonical field be ϕ and the non-canonical, ghost field be χ . We shall assume that the complete action describing these two fields is given by

$$S[\phi, \chi] = - \int d^4x \sqrt{-g} \left[-X^{\phi\phi} + V(\phi) + U_0 (X^{\chi\chi})^2 \right], \quad (3.15)$$

where $X^{\phi\phi}$ is the kinetic term (1.30), U_0 is a positive constant with the dimension

of M_{Pl}^{-4} , and the kinetic term X^{xx} is defined as

$$X^{\text{xx}} = -\frac{1}{2} \partial_\mu \chi \partial^\mu \chi. \quad (3.16)$$

While the stress-energy tensor associated with the ϕ is given by (1.32), the stress-energy tensor corresponding to the field χ can be obtained to be

$$T_{\nu(\chi)}^\mu = -2 U_0 X^{\text{xx}} \partial^\mu \chi \partial_\nu \chi - \delta_\nu^\mu U_0 (X^{\text{xx}})^2. \quad (3.17)$$

Assuming the fields to be homogeneous, let us understand their behavior in a bouncing universe. Let us first consider the χ field. It is straightforward to obtain that

$$T_{0(\chi)}^0 = -\rho_\chi = \frac{3 U_0 \dot{\chi}^4}{4}, \quad (3.18a)$$

$$T_{j(\chi)}^i = p_\chi \delta_j^i = -\frac{U_0 \dot{\chi}^4}{4} \delta_j^i. \quad (3.18b)$$

Note that ρ_χ is negative and $p_\chi = \rho_\chi/3$, corresponding to radiation. In the absence of any potential, the equation of motion governing the field χ is extremely simple and is given by

$$\chi'' = 0. \quad (3.19)$$

This can be immediately integrated to obtain $\chi' = C_2$, where C_2 is a constant of integration. In other words, the field evolves monotonically towards either large or small values as the universe evolves. Such a behavior should not be surprising for a purely kinetic field that is devoid of any potential to guide it. The energy density ρ_χ can be written as

$$\rho_\chi = -\frac{3 U_0 \chi'^4}{4 a^4} = -\frac{3 U_0 C_2^4}{4 a^4}, \quad (3.20)$$

which is indeed the behavior of radiation, albeit with a negative energy density.

Let us now turn to the behavior of the field ϕ . The components of the stress-energy tensor associated with the field are given by equations (1.33). Recall that the field ϕ is expected to behave as ordinary matter. The pressureless condition leads to [cf. equation (1.33b)]

$$\frac{\phi'^2}{2} - a^2 V(\phi) = 0. \quad (3.21)$$

Further, being pressureless, the associated energy density is expected to behave as, say, $\rho_\phi = C_1^2/a^3$, where C_1 is a constant. This implies that we can write [cf. equation (1.33)]

$$\frac{\phi'^2}{2} + a^2 V(\phi) = \frac{C_1^2}{a}. \quad (3.22)$$

Upon adding the above two equations, we obtain that

$$\phi' = \frac{C_1}{\sqrt{a}}. \quad (3.23)$$

Given the scale factor (3.1), this equation can be easily integrated to arrive at

$$\phi = \phi_0 \sinh^{-1}(k_0 \eta), \quad (3.24)$$

where $\phi_0 = C_1/(\sqrt{a_0} k_0)$ and we have set the constant of integration to zero. The above expression can be inverted to write

$$k_0 \eta = \sinh \left(\frac{\phi}{\phi_0} \right). \quad (3.25)$$

Since, according to equations (3.21) and (3.23),

$$V(\phi) = \frac{\phi'^2}{2a^2} = \frac{C_1^2}{2a^3}, \quad (3.26)$$

on using the above solution for ϕ , we can determine the potential to be

$$V(\phi) = \frac{C_1^2}{2 a_0^3 \cosh^6(\phi/\phi_0)}. \quad (3.27)$$

It is straightforward to check that the above expressions for the field and the potential indeed satisfy the standard equation of motion (1.31) governing the canonical scalar field. Note that the evolution of the field is symmetric about the bounce. It starts with large negative values at early times during the contracting phase, rolls *up* the potential (3.27), reaching zero at the bounce¹. Thereafter, the field continues towards positive values, rolling down the potential during the expanding phase.

Now that we have arrived at the behavior of the fields, the remaining task is to fix the constants C_1 and C_2 . They ought to be related to the parameters k_0 and a_0 in terms of which we had expressed the scale factor and the constant U_0 that appears in the part of the action describing the field χ . We find that the first Friedmann equation $3 H^2 M_{\text{Pl}}^2 = \rho = \rho_\phi + \rho_\chi$ can be expressed as

$$3 \mathcal{H}^2 M_{\text{Pl}}^2 = \frac{\dot{\phi}^2}{2} + a^2 V(\phi) - \frac{3 U_0 \chi'^4}{4 a^2}, \quad (3.28)$$

where $\mathcal{H} = a'/a$ is the conformal Hubble parameter. Upon using the various expressions we have obtained above and the scale factor (3.1), we can determine the constants C_1 and C_2 to be

$$C_1 = \sqrt{12 a_0} M_{\text{Pl}} k_0, \quad (3.29a)$$

$$C_2 = \sqrt{\frac{4 M_{\text{Pl}} a_0 k_0}{U_0^{1/2}}}, \quad (3.29b)$$

¹The fact that the field rolls *up* the potential during the contracting phase should not come as a surprise. During an expanding phase such as inflation, H is positive and, as is well known, the $3 H \dot{\phi}$ term leads to friction, slowing down the field that is rolling down a potential. In contrast, during a contracting phase, since H is negative, the $3 H \dot{\phi}$ term acts as ‘anti-friction’, speeding up the field and thereby allowing it to climb the potential.

so that the energy densities associated with the two fields reduce to

$$\rho_\phi = \frac{12 M_{\text{Pl}}^2 a_0 k_0^2}{a^3}, \quad (3.30a)$$

$$\rho_\chi = -\frac{12 M_{\text{Pl}}^2 a_0^2 k_0^2}{a^4}. \quad (3.30b)$$

It is easy to see that $\rho_\phi + \rho_\chi = 0$ at the bounce, and such a behavior would not have been possible without the ghost field χ .

We should point out here that, if we make use the above expression for C_1 , the potential (3.27) can be written as

$$V(\phi) = \frac{6 M_{\text{Pl}}^2 (k_0/a_0)^2}{\cosh^6(\sqrt{12} \phi/M_{\text{Pl}})}. \quad (3.31)$$

In other words, the potential and, hence, the complete model, actually depends *only* on the parameter k_0/a_0 . Therefore, we can expect the power spectra to depend only on this combination. This is already evident in the case of the tensors [*cf.* equation (3.14)]. In due course, we shall see that similar conclusions apply to the scalars as well. We shall comment further on this point in the concluding section.

We should mention here that the matter bounce scenario driven by two scalar fields we are studying is somewhat similar to a system which had been investigated earlier [12]. In the earlier work, the purely kinetic, ghost field χ was described by a linear kinetic term, in contrast to the non-linear term that we are considering. Also, the choice of the potential describing the canonical field ϕ was different. However, since both the models lead to a matter dominated phase at early times, we find that the two potentials behave in a similar manner at large negative values of the field. The difference in the action governing the χ field and the choice of an even function for the potential describing the ϕ field lead to a difference in the behavior of the background around the bounce between the

two models. Our choices not only permit us to solve for the background analytically, but, importantly, the symmetric matter bounce (3.1) of our interest leads to a tensor-to-scalar ratio that is consistent with the observations.

3.5 Equations of motion governing the scalar perturbations

In this section, we shall derive the equations governing the evolution of the scalar perturbations. Since there are two fields involved, evidently, apart from the curvature perturbation, there will be an isocurvature perturbation present as well. We shall derive the equations governing the perturbations $\delta\phi$ and $\delta\chi$ and their corresponding gauge invariant versions $\overline{\delta\phi}$ and $\overline{\delta\chi}$. Thereafter, we shall construct the curvature and isocurvature perturbations for our model and arrive at the corresponding equations governing them.

3.5.1 The first order Einstein's equations

If we take into account the scalar perturbations to the background metric, then the FLRW line-element, in general, can be written as in equation (1.44). At the first order in the perturbations, the Einstein's equations are given by [1]

$$3H \left(HA + \dot{\psi} \right) - \frac{1}{a^2} \nabla^2 \left[\psi - aH \left(B - a\dot{E} \right) \right] = -\frac{1}{2M_{\text{Pl}}^2} (\delta\rho_\phi + \delta\rho_\chi), \quad (3.32a)$$

$$\partial_i \left(HA + \dot{\psi} \right) = \frac{1}{2M_{\text{Pl}}^2} \partial_i (\delta q_\phi + \delta q_\chi), \quad (3.32b)$$

$$\ddot{\psi} + H \left(\dot{A} + 3\dot{\psi} \right) + \left(2\dot{H} + 3H^2 \right) A = \frac{1}{2M_{\text{Pl}}^2} (\delta p_\phi + \delta p_\chi), \quad (3.32c)$$

$$A - \psi + \frac{1}{a} \left[a^2 \left(B - a\dot{E} \right) \right]' = 0, \quad (3.32d)$$

where $\delta\rho_I$ and δp_I , with $I = (\phi, \chi)$, are the perturbations in the energy densities and pressure associated with the two fields ϕ and χ . Further, the quantities δq_I have been defined through the relation $\delta T_{i(I)}^0 = -\partial_i(\delta q_I)$. The last of the above equations follows from the fact that there are no anisotropic stresses present. While the components of the perturbed stress-energy tensor associated with the field ϕ are given by equations (1.51), the components of the perturbed stress-energy tensor corresponding to the field χ can be evaluated to be

$$\delta T_{0(\chi)}^0 = -\delta\rho_\chi = 3U_0\dot{\chi}^3\delta\dot{\chi} - 3AU_0\dot{\chi}^4, \quad (3.33a)$$

$$\delta T_{i(\chi)}^0 = -\partial_i\delta q_\chi = \partial_i(U_0\dot{\chi}^3\delta\chi), \quad (3.33b)$$

$$\delta T_{j(\chi)}^i = \delta p_\chi\delta_j^i = (U_0A\dot{\chi}^4 - U_0\dot{\chi}^3\delta\dot{\chi})\delta_j^i. \quad (3.33c)$$

3.5.2 Equations governing the perturbations in the scalar fields

The equations of motion describing the perturbations in the fields can be arrived at from the following conservation equation governing the perturbation in the energy density of a specific component (see, for instance, Refs. [107, 108]):

$$\dot{\delta\rho}_I + 3H(\delta\rho_I + \delta p_I) - 3(\rho_I + p_I)\dot{\psi} - \nabla^2 \left[\left(\frac{\rho_I + p_I}{a} \right) B + \frac{\delta q_I}{a^2} - (\rho_I + p_I)\dot{E} \right] = 0. \quad (3.34)$$

Upon making use of this equation and the above expressions for the components of the perturbed stress-energy tensor, we obtain the equations of motion governing the Fourier modes, say, $\delta\phi_k$ and $\delta\chi_k$, associated with the perturbations in the two scalar fields to be

$$\begin{aligned} \ddot{\delta\phi}_k + 3H\dot{\delta\phi}_k + V_{\phi\phi}\delta\phi_k + 2V_\phi A_k & - \dot{\phi} \left(\dot{A}_k + 3\dot{\psi}_k \right) \\ & + \frac{k^2}{a^2} \left[\delta\phi_k + a\dot{\phi} \left(B_k - a\dot{E}_k \right) \right] = 0, \end{aligned} \quad (3.35a)$$

$$\delta\ddot{\chi}_k + H \delta\dot{\chi}_k - \dot{\chi} \left(\dot{A}_k + \dot{\psi}_k \right) + \frac{k^2}{3a^2} \left[\delta\chi_k + a \dot{\chi} \left(B_k - a \dot{E}_k \right) \right] = 0, \quad (3.35b)$$

where, evidently, A_k , B_k , ψ_k and E_k denote the Fourier modes that describe the corresponding metric perturbations. The gauge invariant perturbations associated with the two scalar fields can be constructed to be

$$\overline{\delta\phi}_k = \delta\phi_k + \frac{\dot{\phi}}{H} \psi_k, \quad (3.36a)$$

$$\overline{\delta\chi}_k = \delta\chi_k + \frac{\dot{\chi}}{H} \psi_k. \quad (3.36b)$$

Upon using the equations of motion (3.35) and the first order Einstein equations (3.32), we find that these gauge invariant perturbations of the two scalar fields obey the following equations:

$$\begin{aligned} \overline{\delta\phi}_k'' + 2\mathcal{H} \overline{\delta\phi}_k' + \left(k^2 + a^2 V_{\phi\phi} + \frac{2a^2 \phi' V_\phi}{\mathcal{H} M_{\text{Pl}}^2} + \frac{3\phi'^2}{M_{\text{Pl}}^2} - \frac{\phi'^4}{2\mathcal{H}^2 M_{\text{Pl}}^4} + \frac{U_0 \phi'^2 \chi'^4}{a^2 \mathcal{H}^2 M_{\text{Pl}}^4} \right) \overline{\delta\phi}_k \\ = \frac{U_0 \phi' \chi'^3}{a^2 \mathcal{H} M_{\text{Pl}}^2} \overline{\delta\chi}_k' \\ + \left(\frac{U_0 V_\phi \chi'^3}{\mathcal{H} M_{\text{Pl}}^2} + \frac{3U_0 \phi' \chi'^3}{a^2 M_{\text{Pl}}^2} - \frac{U_0 \phi'^3 \chi'^3}{2a^2 \mathcal{H}^2 M_{\text{Pl}}^4} + \frac{U_0^2 \phi' \chi'^7}{a^4 \mathcal{H}^2 M_{\text{Pl}}^4} \right) \overline{\delta\chi}_k, \end{aligned} \quad (3.37a)$$

$$\begin{aligned} \overline{\delta\chi}_k'' + \left(\frac{k^2}{3} - \frac{2U_0 \chi'^4}{a^2 M_{\text{Pl}}^2} + \frac{U_0 \phi'^2 \chi'^4}{3a^2 \mathcal{H}^2 M_{\text{Pl}}^4} - \frac{U_0^2 \chi'^8}{2a^4 \mathcal{H}^2 M_{\text{Pl}}^4} \right) \overline{\delta\chi}_k \\ = \frac{\phi' \chi'}{3\mathcal{H} M_{\text{Pl}}^2} \overline{\delta\phi}_k' \\ - \left(\frac{2\chi' a^2 V_\phi}{3\mathcal{H} M_{\text{Pl}}^2} + \frac{2\phi' \chi'}{M_{\text{Pl}}^2} - \frac{\phi'^3 \chi'}{3\mathcal{H}^2 M_{\text{Pl}}^4} + \frac{U_0 \phi' \chi'^5}{2a^2 \mathcal{H}^2 M_{\text{Pl}}^4} \right) \overline{\delta\phi}_k. \end{aligned} \quad (3.37b)$$

Let us now turn to the construction of the gauge invariant curvature and isocurvature perturbations associated with the two fields. In due course, we shall make use of the above equations to obtain the equations governing the curvature and isocurvature perturbations.

3.5.3 Constructing the curvature and isocurvature perturbations

As is well known, in the presence of more than one field or fluid, apart from the curvature perturbation, isocurvature perturbations are also generated. The isocurvature perturbations source the curvature perturbations. It is the structure of the complete action describing the matter fields that determines the relation between the perturbations in the fields and the curvature and isocurvature perturbations. As we had pointed out earlier, while the fluctuations along the direction of the background trajectory in the field space are referred to as the adiabatic or the curvature perturbation, the perturbations along a direction perpendicular to the background trajectory are called the non-adiabatic, entropic or isocurvature perturbations [10, 107, 108].

The Lagrangian density associated with the action (3.15) is evidently given by

$$\mathcal{L} = X^{\phi\phi} - V(\phi) - U_0 (X^{\chi\chi})^2. \quad (3.38)$$

Let us now define a set of basis vectors along the direction of background evolution, *viz.* the adiabatic basis, and another set of basis vectors along the direction perpendicular to the background evolution, which is referred to as the entropic basis. These two sets of basis vectors obey the following orthonormality condition (see, for instance, Refs. [38, 109]):

$$\mathcal{L}_{x^{IJ}} e_n^I e_m^J = \delta_{nm}, \quad (3.39)$$

where $(I, J) = (\phi, \chi)$, $(n, m) = (1, 2)$ and

$$\mathcal{L}_{x^{IJ}} = \frac{\partial \mathcal{L}}{\partial X^{IJ}}. \quad (3.40)$$

The adiabatic basis vectors can be defined as [38, 109]

$$e_1^I = \frac{\dot{\varphi}^I}{\sqrt{\mathcal{L}_{x^{JK}} \dot{\varphi}^J \dot{\varphi}^K}}, \quad (3.41)$$

where $(\varphi^1, \varphi^2) = (\phi, \chi)^2$. Since

$$\mathcal{L}_{x^{\phi\phi}} = 1 \quad (3.42)$$

and

$$\mathcal{L}_{x^{\chi\chi}} = -2U_0 X^{\chi\chi} = -U_0 \dot{\chi}^2, \quad (3.43)$$

we can define the two adiabatic basis vectors to be

$$e_1^\phi = \frac{\dot{\phi}}{\sqrt{\dot{\phi}^2 - U_0 \dot{\chi}^4}}, \quad (3.44a)$$

$$e_1^\chi = \frac{\dot{\chi}}{\sqrt{\dot{\phi}^2 - U_0 \dot{\chi}^4}}. \quad (3.44b)$$

The curvature perturbation can be defined in terms of these basis vectors as

$$\mathcal{R} = \frac{H}{\mathcal{L}_{x^{IJ}} \dot{\varphi}^I \dot{\varphi}^J} \mathcal{L}_{x^{KL}} \dot{\varphi}^K \overline{\delta\varphi}^L = \frac{H}{\sqrt{\mathcal{L}_{x^{IJ}} \dot{\varphi}^I \dot{\varphi}^J}} \mathcal{L}_{x^{KL}} e_1^K \overline{\delta\varphi}^L, \quad (3.45)$$

where $\overline{\delta\varphi}^L$ is the gauge invariant perturbation associated with the field φ^L . For our model, the curvature perturbation can be constructed to be

$$\mathcal{R} = \frac{H}{\dot{\phi}^2 - U_0 \dot{\chi}^4} \left(\dot{\phi} \overline{\delta\phi} - U_0 \dot{\chi}^3 \overline{\delta\chi} \right). \quad (3.46)$$

It is well known that, when multiple components (fluids and/or fields) are present, the total curvature perturbation is defined as (see, for instance, Refs. [107,

²Actually, since I already represents ϕ and χ , the introduction of φ^I implying $(\varphi^1, \varphi^2) = (\phi, \chi)$ may be considered as redundant notation. However, representing the perturbations in the scalar fields as $\delta\varphi^I = (\delta\phi, \delta\chi)$ seems to be a better choice than denoting them as δI !

108])

$$\mathcal{R} = \sum_I \frac{\rho_I + p_I}{\rho + p} \mathcal{R}_I, \quad (3.47)$$

where \mathcal{R}_I is the curvature perturbation associated with an individual component and is given by

$$\mathcal{R}_I = \psi + \frac{H}{\rho_I + p_I} \delta q_I. \quad (3.48)$$

For our system, it is easy to show that, if we make use of the expressions for the various quantities we have obtained earlier, the definition (3.47) for the total curvature perturbation indeed matches the explicitly gauge invariant expression (3.46) we have arrived at. Note that the expression (3.46) for \mathcal{R} suggests that it may diverge when $\dot{\phi}^2 - U_0 \dot{\chi}^4 = 0$, which corresponds to the condition $\dot{H} = 0$. Recall that, $\dot{H} = 0$ at $\mp\eta_* = \mp\eta_0/\sqrt{3}$, which is where the total energy density ρ reaches its maximum value. As we shall see, the curvature perturbation indeed diverges at these times. The expression (3.46) also suggests that the curvature perturbation may turn out to be zero at the bounce, wherein $H = 0$. However, we find that this actually does not occur at the bounce, but the curvature perturbation vanishes for an instant between the bounce and η_* .

Let us now construct the corresponding basis vectors for the entropic perturbations, *viz.* e_2^ϕ and e_2^χ . Using equations (3.44) and the orthonormality condition (3.39), we obtain that

$$e_2^\phi = \frac{\dot{\chi} \sqrt{-U_0 \dot{\chi}^2}}{\sqrt{\dot{\phi}^2 - U_0 \dot{\chi}^4}}, \quad (3.49a)$$

$$e_2^\chi = \frac{\dot{\phi}}{\sqrt{-U_0 \dot{\chi}^2} \sqrt{\dot{\phi}^2 - U_0 \dot{\chi}^4}}. \quad (3.49b)$$

It is straightforward to check that these two basis vectors are indeed orthogonal to the direction of the background evolution. The isocurvature perturbation can

therefore be defined in terms of the basis vectors (3.49) as

$$\mathcal{S} = \frac{H}{\sqrt{\mathcal{L}_{x^{IJ}} \dot{\phi}^I \dot{\phi}^J}} \mathcal{L}_{x^{KL}} e_2^K \bar{\delta}\varphi^L. \quad (3.50)$$

This can be expressed as

$$\mathcal{S} = \frac{H \sqrt{U_0} \dot{\chi}^2}{\dot{\phi}^2 - U_0 \dot{\chi}^4} \left(\dot{\chi} \bar{\delta}\phi - \dot{\phi} \bar{\delta}\chi \right), \quad (3.51)$$

where, in order for \mathcal{S} to remain a real quantity, we have dropped the minus sign under the square root that appears as an overall coefficient. It is easy to check that, apart from an overall background factor, the isocurvature perturbation we have defined above can be expressed as the difference of the curvature perturbation \mathcal{R}_I [*cf.* equation (3.48)] associated with the two individual fields [107]. Note that, as in the case of the curvature perturbation, the isocurvature perturbation can be expected to diverge at $\mp\eta_*$ and vanish at the bounce. We shall see later that these expectations indeed prove to be true.

3.5.4 Equations governing the curvature and the isocurvature perturbations

Let \mathcal{R}_k and \mathcal{S}_k denote the Fourier modes associated with the curvature and the isocurvature perturbations. The expressions for the curvature and the isocurvature perturbations we have obtained above can be inverted to arrive at the following relations:

$$\bar{\delta}\phi_k = \frac{1}{\mathcal{H}} \left(\phi' \mathcal{R}_k - \frac{1}{a} \sqrt{U_0} \chi'^4 \mathcal{S}_k \right), \quad (3.52a)$$

$$\bar{\delta}\chi_k = \frac{1}{\mathcal{H}} \left(\chi' \mathcal{R}_k - \frac{a \phi'}{\sqrt{U_0} \chi'^2} \mathcal{S}_k \right). \quad (3.52b)$$

Using the equations of motion for the gauge invariant field perturbations (3.37), we obtain the equations governing \mathcal{R}_k and \mathcal{S}_k to be

$$\begin{aligned}
\mathcal{R}_k'' &+ \left\{ \frac{2(\mathcal{H}' - \mathcal{H}^2)}{\mathcal{H}} - 2\mathcal{H} + \frac{a}{M_{\text{Pl}}^2} \left[\frac{2\phi'^2}{3a\mathcal{H}} - \frac{aV_\phi\phi'}{\mathcal{H}' - \mathcal{H}^2} - \frac{\mathcal{H}\phi'^2}{a(\mathcal{H}' - \mathcal{H}^2)} \right] \right. \\
&\quad \left. - \frac{\phi'^4}{3M_{\text{Pl}}^4\mathcal{H}(\mathcal{H}' - \mathcal{H}^2)} \right\} \mathcal{R}_k' + \frac{k^2}{3} \left[1 + \frac{\phi'^2}{M_{\text{Pl}}^2(\mathcal{H}' - \mathcal{H}^2)} \right] \mathcal{R}_k \\
&= \frac{\sqrt{U_0}\chi'^4\phi'}{M_{\text{Pl}}^2(\mathcal{H}' - \mathcal{H}^2)} \left[\frac{aV_\phi}{\phi'} + \frac{\mathcal{H}}{a} - \frac{1}{2M_{\text{Pl}}^2\mathcal{H}} \left(\frac{\phi'^2}{a} - \frac{U_0\chi'^4}{3a^3} \right) \right] \mathcal{S}_k' \\
&\quad + \frac{\sqrt{U_0}\chi'^4\phi'}{aM_{\text{Pl}}^2} \left[\frac{k^2}{3(\mathcal{H}' - \mathcal{H}^2)} + \frac{5}{3} + \frac{5a^2V_\phi}{\mathcal{H}\phi'} - \frac{2\mathcal{H}^2}{\mathcal{H}' - \mathcal{H}^2} + \frac{V_{\phi\phi}a^2}{\mathcal{H}' - \mathcal{H}^2} \right. \\
&\quad \left. - \frac{\mathcal{H}' - \mathcal{H}^2}{3\mathcal{H}^2} + \frac{1}{M_{\text{Pl}}^2} \left(\frac{2V_\phi\phi'a^2}{3\mathcal{H}(\mathcal{H}' - \mathcal{H}^2)} + \frac{\phi'^2}{\mathcal{H}' - \mathcal{H}^2} - \frac{\phi'^2}{3\mathcal{H}^2} \right) \right] \mathcal{S}_k, \quad (3.53a)
\end{aligned}$$

$$\begin{aligned}
\mathcal{S}_k'' &+ \left[\frac{2(\mathcal{H}' - \mathcal{H}^2)}{\mathcal{H}} - 2\mathcal{H} - \frac{1}{M_{\text{Pl}}^2} \left(\frac{2\phi'^2}{3\mathcal{H}} + \frac{V_\phi\phi'a^2}{\mathcal{H}' - \mathcal{H}^2} + \frac{\mathcal{H}\phi'^2}{\mathcal{H}' - \mathcal{H}^2} \right) \right. \\
&\quad \left. + \frac{\phi'^4}{3M_{\text{Pl}}^4\mathcal{H}(\mathcal{H}' - \mathcal{H}^2)} \right] \mathcal{S}_k' \\
&\quad + \left\{ k^2 \left[1 - \frac{\phi'^2}{3M_{\text{Pl}}^2(\mathcal{H}' - \mathcal{H}^2)} \right] \right. \\
&\quad \left. - 2\mathcal{H}^2 + a^2V_{\phi\phi} + \frac{2(\mathcal{H}' - \mathcal{H}^2)^2}{\mathcal{H}^2} - 3(\mathcal{H}' - \mathcal{H}^2) \right. \\
&\quad \left. + \frac{1}{M_{\text{Pl}}^2} \left[\frac{2\mathcal{H}^2\phi'^2}{\mathcal{H}' - \mathcal{H}^2} - \frac{2V_\phi\phi'a^2}{3\mathcal{H}} - \frac{2\phi'^2}{3} - \frac{V_{\phi\phi}\phi'^2a^2}{\mathcal{H}' - \mathcal{H}^2} - \frac{2\phi'^2(\mathcal{H}' - \mathcal{H}^2)}{3\mathcal{H}^2} \right] \right. \\
&\quad \left. + \frac{1}{M_{\text{Pl}}^4} \left[\frac{\phi'^4}{3\mathcal{H}^2} - \frac{2V_\phi\phi'^3a^2}{3\mathcal{H}(\mathcal{H}' - \mathcal{H}^2)} - \frac{2\phi'^4}{3(\mathcal{H}' - \mathcal{H}^2)} \right] \right\} \mathcal{S}_k \\
&= \frac{\sqrt{U_0}\chi'^4\phi'}{M_{\text{Pl}}^2(\mathcal{H}' - \mathcal{H}^2)} \left(\frac{\mathcal{H}' - \mathcal{H}^2}{a\mathcal{H}} - \frac{\mathcal{H}}{a} - \frac{aV_\phi}{\phi'} - \frac{\phi'^2}{3M_{\text{Pl}}^2a\mathcal{H}} \right) \mathcal{R}_k' \\
&\quad + \frac{\sqrt{U_0}\chi'^4\phi'}{3aM_{\text{Pl}}^2(\mathcal{H}' - \mathcal{H}^2)} k^2 \mathcal{R}_k. \quad (3.53b)
\end{aligned}$$

We should stress here that these equations apply to the two-field model described by the action (3.15). For the specific bouncing scenario of our interest characterized by the scale factor (3.1), these equations simplify to be

$$\begin{aligned}
\mathcal{R}_k'' &+ \frac{2(7 + 9k_0^2\eta^2 - 6k_0^4\eta^4)}{\eta(1 - 3k_0^2\eta^2)(1 + k_0^2\eta^2)} \mathcal{R}_k' - \frac{k^2(5 + 9k_0^2\eta^2)}{3(1 - 3k_0^2\eta^2)} \mathcal{R}_k \\
&= \frac{4(5 + 12k_0^2\eta^2)}{\sqrt{3}\eta(1 - 3k_0^2\eta^2)\sqrt{1 + k_0^2\eta^2}} \mathcal{S}_k'
\end{aligned}$$

$$- \frac{4 \left[5 - 22 k_0^2 \eta^2 - 24 k_0^4 \eta^4 + k^2 \eta^2 (1 + k_0^2 \eta^2)^2 \right]}{\sqrt{3} \eta^2 (1 + k_0^2 \eta^2)^{3/2} (1 - 3 k_0^2 \eta^2)} \mathcal{S}_k, \quad (3.54a)$$

$$\begin{aligned} \mathcal{S}_k'' &= \frac{2 (9 + 7 k_0^2 \eta^2 + 6 k_0^4 \eta^4)}{\eta (1 - 3 k_0^2 \eta^2) (1 + k_0^2 \eta^2)} \mathcal{S}_k' \\ &+ \frac{18 - 85 k_0^2 \eta^2 - 25 k_0^4 \eta^4 - 6 k_0^6 \eta^6 + k^2 \eta^2 (3 - k_0^2 \eta^2) (1 + k_0^2 \eta^2)^2}{\eta^2 (1 - 3 k_0^2 \eta^2) (1 + k_0^2 \eta^2)^2} \mathcal{S}_k \\ &= - \frac{4 \sqrt{3} (3 - 2 k_0^2 \eta^2)}{\eta \sqrt{1 + k_0^2 \eta^2} (1 - 3 k_0^2 \eta^2)} \mathcal{R}_k' + \frac{4 k^2 \sqrt{1 + k_0^2 \eta^2}}{\sqrt{3} (1 - 3 k_0^2 \eta^2)} \mathcal{R}_k. \end{aligned} \quad (3.54b)$$

Note that the denominators of some of the coefficients in these equations contain either a factor of η or $(1 - 3 k_0^2 \eta^2)$. Therefore, as one approaches the bounce during the contracting phase, the coefficients will first diverge at $-\eta_*$ and then at the bounce. Later, after the bounce, they will also diverge at η_* , before we get to evaluate the power spectra. Due to this reason, the above equations do not permit us to evolve the quantities \mathcal{R}_k and \mathcal{S}_k across the bounce. This issue can be circumvented by working in a specific gauge and considering two other suitable quantities to characterize the perturbations whose governing equations remain well behaved around the bounce (see Ref. [12], in this context, also see Ref. [110]).

Another related point needs to be emphasized at this stage of our discussion. As we shall describe in some detail in the next section, the initial conditions on the perturbations need to be imposed at sufficiently early times when the modes are well inside the Hubble radius during the contracting phase. Moreover, in order to impose the standard initial conditions on the curvature and isocurvature perturbations, the modes need to be decoupled during these early times. It has been pointed out that a strong coupling between the two modes would not permit the imposition of standard, independent initial conditions on the modes (for a detailed discussion on this issue, see Ref. [111]). In due course, we shall discuss the specific initial conditions that we shall impose on the perturbations (see subsection 3.6.2). We ought to stress here that the equations (3.54) governing \mathcal{R}_k and \mathcal{S}_k indeed decouple at very early times, *i.e.* as $\eta \rightarrow -\infty$ [*cf.* equations (3.61) and

(3.62)]. We should highlight the fact that, in the next two sections, apart from the numerical solutions, we shall also construct analytical solutions, which we shall show match the numerical results very well.

3.5.5 Perturbations in a specific gauge

We now need to identify a suitable gauge wherein the perturbations can be evolved across the bounce without facing the difficulties mentioned above. We find that these difficulties can be avoided if we choose to work in the uniform- χ gauge [12]. In this gauge, the two independent scalar perturbations turn out to be the metric potentials A and ψ and, as we shall soon illustrate, these quantities can be smoothly evolved across the bounce. The curvature and the isocurvature perturbations can then be suitably constructed from these two scalar perturbations.

The uniform χ -gauge corresponds to the situation wherein $\delta\chi_k = 0$. In such a case, equation (3.35b) reduces to

$$\frac{k^2}{3a} \left(B_k - a \dot{E}_k \right) = \left(\dot{A}_k + \dot{\psi}_k \right). \quad (3.55)$$

Upon using this relation, the first order Einstein equations (3.32) and the background equations, we obtain the following equations governing A_k and ψ_k :

$$\begin{aligned} A_k'' + 4\mathcal{H} A_k' + \left[\frac{k^2}{3} - \left(6\mathcal{H}^2 - \frac{\phi'^2}{M_{\text{Pl}}^2} + \frac{2a^2 \mathcal{H} V_\phi}{\phi'} + \frac{2U_0 \chi'^4}{a^2 M_{\text{Pl}}^2} \right) \right] A_k \\ = \frac{2a^2 V_\phi}{\phi'} \psi_k' + \frac{4k^2}{3} \psi_k, \end{aligned} \quad (3.56a)$$

$$\begin{aligned} \psi_k'' + \left(2\mathcal{H} + \frac{2a^2 V_\phi}{\phi'} \right) \psi_k' + k^2 \psi_k = 2\mathcal{H} A_k' \\ - \left(6\mathcal{H}^2 - \frac{\phi'^2}{M_{\text{Pl}}^2} + \frac{2a^2 \mathcal{H} V_\phi}{\phi'} + \frac{2U_0 \chi'^4}{a^2 M_{\text{Pl}}^2} \right) A_k. \end{aligned} \quad (3.56b)$$

We should again mention that these equations correspond to the system described by the action (3.15). For the specific bouncing scenario that we are considering here, the above equations simplify to

$$A_k'' + 4 \mathcal{H} A_k' + \left(\frac{k^2}{3} - \frac{20 a_0^2 k_0^2}{a^2} \right) A_k = -3 \mathcal{H} \psi_k' + \frac{4 k^2}{3} \psi_k, \quad (3.57a)$$

$$\psi_k'' - \mathcal{H} \psi_k' + k^2 \psi_k = 2 \mathcal{H} A_k' - \frac{20 a_0^2 k_0^2}{a^2} A_k. \quad (3.57b)$$

In arriving at these two equations, we have made use of the relation: $\dot{\phi}^2/2 = V(\phi)$, which arises due to the fact that the field ϕ is pressureless. Note that, in the uniform χ -gauge, the curvature and isocurvature perturbations are given by

$$\mathcal{R}_k = \psi_k + \frac{2 H M_{\text{Pl}}^2}{\dot{\phi}^2 - U_0 \dot{\chi}^4} \left(\dot{\psi}_k + H A_k \right), \quad (3.58a)$$

$$\mathcal{S}_k = \frac{2 H M_{\text{Pl}}^2 \sqrt{U_0 \dot{\chi}^4}}{\left(\dot{\phi}^2 - U_0 \dot{\chi}^4 \right) \dot{\phi}} \left(\dot{\psi}_k + H A_k \right). \quad (3.58b)$$

Later, we shall make use of these relations to construct \mathcal{R}_k and \mathcal{S}_k from A_k and ψ_k around the bounce.

3.6 Evolution of the scalar perturbations

Let us now turn to solving the equations governing the scalar perturbations numerically. Since we have analytical solutions to describe the behavior of the background quantities, we need to develop the numerical procedure only for the evolution of the perturbations. Our main aim is to evaluate the scalar power spectra after the bounce, which, obviously, requires us to evolve the perturbations across the bounce. In the case of tensors, we could evolve the perturbations smoothly across the bounce and evaluate the corresponding power spectrum at a suitable time after the bounce. However, in the case of scalars, as we have described

above, it does not seem possible to integrate the equations describing the curvature and the isocurvature perturbations across the bounce due to the presence of diverging coefficients. We shall hence choose to evolve the metric perturbations A_k and ψ_k across the bounce, since the equations governing them are devoid of such divergent terms. Once we have evolved A_k and ψ_k across the bounce, we shall reconstruct the curvature and the isocurvature perturbations \mathcal{R}_k and \mathcal{S}_k from these quantities to arrive at the power spectra.

Recall that, in the case of tensors, when evaluating the perturbations *analytically*, we had divided the period of our interest—*i.e.* from very early times during the contracting phase to a suitable time immediately after the bounce — into two domains, *viz.* $-\infty < \eta \leq -\alpha \eta_0$ and $-\alpha \eta_0 \leq \eta \leq \beta \eta_0$, where we had set $\alpha = 10^5$ and $\beta = 10^2$. In the case of scalars, we shall work over these two domains to evolve the perturbations *analytically as well as numerically*. In the first domain, we shall identify the Mukhanov-Sasaki variables associated with the perturbations \mathcal{R}_k and \mathcal{S}_k and impose the corresponding Bunch-Davies initial conditions on these variables at suitably early times. We shall evolve the perturbations \mathcal{R}_k and \mathcal{S}_k using the governing equations (3.54) until $\eta = -\alpha \eta_0$. At $\eta = -\alpha \eta_0$, we shall match the quantities \mathcal{R}_k and \mathcal{S}_k (and their time derivatives) to the metric perturbations A_k and ψ_k (and their time derivatives) using the relations (3.58). Thereafter, we shall evolve the perturbations A_k and ψ_k [using equations (3.57)] until $\eta = \beta \eta_0$ after the bounce. Once we have evolved A_k and ψ_k across the bounce, we can reconstruct the quantities \mathcal{R}_k and \mathcal{S}_k [using equations (3.58)] and also, eventually, evaluate their power spectra.

3.6.1 Equations in terms of e-N-folds

As in the case of tensors, we shall numerically integrate the equations with e-N-folds as the independent variable. We need to numerically integrate the equations governing the evolution of the quantities \mathcal{R}_k , \mathcal{S}_k , ψ_k and A_k . In terms of the variable e-N-folds, equations (3.54) can be written as

$$\begin{aligned} \frac{d^2 \mathcal{R}_k}{d\mathcal{N}^2} &+ \left[\mathcal{N} + \frac{1}{H} \frac{dH}{d\mathcal{N}} - \frac{1}{\mathcal{N}} + \frac{2a_0 \mathcal{N}}{a^2 H \eta} \left(\frac{7 + 9k_0^2 \eta^2 - 6k_0^4 \eta^4}{1 - 3k_0^2 \eta^2} \right) \right] \frac{d\mathcal{R}_k}{d\mathcal{N}} \\ &- \frac{k^2 \mathcal{N}^2}{3a^2 H^2} \left(\frac{5 + 9k_0^2 \eta^2}{1 - 3k_0^2 \eta^2} \right) \mathcal{R}_k \\ &= \frac{4a_0^{1/2} \mathcal{N}}{\sqrt{3} a^{3/2} H \eta} \left(\frac{5 + 12k_0^2 \eta^2}{1 - 3k_0^2 \eta^2} \right) \frac{d\mathcal{S}_k}{d\mathcal{N}} \\ &- \frac{4\mathcal{N}^2 a_0^{3/2}}{\sqrt{3} a^{7/2} H^2 \eta^2} \left[\frac{5 - 22k_0^2 \eta^2 - 24k_0^4 \eta^4 + k^2 \eta^2 (a/a_0)^2}{1 - 3k_0^2 \eta^2} \right] \mathcal{S}_k, \quad (3.59a) \end{aligned}$$

$$\begin{aligned} \frac{d^2 \mathcal{S}_k}{d\mathcal{N}^2} &+ \left[\mathcal{N} + \frac{1}{H} \frac{dH}{d\mathcal{N}} - \frac{1}{\mathcal{N}} - \frac{2a_0 \mathcal{N}}{a^2 H \eta} \left(\frac{9 + 7k_0^2 \eta^2 + 6k_0^4 \eta^4}{1 - 3k_0^2 \eta^2} \right) \right] \frac{d\mathcal{S}_k}{d\mathcal{N}} \\ &+ \frac{a_0^2 \mathcal{N}^2}{a^4 H^2 \eta^2} \\ &\times \left(\frac{18 - 85k_0^2 \eta^2 - 25k_0^4 \eta^4 - 6k_0^6 \eta^6 + k^2 \eta^2 (3 - k_0^2 \eta^2) (a/a_0)^2}{1 - 3k_0^2 \eta^2} \right) \mathcal{S}_k \\ &= - \frac{4\sqrt{3} a_0^{1/2} \mathcal{N}}{a^{3/2} H \eta} \left(\frac{3 - 2k_0^2 \eta^2}{1 - 3k_0^2 \eta^2} \right) \frac{d\mathcal{R}_k}{d\mathcal{N}} \\ &+ \frac{4k^2 \mathcal{N}^2}{\sqrt{3} a_0^{1/2} a^{3/2} H^2} \left(\frac{1}{1 - 3k_0^2 \eta^2} \right) \mathcal{R}_k. \quad (3.59b) \end{aligned}$$

Similarly, we find that equations (3.57) can be expressed as

$$\begin{aligned} \frac{d^2 A_k}{d\mathcal{N}^2} &+ \left(5\mathcal{N} + \frac{1}{H} \frac{dH}{d\mathcal{N}} - \frac{1}{\mathcal{N}} \right) \frac{dA_k}{d\mathcal{N}} + \left(\frac{k^2 \mathcal{N}^2}{3a^2 H^2} - \frac{20a_0^2 \mathcal{N}^2 k_0^2}{a^4 H^2} \right) A_k \\ &= -3\mathcal{N} \frac{d\psi_k}{d\mathcal{N}} + \frac{4k^2 \mathcal{N}^2}{3a^2 H^2} \psi_k, \quad (3.60a) \end{aligned}$$

$$\begin{aligned} \frac{d^2 \psi_k}{d\mathcal{N}^2} &+ \left(\frac{1}{H} \frac{dH}{d\mathcal{N}} - \frac{1}{\mathcal{N}} \right) \frac{d\psi_k}{d\mathcal{N}} + \frac{k^2 \mathcal{N}^2}{a^2 H^2} \psi_k \\ &= 2\mathcal{N} \frac{dA_k}{d\mathcal{N}} - \frac{20a_0^2 \mathcal{N}^2 k_0^2}{a^4 H^2} A_k. \quad (3.60b) \end{aligned}$$

In the above equations, to avoid rather lengthy and cumbersome expressions, we have not attempted to express the coefficients involving the conformal time coordinate in terms of e-N-folds.

3.6.2 Initial conditions and power spectra

Let us now understand the initial conditions that need to be imposed on the scalar perturbations. Note that, at very early times during the contracting phase, the energy density of the canonical scalar field ϕ dominates the energy density of the non-canonical field χ . In inflationary scenarios driven by two fields, it is well known that, when the background is largely driven by one of the two fields, the isocurvature perturbation can be neglected [10]. This seems to suggest that we can ignore the effect of the isocurvature perturbation on the curvature perturbation at early times. In such a case, we find that the equation (3.54a) governing the curvature perturbation simplifies to be

$$\mathcal{R}'_k + 2 \frac{z'}{z} \mathcal{R}'_k + k^2 \mathcal{R}_k \simeq 0, \quad (3.61)$$

where $z \simeq a \dot{\phi}/H$, which simplifies to $z \simeq \sqrt{3} M_{\text{pl}} a$ in the particular matter bounce scenario that we are considering.

In an expanding universe, we can expect the isocurvature perturbations to decay and, hence, they are not expected to play a significant role at late times. However, since perturbations can grow in a contracting universe, the effect of the isocurvature perturbations may not be negligible as one approaches the bounce. Therefore, though the effects of the isocurvature perturbations may be insignificant at early times, their contribution may need to be accounted for as one approaches the bounce, particularly when the energy density of the second field χ becomes comparable to the energy density of the ϕ field. At early times, we find that the

curvature and the isocurvature perturbations decouple, and the equation (3.54b) describing the isocurvature perturbation simplifies to

$$\mathcal{S}_k'' + 2 \frac{z'}{z} \mathcal{S}_k' + \left(\frac{k^2}{3} + \frac{\phi'^2}{6 M_{\text{Pl}}^2} \right) \mathcal{S}_k \simeq 0. \quad (3.62)$$

Let us define the Mukhanov-Sasaki variable corresponding to the perturbations \mathcal{R}_k and \mathcal{S}_k to be $v_k^\sigma = z \mathcal{R}_k$ and $v_k^s = z \mathcal{S}_k$, where $z = a \dot{\phi}/H$. In terms of these variables, in the matter bounce scenario of our interest, the above two decoupled equations for \mathcal{R}_k and \mathcal{S}_k reduce to

$$v_k^{\sigma''} + \left(k^2 - \frac{2}{\eta^2} \right) v_k^\sigma \simeq 0, \quad (3.63a)$$

$$v_k^{s''} + \frac{k^2}{3} v_k^s \simeq 0. \quad (3.63b)$$

It is useful to note that, in the matter dominated phase, the mode v_k^σ behaves exactly as the Mukhanov-Sasaki variable u_k corresponding to the tensor perturbation. At very early times, *i.e.* when $k^2 \gg 2/\eta^2$, we can impose the following Bunch-Davies initial conditions on these variables:

$$v_k^\sigma(\eta) = \frac{1}{\sqrt{2} k} e^{-ik\eta}, \quad (3.64a)$$

$$v_k^s(\eta) = \frac{3^{1/4}}{\sqrt{2} k} e^{-ik\eta/\sqrt{3}}. \quad (3.64b)$$

These initial conditions can evidently be translated to the corresponding initial conditions on \mathcal{R}_k and \mathcal{S}_k and their derivatives with respect to the e-N-fold.

During early times, when the initial conditions are imposed, the curvature and the isocurvature perturbations are considered to be statistically independent quantities. Therefore, as is usually done in the case of two-field models, we shall numerically integrate the equations (3.59) using two sets of initial conditions (in

this context, see, for instance, Refs. [11]). In the first case, we perform the integration by imposing the Bunch-Davies initial condition corresponding to (3.64a) on \mathcal{R}_k and setting the initial value of \mathcal{S}_k to be zero. While, in the second case, we impose the initial condition corresponding to (3.64b) on \mathcal{S}_k and set the initial value of \mathcal{R}_k to be zero. Let us denote the perturbations \mathcal{R}_k and \mathcal{S}_k evolved according to these two sets of initial conditions to be $(\mathcal{R}_k^{\text{I}}, \mathcal{S}_k^{\text{I}})$ and $(\mathcal{R}_k^{\text{II}}, \mathcal{S}_k^{\text{II}})$, respectively. Then, the power spectra associated with the curvature and the isocurvature perturbations can be defined as [11]

$$\mathcal{P}_{\mathcal{R}}(k) = \frac{k^3}{2\pi^2} \left(|\mathcal{R}_k^{\text{I}}|^2 + |\mathcal{R}_k^{\text{II}}|^2 \right), \quad (3.65a)$$

$$\mathcal{P}_{\mathcal{S}}(k) = \frac{k^3}{2\pi^2} \left(|\mathcal{S}_k^{\text{I}}|^2 + |\mathcal{S}_k^{\text{II}}|^2 \right). \quad (3.65b)$$

3.6.3 Evolution of the perturbations

We impose the initial conditions as we have described above when $k^2 = 10^4 (a''/a)^3$. We integrate the equations (3.59) governing \mathcal{R}_k and \mathcal{S}_k from this initial time up to $\eta = -\alpha \eta_0$, where, as before, we shall set $\alpha = 10^5$ (which corresponds to an e-N-fold of about $\mathcal{N} \simeq -6.79$). As in the case of tensors, we carry out the numerical integration using a fifth order Runge-Kutta algorithm. Having integrated for \mathcal{R}_k and \mathcal{S}_k until $\mathcal{N} = -6.79$, we evaluate the values of A_k and ψ_k (and their derivatives) at this time by inverting the relations (3.58). Using these as initial conditions, we integrate the equations (3.60) across the bounce until $\eta = \beta \eta_0$, with $\beta = 10^2$, which corresponds to $\mathcal{N} = 4.3$. We then reconstruct the evolution of \mathcal{R}_k and \mathcal{S}_k across the bounce using the relations (3.58). In figure 3.3, we have plotted the evolution of curvature perturbation $(\mathcal{R}_k^{\text{I}}, \mathcal{R}_k^{\text{II}})$ and the isocurvature perturbation $(\mathcal{S}_k^{\text{I}}, \mathcal{S}_k^{\text{II}})$, arrived at numerically for a specific wavenumber

³Note that, at early times, since $z \propto a$, $z''/z = a''/a$. This behavior is indeed expected when the scale factor is described by a power law.

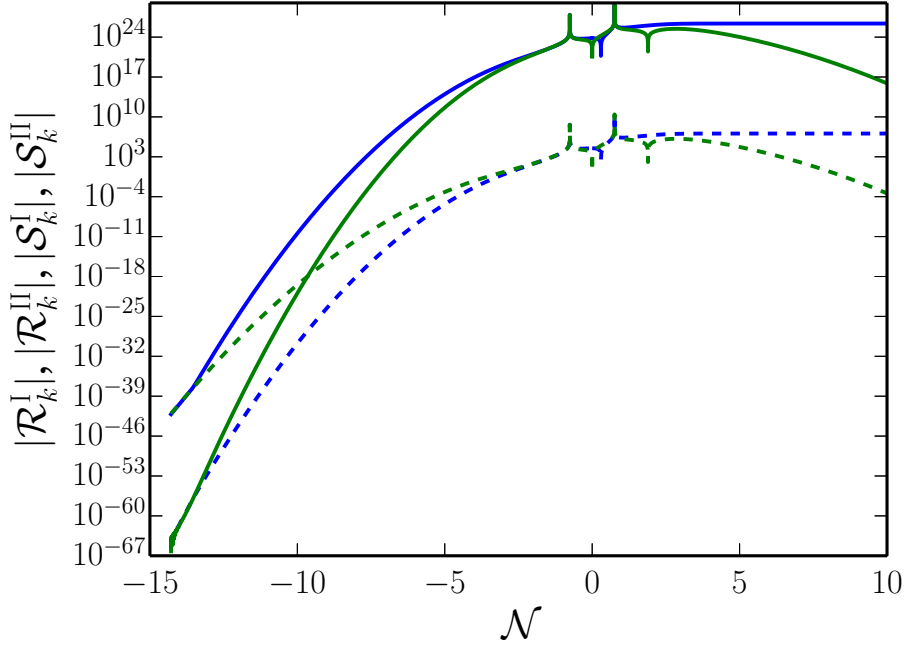


Figure 3.3: The numerical results for the amplitudes of the curvature (in blue, with \mathcal{R}_k^I as solid and \mathcal{R}_k^{II} as dashed) and the isocurvature (in green, with \mathcal{S}_k^I as solid and \mathcal{S}_k^{II} as dashed) perturbations evolved with different sets of initial conditions have been plotted as a function of e-N-folds for $k/k_0 = 10^{-20}$. As in figure 3.1, we have set $k_0 = M_{\text{Pl}}$ and $a_0 = 3 \times 10^7$, corresponding to $k_0/(a_0 M_{\text{Pl}}) = 3.3 \times 10^{-8}$ which, as we shall see, leads to a scale-invariant scalar power spectrum whose amplitude matches COBE normalization [112]. We have plotted the results from the initial e-N-fold \mathcal{N}_i [when $k^2 = 10^4 (a''/a)$] corresponding to the mode. Note that the amplitudes of \mathcal{R}_k^I and \mathcal{S}_k^I are dominant (at suitably late times) when compared to that of \mathcal{R}_k^{II} and \mathcal{S}_k^{II} , respectively. Also, the curvature perturbation behaves largely in a fashion similar to the tensor perturbation [*cf.* figure 3.1]. The upward and downward spikes in the plots correspond to points in time where the perturbations diverge and vanish, respectively. As we had expected, both the curvature and the isocurvature perturbations diverge at $\eta = \mp\eta_*$. However, it is only the isocurvature perturbation that vanishes at the bounce. The curvature perturbation actually goes to zero soon after the bounce (during $0 < \eta < \eta_*$), which in turn leads to the vanishing of the isocurvature perturbation a little time later (soon after $\eta = \eta_*$). While the curvature perturbation is largely constant (after $\eta = \eta_*$) during the expanding phase, the isocurvature perturbation begins to decay.

which corresponds to cosmological scales today.

There are a few points that need to be emphasized concerning the results we have obtained. As we have discussed earlier, the curvature and the isocurvature perturbations are expected to diverge at $\eta = \mp\eta_*$, and it is clear from figure 3.3

that they indeed do so. Moreover, the isocurvature perturbation vanishes at the bounce, as expected. In contrast, we find that the curvature perturbation does not vanish at the bounce as one may naively guess, but does so a little time after the bounce. This behavior seems to be responsible for the isocurvature perturbation too to vanish a little time later. Note that, as in the case of tensors, the amplitude of the curvature perturbation almost freezes at suitably late times (in fact, after $\eta = \eta_*$) during the expanding phase. During the period, the isocurvature perturbations begin to decay. As we shall illustrate later, this leads to a strongly adiabatic scalar power spectrum, with the amplitude of the isocurvature perturbations being much smaller than the curvature perturbations.

3.7 Analytical arguments

In this section, we shall arrive at analytical solutions for the curvature and isocurvature perturbations for scales of cosmological interest under well-motivated approximations. We shall again divide the period of interest into two domains, as we have discussed already. Let us go on to construct the solutions to the equations governing the scalar perturbations in the two domains.

3.7.1 Solutions in the first domain

As we have discussed before, at early times during the matter dominated contraction, we can assume that the equations governing the evolution of the curvature and the isocurvature perturbations are decoupled. We had mentioned earlier that, during this phase, the mode v_k^σ is expected to behave exactly like the Mukhanov-Sasaki variable u_k associated with the tensor mode. This is not surprising since such a behavior is well known in power law expansion and, hence,

can be expected in power law contraction as well. Using the Bunch-Davies initial condition (3.64a), during sufficiently early times, the solution to equation (3.61) can be obtained to be

$$\mathcal{R}_k(\eta) \simeq \frac{1}{\sqrt{6} k M_{\text{Pl}} a_0 k_0^2 \eta^2} \left(1 - \frac{i}{k \eta} \right) e^{-i k \eta}, \quad (3.66)$$

which, it should be emphasized, is the same as the solution (3.4) for the tensor mode apart from an overall constant.

Obtaining the solution to the isocurvature perturbation requires a little more care. In arriving at the equation (3.63b) governing the Mukhanov-Sasaki variable associated with the isocurvature perturbation, we had completely ignored the role of the curvature perturbation. While this seems acceptable for determining the initial condition, we find that the effect of the curvature perturbation needs to be accounted for, in order to achieve a better approximation. During the first domain, upon using the expression (3.66) for \mathcal{R}_k , we find that the solution to equation (3.54b) can be obtained to be [113]

$$\mathcal{S}_k(\eta) \simeq \frac{1}{9 \sqrt{2} k^3 a_0 k_0^3 M_{\text{Pl}} \eta^4} \left(-12 i (1 + i k \eta) e^{-i k \eta} + \frac{9}{3^{1/4}} k k_0 \eta^2 e^{-i k \eta / \sqrt{3}} + 4 k^2 \eta^2 e^{-i k \eta / \sqrt{3}} \left\{ \pi + i \text{Ei} \left[e^{-i(3-\sqrt{3})k\eta/3} \right] \right\} \right), \quad (3.67)$$

where $\text{Ei}[z]$ is the exponential integral function (see, for instance, Ref. [114]). It is straightforward to check that, at early times, it is the second term in the above expression which survives, which exactly corresponds to the initial condition (3.64b).

3.7.2 Solutions in the second domain

As we have discussed, in the second domain (*i.e.* over the period $-\alpha \eta_0 \leq \eta \leq \beta \eta_0$), we shall solve for the metric perturbations A_k and ψ_k . In this domain, for scales of cosmological interest, we can ignore the k -dependent terms in equations (3.57). Under this condition, the two equations can be combined to obtain that

$$(A_k + \psi_k)'' + 2\mathcal{H}(A_k + \psi_k)' \simeq 0, \quad (3.68)$$

which is exactly the equation for the tensor mode h_k that we had arrived in this domain [*cf.* equation (3.5)]. This equation can be integrated once to yield

$$(A_k + \psi_k)' \simeq \frac{k_0 \mathcal{C}_k}{a^2}. \quad (3.69)$$

with \mathcal{C}_k being a constant of integration. Upon further integration, we obtain that

$$A_k(\eta) + \psi_k(\eta) \simeq \frac{\mathcal{C}_k}{2a_0^2} f(k_0 \eta) + \mathcal{D}_k, \quad (3.70)$$

where the function f is given by equation (3.8) and \mathcal{D}_k is a second constant of integration. Upon substituting this result in equation (3.57a), we can arrive at an equation governing A_k . On solving the resulting differential equation (say, using Mathematica [113]), we find that the solution for A_k is given by

$$A_k(\eta) \simeq \frac{\mathcal{C}_k k_0 \eta}{4a_0^2 (1 + k_0^2 \eta^2)} + \mathcal{E}_k e^{-2\sqrt{5} \tan^{-1}(k_0 \eta)} + \mathcal{F}_k e^{2\sqrt{5} \tan^{-1}(k_0 \eta)}, \quad (3.71)$$

where \mathcal{E}_k and \mathcal{F}_k denote two additional constants of integration. The corresponding solution for ψ_k can be obtained by substituting this result in equation (3.70).

Having obtained the solutions for A_k and ψ_k , we can now reconstruct the curvature and the isocurvature perturbations \mathcal{R}_k and \mathcal{S}_k using equations (3.58). We

find that, in the second domain, \mathcal{R}_k and \mathcal{S}_k are given by

$$\begin{aligned} \mathcal{R}_k(\eta) \simeq & \frac{-1}{2 a_0^2 (1 - 2 k_0^2 \eta^2 - 3 k_0^4 \eta^4)} \left(\mathcal{C}_k \left[(1 + 3 k_0^2 \eta^2) k_0 \eta \right. \right. \\ & \left. \left. - (1 - 2 k_0^2 \eta^2 - 3 k_0^4 \eta^4) \tan^{-1}(k_0 \eta) \right] \right. \\ & - 2 a_0^2 (1 + k_0^2 \eta^2) \left[\mathcal{D}_k (1 - 3 k_0^2 \eta^2) \right. \\ & - \mathcal{E}_k \left(1 + 2 \sqrt{5} k_0 \eta - k_0^2 \eta^2 \right) e^{-2 \sqrt{5} \tan^{-1}(k_0 \eta)} \\ & \left. \left. - \mathcal{F}_k \left(1 - 2 \sqrt{5} k_0 \eta - k_0^2 \eta^2 \right) e^{2 \sqrt{5} \tan^{-1}(k_0 \eta)} \right] \right), \end{aligned} \quad (3.72a)$$

$$\begin{aligned} \mathcal{S}_k(\eta) \simeq & \frac{-k_0 \eta}{2 \sqrt{3} a_0^2 (1 + k_0^2 \eta^2)^{1/2} (1 - 3 k_0^2 \eta^2)} \left\{ 3 \mathcal{C}_k \right. \\ & + 8 a_0^2 \left[\mathcal{E}_k \left(\sqrt{5} + k_0 \eta \right) e^{-2 \sqrt{5} \tan^{-1}(k_0 \eta)} \right. \\ & \left. \left. - \mathcal{F}_k \left(\sqrt{5} - k_0 \eta \right) e^{2 \sqrt{5} \tan^{-1}(k_0 \eta)} \right] \right\}. \end{aligned} \quad (3.72b)$$

The four constants \mathcal{C}_k , \mathcal{D}_k , \mathcal{E}_k and \mathcal{F}_k can be determined by matching these solutions with the solutions for \mathcal{R}_k and \mathcal{S}_k we had obtained in the first domain at $\eta = -\alpha \eta_0$. The expressions describing the constants are long and cumbersome and, hence, we relegate the details to an appendix (see appendix A).

3.7.3 Comparison with the numerical results

Let us now compare the above analytical results for \mathcal{R}_k and \mathcal{S}_k with the numerical results. Recall that, numerically, we had obtained two sets of solutions for \mathcal{R}_k and \mathcal{S}_k , *viz.* $(\mathcal{R}_k^I, \mathcal{S}_k^I)$ and $(\mathcal{R}_k^{II}, \mathcal{S}_k^{II})$, corresponding to two different sets of initial conditions. In contrast, while arriving at the analytical results, for convenience, we have imposed the Bunch-Davies initial on both \mathcal{R}_k and \mathcal{S}_k simultaneously. We shall compare the amplitudes of \mathcal{R}_k and \mathcal{S}_k obtained analytically with the amplitudes $\mathcal{R}_k^I + \mathcal{R}_k^{II}$ and $\mathcal{S}_k^I + \mathcal{S}_k^{II}$ arrived at numerically. (Recall that, the amplitudes of

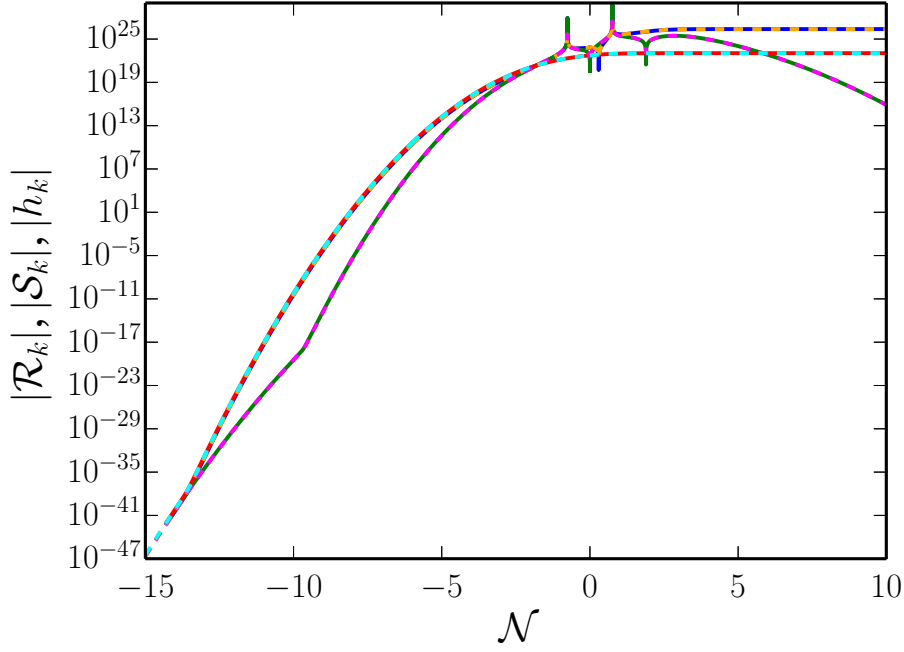


Figure 3.4: A comparison of the numerical results (solid lines) with the analytical results (dashed lines) for the amplitude of the curvature perturbation \mathcal{R}_k (blue solid line and orange dashed line), the isocurvature perturbation \mathcal{S}_k (green solid line and magenta dashed line) and the tensor mode h_k (red solid line and cyan dashed line) corresponding to the wavenumber $k/k_0 = 10^{-20}$. As earlier, we have set $k_0 = M_{\text{pl}}$ and $a_0 = 3 \times 10^7$, corresponding to $k_0/(a_0 M_{\text{pl}}) = 3.3 \times 10^{-8}$ and, for plotting the analytical results, we have chosen $\alpha = 10^5$. We have plotted the numerical results from the initial e-N-fold \mathcal{N}_i [when $k^2 = 10^4 (a''/a)$] corresponding to the mode. Evidently, the analytical and numerical results match extremely well, suggesting that the analytical approximation for the modes works to a very good accuracy. Notice that, around the bounce, the amplitude of the scalar perturbations are enhanced by a few orders of magnitude more than that of the tensor perturbations. It is this feature, which is obviously a result of the specific behavior of the background near the bounce, that leads to a viable tensor-to-scalar ratio.

\mathcal{R}_k^{I} and \mathcal{S}_k^{I} had dominated those of $\mathcal{R}_k^{\text{II}}$ and $\mathcal{S}_k^{\text{II}}$, respectively.) In figures 3.4 and 3.5, we have plotted the analytical and the numerical results for wavenumbers such that $k/k_0 = 10^{-20}$ and $k/k_0 = 10^{-25}$, respectively. As is evident from the figures, the analytical results match the numerical results very well. In fact, we find the difference between the analytical and numerical results to be less than 2%.

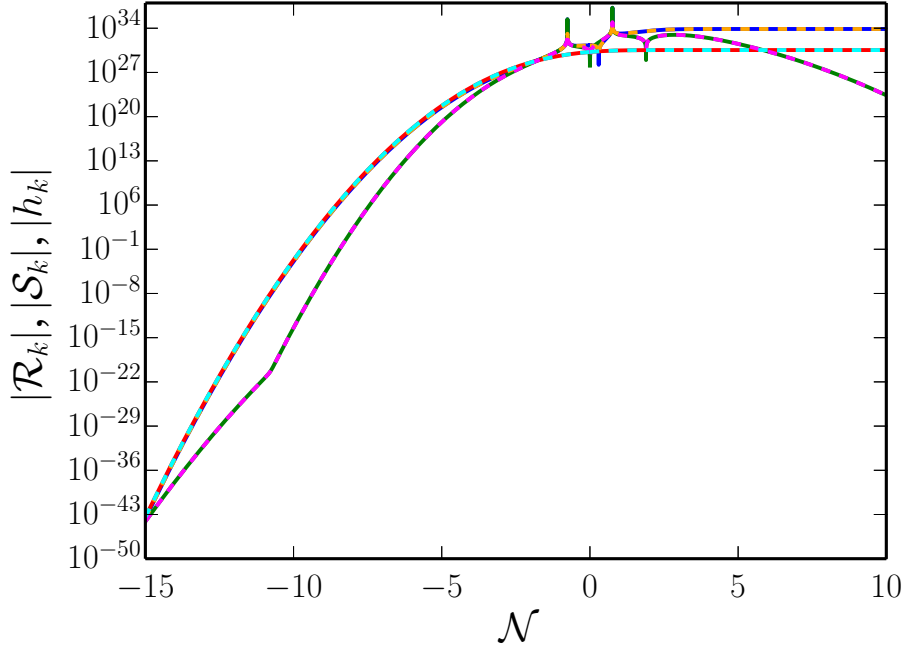


Figure 3.5: The plots as in the previous figure for the wavenumber $k/k_0 = 10^{-25}$. Clearly, the analytical results are in good agreement with the numerical results.

3.8 The scalar power spectra and the tensor-to-scalar ratio

With the analytical and the numerical results at hand, let us now go on to evaluate the scalar power spectra and the tensor-to-scalar ratio. In order to understand the effects of the bounce on these quantities, let us evaluate the scalar and tensor power spectra before as well as after the bounce.

Let us first consider the numerical results, which are exhibited in figure 3.6. All the power spectra are strictly scale-invariant (over scales of cosmological interest) before as well as after the bounce. The power spectra before the bounce have been evaluated at $\eta = -\alpha \eta_0$, with $\alpha = 10^5$, which, as we had mentioned, corresponds to $\mathcal{N} = -6.79$. The power spectra after the bounce have been evaluated at $\eta = \beta \eta_0$, with $\beta = 10^2$, which, recall that, corresponds to $\mathcal{N} = 4.3$. Since the scales of

cosmological interest are much smaller than the scale associated with the bounce, the shapes of the power spectra are indeed expected to remain unaffected by the bounce. While a bounce generically enhances the amplitude of the perturbations, the scalar and tensor perturbations can be expected to be amplified by different amounts, depending on the behavior of the background close to the bounce. Note that, in the scenario of our interest, the tensor-to-scalar ratio is rather large before the bounce. In fact, the tensor-to-scalar ratio well before the bounce proves to be of the order of $\mathcal{O}(24)$, a result that is well known in the literature (see, for instance, Ref. [12]). As we had pointed out, in our case, the bounce amplifies the scalar perturbations much more than the tensor perturbations [*cf.* figures 3.4 and 3.5]. In other words, the bounce suppresses the tensor-to-scalar ratio. Recall that, the only parameter that occurs in our model is the combination k_0/a_0 . We find that, for a choice of k_0/a_0 that leads to a COBE normalized scalar power spectrum after the bounce, *i.e.* $\mathcal{P}_{\mathcal{R}}(k) \simeq 2.31 \times 10^{-9}$ [112], the corresponding tensor-to-scalar ratio proves to be much smaller than the current upper bound of $r \leq 0.07$ from Planck [7]. It is also useful to note that isocurvature perturbations, while they grow across the bounce, begin to decay at late times (actually, after $\eta > \eta_*$). At a sufficiently late time when we evaluate the power spectra, their amplitude proves to be about four orders of magnitude smaller than the amplitude of the curvature perturbation. This suggests that the power spectrum is strongly adiabatic, which is also consistent with the recent observations [7].

Let us now evaluate the scalar power spectra analytically after the bounce. At a sufficiently late time after the bounce (say, when $\eta \gg \eta_*$), we find that the curvature perturbation turns almost a constant [*cf.* equation (3.72a)], and is given by

$$\mathcal{R}_k(\eta) \simeq \mathcal{C}_k \frac{\pi}{4 a_0^2} - \mathcal{E}_k \frac{e^{-\sqrt{5}\pi}}{3} - \mathcal{F}_k \frac{e^{\sqrt{5}\pi}}{3} + \mathcal{D}_k. \quad (3.73)$$

We have plotted the power spectrum associated with this curvature perturbation

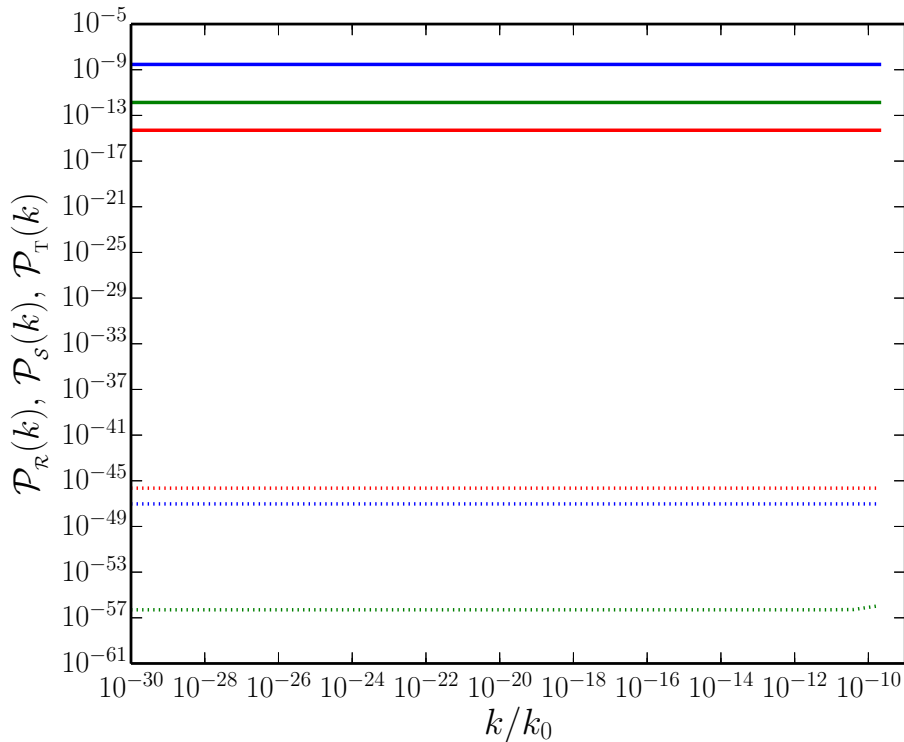


Figure 3.6: The numerically evaluated scalar (the curvature perturbation spectrum in blue and the isocurvature perturbation spectrum in green) and tensor power spectra (in red) have been plotted as a function of k/k_0 for a wide range of wavenumbers. The power spectra have been plotted both before the bounce (as dotted lines) and after (as solid lines). The power spectra have been evaluated at $\eta = -\alpha \eta_0$ (with $\alpha = 10^5$) before the bounce and at $\eta = \beta \eta_0$ (with $\beta = 10^2$) after the bounce. In plotting the figure, we have set $k_0/(a_0 M_{\text{Pl}}) = 3.3 \times 10^{-8}$, as in the previous figures. All the power spectra are evidently scale-invariant over scales of cosmological interest. Also, the above choice of k_0/a_0 leads to a COBE normalized curvature perturbation spectrum. Moreover, the tensor-to-scalar ratio evaluated after the bounce proves to be rather small ($r \simeq 10^{-6}$), which is consistent with the current upper limits on the quantity.

in figure 3.7, which is very similar in shape to the analytical tensor power spectrum we had plotted earlier [*cf.* figure 3.2]. Note that our analytical approximations are valid only when $k \ll k_0/\alpha$, and the spectrum is indeed scale-invariant over this domain, reflecting the behavior obtained numerically. If we now assume that $k \ll k_0/\alpha$, we obtain the scale-invariant amplitude of the curvature

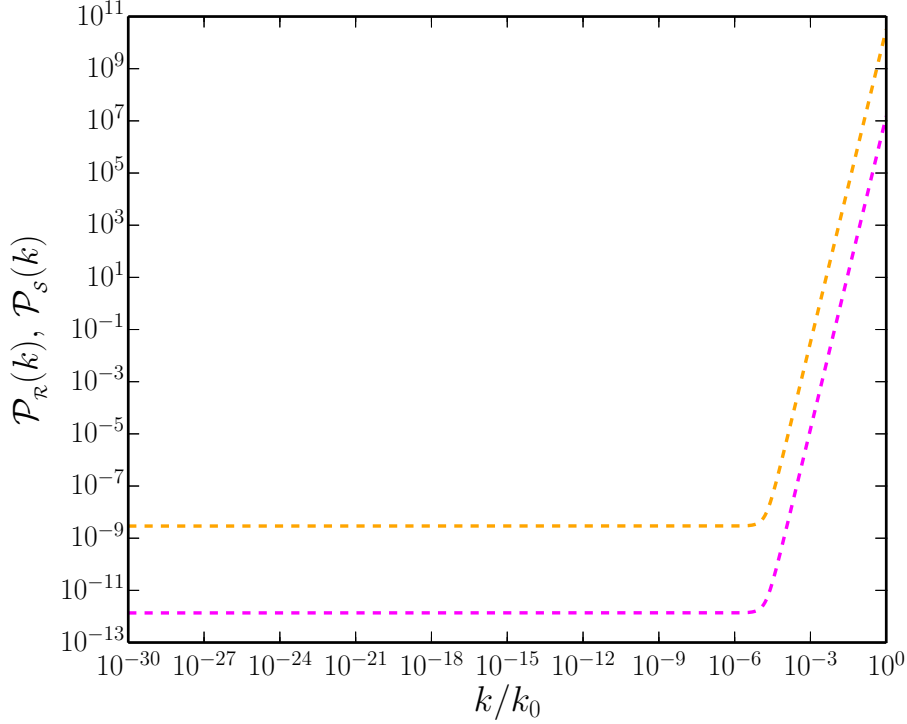


Figure 3.7: The curvature (in orange) and the isocurvature (in magenta) perturbation spectra evaluated analytically after the bounce. In plotting this figure, we have chosen the same values for the various parameters as in figure 3.2, wherein we had plotted the tensor power spectrum obtained analytically. As in the case of the tensor power spectrum, these analytical spectra are valid only for $k \ll k_0/\alpha$. We find that the scale-invariant amplitudes at such small wavenumbers match the numerical results presented in the previous figure very well.

perturbation spectrum to be

$$\mathcal{P}_R(k) \simeq \frac{k_0^2 e^{4\sqrt{5}\pi}}{61440 \pi^2 a_0^2 M_{\text{Pl}}^2}, \quad (3.74)$$

which we find matches the numerical result [of COBE normalized amplitude for $k_0/(a_0 M_{\text{Pl}}) = 3.3 \times 10^{-8}$] very well.

From the analytical and numerical results for the scalar and tensor modes, we can also understand the behavior of the tensor-to-scalar ratio across the bounce. In figure 3.8, we have plotted the evolution of the tensor-to-scalar $r_k = \mathcal{P}_T(k)/\mathcal{P}_R(k)$ for a mode with wavenumber $k/k_0 = 10^{-20}$. We have plotted the numerical as well as the analytical results in the figure. The numerical and the analytical re-

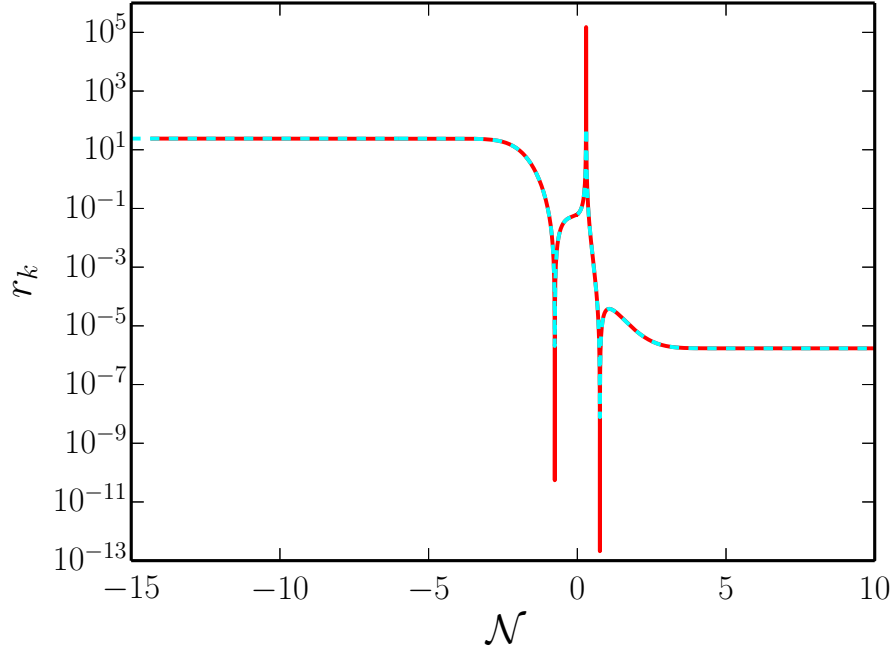


Figure 3.8: The tensor-to-scalar ratio calculated numerically (red solid line) and analytically (cyan dashed line) have been plotted as a function of \mathcal{N} for the wavenumber $k/k_0 = 10^{-20}$. The numerical and the analytical results agree well as expected. Note that the bounce suppresses the tensor-to-scalar ratio from a large value ($r_k \simeq 20$) to a rather small value ($r_k \simeq 10^{-6}$).

sults agree well with each other. Also, r_k vanishes (at $\eta = \mp\eta_*$) and diverges (during $0 < \eta < \eta_*$) exactly reflecting the behavior of the curvature perturbation (which diverges and vanishes at these points, respectively). Importantly, the bounce suppresses the tensor-to-scalar ratio from a large value ($r_k \simeq 20$) to a rather small value ($r_k \simeq 10^{-6}$) that is consistent with the current upper bounds. It is interesting to note that tensor-to-scalar ratio is a pure number and is actually independent of even the single parameter k_0/a_0 that characterizes our model [cf. equations (3.13) and (3.74)].

Our last task is to arrive at the isocurvature power spectrum analytically. At late times after the bounce (such that $\eta \gg \eta_*$), the behavior of the isocurvature perturbation can be shown to be [cf. equation (3.72b)]

$$\mathcal{S}_k(\eta) \simeq \frac{4 \mathcal{F}_k e^{\sqrt{5} \pi}}{3 \sqrt{3} k_0 \eta}. \quad (3.75)$$

Unlike the curvature perturbation, the isocurvature perturbation is not a constant in this domain, but decays with the expansion of the universe. This behavior is also evident from the numerical results [*cf.* figures 3.4 and 3.5]. For scales of cosmological interest such that $k \ll k_0/\alpha$, we find that the isocurvature perturbation spectrum, evaluated at $\eta = \beta \eta_0$, is given by

$$\mathcal{P}_s(k) \simeq \frac{k_0^2 e^{4\sqrt{5}\pi}}{11520 \beta^2 \pi^2 a_0^2 M_{\text{Pl}}^2}. \quad (3.76)$$

For the values of the parameters we have been working with, *viz.* $k_0/(a_0 M_{\text{Pl}}) = 3.3 \times 10^{-8}$ and $\beta = 10^2$, we find that the above analytical estimate agrees well with the numerical results we have obtained.

3.9 Discussion

One of the problems that had plagued completely symmetric bouncing scenarios is the fact that the tensor-to-scalar ratio in such models proves to be large, typically well beyond the current constraints from the cosmological data. In this work, we have constructed a two-field model consisting of a canonical scalar field and a non-canonical ghost field to drive a symmetric matter bounce and have studied the evolution of the scalar and tensor perturbations in the model. For a specific choice of the scale factor describing the matter bounce, we have been able to arrive at completely analytical solutions for all the background quantities. We find that the model we have constructed involves only one parameter, *viz.* the scale associated with the bounce determined by k_0/a_0 . Using the background solutions, we have numerically evolved the perturbations across the bounce and have evaluated the scalar and tensor power spectra after the bounce. In order to circumvent the issues confronting the evolution of the curvature and the isocurvature perturbations in a bouncing scenario, we have worked in a specific gauge

wherein the two independent scalar perturbations behave well across the bounce. Once having evolved the perturbations, we had reconstructed the curvature and the isocurvature perturbations from these quantities and had evaluated the corresponding power spectra. We have shown that the scalar and tensor perturbation spectra in our model prove to be strictly scale-invariant, as is expected to occur in a matter bounce scenario. We have also explicitly illustrated a well understood result, *viz.* while the bounce affects the amplitudes of the power spectra, their shapes remain unmodified across the bounce over scales of cosmological interest. Moreover, we find that, for a value of k_0/a_0 that leads to the COBE normalized power spectrum for the curvature perturbation, the tensor-to-scalar ratio proves to be of the order of $r \simeq 10^{-6}$, which is, obviously, perfectly consistent with the current upper bounds from the recent CMB observations [116]. Further, we have shown that, the amplitude of the isocurvature perturbations are quite small (their power spectrum is about four orders of magnitude below the power spectrum of the curvature perturbation). This indicates that the scenario generates a strongly adiabatic scalar perturbation spectra, again an aspect which is consistent with the observations. Importantly, we have also supported all the numerical results with analytical arguments.

Before, we conclude, we believe we should clarify a few different points. As we have pointed out repeatedly, our model essentially depends on only one parameter, *viz.* k_0/a_0 . This is evident from potential governing the model and this aspect is also reflected in the results we have obtained. Notice that the amplitudes of the scalar as well as the tensor power spectra [*cf.* equations (3.13), (3.74) and (3.76)] actually depend only on the ratio $k_0/(M_{\text{Pl}} a_0)$. We have chosen $k_0/(a_0 M_{\text{Pl}}) = 3.3 \times 10^{-8}$ in order to lead to a COBE normalized curvature perturbation spectrum. It is also important to note that, in terms of cosmic time, the duration of the bounce is, in fact, of the order of $a_0 \eta_* \simeq a_0/k_0$.

Another point that requires some clarification is the assumption of a symmetric bounce. The assumption of a symmetric bounce has proved to be convenient for us to study the problem. Actually, the scale factor and the model that drives the background will be valid only until an early epoch after the bounce. Hence, the term symmetric bounce basically refers to the period close to the bounce. At a suitable time after the bounce, we expect the energy from the scalar fields to be transferred to radiation as is done, for instance, in perturbative reheating after inflation. Though we have not touched upon this issue here, we believe that reheating can be achieved with a simple coupling (such as the conventional $\Gamma \dot{\phi}$ term) between the scalar field and the radiation fluid. Since we expect reheating to be achieved in such a fashion, we have ignored the presence of a radiation fluid in this work.

While it is interesting to have achieved a tensor-to-scalar ratio that is consistent with the observations in a completely symmetric matter bounce scenario, needless to add, many challenges remain. Theoretically, the model needs to be examined in greater detail to understand the fundamental reason as to why it leads to a small tensor-to-scalar ratio. In this context, the best way forward seems to be to consider different models leading to the same factor and investigate the behavior of the perturbations in these different models. Another related point is regarding the concern that has been raised about the situations under which the standard initial conditions can be imposed (in this context, see, for instance, Ref. [111]). In the case of our model, since the curvature and the isocurvature perturbations decouple during the early contracting phase, we have been able to impose the standard Bunch-Davies initial conditions.

From an observational point of view, we need to generate a tilt in the scalar power spectrum to match the CMB observations, an aspect which we shall discuss in the following chapter. Moreover, we need to examine if the scalar non-Gaussianities

generated in the model are indeed consistent with the current constraints from Planck [37]. Further, rather than brush them aside, we need to get around to addressing the different theoretical issues plaguing bouncing models that we had discussed in some detail in the introductory section. We should point out here that a completely non-perturbative analysis of a model very similar to what we have considered seems to suggest such models may not be as pathological as it has been argued to be [115]. Clearly, one needs to explore more complex models beyond the simple model we have constructed here. For instance, the ghost fields we have worked with can be considered to be undesirable and one needs to utilize more sophisticated models involving, say, Galileons or ghost condensates to achieve the bounces (in this context, see, for instance, Refs. [15, 88]). These models are often considered to have emerged from more complete theories. Moreover, they can alleviate or overcome difficulties such as gradient instabilities that can otherwise arise. We are presently investigating a variety of such issues.

Chapter 4

Viabie scalar spectral tilt and tensor-to-scalar ratio in near-matter bounces

4.1 Introduction

In bouncing scenarios, the shape of the primordial spectra generated is largely determined by the form of the contraction during the early stages. In the previous chapter, we had seen that a matter bounce scenario leads to scale-invariant spectra, just as de Sitter inflation does [64,97]. It then seems natural to expect that near-matter bounces will lead to nearly scale-invariant primordial spectra, as is required by the CMB observations.

While it is rather easy to build inflationary models that are consistent with the observations, it proves to be quite involved to construct viable bouncing models. As we have emphasized earlier, the difficulties largely arise due to the fact that the null energy condition has to be violated near the bounce, which leads to

certain pathologies at the level of the background as well as the perturbations. The simplest of the bouncing models are those whose scale factors are symmetric about the bounce. However, as we had discussed, such models can lead to a large tensor-to-scalar ratio beyond the current constraints [12]. In the previous chapter, we had constructed a model consisting of a canonical and a non-canonical (as well as ghost) field to drive a symmetric matter bounce [116]. We had shown (both analytically and numerically) that the model leads to strictly scale-invariant primordial spectra and a viable tensor-to-scalar ratio as well as insignificant isocurvature perturbations. We had found that the amplitude of the scalar perturbations are considerably enhanced during the NEC violating phase resulting in a small tensor-to-scalar ratio after the bounce. In this chapter, we extend our earlier model so that it also leads to a scalar spectral tilt that is consistent with the observations.

This chapter is organized as follows. In the following section, we shall describe the scale factor of our interest and the sources that can drive such a background. In section 4.3, we shall discuss the simpler case of the evolution of the tensor perturbations and evaluate the tensor power spectra prior to the bounce. In section 4.4, we shall arrive at the equations governing the scalar perturbations. In section 4.5, we shall solve the equations numerically to determine their evolution across the bounce. We shall also present the essential results, *viz.* the scalar and tensor power spectra (evaluated after the bounce), that we obtain in the model. In section 4.6, we shall conclude with a brief summary.

4.2 Background and sources

In this section, we shall construct sources involving two scalar fields to drive near-matter bounces. We shall consider the background to be the spatially flat

FLRW metric that is described by the line-element (1.28). We shall assume that the scale factor describing the bounce is given in terms of the conformal time as follows:

$$a(\eta) = a_0 (1 + k_0^2 \eta^2)^{1+\varepsilon}, \quad (4.1)$$

where a_0 is the value of the scale factor at the bounce (*i.e.* at $\eta = 0$), k_0 is the scale associated with the bounce¹, while $\varepsilon \geq 0$. Note that $\varepsilon = 0$ corresponds to the specific case of the matter bounce scenario we had considered in the previous chapter. As we shall see later, a non-zero but small ε (such that $\varepsilon \ll 1$) leads to a scalar spectral tilt suggested by the CMB observations.

We find that the Hubble parameter associated with the scale factor (4.1) can be expressed as

$$H^2 = \left[\frac{2k_0(1+\varepsilon)}{a_0} \right]^2 \left[\frac{1}{(a/a_0)^\gamma} - \frac{1}{(a/a_0)^\delta} \right], \quad (4.2)$$

where $\gamma = (3 + 2\varepsilon)/(1 + \varepsilon)$ and $\delta = 2(2 + \varepsilon)/(1 + \varepsilon)$. Recall that, according to the first Friedmann equation, $H^2 = \rho/(3M_{\text{pl}}^2)$, with ρ being the total energy density of the sources driving the background. Therefore, the right hand side of the expression (4.2) suggests that the scale factor (4.1) can be driven by two sources described by the equations of state $w_1 = -\varepsilon/[3(1 + \varepsilon)]$ and $w_2 = (1 - \varepsilon)/[3(1 + \varepsilon)]$. Moreover, the second source has to have negative energy density, a property which ensures that the Hubble parameter vanishes at the bounce (*i.e.* when $a = a_0$).

These sources can be modeled in terms of two scalar fields—a canonical scalar field, say, ϕ , characterized by the potential $V(\phi)$ and a non-canonical ghost field,

¹To be precise, the energy scale associated with the bounce is actually given by k_0/a_0 . Recall that, in the matter bounce scenario we had considered in the last chapter, the amplitudes of the scalar and tensor power spectra had depended *only* on this combination [116].

say, χ —that are described by the action

$$S[\phi, \chi] = - \int d^4x \sqrt{-g} \left[-X^{\phi\phi} + V(\phi) + U_0 (X^{xx})^q \right] \quad (4.3)$$

where the kinetic terms $X^{\phi\phi}$ and X^{xx} are given by the equations (1.30) and (3.16), respectively, while U_0 and q are positive constants. While the stress-energy tensor associated with the field ϕ is given by equation (1.32), the corresponding stress-energy tensor associated with the field χ can be obtained to be

$$T_{\nu(\chi)}^{\mu} = -q U_0 (X^{xx})^{q-1} \partial^{\mu} \chi \partial_{\nu} \chi - \delta_{\nu}^{\mu} U_0 (X^{xx})^q. \quad (4.4)$$

Let us first consider the behavior of the ghost field χ . For a homogeneous field, it is straightforward to show that

$$T_{0(\chi)}^0 = -\rho_{\chi} = (2q - 1) U_0 (X^{xx})^q, \quad (4.5a)$$

$$T_{j(\chi)}^i = p_{\chi} \delta_j^i = -U_0 (X^{xx})^q \delta_j^i, \quad (4.5b)$$

where, evidently, ρ_{χ} and p_{χ} are the energy density and pressure associated with the χ field. Note that ρ_{χ} is negative for $q > 1/2$ and $p_{\chi} = \rho_{\chi}/(2q - 1)$, corresponding to $w_{\chi} = p_{\chi}/\rho_{\chi} = 1/(2q - 1)$. If we set $w_{\chi} = w_2 = (1 - \varepsilon)/[3(1 + \varepsilon)]$, which corresponds to $q = (2 + \varepsilon)/(1 - \varepsilon)$, then the energy density of the field χ can be expressed as

$$\rho_{\chi} = -3 M_{\text{Pl}}^2 \left[\frac{2k_0(1 + \varepsilon)}{a_0} \right]^2 \frac{1}{(a/a_0)^{\delta}}. \quad (4.6)$$

In this expression for ρ_{χ} , we have chosen the overall constant such that it corresponds to the second term in the expression (4.2) for H^2 through the first Friedmann equation.

Let us now turn to the behavior of the canonical scalar field ϕ . The non-zero components of the stress-energy tensor associated with the homogeneous field ϕ are

given by equations (1.33). In order to lead to the first term in the expression (4.2) for H^2 (through the first Friedmann equation), we require ρ_ϕ to behave as

$$\rho_\phi = 3 M_{\text{Pl}}^2 \left[\frac{2 k_0 (1 + \varepsilon)}{a_0} \right]^2 \frac{1}{(a/a_0)^\gamma}, \quad (4.7)$$

which implies that $w_\phi = p_\phi/\rho_\phi = w_1 = -\varepsilon/[3(1 + \varepsilon)]$. These results and equations (1.33) lead to

$$\dot{\phi}^2 = 2 \left(\frac{3 + 2\varepsilon}{3 + 4\varepsilon} \right) V(\phi). \quad (4.8)$$

Using equations (1.33), (4.7), (4.8) and the scale factor (4.1), it is straightforward to show that the evolution of the field ϕ can be expressed in terms of the scale factor $a(\eta)$ as

$$\phi(a) = 2 \sqrt{(1 + \varepsilon)(3 + 2\varepsilon)} M_{\text{Pl}} \cosh^{-1} \left\{ [a(\eta)/a_0]^{1/[2(1+\varepsilon)]} \right\} + \phi_0, \quad (4.9)$$

where ϕ_0 is the value of ϕ at the bounce, *i.e.* when $a = a_0$. From the above expression for ϕ and equation (4.8), the corresponding potential $V(\phi)$ can be obtained to be

$$V(\phi) = (3 + 4\varepsilon)(1 + \varepsilon) \left(\frac{M_{\text{Pl}} k_0}{a_0} \right)^2 \cosh^{-2(3+2\varepsilon)} \left[\frac{1}{2 \sqrt{(1 + \varepsilon)(3 + 2\varepsilon)}} \left(\frac{\phi - \phi_0}{M_{\text{Pl}}} \right) \right]. \quad (4.10)$$

Two points need to be stressed regarding the model we have constructed. Firstly, note that the potential $V(\phi)$ above as well as the complete system involving the two scalar fields ϕ and χ described by the action (4.3) depend only on the two parameters k_0/a_0 and ε , as ϕ_0 and U_0 do not play any non-trivial role in the dynamics. Secondly, when $\varepsilon = 0$, the action reduces to the model that leads to the matter bounce scenario that we have considered earlier [116].

4.3 The tensor modes and the resulting power spectrum

The tensor perturbations are always simpler to study because the equations governing their evolution depends only on the scale factor that describes the FLRW universe and not on the nature of the sources that drive the background. In this section, we shall discuss the tensor power spectrum arising in the near-matter bounces of our interest. As the scale factor (4.1) reduces to a power law form at early times, *i.e.* when $\eta \ll -\eta_0$, the modes and power spectrum well before the bounce are straightforward to arrive at. In a later section, we shall numerically evolve the tensor perturbations across the bounce and evaluate the power spectrum *after* the bounce. We shall see that, while the bounce alters the amplitude of the tensor power spectrum, it does not change its shape.

Let us quickly summarize a few essential points concerning the tensor perturbations. If the tensor perturbations are characterized by γ_{ij} , then the spatially flat FLRW metric containing the perturbations at the linear order can be expressed as in equation (1.48). The Fourier modes h_k corresponding to the tensor perturbations are governed by the differential equation (1.65) and, if we write $h_k = (\sqrt{2}/M_{\text{Pl}}) u_k/a$, then the Mukhanov-Sasaki variable u_k satisfies the differential equation (1.68). The tensor power spectrum evaluated at a specific time is defined in equation (1.71) and the corresponding tensor spectral index n_T is given by (1.72).

During the early contracting phase, *i.e.* when $\eta \ll -\eta_0$, the scale factor (4.1) behaves as $a(\eta) \propto \eta^{2(1+\epsilon)}$. Due to this reason, the equation (1.68) describing the

Mukhanov-Sasaki variable u_k reduces to

$$u_k'' + \left[k^2 - \frac{2(1+\varepsilon)(1+2\varepsilon)}{\eta^2} \right] u_k \simeq 0. \quad (4.11)$$

For modes of cosmological interest, we can impose the standard Bunch-Davies initial conditions at early times when $k\eta \ll -[2(1+\varepsilon)(1+2\varepsilon)]^{1/2}$. In such a case, the solution to above equation which satisfies the Bunch-Davies initial condition can be expressed in terms of the Hankel function $H_\nu^{(1)}(x)$ as in equation (1.77), with ν now given by $\nu = 3/2 + 2\varepsilon$. Moreover, the tensor power spectrum evaluated as one approaches the bounce can also be expressed as in equation (1.78b), with ν given as above. The corresponding spectral index n_T can be obtained to be

$$n_T = -4\varepsilon, \quad (4.12)$$

which clearly reduces to zero when $\varepsilon = 0$ corresponding to the case of the matter bounce. We shall later evolve the tensor perturbations numerically and compute the power spectra before as well as after the bounce. We shall find that the above analytical spectrum matches the numerical results prior to the bounce and the spectral shape is retained as the modes are evolved across the bounce.

4.4 Arriving at the equations governing the scalar perturbations

Since we are working with two scalar fields, as is well known, there will arise two *independent* scalar degrees of freedom. In fact, amongst the four scalar quantities that describe the perturbations in the metric and the two that describe the perturbations in the scalar fields, we can choose to work with any two of them to evolve the perturbations. The usual choices are the curvature and the isocurva-

ture perturbations, which are actually a linear combination of the perturbations in the scalar fields [10, 107, 108]. In this section, we shall derive the equations governing the evolution of the perturbations in the two scalar fields, say, $\delta\phi$ and $\delta\chi$. Thereafter, we shall construct the curvature and isocurvature perturbations for our model and arrive at the equations describing them. As in the model discussed in last the chapter, we find that some of the coefficients in the equations governing the curvature and the isocurvature perturbations diverge as one approaches the bounce. To circumvent this difficulty, we shall choose two other independent scalar quantities to evolve the perturbations across the bounce and reconstruct the curvature and isocurvature perturbations from these quantities.

4.4.1 The Einstein's equations and the equations describing the perturbations in the scalar fields

In linear perturbation theory, the scalar and tensor perturbations evolve independently. When the scalar perturbations are taken into account, the FLRW line element, in general, can be written as in equation (1.44). At the first order in the perturbations, the Einstein's equations describing the system of our interest are given by equations (3.32). While the components of the perturbed stress-energy tensor associated with the field ϕ are given by equations (1.51), the components of the perturbed stress-energy tensor corresponding to the field χ can be evaluated to be

$$\delta T_{0(\chi)}^0 = -\delta\rho_\chi = -(2q-1)qU_0(X^{xx})^{q-1}\dot{\chi}\left(\delta\dot{\chi}-\dot{\chi}A\right), \quad (4.13a)$$

$$\delta T_{i(\chi)}^0 = -\partial_i\delta q_\chi = qU_0(X^{xx})^{q-1}\dot{\chi}\delta\chi, \quad (4.13b)$$

$$\delta T_{j(\chi)}^i = \delta p_\chi\delta_j^i = \frac{\delta\rho_\chi}{2q-1}\delta_j^i. \quad (4.13c)$$

Note that, when $q = 2$, these quantities reduce to the expressions (3.33), as required.

A straightforward way to arrive at the equations of motion describing the perturbations in the scalar fields would be to utilize the conservation equation governing the perturbation in the stress-energy tensor of the fields. The equation governing the evolution of the perturbation in the energy density of a particular component is given by equation (3.34). On substituting the expressions for the components of the perturbed stress-energy tensor we have obtained in equation (3.34), we find that the equation of motion governing the Fourier mode $\delta\phi_k$ is given by equation (3.35a). While, the equation governing the perturbation $\delta\chi_k$ can be obtained to be

$$\begin{aligned} \delta\ddot{\chi}_k + \frac{3H}{2q-1} \delta\dot{\chi}_k - \dot{\chi} \left(\dot{A}_k + \frac{3\dot{\psi}_k}{2q-1} \right) \\ + \frac{k^2}{(2q-1)a^2} \left[\delta\chi_k + a\dot{\chi} (B_k - a\dot{E}_k) \right] = 0, \end{aligned} \quad (4.14)$$

where, as we have mentioned before, the quantities A_k , B_k , ψ_k and E_k are the Fourier modes associated with the corresponding metric perturbations. We should point out that, when $q = 2$, this equation reduces to the matter bounce case [*cf.* equation (3.35b)] we had considered in the earlier chapter.

In the following subsection, we shall first construct the gauge invariant curvature and isocurvature perturbations. Thereafter, with the aid of the above equations for $\delta\phi_k$ and $\delta\chi_k$, we shall arrive at the equations governing them. As in the case of the matter bounce scenario [116], we shall find that some of the coefficients in the equations governing the curvature and the isocurvature perturbations diverge in the domain where the NEC is violated around the bounce. Lastly, we shall discuss the method by which we can circumvent these difficulties before proceeding to solve the equations numerically.

4.4.2 Equations governing the scalar perturbations, and circumventing the diverging coefficients

Recall that the curvature perturbations are the fluctuations along the direction of the background trajectory in the field space. Whereas, the isocurvature perturbations correspond to fluctuations in a direction perpendicular to the background trajectory [10, 107, 108]. Using the arguments we had presented in the previous chapter, we can construct the curvature and the isocurvature perturbations for the model of our interest here to be

$$\mathcal{R} = \frac{H}{\dot{\phi}^2 - 2qU_0(X^{xx})^q} \left(\dot{\phi} \overline{\delta\phi} - qU_0(X^{xx})^{q-1} \dot{\chi} \overline{\delta\chi} \right), \quad (4.15a)$$

$$\mathcal{S} = \frac{H \sqrt{q} U_0(X^{xx})^{q-1}}{\dot{\phi}^2 - 2qU_0(X^{xx})^q} \left(\dot{\chi} \overline{\delta\phi} - \dot{\phi} \overline{\delta\chi} \right), \quad (4.15b)$$

where $\overline{\delta\phi} = \delta\phi + (\dot{\phi}/H)\psi$ and $\overline{\delta\chi} = \delta\chi + (\dot{\chi}/H)\psi$ are the gauge invariant versions of the perturbations associated with the two scalar fields. Upon using the equations of motion (3.35a) and (4.14) governing the perturbations $\delta\phi_k$ and $\delta\chi_k$ and the first order Einstein's equations (3.32), we can arrive at the following equations governing the Fourier modes \mathcal{R}_k and \mathcal{S}_k of the curvature and the isocurvature perturbations:

$$\mathcal{R}_k'' + \left\{ \frac{2}{3(1+\varepsilon)[1-(3+2\varepsilon)k_0^2\eta^2]} \right\} [C_{rr}\mathcal{R}'_k + D_{rr}\mathcal{R}_k + C_{rs}\mathcal{S}'_k + D_{rs}\mathcal{S}_k] = 0, \quad (4.16a)$$

$$\mathcal{S}_k'' + \left\{ \frac{2}{3(1+\varepsilon)[1-(3+2\varepsilon)k_0^2\eta^2]} \right\} [C_{ss}\mathcal{S}'_k + D_{ss}\mathcal{S}_k + C_{sr}\mathcal{R}'_k + D_{sr}\mathcal{R}_k] = 0, \quad (4.16b)$$

where the quantities ($C_{rr}, D_{rr}, C_{rs}, D_{rs}$) are given by

$$C_{rr} = \frac{1}{(1-\varepsilon)(1+k_0^2\eta^2)\eta} \left[21 + 124\varepsilon + 219\varepsilon^2 + 144\varepsilon^3 + 32\varepsilon^4 \right. \\ \left. + (1+2\varepsilon)(27+76\varepsilon+61\varepsilon^2+16\varepsilon^3)k_0^2\eta^2 \right. \\ \left. - 6(1+\varepsilon)^2(1-\varepsilon)(3+2\varepsilon)k_0^4\eta^4 \right], \quad (4.17a)$$

$$D_{rr} = -\frac{k^2}{2} \left[5 + 17\varepsilon + 8\varepsilon^2 + 3(1+\varepsilon)(3+2\varepsilon)k_0^2\eta^2 \right], \quad (4.17b)$$

$$C_{rs} = -\frac{\sqrt{2(2+\varepsilon)(3+2\varepsilon)}}{(1-\varepsilon)\sqrt{1+k_0^2\eta^2}\eta} \left[(1+2\varepsilon)(5+17\varepsilon+8\varepsilon^2) \right. \\ \left. + 3(1+\varepsilon)(4+7\varepsilon+4\varepsilon^2)k_0^2\eta^2 \right], \quad (4.17c)$$

$$D_{rs} = \frac{2\sqrt{2(2+\varepsilon)(3+2\varepsilon)}}{(1-\varepsilon)(1+k_0^2\eta^2)^{3/2}\eta^2} \left[(1+2\varepsilon)(5+17\varepsilon+8\varepsilon^2) \right. \\ \left. + (1-\varepsilon)(1+2\varepsilon)(1+k_0^2\eta^2)^2 k^2\eta^2 \right. \\ \left. - 6(1+\varepsilon)(1+2\varepsilon)(4+7\varepsilon+4\varepsilon^2)k_0^4\eta^4 \right. \\ \left. - (1+\varepsilon)(22+87\varepsilon+84\varepsilon^2+32\varepsilon^3)k_0^2\eta^2 \right], \quad (4.17d)$$

while the quantities ($C_{ss}, D_{sr}, C_{sr}, D_{ss}$) are given by

$$C_{ss} = -\frac{1}{(1-\varepsilon)(1+k_0^2\eta^2)\eta} \left[27 + 124\varepsilon + 213\varepsilon^2 + 144\varepsilon^3 + 32\varepsilon^4 \right. \\ \left. + (1+2\varepsilon)(21+76\varepsilon+67\varepsilon^2+16\varepsilon^3)k_0^2\eta^2 \right. \\ \left. + 6(1+\varepsilon)^2(1-\varepsilon)(3+2\varepsilon)k_0^4\eta^4 \right], \quad (4.18a)$$

$$D_{ss} = \frac{1}{2(1-\varepsilon)(1+k_0^2\eta^2)^2\eta^2} \left\{ 2(27+124\varepsilon+213\varepsilon^2+144\varepsilon^3+32\varepsilon^4) \right. \\ \left. - (255+1076\varepsilon+1753\varepsilon^2+1500\varepsilon^3+688\varepsilon^4+128\varepsilon^5)k_0^2\eta^2 \right. \\ \left. - (1+\varepsilon)(75+691\varepsilon+1314\varepsilon^2+936\varepsilon^3+224\varepsilon^4)k_0^4\eta^4 \right. \\ \left. - 6(1-\varepsilon)(1+\varepsilon)(1+2\varepsilon)(3+2\varepsilon)k_0^6\eta^6 \right. \\ \left. + (1-\varepsilon)[9+19\varepsilon+8\varepsilon^2-(1-\varepsilon)(3+2\varepsilon)k_0^2\eta^2](1+k_0^2\eta^2)^2 k^2\eta^2 \right\}, \quad (4.18b)$$

$$C_{sr} = \frac{\sqrt{2(2+\varepsilon)(3+2\varepsilon)}}{(1-\varepsilon)\sqrt{1+k_0^2\eta^2}\eta} \left[(1+2\varepsilon)(9+19\varepsilon+8\varepsilon^2) - (1-\varepsilon)(2+\varepsilon)(3+4\varepsilon)k_0^2\eta^2 \right], \quad (4.18c)$$

$$D_{sr} = -\sqrt{2(2+\varepsilon)(3+2\varepsilon)}(1+2\varepsilon)k^2\sqrt{1+k_0^2\eta^2}. \quad (4.18d)$$

We find that some of these coefficients diverge either at the time when $\dot{H} = 0$ or at the bounce. This poses a difficulty in evolving the curvature and the isocurvature perturbations across these instances. As we had done in the previous chapter, around the bounce, we shall work in a specific gauge wherein the two scalar quantities describing the perturbations behave well at such points. We shall evolve these two scalar quantities across these domains and eventually reconstruct the curvature and the isocurvature perturbations from these quantities. Note that $\dot{H} = 0$ when $\eta_* = \mp 1/[\sqrt{(3+2\varepsilon)}k_0]$. As we shall illustrate later, the curvature and the isocurvature perturbations indeed diverge at this point. Also, we shall find that, while the isocurvature perturbations vanish exactly at the bounce, the curvature perturbations go to zero a little time later.

As we mentioned, we shall circumvent the problem of diverging coefficients by working in a specific gauge. It has been observed that the difficulties of evolving the curvature and the isocurvature perturbations across the bounce can be avoided if we choose to work in the uniform- χ gauge, *i.e.* the gauge wherein $\delta\chi_k = 0$ [12,116]. In this gauge, we can use A and ψ as the two independent scalar functions and these quantities can be smoothly evolved across the bounce. The curvature and the isocurvature perturbations can then be suitably constructed from these two scalar perturbations. In uniform- χ gauge, equation (3.35b) reduces to

$$\frac{k^2}{a} \left(B_k - a \dot{E}_k \right) = (2b-1) \dot{A}_k + 3 \dot{\psi}_k. \quad (4.19)$$

Upon using this relation, the first order Einstein equations (3.32) and the back-

ground equations, we obtain the following equations governing A_k and ψ_k :

$$\begin{aligned} A_k'' &+ \frac{4(2+3\varepsilon)k_0^2\eta}{1+k_0^2\eta^2} A_k' + \frac{k^2(1+k_0^2\eta^2)^2(1-\varepsilon) - 12k_0^2(1+\varepsilon)^2(5+4\varepsilon)}{3(1+\varepsilon)(1+k_0^2\eta^2)^2} A_k \\ &= -\frac{2(1-\varepsilon)(3+4\varepsilon)k_0^2\eta}{(1+\varepsilon)(1+k_0^2\eta^2)} \psi_k' + \frac{4(1-\varepsilon)}{3(1+\varepsilon)} k^2 \psi_k, \end{aligned} \quad (4.20a)$$

$$\begin{aligned} \psi_k'' &- \frac{2(1+2\varepsilon)k_0^2\eta}{1+k_0^2\eta^2} \psi_k' + k^2 \psi_k \\ &= \frac{4(1+\varepsilon)(1+2\varepsilon)k_0^2\eta}{(1-\varepsilon)(1+k_0^2\eta^2)} A_k' - \frac{4(1+\varepsilon)^2(5+4\varepsilon)}{(1-\varepsilon)(1+k_0^2\eta^2)^2} k_0^2 A_k. \end{aligned} \quad (4.20b)$$

Note that, in the uniform χ -gauge, the curvature and the isocurvature perturbations are given by

$$\mathcal{R}_k = \psi_k + \frac{2H M_{\text{Pl}}^2}{\dot{\phi}^2 - 2q U_0 (X^{\text{xx}})^q} \left(\dot{\psi}_k + H A_k \right), \quad (4.21a)$$

$$\mathcal{S}_k = \frac{2H M_{\text{Pl}}^2 \sqrt{q U_0 (X^{\text{xx}})^{q-1}} \dot{\chi}}{\left[\dot{\phi}^2 - 2q U_0 (X^{\text{xx}})^q \right] \dot{\phi}} \left(\dot{\psi}_k + H A_k \right). \quad (4.21b)$$

Later, we shall make use of these relations to construct \mathcal{R}_k and \mathcal{S}_k from A_k and ψ_k around the bounce.

4.5 Evolution of the perturbations and power spectra

In the previous chapter on the matter bounce scenario, we had constructed analytical as well as numerical solutions for the perturbations at early times (*i.e.* when $\eta \ll -\eta_0$) as well across the bounce. For the case of near-matter bounces of our interest here, we do not seem to be able to analytically solve the equations (4.20) governing A_k and ψ_k across the bounce. Therefore, we evolve the perturbations numerically. In the case of bounces driven by two fields, one of the concerns that has been raised is whether the fields will be decoupled at early times allowing one to impose the required Bunch-Davies initial conditions (in this context, see

Ref. [111]). Note that, in the model governed by the action (4.3), the two fields ϕ and χ do not interact directly and are coupled only gravitationally. It should be clear from the first Friedmann equation (4.2) that the energy densities of the two fields are equal *only at the bounce*. Clearly, at very early times, the background universe is effectively driven by a single field, with the field ϕ dominating the evolution. This behavior ensures that the curvature and the isocurvature perturbations are completely decoupled during the early contracting phase permitting us to impose the standard initial conditions on the modes.

As we can construct the background quantities analytically, we shall require the numerical procedure only for the evolution of the perturbations. The tensor perturbations can be evolved across the bounce without any difficulty. In the case of scalars, we evolve the curvature and the isocurvature perturbations until close to the bounce and thereafter we shall choose to evolve the metric perturbations A_k and ψ_k across the bounce (for reasons discussed in the last section). We shall evaluate the final perturbation spectra at a suitable time after the bounce.

4.5.1 Analytical solutions at early times

Since the scale factor (4.1) reduces to a power law form for $\eta \ll -\eta_0$, the scalar modes can be obtained analytically during the contracting phase as in the case of tensors. Also, as we mentioned, during these early times, it is the energy density of the scalar field ϕ that dominates the background evolution. Due to this reason, as we discussed, when $\eta \ll -\eta_0$, the curvature and the isocurvature perturbations decouple so that the equations (4.16) governing \mathcal{R}_k and \mathcal{S}_k simplify to

$$\mathcal{R}_k'' + 2 \frac{z'}{z} \mathcal{R}_k' + k^2 \mathcal{R}_k \simeq 0, \quad (4.22a)$$

$$\mathcal{S}_k'' + 2 \frac{z'}{z} \mathcal{S}_k' + \left[w_\chi k^2 + \frac{2(1+2\varepsilon)}{\eta^2} \right] \mathcal{S}_k \simeq 0, \quad (4.22b)$$

where $z \simeq a \dot{\phi}/H \simeq \sqrt{3(1+w_\phi)} M_{\text{Pl}} a$ and, recall that, while $w_\phi = -\varepsilon/[3(1+\varepsilon)]$, $w_\chi = (1-\varepsilon)/[3(1+\varepsilon)]$. We find that the equations describing the Mukhanov-Sasaki variables corresponding to the curvature and the isocurvature perturbations, *viz.* $v_k^\sigma = z \mathcal{R}_k$ and $v_k^s = z \mathcal{S}_k$, reduce to

$$v_k^{\sigma''} + \left[k^2 - \frac{2(1+\varepsilon)(1+2\varepsilon)}{\eta^2} \right] v_k^\sigma \simeq 0, \quad (4.23a)$$

$$v_k^{s''} + \left[w_\chi k^2 - \frac{2\varepsilon(1+2\varepsilon)}{\eta^2} \right] v_k^s \simeq 0. \quad (4.23b)$$

At very early times during the contracting phase, *i.e.* when $\eta \ll -\eta_0$, we can impose the standard Bunch-Davies initial conditions on the Mukhanov-Sasaki variables v_k^σ and v_k^s . Recall that the initial condition on the variable v_k^σ is given by equation (1.75). Whereas, the initial condition on the variable v_k^s is given by

$$v_k^s(\eta) = \frac{1}{\sqrt{2w_\chi^{\frac{1}{2}}k}} e^{-i\sqrt{w_\chi}k\eta}. \quad (4.24)$$

For convenience, let us simply assume that, while the curvature spectrum $\mathcal{P}_\mathcal{R}(k)$ is given by equation (1.64), the spectrum associated with the isocurvature perturbation is defined to be (in this context, see the following sub-section where we discuss the numerical evolution of the perturbations)

$$\mathcal{P}_s(k) = \frac{k^3}{2\pi^2} |\mathcal{S}_k|^2. \quad (4.25)$$

Note that the equation governing the tensor and the scalar Mukhanov-Sasaki variables u_k and v_k^σ [*cf.* equations (4.11) and (4.23a)] at early times during the contracting phase have the same form, as is expected in a power law background. Therefore, the spectrum of curvature perturbations evaluated prior to the bounce has the same shape as the tensor power spectrum. As a result, we find that, we

can write

$$\mathcal{P}_{\mathcal{R}}(k) = r \mathcal{P}_{\mathcal{T}}(k), \quad (4.26)$$

where the tensor-to-scalar ratio r is a constant and is given by

$$r = \frac{8(3 + 2\varepsilon)}{1 + \varepsilon}. \quad (4.27)$$

Evidently, $r = 24$ when $\varepsilon = 0$, a well known result in the matter bounce scenarios (see, for instance, Ref. [12]). It should also be mentioned that the spectral index $n_{\mathcal{R}}$ [cf. equation (1.72a)] is given by

$$n_{\mathcal{R}} = 1 - 4\varepsilon. \quad (4.28)$$

4.5.2 Numerical evolution across the bounce

We evolve the perturbations numerically just as we had done in the previous chapter. To begin with, we use e-N-folds \mathcal{N} —defined as $a(\mathcal{N}) = a_0 \exp(\mathcal{N}^2/2)$ —to be our independent variable. The e-N-fold proves to be very convenient to describe symmetric bounces and it replaces the more conventional e-fold to evolve the perturbations over a wide domain in time efficiently [101, 102, 116]. We express the equations (1.65) and (4.16) governing the tensor and scalar perturbations h_k , \mathcal{R}_k and \mathcal{S}_k in terms of the new variable \mathcal{N} and integrate the equations using a fifth order Runge-Kutta algorithm. In the case of the scalar perturbations, as is often done in the case of two-field models, we shall numerically integrate the equations (4.16) using two sets of initial conditions, as we have described in the previous chapter [11].

We had discussed earlier as to how the model of our interest depends only on two parameters, *viz.* k_0/a_0 and ε . If we multiply the modes \mathcal{R}_k , \mathcal{S}_k and h_k by the quan-

tity $\sqrt{k_0} a_0 M_{\text{Pl}}$, we find that, we do not have to specify k_0 or a_0 independently in order to evolve them from the given initial conditions. In fact, the resulting scalar and tensor power spectra depend only on k_0/a_0 and ε . We shall choose to work with $k_0/(a_0 M_{\text{Pl}}) = 9.61 \times 10^{-9}$ and $\varepsilon = 0.01$. This value of k_0/a_0 ensures that the curvature perturbation spectrum $\mathcal{P}_{\mathcal{R}}(k)$ evaluated after the bounce is COBE normalized corresponding to the value of 2.31×10^{-9} at a suitable pivot scale. Also, the value of ε we shall work with leads to the scalar spectral index of $n_{\mathcal{R}} \simeq 0.96$ [cf. equation (4.28)], as required by the Planck data.

We impose the initial conditions on the perturbations when $k^2 = 10^4 (a''/a)$. In the case of tensors, we evolve the equation (1.65) across the bounce (with \mathcal{N} as the independent variable) until $\eta = \beta \eta_0$, with $\beta = 10^2$, after the bounce. We evolve the scalar perturbations using the equations (4.16) until $\eta = -\alpha \eta_0$ and we shall assume that $\alpha = 10^5$. Since the equations (4.16) contain coefficients which diverge close to the bounce, as we had discussed, we instead use equations (4.20) to evolve the scalar perturbations A_k and ψ_k across the bounce from $\eta = -\alpha \eta_0$ to $\eta = \beta \eta_0$. Evidently, the quantities \mathcal{R}_k and \mathcal{S}_k evolved during the early contracting phase can provide us the initial conditions for A_k and ψ_k at $\eta = -\alpha \eta_0$ through the relations (4.21). Once we have A_k and ψ_k in hand, we shall reconstruct \mathcal{R}_k and \mathcal{S}_k using the same relations. It is useful to mention here that, for the values of k_0/a_0 and ε that we are working with, $\eta = -\alpha \eta_0$ with $\alpha = 10^5$ corresponds to $\mathcal{N} \simeq -6.78$, while $\eta = \beta \eta_0$ with $\beta = 10^2$ corresponds to $\mathcal{N} = 4.29$.

4.5.3 Behavior of the perturbations and the power spectra

In figure 4.1, we have plotted the evolution of the perturbations \mathcal{R}_k and \mathcal{S}_k and h_k for a typical cosmological scale as a function of e-N-folds \mathcal{N} . As we had expected, the curvature and the isocurvature perturbations diverge at the points

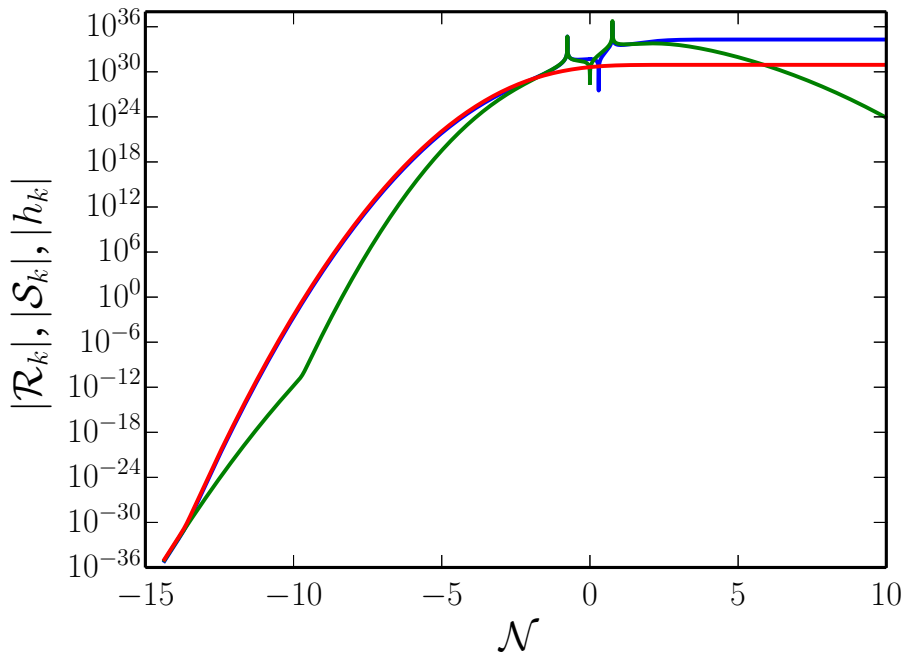


Figure 4.1: Evolution of the amplitudes of the curvature perturbation \mathcal{R}_k (in blue), the isocurvature perturbation \mathcal{S}_k (in green) and the tensor mode h_k (in red) corresponding to the wavenumber $k/k_0 = 10^{-20}$ have been plotted as a function of e-N-folds \mathcal{N} . We have chosen the background parameters to be $k_0/(a_0 M_{\text{Pl}}) = 9.6 \times 10^{-9}$ and $\varepsilon = 0.01$ in plotting this figure. We should clarify that we have, in fact, multiplied \mathcal{R}_k , \mathcal{S}_k and h_k by the quantity $\sqrt{k_0} a_0 M_{\text{Pl}}$ to ensure that they depend only on the parameters k_0/a_0 and ε . We have plotted the numerical results from the initial e-N-fold when $k^2 = 10^4 (a''/a)$ corresponding to the mode. The behavior of the modes is essentially similar to their behavior in the matter bounce scenario we had considered in the previous chapter. The sharp rise in the amplitude of the curvature perturbation close to the bounce ensures that the tensor-to-scalar ratio is strongly suppressed after the bounce leading to levels of r that are consistent with the upper bounds from Planck. Moreover, note that the isocurvature perturbation decays after the bounce, which leads to a strongly adiabatic spectrum, also required by the observations.

where $\dot{H} = 0$, *i.e.* at $\eta_* = \mp 1/[\sqrt{(3+2\varepsilon)} k_0]$, corresponding to $\mathcal{N} = \mp 0.76$ (in this context, see appendix B). Moreover, as expected, the isocurvature perturbations vanish at the bounce. We find that, in fact, the curvature perturbation also vanishes at a point soon after the bounce. Further, while the amplitude of the curvature and the tensor perturbations freeze after $\eta = \eta_*$, the isocurvature perturbations decay soon after². Such a decay leads to a strongly adiabatic spectrum

²In fact, in the case of the tensor perturbations, it is possible to construct analytical solutions across the bounce as well (in this context, see Ref. [33]). We find that our numerical solutions

of scalar perturbations, as is required by the observations. All these points should be evident from figure 4.1. Essentially, the scalar and tensor perturbations behave just as in the matter bounce scenario we had considered in the last chapter [116].

Having obtained the solutions for the modes, we can now evaluate the resulting power spectra. We compute the scalar and tensor power spectra after the bounce at $\eta = \beta \eta_0$, with $\beta = 10^2$ (corresponding to $\mathcal{N} = 4.29$). In figure 4.2, we have plotted the power spectra prior to the bounce (evaluated at $\eta = -\alpha \eta_0$, with $\alpha = 10^5$, corresponding to $\mathcal{N} = -6.78$) as well as after the bounce. It is evident from the figure that the shape of the power spectra are preserved as the perturbations evolve across the bounce. We find that the value of $k_0/(a_0 M_{\text{Pl}}) = 9.61 \times 10^{-9}$ leads to the COBE normalized value of 2.31×10^{-9} for the curvature perturbation spectrum at the scale of $k/k_0 = 10^{-23}$. Recall that, our main goal here is introduce a suitable tilt to the curvature perturbation spectrum so as to be consistent with the observations. As we had mentioned, for $\varepsilon = 0.01$, we find that $n_{\mathcal{R}} = 0.96$, perfectly consistent with the observations. Lastly, we find that, as the perturbations evolve across the bounce, the tensor-to-scalar ratio drops from the value of $r = 23.92$ prior to the bounce to $r = 1.46 \times 10^{-6}$ after the bounce. Needless to add, this value of the r is much smaller than the current upper bound of $r \lesssim 0.07$ from Planck [7].

match the analytical solutions quite well.

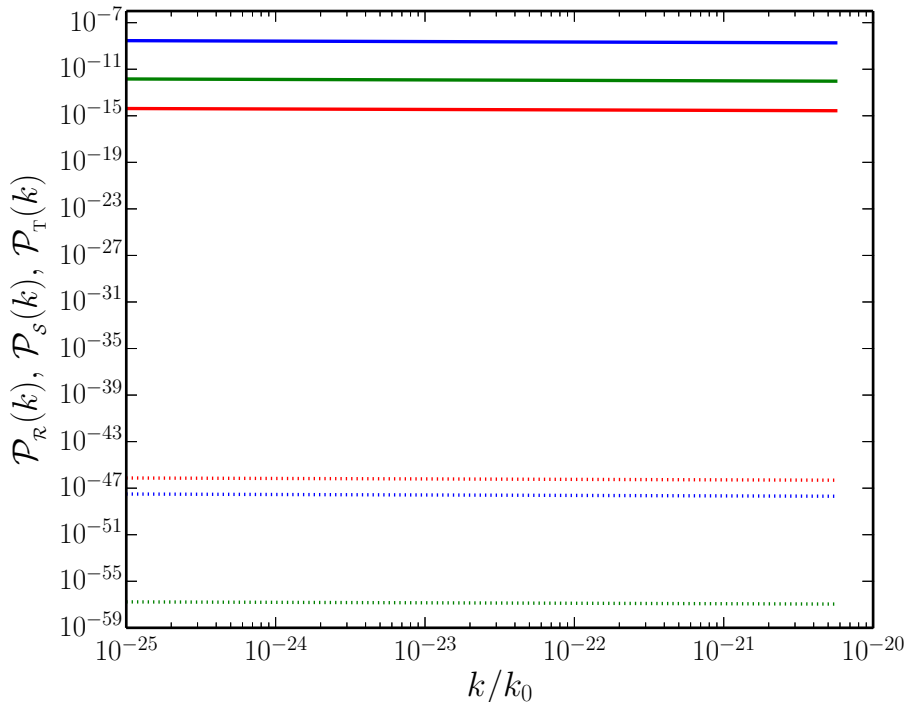


Figure 4.2: The numerically evaluated scalar (the curvature perturbation spectrum in blue and the isocurvature perturbation spectrum in green) and tensor power spectra (in red) have been plotted as a function of k/k_0 for a range of wavenumbers that correspond to cosmological scales today. We have worked with the same set of values for the parameters k_0/a_0 and ε as in the previous figure. The power spectra have been plotted both before the bounce (as dotted lines) and after (as solid lines). The power spectra have been evaluated at $\eta = -\alpha \eta_0$ (with $\alpha = 10^5$) before the bounce and at $\eta = \beta \eta_0$ (with $\beta = 10^2$) after the bounce. The values for the parameters we have worked with lead to the COBE normalized value of 2.31×10^{-9} for the curvature perturbation spectrum at the scale of $k/k_0 = 10^{-23}$. Also, the value of ε we have chosen leads a curvature perturbation spectrum with a red tilt corresponding to $n_{\mathcal{R}} \simeq 0.96$, as required by the CMB observations. Moreover, the tensor-to-scalar ratio evaluated after the bounce proves to be rather small ($r \simeq 10^{-6}$), which is consistent with the current upper limits from Planck on the quantity [7].

4.6 Discussion

In this chapter, extending our discussions from our previous chapter, we have constructed a two-field model consisting of a canonical scalar field and a non-canonical ghost field to drive near-matter bounces. Near-matter bounces are in some sense similar to slow roll inflation as they lead to nearly scale-invariant

spectra. The model we have constructed consisted of two parameters k_0/a_0 and ε . While k_0/a_0 determines the amplitudes of the scalar and tensor power spectra, a non-zero value for ε leads to a tilt in the power spectra. We have been able to numerically evaluate the scalar and tensor power spectra in the model and show that, for suitable values of the parameters, the resulting spectra are consistent with the current constraints from the CMB observations [117].

It is interesting to have extended our original matter bounce scenario and have achieved a red tilt in the scalar power spectrum in order to be consistent with the observations. The next obvious challenge is to examine if the scalar non-Gaussianities generated in the model are indeed consistent with the current constraints from Planck [37]. We are presently investigating this issue.

Chapter 5

Primordial features from ekpyrotic bounces

5.1 Introduction

The precise observations of the anisotropies in the CMB by WMAP and Planck [4, 54] point to a primordial scalar power spectrum that is nearly independent of scale and is largely adiabatic [6]. The most popular paradigm to generate perturbations of such nature is the inflationary scenario [7]. As is well known, inflation is driven by scalar fields (see, for instance, the reviews [2]). There exist many models which permit inflation of the slow roll type leading to power spectra that are consistent with the cosmological data (for a comprehensive list, see Ref. [8]).

Though a nearly scale-invariant primordial power spectrum as generated by slow roll inflation is consistent with the observational data, there have been repeated (model dependent as well as model independent) efforts to examine if the power spectrum contains features [7, 18]. It has been found that certain features improve the fit to the CMB data [7, 18–23]. The possibility of such features gains impor-

tance because of the reason that, if they are confirmed by future observations, they can strongly limit the space of viable models. While such features can be produced in inflationary models which permit deviations from slow roll [19–22], it is imperative to examine if they can also be generated in alternative scenarios.

Even as inflation has been remarkably successful, alternative scenarios have been explored for the origin of primordial perturbations. Amongst these alternatives, the most investigated are the classical bouncing scenarios (for recent reviews, see Refs. [3]). Recall that, the primary goal of the inflationary paradigm is to overcome the horizon problem and provide natural initial conditions for the perturbations when they are well inside the Hubble radius during the early stages of the accelerated expansion. The bouncing scenarios can permit similar initial conditions to be imposed on the perturbations during the contracting phase, provided the early phase is undergoing *decelerated* contraction. More than a handful of bouncing scenarios have been constructed that result in primordial power spectra that are consistent with the observations (see, for instance, Refs. [13]).

It is rather straightforward to construct a model of inflation and, as we mentioned, there exist many models of inflation that perform well against the cosmological data. In contrast, it proves to be an intricate task to construct bouncing models that are free of pathologies (for a list of difficulties faced, see, for example, Refs. [3, 16]). Moreover, the inflationary trajectory is almost always an attractor, which permits inflation to be achieved easily. However, bouncing scenarios often require fine tuned initial conditions. It is the attractor nature of the inflationary trajectory which allows for the generation of features in the primordial spectrum through brief periods of deviation from slow roll. The fact that the trajectory is an attractor ensures that slow roll inflation is restored after such departures. The fine tuned conditions required for bouncing scenarios implies that features cannot be generated in these models. For instance, near matter bounces, which can

be easily constructed, do not behave as attractors and hence they cannot return to the original trajectory if departures are introduced [24]. This implies that such models will be ruled out if cosmological data confirm the presence of features in the primordial spectrum.

Amongst the bouncing models, it is *only* the ekpyrotic scenario that permits trajectories which are attractors (for the original ideas, see Refs. [25]; for more recent discussions, see Refs. [26]). Another advantage of the ekpyrotic model is the fact that the anisotropic instabilities which may arise during the contracting phase can be suppressed since the energy density of the ekpyrotic source dominates the evolution. However, ekpyrotic models driven by a single scalar field generate spectra of curvature perturbations that have a strong blue tilt. Therefore, models involving more than one field are considered, with the ekpyrotic contracting phase being dominated by isocurvature perturbations with a nearly scale-invariant spectrum. The second field is utilized to convert the isocurvature perturbations into adiabatic perturbations, eventually resulting in a nearly scale-invariant curvature perturbation spectrum as is required by the observations (see, for example, Refs. [46, 118]). In this chapter, *for the first time in the literature*, we examine if features can be generated in the curvature perturbation spectrum in ekpyrotic bounces. We shall explicitly construct ekpyrotic potentials which permit the generation of features that have been considered in the context of inflation.

This chapter is organized as follows. In the following section, we shall discuss the attractor nature of the ekpyrotic phase driven by a negative potential. In section 5.3, we shall discuss the generation of the curvature and isocurvature perturbations during the ekpyrotic phase. We shall show that the ekpyrotic phase generates a curvature perturbation spectrum with a strong blue tilt and a nearly scale-invariant isocurvature perturbation spectrum. In section 5.4, we shall nu-

merically illustrate that a sharp turn in the field space converts the isocurvature perturbations into curvature perturbations, leading to a nearly scale independent curvature perturbation spectrum. In section 5.5, we shall introduce suitable modifications to the ekpyrotic potential to generate features in the curvature perturbation spectrum which have often been considered in the context of inflation. We shall finally conclude this chapter with a brief discussion on the prospects of ekpyrotic features in section 5.6.

5.2 Ekpyrotic attractor

In this section, we shall discuss the dynamics of the background in an ekpyrotic model, specifically showing that a negative definite potential for the scalar field admits an attractor during the contracting phase.

The model we shall consider involves two scalar fields ϕ and χ , which are governed by the following action consisting of the potential $V(\phi, \chi)$ and a function $b(\phi)$ [26]:

$$S[\phi, \chi] = \int d^4x \sqrt{-g} \left[-\frac{1}{2} \partial_\mu \phi \partial^\mu \phi - \frac{e^{2b(\phi)}}{2} \partial_\mu \chi \partial^\mu \chi - V(\phi, \chi) \right]. \quad (5.1)$$

We shall begin by working with the potential [the same as in equation (1.34), which we are repeating here for convenience]

$$V(\phi, \chi) = V_{\text{ek}}(\phi) = V_0 e^{\lambda \phi / M_{\text{Pl}}}, \quad (5.2)$$

and choose

$$b(\phi) = \frac{\mu \phi}{2 M_{\text{Pl}}}, \quad (5.3)$$

where λ and μ are positive constants. Upon varying the action (5.1), we obtain

the equations of motion governing the homogeneous scalar fields ϕ and χ to be

$$\ddot{\phi} + 3H\dot{\phi} + V_\phi = b_\phi e^{2b}\dot{\chi}^2, \quad (5.4a)$$

$$\ddot{\chi} + 3H\dot{\chi} + e^{-2b}V_\chi = -2b_\phi\dot{\phi}\dot{\chi}, \quad (5.4b)$$

where, we have introduced earlier, $V_\phi = \partial V/\partial\phi$, while $V_\chi = \partial V/\partial\chi$ and $b_\phi = db/d\phi$. The first Friedmann equation for the system of our interest is given by

$$H^2 = \frac{1}{3M_{\text{Pl}}^2} \left[\frac{1}{2}\dot{\phi}^2 + \frac{e^{2b}}{2}\dot{\chi}^2 + V \right]. \quad (5.5)$$

To examine the stability of the background, it is convenient to write the above background equations in terms of the following dimensionless variables [26]:

$$(x, y, z) \equiv \left(\frac{\dot{\phi}}{\sqrt{6}H M_{\text{Pl}}}, \frac{\sqrt{V}}{\sqrt{3}H M_{\text{Pl}}}, \frac{e^b\dot{\chi}}{\sqrt{6}H M_{\text{Pl}}} \right). \quad (5.6)$$

In terms of the variables (x, y, z) , the equations (5.4) governing the two homogeneous scalar fields can be written as

$$\frac{dx}{dN} = -3xy^2 + \frac{\sqrt{3}}{\sqrt{2}}(\mu z^2 - \lambda y^2), \quad (5.7a)$$

$$\frac{dz}{dN} = -3y^2z - \frac{\sqrt{3}}{\sqrt{2}}\mu xz, \quad (5.7b)$$

where $N = \log a$, as usual, denotes e-folds. We should point out that, during the contracting phase of our interest here, N runs from large positive values at early times to small positive values as one approaches the bounce. Also, the first Friedmann equation (5.5) leads to the constraint

$$x^2 + y^2 + z^2 = 1. \quad (5.8)$$

To illustrate our main points concerning the stability of the background evolution, we shall focus in this section on the simpler situation wherein $\mu = \lambda$. Note that, during the contracting phase, H is negative. When $\mu = \lambda$, upon further assuming that $\dot{\phi}$ is positive, it is easy to show that either of the two fixed points

$$(x_*, y_*, z_*) = \left(-\lambda/\sqrt{6}, \pm\sqrt{1 - \lambda^2/6}, 0 \right) \quad (5.9)$$

lead to the desired conditions. Firstly, they prove to be stable provided $\lambda^2 > 6$. Secondly, we find that the corresponding equation of state parameter describing the background is given by

$$w = \frac{p}{\rho} = \frac{\lambda^2}{3} - 1, \quad (5.10)$$

where ρ and p represent the total energy density and pressure associated with the two scalar fields. This implies that the contracting phase is driven by super stiff matter (as $w > 1$ when $\lambda^2 > 6$). Moreover, since $w > 1$, the energy density ρ grows faster than a^{-6} during ekpyrotic contraction. Such a behavior allows one to circumvent the difficulty posed by the rapid growth of anisotropies (which behave as a^{-6}) that proves to be a great drawback afflicting many of the bouncing scenarios [24]. Lastly, as alluded to earlier, the condition $\lambda^2 > 6$ implies that the potential is negative. It is evident from the above analysis that, at this fixed point, the background dynamics is essentially determined by the scalar field ϕ . In such a case, the scale factor corresponding to this attractor solution can be expressed as in equation (1.35), with the constant V_0 [*cf.* equation (5.2)] being given by equation (1.36).

5.3 Featureless power spectra in ekpyrosis

In this section, we shall first describe the equations governing the perturbations and then go on to evaluate the featureless scalar power spectra generated during the ekpyrotic phase.

5.3.1 Equations governing the scalar perturbations

Let us now turn to the evaluation of the scalar power spectra in the model. Since the model involves two fields, as we have repeatedly emphasized, apart from the curvature perturbation, isocurvature perturbations also arise. In the spatially flat gauge [*viz.* when $\psi = E = 0$ in the line-element (1.44)], for instance, the Mukhanov-Sasaki variables associated with the curvature and the isocurvature perturbations v^σ and v^s are given by

$$v^\sigma = a (\cos \theta \delta\phi + e^b \sin \theta \delta\chi), \quad (5.11a)$$

$$v^s = a (-\sin \theta \delta\phi + e^b \cos \theta \delta\chi), \quad (5.11b)$$

where

$$\cos \theta = \frac{\dot{\phi}}{\dot{\sigma}}, \quad \sin \theta = e^b \dot{\chi}/\dot{\sigma}, \quad \dot{\sigma}^2 = \dot{\phi}^2 + e^{2b} \dot{\chi}^2. \quad (5.12)$$

The curvature and the isocurvature perturbations are defined as $\mathcal{R} = v^\sigma/z$ and $\mathcal{S} = v^s/z$, respectively, with $z = a \dot{\sigma}/H$ [26].

One can show that, at the quadratic order, the action governing the Mukhanov-Sasaki variables associated with the curvature and the isocurvature perturbations is given by (see for instance, Ref. [109])

$$\mathcal{S}_2[v^\sigma, v^s] = \frac{1}{2} \int d\eta \int d^3\mathbf{x} \left\{ v^{\sigma'2} + v^{s'2} - (\partial v^\sigma)^2 - (\partial v^s)^2 + \frac{z'^2}{z^2} v^{\sigma 2} \right.$$

$$+ \left(\frac{a'^2}{a^2} - a^2 \mu_s^2 \right) v^{s2} - 2 \left[\frac{z'}{z} v^{\sigma'} v^\sigma + \frac{a'}{a} v^{s'} v^s + z \xi \left(\frac{v^\sigma}{z} \right)' v^s \right] \Bigg\}, \quad (5.13)$$

where

$$\xi = -\frac{2aV_s}{\dot{\sigma}}, \quad (5.14)$$

$$\mu_s^2 = V_{ss} - \left(\frac{V_s}{\dot{\sigma}} \right)^2 + b_\phi (1 + \sin^2 \theta) \cos \theta V_\sigma + b_\phi \cos^2 \theta \sin \theta V_s - (b_\phi^2 + b_{\phi\phi}) \dot{\sigma}^2. \quad (5.15)$$

Also, the quantities V_σ , V_s and V_{ss} are given by

$$V_\sigma = e_\sigma^I V_I, \quad V_s = e_s^I V_I, \quad V_{ss} = e_s^I e_s^J V_{IJ}, \quad (5.16)$$

with e_σ and e_s being the adiabatic and entropy vectors in the space of the two fields, defined as

$$e_\sigma = (\cos \theta, e^{-b} \sin \theta), \quad (5.17a)$$

$$e_s = (-\sin \theta, e^{-b} \cos \theta), \quad (5.17b)$$

where $I = \{\phi, \chi\}$, and we have assumed implicit summations over the repeated indices I and J . By varying the action (5.13), the equations governing the Fourier modes of the Mukhanov-Sasaki variables, *viz.* v_k^σ and v_k^s , can be obtained to be [26, 109]

$$v_k^{\sigma''} + \left(k^2 - \frac{z''}{z} \right) v_k^\sigma = \frac{1}{z} (z \xi v_k^s)', \quad (5.18a)$$

$$v_k^{s''} + \left(k^2 - \frac{a''}{a} + a^2 \mu_s^2 \right) v_k^s = -z \xi \left(\frac{v_k^\sigma}{z} \right)'. \quad (5.18b)$$

It should be stressed that these equations (5.18) apply for an arbitrary potential

$V(\phi, \chi)$ and function $b(\phi)$.

5.3.2 The scalar power spectra

The ekpyrotic contracting phase can be modeled by the potential $V_{\text{ek}}(\phi)$ and the function $b(\phi)$ we had mentioned before [26]. We shall now assume that V_0 is negative (to lead to an attractor) and that $\mu \neq \lambda$. During this ekpyrotic phase, we find that the contribution of χ to the background energy density can be ignored and the function ξ , which couples the curvature and the isocurvature perturbations, is negligible (in this context, see figure 5.1). Therefore, the equations governing the Mukhanov-Sasaki variables (5.18) decouple. In such a case, the quantity v_k^σ satisfies the equation (1.76), while v_k^s obeys the equation

$$v_k^{s''} + \left[k^2 + \frac{\lambda^2 (2 - \mu \lambda - \mu^2) + 6 \mu \lambda - 8}{(\lambda^2 - 2)^2 \eta^2} \right] v_k^s = 0. \quad (5.19)$$

These equations can be solved analytically and, upon imposing the Bunch-Davies initial conditions at early times, the scalar power spectra can be evaluated at later times closer to the bounce. The two scalar power spectra can be expressed as in equation (1.78a), where $\nu = (\lambda^2 - 6)/[2(\lambda^2 - 2)]$ and $(\lambda^2 + 2\mu\lambda - 6)/[2(\lambda^2 - 2)]$ for the cases of the curvature and the isocurvature perturbations, respectively. While the spectral index $n_{\mathcal{R}}$ associated with the curvature perturbation is given by equation (1.79), the spectral index n_s associated with the isocurvature perturbation can be obtained to be

$$n_s = 4 - \left| \frac{2(\lambda\mu - 2)}{\lambda^2 - 2} + 1 \right|. \quad (5.20)$$

Since $\lambda^2 > 6$, one obtains a very blue, *i.e.* $n_{\mathcal{R}} > 3$, curvature perturbation spectrum $\mathcal{P}_{\mathcal{R}}(k)$. We can choose μ suitably to arrive at a nearly scale-invariant isocur-

vature perturbation spectrum $\mathcal{P}_s(k)$ (such that $n_s \simeq 1$). Note that, had μ been zero [corresponding to a vanishing $b(\phi)$], the isocurvature perturbation spectrum would also have been blue like the curvature perturbation spectrum. Clearly, the presence of the non-minimal coupling function $b(\phi)$ seems essential to arrive at a scale-invariant isocurvature perturbation spectrum. In what follows, we shall construct a mechanism to convert the isocurvature perturbations into curvature perturbations and also modify the tilt of the curvature perturbation spectrum so as to be consistent with the observations.

5.4 Converting the isocurvature perturbations into curvature perturbations

As is well known, the isocurvature perturbations can be converted into curvature perturbations if there arises a turn in the background trajectory in the field space [26, 46]. Since the field ϕ dominates the background during the ekpyrotic phase, we shall require the field to take a turn along the χ direction. We achieve such a turn by multiplying the original potential $V_{\text{ek}}(\phi)$ by the term

$$V_c(\phi, \chi) = 1 + \beta \chi \exp - [(\phi - \phi_c)/\Delta\phi_c]^2, \quad (5.21)$$

where β , ϕ_c and $\Delta\phi_c$ are constants. Clearly, in V_c , the dependence on the field χ is the strongest within $\Delta\phi_c$ of ϕ_c . The introduction of the term V_c in the potential makes the dynamics difficult to study analytically. Therefore, we resort to numerics. We find that, as the field ϕ approaches ϕ_c , there arises an abrupt change of direction in the field space with a rapid variation of the field χ . This behavior leads to a sharp rise in the function ξ which determines the coupling between curvature and the isocurvature perturbations [*cf.* equations (5.18)]. The sudden

rise in ξ considerably amplifies the curvature perturbation. These behavior are illustrated in figure 5.1. The analytical expressions for the power spectra we have presented above correspond to spectra evaluated prior to the turn. The power spectra evaluated numerically before and at the turn in field space (when $\phi = \phi_c$, corresponding to $\eta = \eta_c$) are illustrated in figure 5.2. A few points regarding the figure need emphasis. As we discussed, when evaluated prior to the turn, while $\mathcal{P}_{\mathcal{R}}(k)$ is strongly blue, $\mathcal{P}_{\mathcal{S}}(k)$ is nearly scale-invariant. Also, note that, over the scales of interest, the amplitude of $\mathcal{P}_{\mathcal{S}}(k)$ is considerably larger than the amplitude of $\mathcal{P}_{\mathcal{R}}(k)$. However, as the turn occurs, we find that both the scalar power spectra have roughly the same amplitude. Moreover, importantly, due to its strong effects, the isocurvature perturbations have altered the shape of the curvature perturbation spectrum $\mathcal{P}_{\mathcal{R}}(k)$ and, in fact, for suitable values of the parameters (actually, for $\lambda = \sqrt{20}$ and $\mu \simeq 4.54$), we obtain a nearly scale-invariant spectrum with $n_{\mathcal{R}} \simeq 0.96$, completely consistent with the observations. We have chosen the parameters such that the nearly scale-invariant $\mathcal{P}_{\mathcal{R}}(k)$ is COBE normalized. In the next section, we shall modify the ekpyrotic potential $V_{\text{ek}}(\phi)$ to generate features in the scalar power spectra.

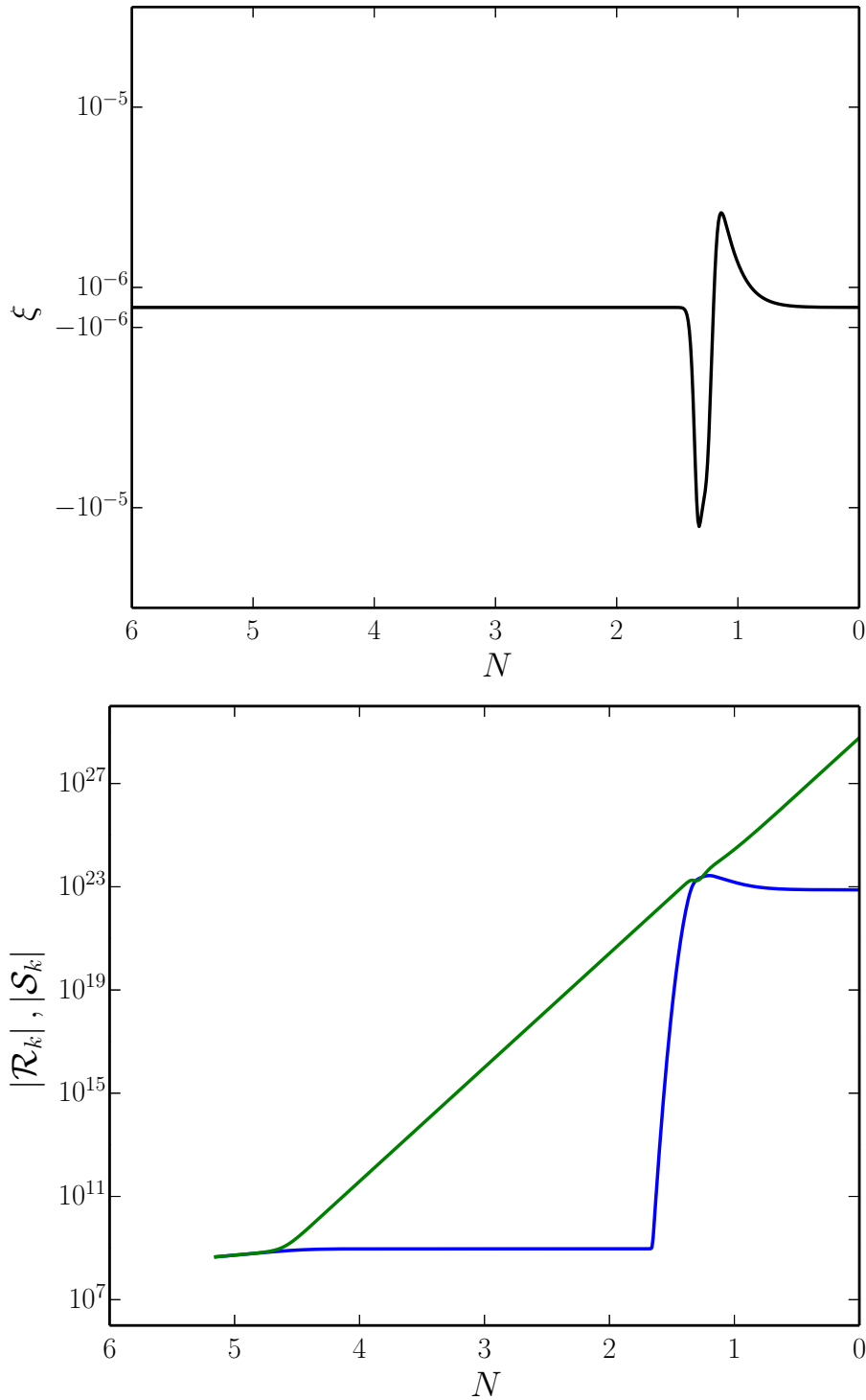


Figure 5.1: The behavior of the coupling function ξ (on top) and the corresponding effects on the curvature (in blue) and the isocurvature (in green) perturbations (at the bottom) have been plotted as a function of e-folds N . Recall that time runs forward from left to right and the choice of $N = 0$ is arbitrary. There arises a sharp rise in ξ when the direction of evolution changes in the field space. It should be clear from the plots that the amplitude of the curvature perturbation is enhanced exactly around this time.

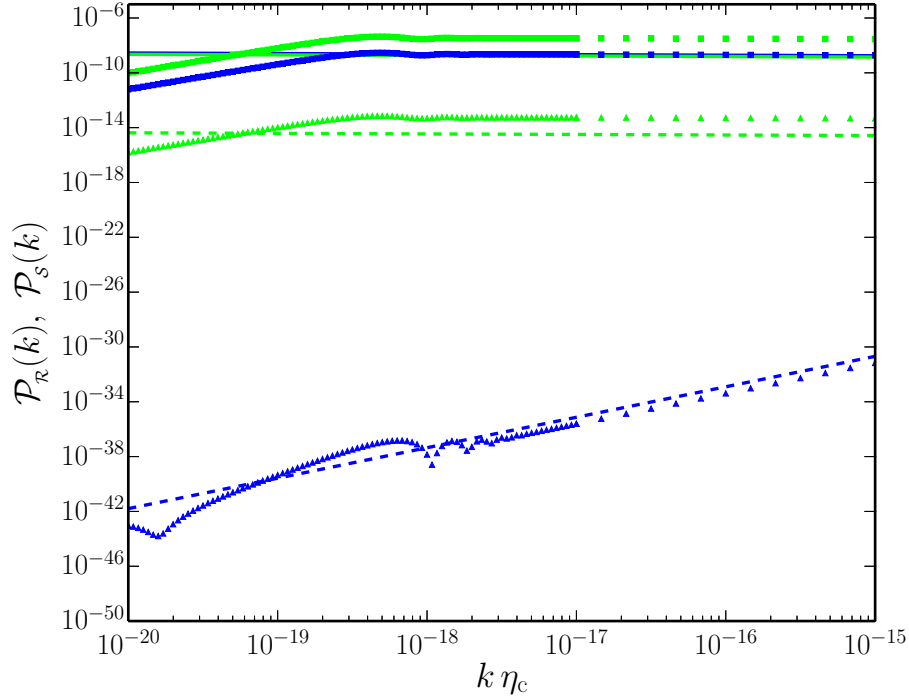


Figure 5.2: The curvature and isocurvature perturbation spectra, *viz.* $\mathcal{P}_{\mathcal{R}}(k)$ and $\mathcal{P}_{\mathcal{S}}(k)$ (in blue and green, respectively), have been plotted prior to (as dashed lines) as well as during the turn (as solid lines) in field space. Note that $\mathcal{P}_{\mathcal{S}}(k)$ is nearly scale-free both prior to and during the turn. However, while $\mathcal{P}_{\mathcal{R}}(k)$ is blue before the turn, it is red later. Also, the isocurvature perturbations are extremely dominant prior to the turn. But, the amplitude of the curvature perturbation becomes comparable to that of the isocurvature perturbations during the turn in field space. The range of wavenumbers over which the spectra have been plotted are expected to correspond to cosmological scales today. Moreover, we have chosen to work with values of the various parameters involved so that $\mathcal{P}_{\mathcal{R}}(k)$ is COBE normalized. The figure also contains the scalar power spectra with a specific feature before (as triangles) and during the turn (as squares). We should highlight that it is the feature in the initial $\mathcal{P}_{\mathcal{S}}(k)$ which is imprinted as a feature in the final $\mathcal{P}_{\mathcal{R}}(k)$.

5.5 Generating ekpyrotic features

The primordial features that have been found to improve the fit to the data can be broadly classified into the following three types: (1) sharp drop in power at large scales corresponding to the Hubble radius today, (2) a burst of oscillations over an intermediate range of scales, and (3) persisting oscillations over a wide range of scales. While a feature of the first type improves the fit to the CMB data at the very low multipoles (specifically, the low quadrupole, *i.e.* corresponding to $\ell = 2$) [19], the second type has been shown to provide a better fit to the outliers (to the nearly scale-invariant case) around the multipoles of $\ell \simeq 20\text{--}40$ [20]. The third type of feature has been found to fit the data over a wide range of multipoles [21].

Smooth scalar field potentials cannot generate features. It is the features in the potential and the resulting non-trivial dynamics that translates to features in the power spectra. As we had discussed in the introductory section of this chapter, in inflation, features in the potential lead to deviations from slow roll which, in turn, generate spectra containing departures from near scale-invariance. For instance, in single field inflationary models, a point of inflection can lead to the first type of feature we had mentioned above [19], while the second type of feature can be generated with the introduction of a simple step in the inflationary potential [20]. The last type of feature is generated with the aid of corresponding oscillations in the inflationary potential [21]. In fact, there have been attempts to construct inflationary models that can simultaneously generate more than one type of features [22].

Since the background dynamics in the ekpyrotic scenario is rather distinct from the inflationary case, prior experience with inflationary features does not necessarily help in constructing ekpyrotic potentials leading to the desired features. We find that multiplying the original ekpyrotic potential $V_{\text{ek}}(\phi)$ by the following

oscillating term:

$$V_f(\phi) = 1 + \alpha \cos(\omega \phi / M_{\text{Pl}}) \quad (5.22)$$

does indeed lead to persistent oscillations in the power spectrum as in the context of inflation [21]. However, the potentials for generating the other two types of features prove to be considerably different. We had to experiment with different multiplicative functions $V_f(\phi)$ before arriving at the required forms. Interestingly, we find that, introducing a step by multiplying $V_{\text{ek}}(\phi)$ with the term

$$V_f(\phi) = 1 + \alpha \tanh[(\phi - \phi_0) / \Delta\phi_f] \quad (5.23)$$

results in the first type of feature we had mentioned, *viz.* a sharp drop in power at large scales. Lastly, introducing a well in the potential with the help of a term such as

$$V_f(\phi) = 1 - \alpha \exp - [(\phi - \phi_0) / \Delta\phi_f]^2 \quad (5.24)$$

generates a burst of oscillations over an intermediate range of scales, which is the second type of feature we had discussed. We have plotted the power spectra of curvature perturbations arising in these three cases in figure 5.3. In the figure, we have also plotted inflationary power spectra with features that lead to a better fit to the most recent Planck data (in this context, see Refs. [4]). It is clear from the figure that the ekpyrotic features match the inflationary features reasonably well.

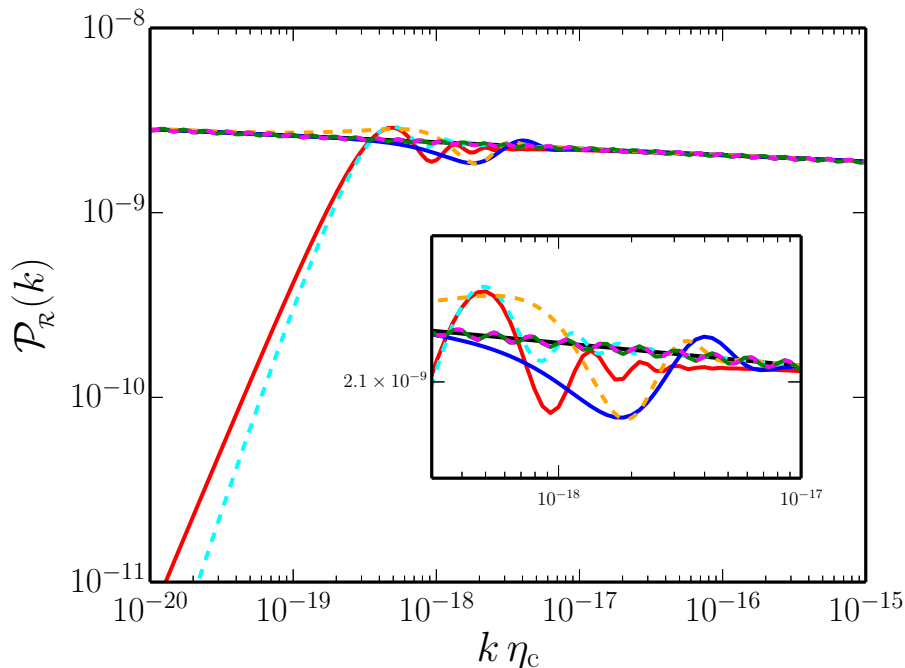


Figure 5.3: The power spectra of the curvature perturbations with the three types of features (type 1 in red and cyan, type 2 in blue and orange, and type 3 in green and pink) generated in the ekpyrotic (solid lines) and the inflationary (dashed lines) scenarios have been plotted over scales of cosmological interest. The inflationary spectra correspond to those that lead to an improved fit to the CMB data [7]. Clearly (as also highlighted in the inset), the ekpyrotic spectra closely resemble the inflationary spectra with features.

5.6 Prospects

Features in the primordial spectra can lead to strong constraints on the physics of the early universe [18]. However, there is no significant observational evidence for deviations from a nearly scale-invariant primordial power spectrum as yet. Many of the simpler and fine tuned bouncing models would prove to be unsustainable if future observations confirm the presence of features [4]. We have examined if the bouncing scenarios can remain viable after such a possibility. *For the first time in the literature*, we have constructed ekpyrotic potentials that lead to features that have often been found to provide an improved fit to the CMB data [119]. Though we have evaluated the spectra prior to the bounce, since the

scales associated with the bounce are significantly different from the scales of cosmological interest, the shape of the spectra we have arrived at will not be altered by the dynamics of the bounce. Therefore, these power spectra can be expected to retain their form after the bounce. Moreover, experience with related models suggests that the isocurvature perturbations would decay after the bounce leading to an adiabatic spectrum consistent with the observations [26, 46].

We have focused on the power spectra generated in the ekpyrotic models. Currently, there also exist strong limits on the primordial scalar non-Gaussianities [37]. The concern has been that, quite generically, the scalar non-Gaussianities generated in bounces may turn out be larger than the current constraints [37]. However, it has been argued that the non-Gaussianities in the type of models we have considered will prove to be small (in this context, see the third reference in Refs. [26]). We are currently investigating this issue.

Chapter 6

Quantum-to-classical transition of primordial perturbations in inflationary and bouncing scenarios

6.1 Introduction

As we have discussed in the previous chapters, the inflationary and the non-singular, classical bouncing scenarios offer alternative paradigms for the origin of perturbations in the early universe. In both these scenarios, the background is often assumed to be driven by one or more scalar fields. It is the quantum fluctuations associated with the scalar fields that are supposed to be responsible for the primordial scalar perturbations. These primordial perturbations, in turn, are expected to lead to the anisotropies in the CMB and the formation of the large scale structure. The statistical properties of the anisotropies in the CMB and the distribution of the large scale structure are described in terms of classical correlation functions. While the perturbations have a quantum origin, when examining

their imprints on the CMB and the large scale structure, the correlation functions describing the primordial perturbations are treated as classical quantities. It would be fair to say that, despite considerable effort, the quantum-to-classical transition of the primordial perturbations remains to be understood satisfactory (in this context, see Refs. [28,29]).

Inflation is often easy to achieve with the aid of a single scalar field. In contrast, as described in the last three chapters, one seems to require more than one scalar field to achieve non-singular, classical bounces. As we have seen, such multi-field models result in a richer dynamics as far as the background is concerned. Moreover, apart from the curvature perturbation, isocurvature perturbations also arise in the multi-field models. For instance, in the ekpyrotic scenario discussed in the previous chapter, the isocurvature perturbation plays an important role in converting a strongly blue curvature perturbation spectrum into a nearly scale-invariant spectrum, as is demanded by the observations. It will be interesting to examine the role of the isocurvature perturbations in the quantum-to-classical transition of the primordial scalar perturbations [30,32].

With a such motivation in mind, in this chapter, we shall compare and contrast the quantum-to-classical transition in two-field models of inflationary and bouncing scenarios [28–33,121]. Specifically, in the context of inflation, we shall consider the case of double inflation driven by two scalar fields described by the quadratic potential. In the context of bounces, we shall consider the ekpyrotic scenario which we discussed in the previous chapter. We shall investigate the nature of the quantum-to-classical transition in these situations with the aid of the Wigner function characterizing the evolution of the curvature perturbation associated with a typical mode of cosmological interest. As is well known, the modes of a quantum field are expected to be increasingly squeezed as the universe evolves. We shall also examine the extent of squeezing of the curvature

perturbation in the inflationary and bouncing scenarios.

This chapter is organized as follows. In the following section, we shall review the quantum-to-classical transition of the curvature perturbation in single field models. We shall study the behavior of the Wigner function and the extent of squeezing in power law inflation and during the contracting phase in matter as well as ekpyrotic bounces. In section 6.3, we shall solve the Schrodinger equation describing a single mode of the curvature and the isocurvature perturbations in two-field models. We shall then obtain the corresponding Wigner function as well as the reduced density matrix describing the curvature perturbation. We shall also construct the squeezing parameters characterizing the curvature and the isocurvature perturbations. In section 6.4, we shall apply the formalism developed to the cases of double inflation and ekpyrotic contraction. We shall examine the behavior of the Wigner function, the reduced density matrix and the squeezing parameter describing the curvature perturbation in both these scenarios. In section 6.5, we shall conclude the chapter with a brief discussion highlighting the primary differences in the behavior of the quantum-to-classical transition in double inflation and ekpyrotic contraction.

6.2 Review of the single field case

In this section, we shall rapidly review the quantum-to-classical transition of perturbations generated in the inflationary and bouncing scenarios driven by a single, canonical, scalar field.

6.2.1 Action governing the scalar perturbations

Recall that, during inflation or a contracting phase driven by a single, canonical scalar field, the scalar perturbations can be described completely in terms of the curvature perturbation \mathcal{R} . In such a case, the curvature perturbation \mathcal{R} is governed by the action (1.54). We shall work here with the corresponding Mukhanov-Sasaki variable v defined as $v = z\mathcal{R}$. In terms of the variable v , one can show that the action (1.29) reduces to the following form [28]:

$$\mathcal{S}_2[v] = \frac{1}{2} \int d\eta \int d^3\mathbf{x} \left[v'^2 - (\partial v)^2 - \frac{z'}{z} v' v + \frac{z'^2}{z^2} v^2 \right]. \quad (6.1)$$

As we had done with the operator describing the curvature perturbation \mathcal{R} [cf. equation (1.58)], we can decompose the classical Mukhanov-Sasaki variable v in terms of the corresponding Fourier modes $v_{\mathbf{k}}$ as

$$v(\eta, \mathbf{x}) = \int \frac{d^3\mathbf{k}}{(2\pi)^{3/2}} v_{\mathbf{k}}(\eta) e^{i\mathbf{k}\cdot\mathbf{x}}. \quad (6.2)$$

In terms of the Fourier modes $v_{\mathbf{k}}$, the action (6.1) can be expressed as

$$\mathcal{S}_2[v] = \frac{1}{2} \int d\eta \int d^3\mathbf{k} \left[v'_{\mathbf{k}} v'^*_{\mathbf{k}} - \frac{z'}{z} (v'_{\mathbf{k}} v^*_{\mathbf{k}} + v'^*_{\mathbf{k}} v_{\mathbf{k}}) - \left(k^2 - \frac{z'^2}{z^2} \right) v^*_{\mathbf{k}} v_{\mathbf{k}} \right]. \quad (6.3)$$

If we now write $v_{\mathbf{k}} = v_{\mathbf{k}}^{\text{R}} + i v_{\mathbf{k}}^{\text{I}}$, where, evidently, $v_{\mathbf{k}}^{\text{R}}$ and $v_{\mathbf{k}}^{\text{I}}$ denote the real and imaginary parts of $v_{\mathbf{k}}$, then the above action reduces to

$$\begin{aligned} \mathcal{S}_2[v] = & \frac{1}{2} \int d\eta \int d^3\mathbf{k} \left[v_{\mathbf{k}}^{\text{R}2} + v_{\mathbf{k}}^{\text{I}2} - \frac{z'}{z} (v_{\mathbf{k}}^{\text{R}} v_{\mathbf{k}}^{\text{R}'} + v_{\mathbf{k}}^{\text{I}} v_{\mathbf{k}}^{\text{I}'}) \right. \\ & \left. - \left(k^2 - \frac{z'^2}{z^2} \right) (v_{\mathbf{k}}^{\text{R}2} + v_{\mathbf{k}}^{\text{I}2}) \right]. \end{aligned} \quad (6.4)$$

Since we are working at the linear order in perturbation theory, the modes $v_{\mathbf{k}}$ evolve independently. Due to this reason, in this chapter, we shall focus on the

behavior of a single mode v_k , and drop the subscript k . Further, it should be clear from that the structure of the above action that the real and imaginary parts v_k^R and v_k^I (which, we should emphasize, are real quantities themselves) are not coupled to each other and evolve independently. Therefore, for convenience in notation, we shall also drop the superscripts R and I and refer to *all* these variables simply as v . Needless to add, the discussion below shall apply to each of the components v_k^R and v_k^I and for all modes k of cosmological interest.

6.2.2 Schrodinger equation, wave function and variances

In this section, we shall solve the Schrodinger equation describing the wave function associated with the variable v . Note that the variable v satisfies the scalar Mukhanov-Sasaki equation (1.62), which is essentially the equation of motion describing an oscillator with the time-dependent frequency

$$\omega^2(\eta) = k^2 - \frac{z''}{z}. \quad (6.5)$$

As is well known, the solution to the Schrodinger equation describing a time-dependent oscillator can be expressed in terms of the solutions to the classical equation of motion. It is this approach that we shall adopt to construct the wave function describing the system.

It should be clear from the action (6.4) that the conjugate momentum associated with the variable v is given by

$$p = v' - \frac{z'}{z} v. \quad (6.6)$$

The corresponding Hamiltonian can be immediately constructed to be

$$H = \frac{p^2}{2} + 2 \frac{z'}{z} p v + \frac{k^2}{2} v^2. \quad (6.7)$$

In the Schrodinger picture that we shall be working in, while the operator \hat{v} is a simple multiplicative operator, the corresponding momentum operator \hat{p} can be represented as $\hat{p} = -i \partial / (\partial v)$. If the wave function describing the system is $\Psi(v, \eta)$, then the Schrodinger equation governing the wave function is given by

$$i \frac{\partial \Psi}{\partial \eta} = -\frac{1}{2} \frac{\partial^2 \Psi}{\partial v^2} - \frac{i}{2} \frac{z'}{z} \left(\Psi + 2v \frac{\partial \Psi}{\partial v} \right) + \frac{k^2}{2} v^2 \Psi. \quad (6.8)$$

We shall be interested in situations wherein the wave function evolves from an initial ground state defined at very early times when the modes can be expected to be in the sub-Hubble domain. In such a case, we can propose the following Gaussian ansatz to describe the wave function [28,29]:

$$\Psi(v, \eta) = N(\eta) \exp - \left[\frac{\Omega(\eta) v^2}{2} \right], \quad (6.9)$$

where N and Ω are functions that depend on time which need to be determined by solving the Schrodinger equation (6.8). Actually, upon normalizing the wave function, *i.e.* demanding that

$$\int_{-\infty}^{\infty} dv |\Psi(v, \eta)|^2 = 1, \quad (6.10)$$

we find that N and Ω are related as follows:

$$|N| = \left(\frac{\Omega + \Omega^*}{2\pi} \right)^{1/4} = \left(\frac{\Omega^{\text{R}}}{\pi} \right)^{1/4}, \quad (6.11)$$

where Ω^{R} denotes the real part of Ω . Upon substituting the ansatz (6.9) in the

Schrodinger equation (6.8), we find that the functions N and Ω satisfy the differential equations

$$i \frac{N'}{N} = \frac{\Omega}{2} - \frac{i}{2} \frac{z'}{z}, \quad (6.12a)$$

$$\Omega' = -i\Omega^2 - 2 \frac{z'}{z} \Omega + ik^2. \quad (6.12b)$$

Let us now write the quantity Ω as

$$\Omega = -\frac{ig^*}{f^*}, \quad (6.13)$$

where g is given by

$$g = f' - \frac{z'}{z} f, \quad (6.14)$$

i.e. it has the same structure as the conjugate momentum p . In such a case, we find that equation (6.12b) leads to

$$f'' + \omega^2(\eta) f = 0, \quad (6.15)$$

with $\omega^2(\eta)$ defined as in equation (6.5). Clearly, the above differential equation for f is the same as the scalar Mukhanov-Sasaki equation (1.62). In other words, as in the case of a time-dependent oscillator, the classical solution to the Mukhanov-Sasaki variable v allows us to construct the wave function describing the quantum system. It should be evident that, in a state described by the Gaussian wave function (6.9), the expectation values $\langle \hat{v} \rangle$ and $\langle \hat{p} \rangle$ are zero. The variances associated with these quantities can be easily evaluated to be

$$\langle \hat{v}^2 \rangle = \frac{1}{2\Omega^R} = |f|^2, \quad (6.16a)$$

$$\langle \hat{p}^2 \rangle = |g|^2, \quad (6.16b)$$

where Ω^{R} denotes the real part of Ω . Note that the variances are determined by the amplitudes of the classical solutions to v and the corresponding conjugate momentum p . Moreover, one can show that

$$\frac{1}{2} \langle \hat{v} \hat{p} + \hat{p} \hat{v} \rangle = f g^* + f^* g. \quad (6.17)$$

As we shall see later, the Wigner function and the squeezing parameters can be completely expressed in terms of the above three quantities.

6.2.3 The Wigner function

In order to examine the quantum-to-classical transition of the cosmological perturbations, we utilize the standard tool called the Wigner function [28, 29]. The Wigner function is a quasi-probability distribution that helps us visualize the dynamics of a quantum system in phase space. Given a wave function $\Psi(x, t)$, the Wigner function $W(x, p, t)$ is defined by the following integral:

$$W(x, p, t) = \frac{1}{\pi} \int_{-\infty}^{\infty} dy \Psi(x - y, t) \Psi^*(x + y, t) e^{2ipy}. \quad (6.18)$$

While it is straightforward to show that the Wigner function $W(x, p, t)$ is always real, one finds that it does *not* prove to be positive definite for all states of a system. Hence, it is often referred to as a 'quasi'-probability distribution. However, for the Gaussian wave function of our interest here, it does remain positive.

Using the wave function (6.9), one can obtain the corresponding Wigner function in the phase space v - p by substituting it in the expression (6.18), and evaluating the Gaussian integrals involved. One obtains that

$$W(v, p) = \frac{1}{\pi} \exp - \left[\Omega^{\text{R}} v^2 + \frac{1}{\Omega^{\text{R}}} (p + \Omega^{\text{I}} v)^2 \right], \quad (6.19)$$

where Ω^I represents the imaginary part of Ω . As we shall see, as time evolves, the Wigner function becomes increasingly squeezed along the direction of the asymptotic classical trajectory in phase space. Moreover, one finds that, at these late times, the quantum correlations become indistinguishable from classical, stochastic, correlation functions. When such a behavior occurs, the system can be said to have approached classicality. The extent of squeezing can be characterized by the behavior of the so-called Wigner ellipse, which is defined as the locus of points in the phase space wherein the Wigner function has a specific amplitude. In our case, the Wigner ellipse can be, for instance, chosen as the contour wherein the exponent of the Wigner function (6.19) is unity, *i.e.* the curve described by the condition

$$\Omega^R v^2 + \frac{1}{\Omega^R} (p + \Omega^I v)^2 = 1. \quad (6.20)$$

6.2.4 The squeezing parameter and the squeezing angle

While one may visually ascertain the extent of squeezing using the Wigner function, it is useful to have a measure that will allow us to quantify the amount of squeezing. The squeezing parameters provides such a measure. We shall now turn to a brief discussion of these parameters.

Using equation (6.15), it is easy to establish that the following Wronskian:

$$\mathcal{W} = f g^* - f^* g, \quad (6.21)$$

is a conserved quantity. As we have discussed earlier, in inflation as well as bounces, one imposes the initial conditions on the modes in the sub-Hubble domain wherein $k^2 \gg z''/z$. Also, one imposes the standard Bunch-Davies initial condition, which corresponds to choosing $f(\eta) \rightarrow (1/\sqrt{2k}) \exp - (i k \eta)$ in the sub-Hubble limit. In such a case, $\Omega \rightarrow k$, so that the Gaussian ansatz (6.9) reduces

to the ground state wave function of an oscillator with unit mass and frequency k , as expected. Demanding the Bunch-Davies initial condition also fixes the value of the above Wronskian to be $\mathcal{W} = i$.

Let us now introduce the parametrization

$$f = \frac{1}{\sqrt{2k}} (\tilde{\alpha} + \tilde{\beta}), \quad (6.22a)$$

$$g = -i \sqrt{\frac{k}{2}} (\tilde{\alpha} - \tilde{\beta}). \quad (6.22b)$$

The Wronskian (6.21) and the fact that $\mathcal{W} = i$ leads to the constraint

$$|\tilde{\alpha}|^2 - |\tilde{\beta}|^2 = 1. \quad (6.23)$$

It should be evident that the quantities $\tilde{\alpha}$ and $\tilde{\beta}$ are essentially the so-called Bogoliubov coefficients which relate the modes of a quantum field at different times in a time-dependent background. These coefficients would also relate the annihilation and the creation operators at different times, had we been working in the Heisenberg picture (in this context, see, for example, the texts [120]).

The constraint (6.23) permits us to parametrize the quantities $\tilde{\alpha}$ and $\tilde{\beta}$ in terms of three parameters, say, (r, θ, ϕ) , as follows¹:

$$\tilde{\alpha} = \cosh r e^{i\theta}, \quad (6.24a)$$

$$\tilde{\beta} = \sinh r e^{i(2\phi - \theta)}. \quad (6.24b)$$

The quantity r is the primary parameter which reflects the extent of squeezing of the original vacuum state due to the time dependence of the background. As we shall illustrate in due course, the Wigner ellipse initially starts as a circle when

¹We seem unable to ensure clarity and simultaneously avoid degeneracy in our notation! Earlier, while ϕ had denoted a canonical scalar field, r had represented the tensor-to-scalar ratio. In this section, r and ϕ shall denote the squeezing parameter and the squeezing angle, respectively.

the Bunch-Davies initial condition is imposed in the sub-Hubble domain. The circle gets increasingly squeezed into an ellipse and the ellipse rotates as time evolves. While the quantity r shall reflect the extent of squeezing of the circle into an ellipse, the angle ϕ determines the direction of squeezing. Using the definitions (6.22) and (6.24) and the expressions (6.16) for the variances in the operators \hat{v} and \hat{p} , we can write the variances in terms of the squeezing parameters as follows:

$$\langle \hat{v}^2 \rangle = |f|^2 = \frac{1}{2k} [\cosh(2r) + \sinh(2r) \cos(2\phi)], \quad (6.25a)$$

$$\langle \hat{p}^2 \rangle = |g|^2 = \frac{k}{2} [\cosh(2r) - \sinh(2r) \cos(2\phi)]. \quad (6.25b)$$

We can invert these relations to express the squeezing parameters in terms of the variances as

$$\cosh(2r) = k \langle \hat{v}^2 \rangle + \frac{\langle \hat{p}^2 \rangle}{k} = k |f|^2 + \frac{|g|^2}{k}, \quad (6.26a)$$

$$\cos(2\phi) = \frac{1}{\sinh(2r)} \left(k \langle \hat{v}^2 \rangle - \frac{\langle \hat{p}^2 \rangle}{k} \right) = \frac{1}{\sinh(2r)} \left(k |f|^2 - \frac{|g|^2}{k} \right). \quad (6.26b)$$

Since the variances $\langle \hat{v}^2 \rangle$ and $\langle \hat{p}^2 \rangle$ are completely determined by the amplitudes of the classical solutions f and g , we can determine the squeezing parameter r and the rotation angle ϕ from these quantities. In the remainder of this section, utilizing the classical solutions for the Mukhanov-Sasaki variable, we shall examine the behavior of the squeezing parameters r and ϕ in the cases wherein the universe inflates or contracts with the scale factor described by a power law.

6.2.5 Power law inflation and contraction

In this subsection, we shall understand the essential differences in the quantum-to-classical transition of the curvature perturbation in single field models driving

power law expansion or contraction. As we had discussed in chapter 1, a canonical scalar field governed by the exponential potential (1.34) leads to a power law scale factor as given in equation (1.35). Recall that, in this case, the solution to the Mukhanov-Sasaki variable is given by equation (1.77). Upon using this solution, we can express the corresponding conjugate momentum in terms of the Hankel function $H_\nu^{(1)}(x)$ as

$$g(\eta) = \sqrt{\frac{\pi}{-4\eta}} e^{i(\nu+1/2)\pi/2} \left\{ k\eta H_{\nu-1}^{(1)}(-k\eta) + \left[\frac{\lambda^2 - 6}{2(\lambda^2 - 2)} - \nu \right] H_\nu^{(1)}(-k\eta) \right\}, \quad (6.27)$$

where $\nu = |(\lambda^2 - 6)/[2(\lambda^2 - 2)]|$. From the solution (1.77) for the mode v and the conjugate momentum above, for $\nu = \pm(\lambda^2 - 6)/[2(\lambda^2 - 2)]$, the resulting squeezing parameters r and ϕ can be obtained to be

$$\cosh(2r) = -\frac{\pi k \eta}{4} \left[|H_\nu^{(1)}(-k\eta)|^2 + |H_{|\nu\mp 1|}^{(1)}(-k\eta)|^2 \right], \quad (6.28a)$$

$$\cos(2\phi) = -\frac{\pi k \eta}{4} \frac{1}{\sinh(2r)} \left[|H_\nu^{(1)}(-k\eta)|^2 - |H_{|\nu\mp 1|}^{(1)}(-k\eta)|^2 \right]. \quad (6.28b)$$

These expressions are exact. Using these results, we have plotted the behavior of the parameters r and ϕ in figure 6.1 for the cases of de Sitter inflation (wherein $\lambda = 0$) and matter dominated contraction (*i.e.* when $\lambda^2 = 3$). We shall attempt to understand these results below.

One finds that, during inflation (*i.e.* when $\lambda^2 < 2$), the amplitude of the mode f dominates its momentum g at late times. In fact, it is the first term in equations (6.28) that dominate so that squeezing parameters at late times (when $-k\eta \ll 1$) reduce to

$$\cosh(2r) \simeq -\frac{\pi k \eta}{4} |H_\nu^{(1)}(-k\eta)|^2 \simeq \frac{|\Gamma(\nu)|^2}{2\pi} \left(\frac{-k\eta}{2} \right)^{1-2\nu} \propto a^2, \quad (6.29a)$$

$$\cos(2\phi) \simeq -\frac{\pi k \eta}{4 \sinh(2r)} |H_\nu^{(1)}(-k\eta)|^2 \simeq \tanh(2r) \simeq 1. \quad (6.29b)$$

In a contracting universe wherein $2 < \lambda^2 < \infty$, one finds that g dominates f . As a result, when $2 < \lambda^2 < 6$ (which includes the matter and near-matter bounces we have discussed in the earlier chapters), the equations (6.28) simplify to

$$\cosh(2r) \simeq -\frac{\pi k \eta}{4} \left| H_{\nu+1}^{(1)}(-k\eta) \right|^2 \simeq \frac{|\Gamma(\nu+1)|^2}{2\pi} \left(\frac{-k\eta}{2} \right)^{-1-2\nu} \propto \frac{1}{a^2}, \quad (6.30a)$$

$$\cos(2\phi) \simeq \frac{\pi k \eta}{4 \sinh(2r)} \left| H_{\nu+1}^{(1)}(-k\eta) \right|^2 \simeq -\tanh(2r) \simeq -1. \quad (6.30b)$$

Whereas, in an ekpyrotic phase of slow contraction (*i.e.* when $\lambda^2 > 6$), the equations (6.28) simplify to

$$\cosh(2r) \simeq -\frac{\pi k \eta}{4} \left| H_{1-\nu}^{(1)}(-k\eta) \right|^2 \simeq \frac{|\Gamma(1-\nu)|^2}{2\pi} \left(\frac{-k\eta}{2} \right)^{2\nu-1} \propto \frac{1}{a^2}, \quad (6.31a)$$

$$\cos(2\phi) \simeq \frac{\pi k \eta}{4 \sinh(2r)} \left| H_{1-\nu}^{(1)}(-k\eta) \right|^2 \simeq \tanh(2r) \simeq -1. \quad (6.31b)$$

It should be clear from the above analysis that the squeezing parameter r always increases at late times in both expanding and contracting universes. Further, in the super-Hubble limit, the squeezing angle ϕ tends to zero in the case of inflation and $\pi/2$ in the case of a contracting universe [121]. These conclusions are also corroborated by the exact results plotted in figure 6.1.

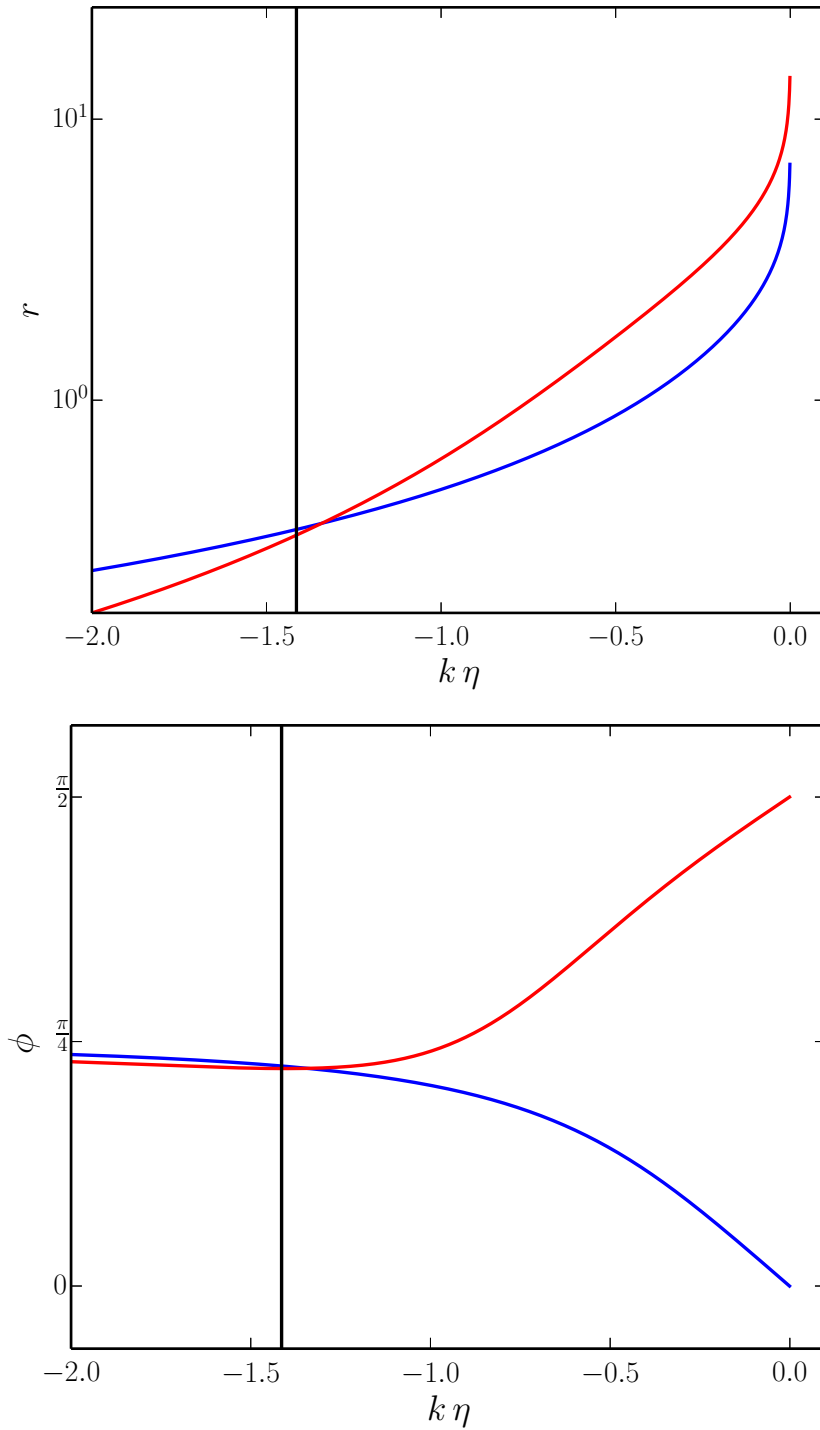


Figure 6.1: Evolution of the squeezing parameter r (on top) and the squeezing angle ϕ (at the bottom) in de Sitter inflation (in blue) and matter dominated contraction (in red). The vertical black line denotes the time when the mode associated with the curvature perturbation exits the Hubble radius. While the squeezing parameter increases in the super-Hubble limit in both the cases, the squeezing angle approaches $\pi/2$ in de Sitter inflation and zero in the case of matter dominated contraction. The difference in the behavior of the squeezing angle ϕ can be attributed to the fact that, at late times, f dominates during expansion, while g dominates during contraction.

6.3 Two-field models: Essential formalism

Even though single field models of inflation are consistent with the observational data, high energy theories, such as string theory, which are expected to describe the early universe, often involve many scalar fields (in this context, see Refs. [58,122]). It also seems that one may require more than scalar field to achieve bounces. For these reasons, as we have already outlined in the introduction of this chapter, in this section, we shall examine the quantum-to-classical transition of the perturbations in two-field models of inflationary and bouncing scenarios. As far as the background is concerned, two-field models are interesting due to the possibility of different types of trajectories in the field space. At the level of perturbations, recall that, apart from the curvature perturbation, isocurvature perturbations also arise in such models (see, for instance, Refs. [9, 10, 109]). Importantly, in the case of the ekpyrotic scenario we had discussed in the previous chapter, the isocurvature perturbations induced by the second field played an essential role to eventually lead to a nearly scale-invariant spectrum of curvature perturbations [26,46].

6.3.1 The action and the equations of motion

As we had discussed in the case of the ekpyrotic scenario discussed in the previous chapter, in any two-field model, we can define Mukhanov-Sasaki variables, say, v_σ and v_s , associated with the curvature and the isocurvature perturbations. The homogeneity of the FLRW background permits us to decompose these variables in terms of Fourier modes as we had done in the case of the Mukhanov-Sasaki variable v associated with the curvature perturbation in the previous section [*cf.* equation (6.2)]. Since we are working at the linear order in perturbation

theory, the Mukhanov-Sasaki variables v_σ^k and v_s^k associated with the different modes k evolve independently. Hence, as we had done in the single field case, for simplicity, we shall omit the index k that denotes the particular mode under consideration. Moreover, if we express the Fourier modes of the Mukhanov-Sasaki variables as $v_\sigma = v_\sigma^R + v_\sigma^I$ and $v_s = v_s^R + v_s^I$, we find that the real parts (v_σ^R, v_s^R) and the imaginary parts (v_σ^I, v_s^I) evolve independently and are governed by action which have identical forms. Therefore, for convenience, we shall hereafter drop the superscripts R and I as well. Our discussion below shall refer to one set of these variables corresponding to a typical scale of cosmological interest.

One can show that the quadratic action governing a single set of the Mukhanov-Sasaki variables v_σ and v_s characterizing the curvature and the isocurvature perturbations in a generic two-field model can be written as (in this context, see the appendix of Ref. [32])

$$\begin{aligned} \mathcal{S}_2[v_\sigma, v_s] = & \int d\eta \left(\frac{\kappa_\sigma}{2} v_\sigma'^2 - \ell_{\sigma\sigma} v_\sigma v_\sigma' + \frac{\kappa_s}{2} v_s'^2 - \ell_{ss} v_s v_s' + \kappa_{\sigma s} v_\sigma' v_s' - \ell_{\sigma s} v_\sigma' v_s \right. \\ & \left. - \ell_{s\sigma} v_\sigma v_s' - \frac{m_\sigma^2}{2} v_\sigma^2 - \frac{m_s^2}{2} v_s^2 - m_{\sigma s}^2 v_\sigma v_s \right). \end{aligned} \quad (6.32)$$

In this action, depending on the two-field model, all the coefficients— $\kappa_\sigma, \ell_{\sigma\sigma}, \kappa_s, \ell_{ss}, \kappa_{\sigma s}, \ell_{\sigma s}, \ell_{s\sigma}, m_\sigma^2$ and m_s^2 —can be dependent on time. We should stress that the above form for the action includes all the cases of two-field models we have considered in this thesis so far, *viz.* the model involving two canonical scalar fields we had discussed in chapter 2, the models involving a canonical scalar field and non-canonical ghost fields that we had studied in chapters 3 and 4 as well as the ekpyrotic model leading to features we had investigated in chapter 5. Upon varying the action (6.32), we can obtain equations of motion governing v_σ and v_s to be

$$(\kappa_\sigma v_\sigma' + \kappa_{\sigma s} v_s')' = -\bar{m}_\sigma^2 v_\sigma + \ell v_s' - \bar{m}_{\sigma s}^2 v_s, \quad (6.33a)$$

$$(\kappa_s v'_s + \kappa_{\sigma s} v'_\sigma)' = -\bar{m}_s^2 v_s - \ell v'_\sigma - \ell' v_\sigma - \bar{m}_{\sigma s}^2 v_\sigma, \quad (6.33b)$$

where the quantities \bar{m}_σ^2 , \bar{m}_s^2 , ℓ and $\bar{m}_{\sigma s}^2$ are defined as

$$\bar{m}_\sigma^2 = m_\sigma^2 - \ell'_{\sigma\sigma}, \quad (6.34a)$$

$$\bar{m}_s^2 = m_s^2 - \ell'_{ss}, \quad (6.34b)$$

$$\ell = \ell_{\sigma s} - \ell_{s\sigma}, \quad (6.34c)$$

$$\bar{m}_{\sigma s}^2 = m_{\sigma s}^2 - \ell'_{\sigma s} = m_{\sigma s}^2 - \ell'_{s\sigma} - \ell'. \quad (6.34d)$$

6.3.2 The Gaussian ansatz for the wave function

In this section, as we have done in the case of single field models, we shall consider a Gaussian ansatz for the wave function describing the system involving the Mukhanov-Sasaki variables v_σ and v_s . We shall begin by constructing the classical Hamiltonian for the system. From the action (6.32), one can immediately obtain the canonical momenta, say, p_σ and p_s , corresponding to the variables v_σ and v_s , to be

$$p_\sigma = \kappa_\sigma v'_\sigma + \kappa_{\sigma s} v'_s - \ell_{\sigma s} v_s - \ell_{\sigma\sigma} v_\sigma, \quad (6.35a)$$

$$p_s = \kappa_s v'_s + \kappa_{\sigma s} v'_\sigma - \ell_{ss} v_s - \ell_{s\sigma} v_\sigma. \quad (6.35b)$$

Then, the Hamiltonian of the complete system can be constructed to be

$$\begin{aligned} H = & \frac{\kappa_s}{2\kappa} (p_\sigma + \ell_{\sigma\sigma} v_\sigma + \ell_{\sigma s} v_s)^2 + \frac{\kappa_\sigma}{2\kappa} (p_s + \ell_s v_s + \ell_{s\sigma} v_\sigma)^2 \\ & - \frac{\kappa_{\sigma s}}{\kappa} (p_\sigma + \ell_{\sigma\sigma} v_\sigma + \ell_{\sigma s} v_s) (p_s + \ell_s v_s + \ell_{s\sigma} v_\sigma) \\ & + \frac{m_\sigma^2}{2} v_\sigma^2 + \frac{m_s^2}{2} v_s^2 + m_{\sigma s}^2 v_\sigma v_s, \end{aligned} \quad (6.36)$$

where we have set

$$\kappa = \kappa_\sigma \kappa_s - \kappa_{\sigma s}^2. \quad (6.37)$$

Evidently, upon quantization, in the Schrodinger picture, while the operators \hat{v}_σ and \hat{v}_s will turn out to be simple multiplicative operators, the operators representing the conjugate momenta will be given by $\hat{p}_\sigma = -i \partial / (\partial v_\sigma)$ and $\hat{p}_s = -i \partial / (\partial v_s)$. The operator corresponding to the classical Hamiltonian (6.36) is straightforward to construct in terms of the above sets of conjugate operators, but the resulting Hamiltonian operator proves to be rather lengthy and cumbersome. Therefore, we do not explicitly write down the Schrodinger equation governing the wave function that describes the system. As in the single field case, we propose a Gaussian ansatz for the wave function of the following form (in this context, see Ref. [32]):

$$\Psi(v_\sigma, v_s, \eta) = N(\eta) \exp - \frac{1}{2} \left[\Omega_{\sigma\sigma}(\eta) v_\sigma^2 + 2 \Omega_{\sigma s}(\eta) v_\sigma v_s + \Omega_{ss}(\eta) v_s^2 \right], \quad (6.38)$$

where N , $\Omega_{\sigma\sigma}$, $\Omega_{\sigma s}$ and Ω_{ss} are, in general, complex quantities. On normalizing the above wave function, *i.e.* demanding that,

$$\int_{-\infty}^{\infty} dv_s \int_{-\infty}^{\infty} dv_\sigma |\Psi(v_\sigma, v_s, \eta)|^2 = 1, \quad (6.39)$$

we obtain the relation between the normalization factor N and the quantities $\Omega_{\sigma\sigma}$, $\Omega_{\sigma s}$ and Ω_{ss} to be

$$N = \left[\frac{\Omega_{\sigma\sigma}^R \Omega_{ss}^R - (\Omega_{\sigma s}^R)^2}{\pi} \right]^{1/4}, \quad (6.40)$$

where, as before, the superscript R denotes the real parts of the corresponding complex quantities.

Our aim now is to construct the quantities $\Omega_{\sigma\sigma}$, $\Omega_{\sigma s}$ and Ω_{ss} in terms of the classical solutions to the variables v_σ and v_s and the corresponding conjugate momenta

p_σ and p_s , as we had done in the single field case. Recall that, in the case of two-field models, the curvature and the isocurvature perturbations are assumed to be decoupled in the sub-Hubble domain when the initial conditions are imposed on the perturbations [11]. As we have discussed in the earlier chapters, the equations of motion governing, say, v_σ and v_s , are solved twice with two sets of initial conditions, one wherein the Bunch-Davies initial condition is imposed on v_σ , while v_s is chosen to be zero, and the other wherein v_σ is set to be zero and the Bunch-Davies initial condition is imposed on v_s . Let $\{f_{\sigma_1}, f_{s_1}\}$ and $\{f_{\sigma_2}, f_{s_2}\}$ represent these two sets of solutions for v_σ and v_s , and let $\{g_{\sigma_1}, g_{s_1}\}$ and $\{g_{\sigma_2}, g_{s_2}\}$ denote the corresponding conjugate momenta which are given by [cf. equations (6.35)]

$$g_{\sigma_1} = (\kappa_\sigma f'_{\sigma_1} + \kappa_{\sigma s} f'_{s_1} - \ell_{\sigma s} f_{s_1} - \ell_{\sigma\sigma} f_{\sigma_1}), \quad (6.41a)$$

$$g_{\sigma_2} = (\kappa_\sigma f'_{\sigma_2} + \kappa_{\sigma s} f'_{s_2} - \ell_{\sigma s} f_{s_2} - \ell_{\sigma\sigma} f_{\sigma_2}), \quad (6.41b)$$

$$g_{s_1} = (\kappa_s f'_{s_1} + \kappa_{\sigma s} f'_{\sigma_1} - \ell_{ss} f_{s_1} - \ell_{s\sigma} f_{\sigma_1}), \quad (6.41c)$$

$$g_{s_2} = (\kappa_s f'_{s_2} + \kappa_{\sigma s} f'_{\sigma_2} - \ell_{ss} f_{s_2} - \ell_{s\sigma} f_{\sigma_2}). \quad (6.41d)$$

If we now define $\Omega_{\sigma\sigma}$, $\Omega_{\sigma s}$ and Ω_{ss} in terms of these quantities to be

$$\Omega_{\sigma\sigma} = -\frac{i(f_{s_2}^* g_{\sigma_1}^* - f_{s_1}^* g_{\sigma_2}^*)}{f_{s_2}^* f_{\sigma_1}^* - f_{s_1}^* f_{\sigma_2}^*}, \quad (6.42a)$$

$$\Omega_{\sigma s} = -\frac{i(f_{\sigma_1}^* g_{\sigma_2}^* - f_{\sigma_2}^* g_{\sigma_1}^*)}{f_{\sigma_1}^* f_{s_2}^* - f_{\sigma_2}^* f_{s_1}^*} = -\frac{i(f_{s_2}^* g_{s_1}^* - f_{s_1}^* g_{s_2}^*)}{f_{s_2}^* f_{\sigma_1}^* - f_{s_1}^* f_{\sigma_2}^*}, \quad (6.42b)$$

$$\Omega_{ss} = -\frac{i(f_{\sigma_1}^* g_{s_2}^* - f_{\sigma_2}^* g_{s_1}^*)}{f_{\sigma_1}^* f_{s_2}^* - f_{\sigma_2}^* f_{s_1}^*}, \quad (6.42c)$$

then we find that the Schrodinger equation governing the wave function (6.38) indeed leads to the classical equations of motion governing the variables v_σ and v_s [cf. equations (6.33)]. Thus, we have constructed the wave function completely in terms of the classical solutions, as we had desired. Our choice of initial conditions

lead to the following values for the various Wronskians involved:

$$\mathcal{W}_1 = f_{\sigma_1} g_{\sigma_1}^* + f_{s_1} g_{s_1}^* - (f_{\sigma_1} g_{\sigma_1}^* + f_{s_1} g_{s_1}^*)^* = i, \quad (6.43a)$$

$$\mathcal{W}_2 = f_{\sigma_2} g_{\sigma_2}^* + f_{s_2} g_{s_2}^* - (f_{\sigma_2} g_{\sigma_2}^* + f_{s_2} g_{s_2}^*)^* = i, \quad (6.43b)$$

$$\mathcal{W}_3 = f_{\sigma_1} g_{\sigma_2} + f_{s_1} g_{s_2} - f_{\sigma_2} g_{\sigma_1} - f_{s_2} g_{s_1} = 0, \quad (6.43c)$$

$$\mathcal{W}_4 = f_{\sigma_1} g_{\sigma_2}^* + f_{s_1} g_{s_2}^* - f_{\sigma_2} g_{\sigma_1}^* - f_{s_2} g_{s_1}^* = 0, \quad (6.43d)$$

$$\mathcal{W}_5 = f_{s_1}^* f_{\sigma_1} + f_{s_2}^* f_{\sigma_2} - (f_{s_1}^* f_{\sigma_1} + f_{s_2}^* f_{\sigma_2})^* = 0. \quad (6.43e)$$

It should be noted that, in the case of single field models, $f_{s_1} = f_{s_2} = 0$ and, in such a case, $\mathcal{W}_1 = \mathcal{W}_2$.

In what follows, we shall be focusing on the behavior of the curvature perturbation. It is easy to show that, for the Gaussian ansatz for the wave function [cf. equation (6.38)], the expectation values $\langle \hat{v}_\sigma \rangle$ and $\langle \hat{p}_\sigma \rangle$ prove to be zero. One can also show that the variances in these quantities are given by

$$\langle \hat{v}_\sigma^2 \rangle = \frac{\Omega_{ss}^R}{2 (\Omega_{\sigma\sigma}^R \Omega_{ss}^R - \Omega_{\sigma s}^R)^2} = |f_{\sigma_1}|^2 + |f_{\sigma_2}|^2, \quad (6.44a)$$

$$\langle \hat{p}_\sigma^2 \rangle = \frac{|\Omega_{\sigma\sigma}|^2 \Omega_{ss}^R + \Omega_{\sigma\sigma}^R [(\Omega_{\sigma s}^I)^2 - (\Omega_{\sigma s}^R)^2] - 2 \Omega_{\sigma\sigma}^I \Omega_{\sigma s}^R \Omega_{\sigma s}^I}{2 [\Omega_{ss}^R \Omega_{\sigma\sigma}^R - (\Omega_{\sigma s}^R)^2]} = |g_{\sigma_1}|^2 + |g_{\sigma_2}|^2, \quad (6.44b)$$

with the superscripts I denoting the imaginary parts of the corresponding complex quantities. Moreover, we find that

$$\frac{1}{2} \langle \hat{v}_\sigma \hat{p}_\sigma + \hat{p}_\sigma \hat{v}_\sigma \rangle = f_{\sigma_1} g_{\sigma_1}^* + f_{\sigma_2} g_{\sigma_2}^*. \quad (6.45)$$

As in the single field case, we shall see that the Wigner function and the squeezing parameters describing the curvature perturbation can be completely expressed in terms of the above quantities.

6.3.3 The Wigner function and the reduced density matrix

The Wigner function associated with the wave function (6.38) describing the Mukhanov-Sasaki variables v_σ and v_s can be defined to be [30,32]

$$W(v_\sigma, p_\sigma, v_s, p_s, \eta) = \frac{1}{\pi} \int_{-\infty}^{\infty} dx \int_{-\infty}^{\infty} dy \Psi(v_\sigma - x, v_s - y, \eta) \Psi(v_\sigma + x, v_s + y, \eta) \times e^{-2ixp_\sigma} e^{-2iy p_s}. \quad (6.46)$$

As we had mentioned, we shall be interested in examining the quantum-to-classical transition of the curvature perturbation. Therefore, we shall integrate out the isocurvature degrees of freedom v_s to arrive at the reduced Wigner function describing the conjugate variables v_σ and p_σ . Upon doing so, the reduced Wigner function corresponding to the wave function (6.38) can be obtained to be

$$W(v_\sigma, p_\sigma) = \frac{W_{11}^{1/2}}{2\pi W_{22}^{1/2}} \exp - \left[\frac{W_{11}}{2} v_\sigma^2 + \frac{1}{2W_{22}} (p_\sigma + W_{12} v_\sigma)^2 \right], \quad (6.47)$$

where the quantities W_{11} , W_{12} and W_{22} are given by

$$W_{11} = 2\Omega_{\sigma\sigma}^R \left[1 - \frac{(\Omega_{\sigma s}^R)^2}{\Omega_{ss}^R \Omega_{\sigma\sigma}^R} \right] = \frac{1}{|f_{\sigma_1}|^2 + |f_{\sigma_2}|^2}, \quad (6.48a)$$

$$W_{12} = \Omega_{\sigma\sigma}^I \left[1 - \frac{\Omega_{\sigma s}^I \Omega_{\sigma s}^R}{\Omega_{ss}^R \Omega_{\sigma\sigma}^I} \right] = \frac{W_{11}}{2} [(f_{\sigma_1} g_{\sigma_1}^* + f_{\sigma_2} g_{\sigma_2}^*) + (f_{\sigma_1} g_{\sigma_1}^* + f_{\sigma_2} g_{\sigma_2}^*)^*], \quad (6.48b)$$

$$W_{22} = \frac{\Omega_{\sigma\sigma}^R}{2} \left[1 + \frac{(\Omega_{\sigma s}^I)^2}{\Omega_{ss}^R \Omega_{\sigma\sigma}^R} \right] = \frac{W_{11}}{4} (1 + 4|f_{\sigma_2} g_{\sigma_1} - f_{\sigma_1} g_{\sigma_2}|^2). \quad (6.48c)$$

Clearly, as in the single field case, the corresponding Wigner ellipse can be defined to be

$$\frac{W_{11}}{2} v_\sigma^2 + \frac{1}{2W_{22}} (p_\sigma + W_{12} v_\sigma)^2 = 1. \quad (6.49)$$

As we had discussed, as time evolves, the Wigner ellipse, which is originally a circle when the initial conditions are imposed, gets squeezed more and more into an ellipse, and the axis of the ellipse also rotates. The angle made by the direction of the elongation of the ellipse with respect to the v_σ -axis, say, θ_w , can be determined to be

$$\tan(2\theta_w) = \frac{2k W_{12}}{k^2 - W_{11} W_{22} - W_{12}^2}. \quad (6.50)$$

Note that, in single field models, $W_{11} = 4W_{22}$.

Another useful quantity that describes the behavior of the curvature perturbations is the reduced density matrix, obtained by tracing out the contributions due to the isocurvature degrees of freedom in the complete density matrix describing the system. Such a reduced density matrix is given by

$$\rho(v_\sigma, \bar{v}_\sigma) = \int_{-\infty}^{\infty} dv_s \Psi(v_\sigma, v_s, \eta) \Psi^*(\bar{v}_\sigma, v_s, \eta). \quad (6.51)$$

Upon using the wave function (6.38) and carrying out the integral involved, we obtain that

$$\begin{aligned} \rho(v_\sigma, \bar{v}_\sigma, \eta) = & \bar{N} \exp - \left[\frac{1}{2} \left(\frac{W_{11}}{4} + W_{22} \right) (v_\sigma^2 + \bar{v}_\sigma^2) + \frac{i W_{12}}{2} (v_\sigma^2 - \bar{v}_\sigma^2) \right. \\ & \left. + \left(W_{22} - \frac{W_{11}}{4} \right) v_\sigma \bar{v}_\sigma \right]. \end{aligned} \quad (6.52)$$

Note that the off-diagonal term gets suppressed in the domain wherein $\mathcal{D} = 4W_{22}/W_{11} \gg 1$. As we shall illustrate later, the quantity \mathcal{D} increases when there is a strong influence of the isocurvature perturbation on the curvature perturbation. We should also point out that \mathcal{D} is proportional to the area of the Wigner ellipse.

6.3.4 The squeezing parameters

In the two-field case, the two sets of initial conditions for the two sets of modes had led to the quantities f_{σ_1} , f_{s_1} , f_{σ_2} and f_{s_2} that we had introduced earlier. As we had done in the single field case, let us now parametrize each of these quantities in terms of four sets of Bogoliubov coefficients, *viz.* $(\alpha_{\sigma_1}, \beta_{\sigma_1})$, $(\alpha_{s_1}, \beta_{s_1})$, $(\alpha_{\sigma_2}, \beta_{\sigma_2})$ and $(\alpha_{s_2}, \beta_{s_2})$, as follows:

$$f_{\sigma_1} = \frac{1}{\sqrt{2k}} \left(\tilde{\alpha}_{\sigma_1} + \tilde{\beta}_{\sigma_1}^* \right), \quad f_{s_1} = \frac{1}{\sqrt{2k}} \left(\tilde{\alpha}_{s_1} + \tilde{\beta}_{s_1}^* \right), \quad (6.53a)$$

$$f_{\sigma_2} = \frac{1}{\sqrt{2k}} \left(\tilde{\alpha}_{\sigma_2} + \tilde{\beta}_{\sigma_2}^* \right), \quad f_{s_2} = \frac{1}{\sqrt{2k}} \left(\tilde{\alpha}_{s_2} + \tilde{\beta}_{s_2}^* \right). \quad (6.53b)$$

We can then express the corresponding momenta as

$$g_{\sigma_1} = -i \sqrt{\frac{k}{2}} \left(\tilde{\alpha}_{\sigma_1} - \tilde{\beta}_{\sigma_1}^* \right), \quad g_{s_1} = -i \sqrt{\frac{k}{2}} \left(\tilde{\alpha}_{s_1} - \tilde{\beta}_{s_1}^* \right), \quad (6.54a)$$

$$g_{\sigma_2} = -i \sqrt{\frac{k}{2}} \left(\tilde{\alpha}_{\sigma_2} - \tilde{\beta}_{\sigma_2}^* \right), \quad g_{s_2} = -i \sqrt{\frac{k}{2}} \left(\tilde{\alpha}_{s_2} - \tilde{\beta}_{s_2}^* \right). \quad (6.54b)$$

Under the above parametrization, the equations (6.43) lead to the following conditions on the Bogoliubov coefficients:

$$|\tilde{\alpha}_{\sigma_1}|^2 - |\tilde{\beta}_{\sigma_1}|^2 + |\tilde{\alpha}_{\sigma_2}|^2 - |\tilde{\beta}_{\sigma_2}|^2 = 1, \quad (6.55a)$$

$$|\tilde{\alpha}_{s_1}|^2 - |\tilde{\beta}_{s_1}|^2 + |\tilde{\alpha}_{s_2}|^2 - |\tilde{\beta}_{s_2}|^2 = 1, \quad (6.55b)$$

$$\tilde{\alpha}_{\sigma_1} \tilde{\beta}_{s_2} - \tilde{\alpha}_{s_1} \tilde{\beta}_{\sigma_2} + \tilde{\alpha}_{\sigma_2} \tilde{\beta}_{s_1} - \tilde{\alpha}_{s_2} \tilde{\beta}_{\sigma_1} = 0, \quad (6.55c)$$

$$\tilde{\alpha}_{\sigma_1} \tilde{\alpha}_{s_2}^* - \tilde{\beta}_{\sigma_1} \tilde{\beta}_{s_2}^* + \tilde{\alpha}_{\sigma_2} \tilde{\alpha}_{s_1}^* - \tilde{\beta}_{\sigma_2} \tilde{\beta}_{s_1}^* = 0. \quad (6.55d)$$

These invariants allow us to parameterize the four sets of Bogoliubov coefficients $(\alpha_{\sigma_1}, \beta_{\sigma_1})$, $(\alpha_{s_1}, \beta_{s_1})$, $(\alpha_{\sigma_2}, \beta_{\sigma_2})$ and $(\alpha_{s_2}, \beta_{s_2})$ in the following fashion:

$$\tilde{\alpha}_{\sigma_1} = \cosh r_\sigma \cos \alpha_{\sigma \tilde{\alpha}_1 \tilde{\alpha}_2} e^{i\theta_{\sigma \tilde{\alpha}_1 \tilde{\beta}_1}}, \quad (6.56a)$$

$$\tilde{\beta}_{\sigma_1} = \sinh r_\sigma \cos \alpha_{\sigma\tilde{\beta}_1\tilde{\beta}_2} e^{i(2\phi_{\sigma\tilde{\beta}_1} - \theta_{\sigma\tilde{\alpha}_1\tilde{\beta}_1})}, \quad (6.56b)$$

$$\tilde{\alpha}_{\sigma_2} = \cosh r_\sigma \sin \alpha_{\sigma\tilde{\alpha}_1\tilde{\alpha}_2} e^{i\theta_{\sigma\tilde{\alpha}_2\tilde{\beta}_2}}, \quad (6.56c)$$

$$\tilde{\beta}_{\sigma_2} = \sinh r_\sigma \sin \alpha_{\sigma\tilde{\beta}_1\tilde{\beta}_2} e^{i(2\phi_{\sigma\tilde{\beta}_2} - \theta_{\sigma\tilde{\alpha}_2\tilde{\beta}_2})}, \quad (6.56d)$$

$$\tilde{\alpha}_{s_1} = \cosh r_s \cos \alpha_{s\tilde{\alpha}_1\tilde{\alpha}_2} e^{i\theta_{s\tilde{\alpha}_1\tilde{\beta}_1}}, \quad (6.56e)$$

$$\tilde{\beta}_{s_1} = \sinh r_s \cos \alpha_{s\tilde{\beta}_1\tilde{\beta}_2} e^{i(2\phi_{s\tilde{\beta}_1} - \theta_{s\tilde{\alpha}_1\tilde{\beta}_1})}, \quad (6.56f)$$

$$\tilde{\alpha}_{s_2} = \cosh r_s \sin \alpha_{s\tilde{\alpha}_1\tilde{\alpha}_2} e^{i\theta_{s\tilde{\alpha}_2\tilde{\beta}_2}}, \quad (6.56g)$$

$$\tilde{\beta}_{s_2} = \sinh r_s \sin \alpha_{s\tilde{\beta}_1\tilde{\beta}_2} e^{i(2\phi_{s\tilde{\beta}_2} - \theta_{s\tilde{\alpha}_2\tilde{\beta}_2})}. \quad (6.56h)$$

In the above expressions, the parameters r_σ and r_s are the squeezing parameters corresponding to v_σ and v_s . In this chapter, we shall be focusing on the behavior of the curvature perturbation and, hence, on the behavior of r_σ alone.

We find that the variances in the operator \hat{v}_σ and the operator \hat{p}_σ representing the corresponding conjugate momentum can be expressed in terms of the squeezing parameters as

$$\langle \hat{v}_\sigma^2 \rangle = |f_{\sigma_1}|^2 + |f_{\sigma_2}|^2 = \frac{1}{2k} [\cosh(2r_\sigma) + \sinh(2r_\sigma) \cos(2\phi_\sigma)], \quad (6.57a)$$

$$\langle \hat{p}_\sigma^2 \rangle = |g_{\sigma_1}|^2 + |g_{\sigma_2}|^2 = \frac{k}{2} [\cosh(2r_\sigma) - \sinh(2r_\sigma) \cos(2\phi_\sigma)], \quad (6.57b)$$

where we have defined the quantity $\cos(2\phi_\sigma)$ to be

$$\cos(2\phi_\sigma) = \cos \alpha_{\sigma\tilde{\alpha}_1\tilde{\alpha}_2} \cos \alpha_{\sigma\tilde{\beta}_1\tilde{\beta}_2} \cos(2\phi_{\sigma\tilde{\beta}_1}) + \sin \alpha_{\sigma\tilde{\alpha}_1\tilde{\alpha}_2} \sin \alpha_{\sigma\tilde{\beta}_1\tilde{\beta}_2} \cos(2\phi_{\sigma\tilde{\beta}_2}). \quad (6.58)$$

From above relations we can arrive at

$$\cosh(2r_\sigma) = k \langle \hat{v}_\sigma^2 \rangle + \frac{\langle \hat{p}_\sigma^2 \rangle}{k} = k (|f_{\sigma_1}|^2 + |f_{\sigma_2}|^2) + \frac{1}{k} (|g_{\sigma_1}|^2 + |g_{\sigma_2}|^2), \quad (6.59)$$

and it is using this expression and the solutions for the modes f_{σ_1} and f_{σ_2} that we shall eventually construct r_σ . It is useful to note here that the rotation angle of the

Wigner ellipse θ_w can be expressed as

$$\tan(2\theta_w) = \frac{\sin(2\psi_\sigma)}{\cos(2\phi_\sigma)}, \quad (6.60)$$

where the quantity $\sin(2\psi_\sigma)$ is defined to be

$$\sin(2\psi_\sigma) = \cos\alpha_{\sigma\tilde{\alpha}_1\tilde{\alpha}_2} \cos\alpha_{\sigma\tilde{\beta}_1\tilde{\beta}_2} \sin(2\phi_{\sigma\tilde{\beta}_1}) + \sin\alpha_{\sigma\tilde{\alpha}_1\tilde{\alpha}_2} \sin\alpha_{\sigma\tilde{\beta}_1\tilde{\beta}_2} \sin(2\phi_{\sigma\tilde{\beta}_2}). \quad (6.61)$$

In the single field case $\psi_\sigma = \phi_\sigma$, which implies that $\theta_w = \phi_\sigma$. Lastly, we find that the quantity \mathcal{D} which quantifies the amount of decoherence can be expressed as

$$\begin{aligned} \mathcal{D} &= 1 + 4|(f_{\sigma_2}g_{\sigma_1} - f_{\sigma_1}g_{\sigma_2})|^2 \\ &= \cosh^2(2r_\sigma) - [\cos^2(2\phi_\sigma) + \sin^2(2\psi_\sigma)] \sinh^2(2r_\sigma). \end{aligned} \quad (6.62)$$

In the case of single field models, $f_{\sigma_2} = g_{\sigma_2} = 0$ (*i.e.* $\phi_\sigma = \psi_\sigma$) and, hence, $\mathcal{D} = 1$.

6.4 Application to double inflation and ekpyrotic contraction

In this section, we shall apply the formalism we have developed in the previous section to the cases of double inflation and ekpyrotic contraction. In the case of double inflation, we shall specifically consider a situation wherein the isocurvature perturbation becomes important due to a turn in the field space. In the case of ekpyrotic contraction, we shall examine the effects of the conversion of the isocurvature perturbation into curvature perturbation. Since these situations do not seem to permit analytic solutions to the equations governing the curvature and the isocurvature perturbations, we shall evaluate them numerically.

6.4.1 The case of double inflation

Let us first discuss the case of the double inflation model described by the action (2.1) and the potential (2.21). The potential consists of a sum of two quadratic potentials in the fields ϕ and χ . Note that the model we are considering here corresponds to the case wherein $b = 0$ in the action (5.1). Also, the curvature and the curvature perturbations are given by $\mathcal{R} = v_\sigma/z$ and $\mathcal{S} = v_s/z$ with $z = a\dot{\sigma}/H$, $\dot{\sigma}$ defined as in equation (5.12) and b chosen to be zero. We shall focus on the situation wherein $m_\chi = 8m_\phi$. In this case, the trajectory in the field space is characterized by a sharp turn from a χ dominated phase to a valley along the χ direction (*cf.* figure 2.1). Thereafter, the evolution in the field ϕ along the valley continues to drive inflation. The turn in the field space leads to a brief change in the amplitude of the coupling function ξ given by equation (5.14) (with b set to be zero), which determines the effects of the isocurvature perturbation on the curvature perturbation. The fall and rise in the coupling function ξ alters the amplitude of the isocurvature perturbation which, in turn, affects the amplitude of the curvature perturbation. These behaviors are clear from figure 6.2 wherein we have plotted the evolution of the coupling function ξ as well as the amplitudes of the curvature and the isocurvature perturbations \mathcal{R} and \mathcal{S} .

6.4.2 The case of ekpyrotic contraction

The second model we shall consider is the ekpyrotic scenario that we had discussed in detail in the previous chapter. Let us recall a few essential points concerning the scenario described by the action (5.1). The phase of slow ekpyrotic contraction driven by the field ϕ generates a curvature perturbation spectrum with a strong blue tilt. The presence of the second field χ results in isocurvature perturbations which, interestingly, prove to be dominant in amplitude and have

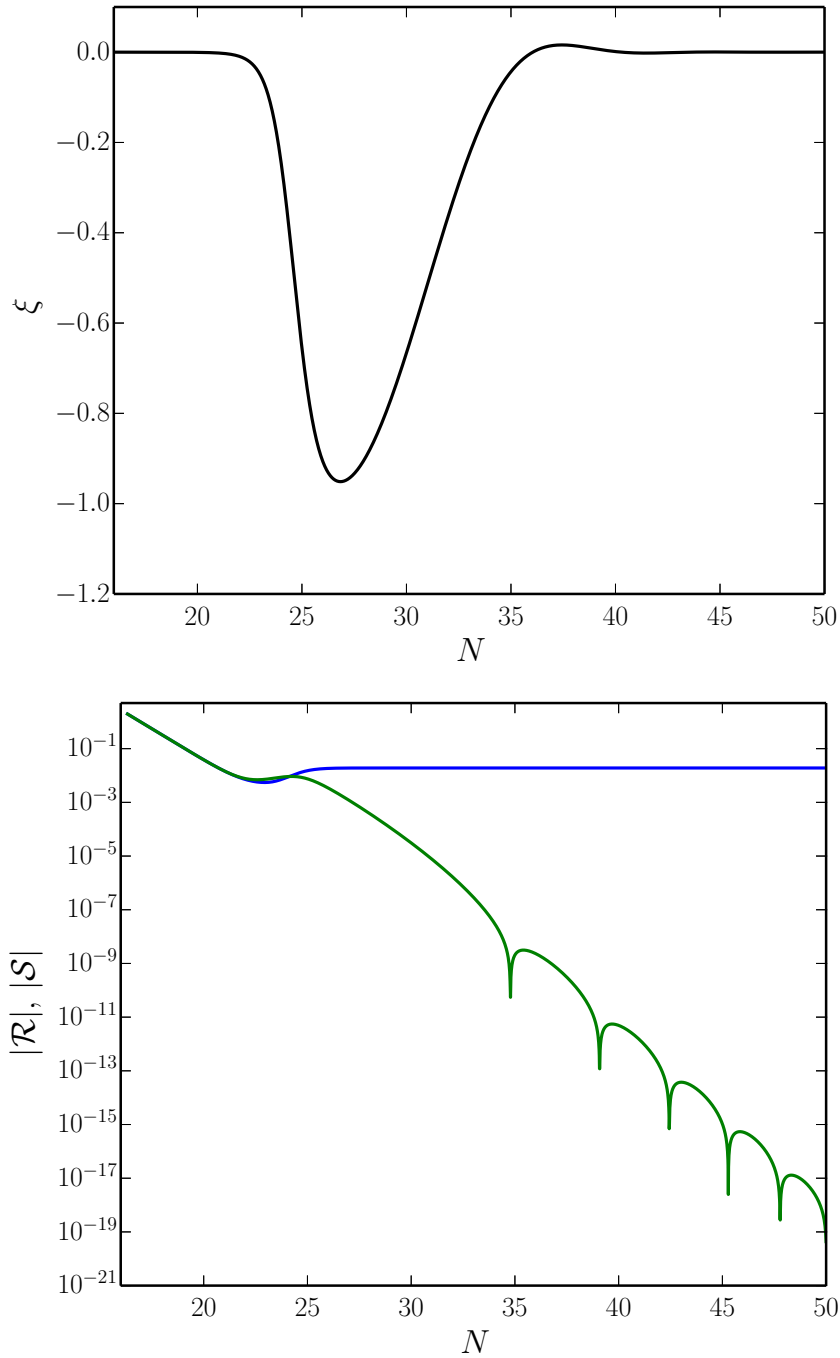


Figure 6.2: Evolution of the coupling function ξ (on top) and the amplitudes of the curvature and the isocurvature perturbations \mathcal{R} and S (at the bottom, in blue and in green, respectively) for a typical cosmological scale, has been plotted as a function of e-folds N in the case of double inflation with $m_\chi = 8m_\phi$. It is clear from the figures that, as the coupling function ξ falls and rises due to the turn in the field space, the amplitude of the isocurvature perturbation is altered briefly leading to a concomitant change in the amplitude of the curvature perturbation. Thereafter, as expected, while the isocurvature perturbation decays rapidly, the amplitude of the curvature perturbation quickly freezes to a constant value.

a nearly scale-invariant spectrum at the end of the ekpyrotic phase. By introducing a turn in the field space along the χ -direction [*cf.* equation (5.21)], we had allowed the isocurvature perturbations to influence the curvature perturbations and eventually give rise to a nearly scale-invariant perturbation spectrum (see figures 5.1 and 5.2). In our discussion below, for simplicity, we shall work with the case wherein $\mu = \lambda$, which produces a strictly scale-invariant spectrum.

6.4.3 Approach to classicality

We shall now turn to understanding the evolution of the cosmological perturbations towards classicality using the tools we have introduced, *viz.* the Wigner function, the squeezing parameters and the reduced density matrix.

In figure 6.3, we have plotted the evolution of the Wigner ellipses arising from the reduced Wigner function [*cf.* equations (6.47) and (6.49)] describing the conjugate pairs v_σ and p_σ in the cases of the double inflationary and the ekpyrotic scenario involving two fields. We have scaled the axes suitably (with the aid of the wavenumber k) so that we begin with a circle when the initial conditions are imposed on the quantum field. In the case of double inflation, the Wigner ellipse of interest is increasingly squeezed along the v_σ -axis, with the contribution due to the isocurvature perturbation (which becomes important as the turn occurs in the field space) hastening the process. This is essentially the behavior we had discussed in the context of power law inflation driven by a single scalar field in section 6.2. However, in the ekpyrotic scenario of interest, during the initial contracting phase prior to the turn induced by the χ -field, the Wigner ellipse orients itself along the p_σ -axis, which is again the behavior we had encountered earlier (in section 6.2) in the case of a contracting phase driven by a single field. As the isocurvature perturbation begins to play a role, the Wigner ellipse rotates and

eventually orients itself along the v_σ -axis.

In figure 6.4, we have plotted the evolution of the squeezing parameter r_σ in both the scenarios of interest. The figure clearly corroborates the conclusion arrived at from the behavior of the Wigner ellipses. We find that, after the mode of interest leaves the Hubble radius, the squeezing parameter r_σ increases constantly in the case of inflation, reflecting the increased squeezing of the Wigner ellipse along the v_σ -axis. Whereas, in the ekpyrotic case, the parameter r_σ exhibits a sharp rise as the isocurvature perturbations are converted to curvature perturbations, which again reflects the behavior of the Wigner ellipse.

In figure 6.5, we have plotted the evolution of the so-called decoherence term $\mathcal{D} = 4W_{22}/W_{11}$ for the two cases of interest. In the double inflation model of our interest, the term has a value of unity during the initial χ -dominated phase, just as in the case of a single field inflationary model. It exhibits a jump as the bend in the background trajectory occurs, and it becomes constant during later ϕ -dominated phase. A similar behavior occurs in the ekpyrotic case as well. Since, in this scenario, the isocurvature perturbations play a rather strong role, we find that the extent of the rise in the quantity \mathcal{D} is considerable. The quantum-to-classical transition of the perturbations in the ekpyrotic scenario can be attributed to the sharp rise in the decoherence term.

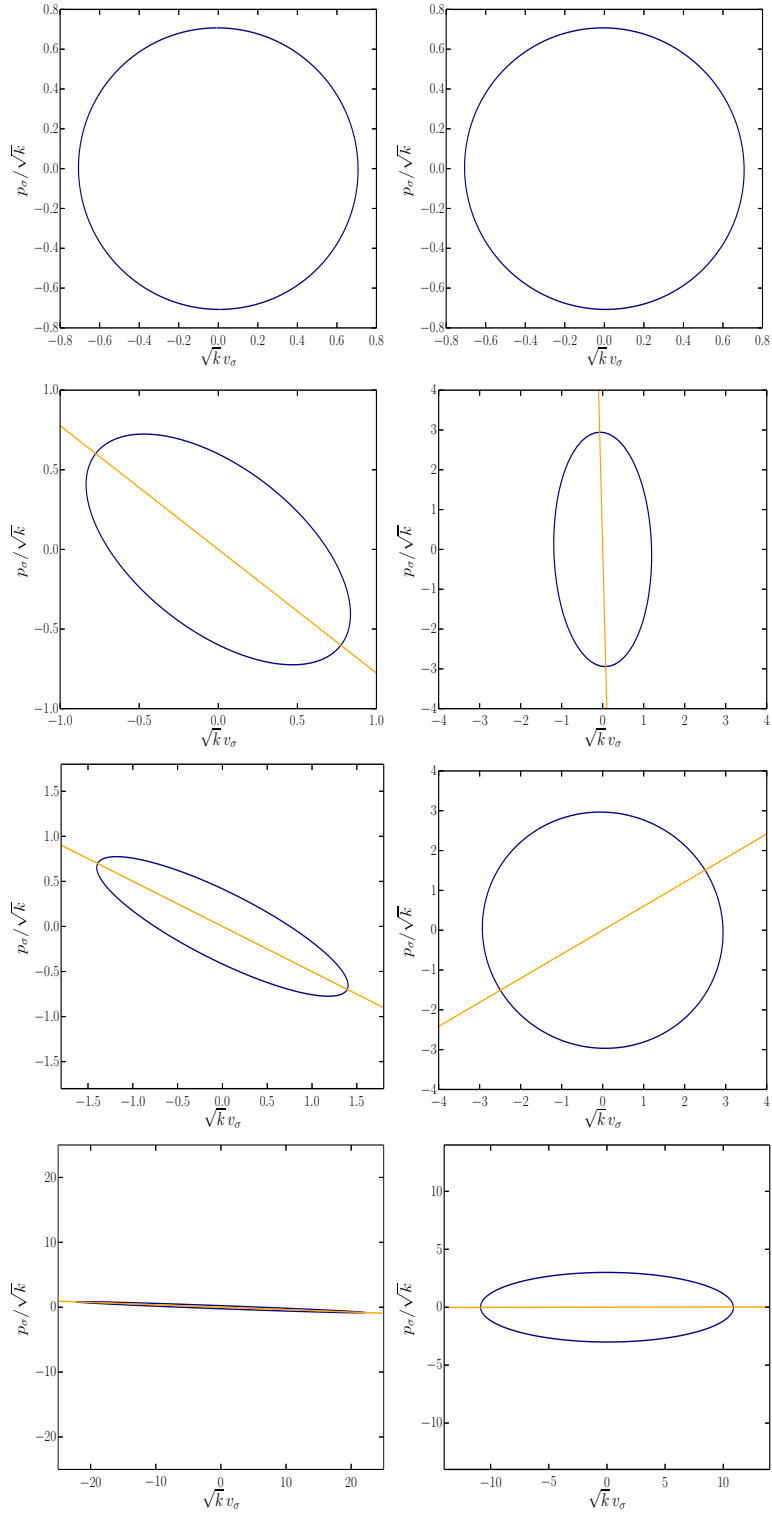


Figure 6.3: Evolution of Wigner ellipse describing the reduced Wigner function $W(v_\sigma, p_\sigma)$ during double inflation with $m_\chi = 8 m_\phi$ (on the left) and the ekpyrotic scenario involving two fields (on the right). In the case of double inflation, the Wigner function becomes increasingly squeezed along the v_σ -axis as in the case of inflation driven by a single scalar field. In contrast, in the ekpyrotic scenario, as the isocurvature perturbations begin to play a role, the Wigner ellipse, which was originally squeezed along the p_σ -axis, gets eventually squeezed along the v_σ -axis.

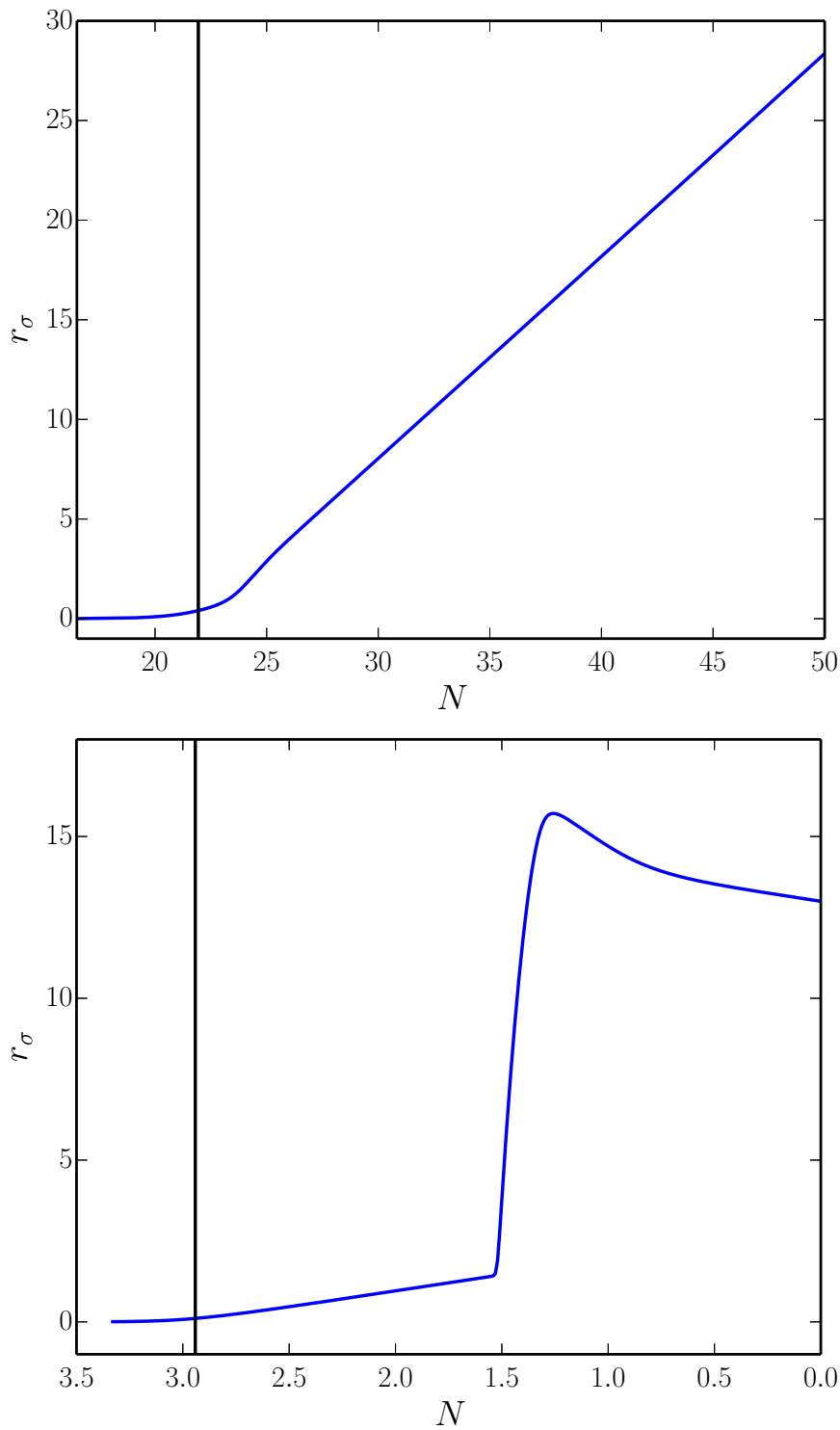


Figure 6.4: Evolution of squeezing parameter r_σ in the cases of double inflation (on top) and the ekpyrotic scenario driven by two fields (at the bottom), has been plotted as a function of e-folds N . The vertical black line indicates the time when the mode of interest leaves the Hubble radius. Note that the extent of growth in r_σ is roughly of the same order in both the scenarios. It is the sudden rise in the ekpyrotic case that makes the Wigner ellipse change direction as the isocurvature perturbations are converted to curvature perturbations.

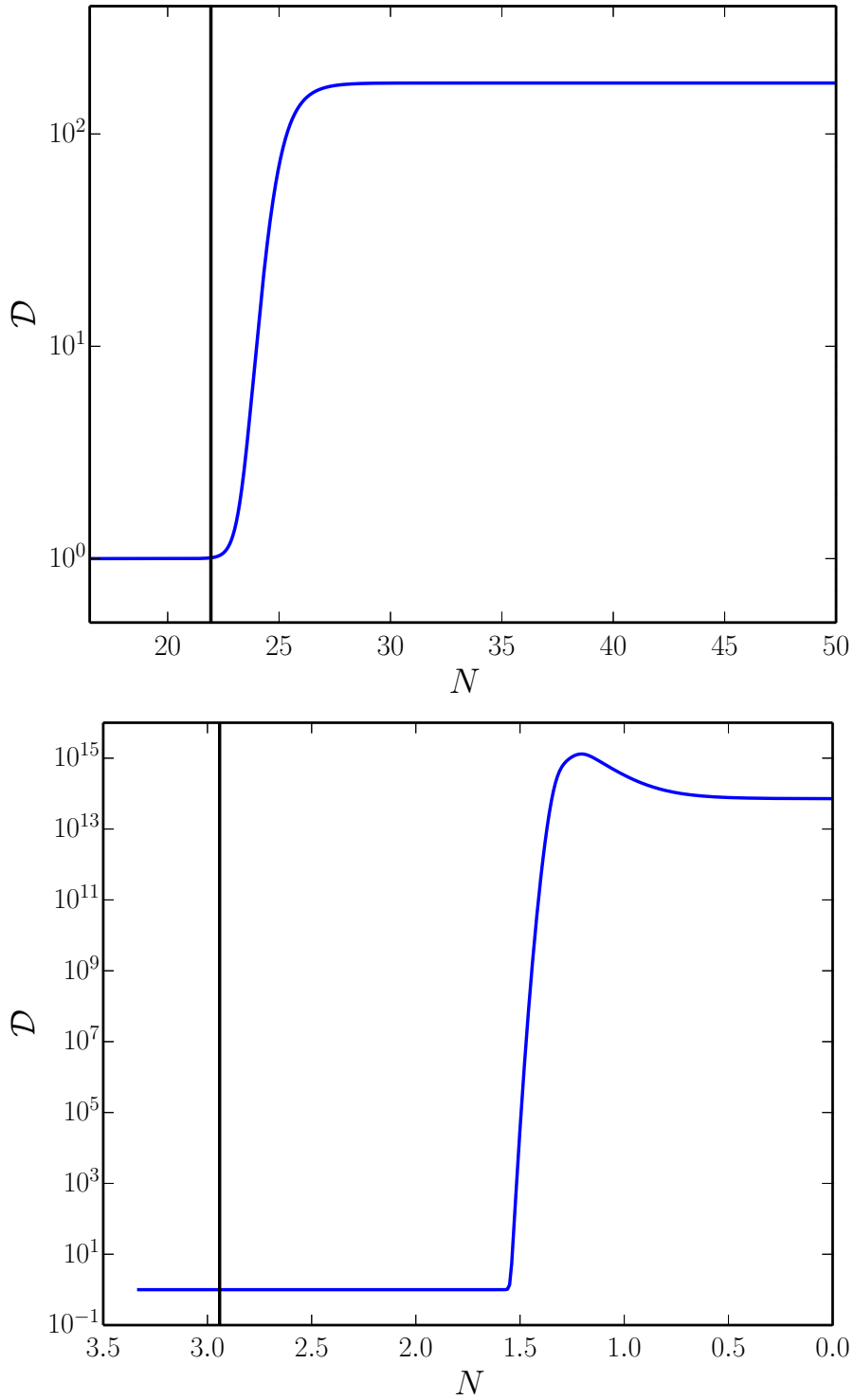


Figure 6.5: Evolution of the decoherence parameter $\mathcal{D} = 4W_{22}/W_{11}$ in double inflation (on top) and in the ekpyrotic scenario (at the bottom). The vertical line again indicates the time when the mode of interest leaves the Hubble radius. Clearly, the decoherence term exhibits a rise exactly when the squeezing parameter does. Note that the rise in the ekpyrotic case is considerably larger than the inflationary case.

6.5 Discussion

In this chapter, we have examined the quantum-to-classical transition of the primordial perturbations generated in two-field models of inflationary and bouncing scenarios. After reviewing scenarios involving a single scalar field, we had compared and contrasted the behavior of the perturbations in two-field models wherein the isocurvature perturbations play a role. We had used a variety of common tools, *viz.* the Wigner function, the squeezing parameters and the reduced to density matrix, to examine the quantum-to-classical transition. We had focused on the behavior of the curvature perturbations. We find that the Wigner ellipses describing the curvature perturbation orient themselves along the asymptotic classical trajectory in the v_σ - p_σ phase space, which is an indication that the perturbations turn classical during the late stages of the evolution. This conclusion is also corroborated by the growth in the squeezing parameter r_σ as well as the decoherence term \mathcal{D} . It should be clarified that the quantum-to-classical transition does not occur abruptly, say, at a specific time. The transition is a continuous process, which is reflected in the constant rise in the amplitude of the squeezing parameter r_σ , an enhancement in the value of the decoherence parameter \mathcal{D} and the eventual orientation of the Wigner ellipse along the classical trajectory.

Apart from examining the behavior of the curvature perturbation, it may be worthwhile to examine the evolution of the Wigner function and the squeezing parameters that characterize the isocurvature perturbation. In particular, investigating the extent of quantum discord in such scenarios may provide us with further insight into the quantum-to-classical transition of the primordial perturbations. We are presently studying such problems.

Chapter 7

Conclusions

7.1 Summary of work done

The inflationary and bouncing scenarios offer alternative mechanisms for the generation of primordial perturbations in the early universe. While inflation can be easily achieved with the aid of a single scalar field, often, one finds that at least two fields are required to drive bounces. Due to this reason, in this thesis, we have studied different issues related to the inflationary and bouncing scenarios driven by two scalar fields. In what follows, after briefly summarizing the main conclusions of this thesis, we shall outline some of the issues that we are presently investigating.

Over the last decade or so, it has been realized that the primordial three-point functions can provide additional constraints to help us discriminate between the inflationary models that are indistinguishable at the level of the two-point functions. The non-Gaussianities generated by single field models have been investigated in great detail. However, it would be fair to say that the non-Gaussianities generated in multi-field models have not been examined to an equal extent.

Specifically, while numerical procedures have been developed to compute the three-point functions generated in single field models, until recently, there has not been a similar effort involving, say, two-field models [44]. As a first step towards this aim, in chapter 2, we had evaluated the dimensionless non-Gaussianity parameter h_{NL} that characterizes the amplitude of the tensor bispectrum numerically for a class of two-field inflationary models. We had also explicitly verified the validity of the consistency relation governing the tensor three-point function in the so-called squeezed limit (*i.e.* when one of the three wavenumbers involved is much smaller than the other two) even in situations involving deviations from slow roll.

While it is easy to construct a model of inflation that is consistent with the cosmological data, constructing pathology-free bounces remain a challenge. The strong point of the matter bounce scenarios is the fact that they can easily lead to scale-invariant spectra. However, one finds that matter bounce scenarios often lead to a tensor-to-scalar ratio that is larger than the current upper bounds from Planck [12]. In chapter 3, we had studied a symmetric matter bounce scenario driven by a canonical scalar field and a non-canonical, ghost scalar field. The model was characterized by a single parameter, *viz.* the scale associated with the bounce. We had solved the equations of motion describing the scalar and tensor perturbations in the model analytically as well as numerically and had evaluated the perturbation spectra at a suitable time after the bounce. We had shown that the model leads to strictly scale-invariant adiabatic scalar and tensor perturbation spectra and a very small tensor-to-scalar ratio that is consistent with the recent observational bounds.

Apart from a suitably small tensor-to-ratio, a red spectral tilt is also required if a bouncing scenario is to be consistent with the observations, since a strictly scale-invariant scalar power spectrum has been ruled to a good level of confidence [7].

In chapter 4, we had extended the matter bounce model we had constructed in the previous chapter to achieve near-matter bounces. The model had now involved an additional parameter, apart from the original scale associated with the bounce. The new parameter had determined the tilt in the scalar and tensor power spectra. Using the numerical procedures developed in the previous chapter, we had evolved the perturbations across the bounce. We had found that, for a certain value of the new parameter, we were able to achieve a red scalar spectral tilt as suggested by the recent CMB data.

As we have repeatedly discussed, nearly scale-free primordial power spectra prove to remarkably consistent with the CMB data. However, tantalizingly, it has been repeatedly shown that specific features in the primordial scalar power spectrum can improve the fit to the data. Since the inflationary trajectory is an attractor, these features can be generated by introducing brief period of deviations from slow roll. In complete contrast, often, bouncing scenarios such as the matter and near-matter bounce models we had considered in chapters 3 and 4 are repellers and they require fine tuned initial conditions. In other words, while inflation can restore the field to its original trajectory when departures are introduced, matter bounces cannot do so. Actually, the high sensitivity to initial conditions will make the field deviate rapidly from the original trajectory. Therefore, it is not possible to generate features in matter or near-matter bounces and, in fact, these models will be ruled out if the presence of features in the primordial spectra are confirmed by future observations. Utilizing the attractive nature of the ekpyrotic bounces, in chapter 5, we had discussed the generation of features during an ekpyrotic phase of contraction. By constructing different ekpyrotic potentials, we had shown that it is possible to generate features in these scenarios often considered in the context of inflation.

One of the issues that remains to be satisfactorily understood is the mechanism of

the quantum-to-classical transition of the primordial perturbations. In chapter 6, we had compared the quantum-to-classical transition of the primordial perturbations in double inflation and the ekpyrotic scenario. We had examined the quantum-to-classical transition with the help of the Wigner function associated with the curvature perturbation. We had found that, in the case of double inflation, the classicality of the curvature perturbation emerges due to the constant increase in the extent of squeezing in a fashion similar to the case of single field inflation. On the other hand, in the ekpyrotic contracting phase, the curvature perturbation turns classical largely due to its interaction with the isocurvature perturbation. We had shown that this mechanism leads to a sharp change in the direction of squeezing of the Wigner function. These conclusions were also supported by the behavior of the squeezing parameter describing the curvature perturbation, which had rapidly increased during the process.

7.2 Outlook

In this final section of the thesis, we shall briefly outline the directions in which we intend to carry our investigations further over the next few years.

One of the primary directions towards which we plan to dedicate our efforts is the numerical computation of the three-point functions involving the scalar perturbations in multi-field inflation. Recently, the so-called transport method has been adopted to compute the non-Gaussianities in multi-field inflation [44]. Extending the more conventional approach adopted in single field models [41, 43], we are presently developing a code to calculate the three-point functions involving the scalar as well as the tensor perturbations in two-field models. In particular, we are aiming to evaluate the amplitude and shape of the non-Gaussianities generated when features are present in the primordial curvature perturbation spec-

trum [123].

In chapters 3 and 4, we had constructed models driving matter and near-matter bounces involving two scalar fields. We had shown that near-matter bounces are consistent with the CMB data at the level of the power spectra. However, we had considered scenarios involving ghost fields which are undesirable. Also, the specific models of non-canonical fields we had considered can be deemed ill-motivated. We are presently constructing similar scenarios involving ghost condensates and Galileons, which circumvent the difficulties associated with the ghost fields. A related question that arises concerning such models is the extent of non-Gaussianities generated in these scenarios. It has been shown that, in matter bounce scenarios driven by a single scalar field, it would *not* be possible to obtain sufficiently small values for both the tensor-to-scalar ratio and the scalar non-Gaussianity parameter simultaneously [124]. It will be interesting to examine the validity of such a ‘no-go theorem’ in multi-field models. We are presently working towards determining the shape as well as the amplitude of the scalar non-Gaussianity parameter that arises in the near-matter bounce models we had considered in chapter 4.

In chapter 5, we had discussed the generation of features in ekpyrotic models that permit attractor solutions for the background. It is important to note that we had calculated the power spectra prior to the bounce. Since the scales associated with the bounce are often widely separated from the scales of cosmological interest, it seems natural to expect that the details of the bounce will not affect the shape of the power spectra. In general, bounces are bound to alter only the amplitudes of the scalar and tensor spectra. Therefore, the natural next step is to construct sources, such as involving the Galileon, to drive the bounce phase, and evolve the perturbations across the bounce (in this context, see Refs. [46]. Apart from examining the effect of the bounce on the amplitudes of the curva-

ture and the tensor perturbation spectra, we need to ensure that the isocurvature perturbations (which were dominant towards the end of the ekpyrotic phase) indeed decay as the universe begins to expand after the bounce. We are presently investigating this issue.

Appendix A

Fixing the coefficients

Recall that, in section 3.7, the expressions (3.72a) and (3.72b) that describe the analytical solutions for \mathcal{R}_k and \mathcal{S}_k in the second domain had contained four time-independent constants, *viz.* \mathcal{C}_k , \mathcal{D}_k , \mathcal{E}_k and \mathcal{F}_k . As we had described, these four constants are to be determined by matching the solutions for \mathcal{R}_k and \mathcal{S}_k in the first domain [*cf.* equations (3.66) and (3.67)] and their time derivatives with the corresponding quantities in the second domain. This matching has to be carried out at the junction of the two domains, *viz.* at $\eta = -\alpha \eta_0$. These matching conditions lead to four equations which need to be solved simultaneously to arrive at the constants \mathcal{C}_k , \mathcal{D}_k , \mathcal{E}_k and \mathcal{F}_k . These constants can be determined to be

$$\begin{aligned} \mathcal{C}_k = & \frac{(\alpha^2 + 1) a_0}{54 \sqrt{2} \alpha^7 k_0^2 M_{\text{Pl}} k^{3/2}} \left\{ 16 \alpha^2 \sqrt{\alpha^2 + 1} k^2 e^{i \alpha k / (\sqrt{3} k_0)} \right. \\ & \times \left[\alpha (\alpha^2 + 1) k - 3 \sqrt{3} i (\alpha^2 - 1) k_0 \right] \\ & \times \text{Ei} \left[i \left(3 - \sqrt{3} \right) \alpha k / (3 k_0) \right] \\ & + \sqrt{3} e^{i \alpha k / k_0} \left[i \alpha^2 (\alpha^2 + 1) \left(-9 \alpha^3 + 32 \sqrt{\alpha^2 + 1} + 27 \alpha \right) k_0 k^2 \right. \\ & \left. + \left(9 \alpha^5 - 18 \alpha^3 + 16 \alpha^2 \sqrt{\alpha^2 + 1} - 80 \sqrt{\alpha^2 + 1} - 27 \alpha \right) \right] \end{aligned}$$

$$\begin{aligned}
& \times \left(3\alpha k_0^2 k + 3i k_0^3 \right) \Big] \\
& - 4\alpha^2 \sqrt{\alpha^2 + 1} \left(4\pi k^2 + 3^{7/4} k_0 k \right) e^{i\alpha k/(\sqrt{3}k_0)} \\
& \times \left[3\sqrt{3} (\alpha^2 - 1) k_0 + i\alpha (\alpha^2 + 1) k \right] \Big\}, \tag{A.1}
\end{aligned}$$

$$\begin{aligned}
\mathcal{D}_k = & \frac{1}{108\sqrt{2} 3^{3/4} \alpha^7 a_0 k_0^2 M_{\text{Pl}} k^{3/2}} \left\{ 4 3^{1/4} \alpha^2 \sqrt{\alpha^2 + 1} \right. \\
& \times \left(\sqrt{3} \alpha^2 (\alpha^2 + 1) k^3 - 9i\alpha (4\alpha^2 - 1) k_0 k^2 \right. \\
& + \left[4\sqrt{3} \alpha (\alpha^2 + 1)^2 k - 36i (\alpha^4 - 1) k_0 \right] \\
& \times k^2 \tan^{-1}(\alpha) \text{Ei} \left[i \left(3 - \sqrt{3} \right) \alpha k / (3 k_0) \right] e^{i\alpha k/(\sqrt{3}k_0)} \\
& + 3^{5/4} \alpha e^{i\alpha k/k_0} \left[i\alpha^2 (\alpha^2 + 1) \left(-9\alpha^3 + 8\sqrt{\alpha^2 + 1} + 9\alpha \right) k_0 k^2 \right. \\
& + \left. \left(9\alpha^5 + 12\alpha^3 + 40\alpha^2 \sqrt{\alpha^2 + 1} - 20\sqrt{\alpha^2 + 1} - 9\alpha \right) \right. \\
& \times \left. \left. \left(3\alpha k_0^2 k + 3i k_0^3 \right) \right] \right. \\
& + \alpha^2 \sqrt{\alpha^2 + 1} \left(4 3^{1/4} \pi k^2 + 9 k_0 k \right) e^{i\alpha k/(\sqrt{3}k_0)} \\
& \times \left[\left(9 - 36\alpha^2 \right) k_0 - i\sqrt{3} \alpha (\alpha^2 + 1) k \right] \\
& + \left(\alpha^2 + 1 \right) \tan^{-1}(\alpha) \left[3^{5/4} i \alpha^2 (\alpha^2 + 1) \right. \\
& \times \left. \left(-9\alpha^3 + 32\sqrt{\alpha^2 + 1} + 27\alpha \right) k_0 k^2 \right. \\
& + 3^{9/4} \left(9\alpha^5 - 18\alpha^3 + 16\sqrt{\alpha^2 + 1} \alpha^2 - 80\sqrt{\alpha^2 + 1} - 27\alpha \right) \\
& \times \left. \left. \left(\alpha k_0^2 k + i k_0^3 \right) \right] e^{i\alpha k/k_0} \right. \\
& + 4\alpha^2 (\alpha^2 + 1)^{3/2} \tan^{-1}(\alpha) \left(4 3^{1/4} \pi k + 9 k_0 \right) \\
& \times \left. \left. \left. \left[-9 (\alpha^2 - 1) k_0 k - \sqrt{3} i \alpha (\alpha^2 + 1) k^2 \right] e^{i\alpha k/(\sqrt{3}k_0)} \right\}, \tag{A.2}
\end{aligned}$$

$$\begin{aligned}
\mathcal{E}_k = & \frac{e^{-2\sqrt{5} \tan^{-1}(\alpha)}}{864 3^{3/4} \sqrt{10} \alpha^7 (\alpha + \sqrt{5}) a_0 k_0^2 M_{\text{Pl}} k^{3/2}} \left\{ -16 3^{1/4} \alpha^2 \sqrt{\alpha^2 + 1} k^2 \right. \\
& \times e^{i\alpha k/(\sqrt{3}k_0)} \left[\sqrt{3} \alpha (\alpha^2 + 1) \left(4\alpha^3 + 5\sqrt{5} \alpha^2 + 8\alpha + 3\sqrt{5} \right) k \right. \\
& + \left. \left. \left. \left. 9i \left(\sqrt{5} \alpha^2 + 8\alpha + 3\sqrt{5} \right) k_0 \right] \text{Ei} \left[i \left(3 - \sqrt{3} \right) \alpha k / (3 k_0) \right] \right\}
\end{aligned}$$

$$\begin{aligned}
& + \left(-i \alpha^2 (\alpha^2 + 1) \left[-9 \alpha^6 + 9 \sqrt{5} \alpha^5 + 162 \alpha^4 \right. \right. \\
& + \left. \left. \left(160 \sqrt{5(\alpha^2 + 1)} + 171 \right) \alpha^2 \left(256 \sqrt{\alpha^2 + 1} + 81 \sqrt{5} \right) \alpha \right. \right. \\
& + \left. \left. 96 \sqrt{5(\alpha^2 + 1)} + 2 \left(64 \sqrt{\alpha^2 + 1} + 45 \sqrt{5} \right) \alpha^3 \right] k^2 \right. \\
& + \left[-9 \alpha^8 + 9 \sqrt{5} \alpha^7 + 153 \alpha^6 + 19 \left(16 \sqrt{5(\alpha^2 + 1)} + 9 \right) \alpha^2 \right. \\
& + \left. \left(640 \sqrt{\alpha^2 + 1} + 81 \sqrt{5} \right) \alpha + 240 \sqrt{5(\alpha^2 + 1)} \right. \\
& + \left. \left(128 \sqrt{\alpha^2 + 1} + 99 \sqrt{5} \right) \alpha^5 + \left(160 \sqrt{5(\alpha^2 + 1)} + 333 \right) \alpha^4 \right. \\
& + \left. \left. 3 \left(128 \sqrt{\alpha^2 + 1} + 57 \sqrt{5} \right) \alpha^3 \right] \left(3 \alpha k_0 k + 3 i k_0^2 \right) \right) 3^{5/4} k_0 e^{i \alpha k / k_0} \\
& + 4 i \alpha^2 \sqrt{\alpha^2 + 1} \left(43^{1/4} \pi k^2 + 9 k_0 k \right) e^{i \alpha k / (\sqrt{3} k_0)} \\
& \times \left[9 i \left(\sqrt{5} \alpha^2 + 8 \alpha + 3 \sqrt{5} \right) k_0 \right. \\
& + \left. \left. \sqrt{3} \alpha (\alpha^2 + 1) \left(4 \alpha^3 + 5 \sqrt{5} \alpha^2 + 8 \alpha + 3 \sqrt{5} \right) k \right] \right\}, \tag{A.3}
\end{aligned}$$

$$\begin{aligned}
\mathcal{F}_k & = \frac{e^{2 \sqrt{5} \tan^{-1}(\alpha)}}{864 \cdot 3^{3/4} \sqrt{10} \alpha^7 (\alpha + \sqrt{5}) a_0 k_0^2 M_{\text{Pl}} k^{3/2}} \left\{ 16 \cdot 3^{1/4} \alpha^2 \sqrt{\alpha^2 + 1} k^2 \right. \\
& \times \left[\sqrt{3} \alpha (\alpha^2 + 1) \left(4 \alpha^3 + 3 \sqrt{5} \alpha^2 - 2 \alpha + 3 \sqrt{5} \right) k \right. \\
& - \left. \left. 9 i \left(\sqrt{5} \alpha^2 + 2 \alpha - 3 \sqrt{5} \right) k_0 \right] \right. \\
& \times \text{Ei} \left[i \left(3 - \sqrt{3} \right) \alpha k / (3 k_0) \right] e^{i \alpha k / (\sqrt{3} k_0)} \\
& + \left(i \alpha^2 (\alpha^2 + 1) k^2 \left[-9 \alpha^6 - 27 \sqrt{5} \alpha^5 - 18 \alpha^4 \right. \right. \\
& + \left. \left. \left(96 \sqrt{5(\alpha^2 + 1)} - 9 \right) \alpha^2 + \left(81 \sqrt{5} - 64 \sqrt{\alpha^2 + 1} \right) \alpha \right. \right. \\
& + \left. \left. 96 \sqrt{5(\alpha^2 + 1)} + 2 \left(64 \sqrt{\alpha^2 + 1} + 27 \sqrt{5} \right) \alpha^3 \right] \right. \\
& - \left[-9 \alpha^8 - 27 \sqrt{5} \alpha^7 - 27 \alpha^6 + 9 \left(16 \sqrt{5(\alpha^2 + 1)} - 1 \right) \alpha^2 \right. \\
& + \left. \left(81 \sqrt{5} - 160 \sqrt{\alpha^2 + 1} \right) \alpha + 240 \sqrt{5(\alpha^2 + 1)} \right. \\
& + \left. \left(128 \sqrt{\alpha^2 + 1} + 27 \sqrt{5} \right) \alpha^5 + 3 \left(32 \sqrt{5(\alpha^2 + 1)} - 9 \right) \alpha^4 \right. \\
& + \left. \left. \left. \left(64 \sqrt{\alpha^2 + 1} + 135 \sqrt{5} \right) \alpha^3 \right] \left(3 \alpha k_0 k + 3 i k_0^2 \right) \right) 3^{5/4} k_0 e^{i \alpha k / k_0} \right.
\end{aligned}$$

$$\begin{aligned}
& -4\alpha^2 \sqrt{\alpha^2 + 1} (43^{1/4} \pi k^2 + 9k_0 k) e^{i\alpha k/(\sqrt{3}k_0)} \\
& \times \left[9 \left(\sqrt{5}\alpha^2 + 2\alpha - 3\sqrt{5} \right) k_0 \right. \\
& \left. + \sqrt{3}i\alpha (\alpha^2 + 1) \left(4\alpha^3 + 3\sqrt{5}\alpha^2 - 2\alpha + 3\sqrt{5} \right) k \right] \Bigg\}. \tag{A.4}
\end{aligned}$$

Appendix B

Is a diverging curvature perturbation acceptable?

We have seen that, in the model driving near-matter bounces we have constructed in chapter 4 as well as in the earlier model leading to the matter bounce scenario considered in chapter 3, the curvature and the isocurvature perturbations diverge when $\dot{H} = 0$. This may cause concern as to whether the perturbation theory breaks down around such instances. We believe that this behavior should not be of any concern. The reason being that the curvature and the isocurvature perturbations diverge due to the fact that a background quantity which appears in the denominator of their definitions vanish. As we have discussed in chapters 3 and 4, it is possible to overcome such hurdles by working with perturbed quantities that behave well at these points.

In fact, such a behavior also occurs during the reheating phase that succeeds inflation. To illustrate this point, let us consider the often studied case of inflation driven by a single, canonical scalar field, say, φ . As is well known, once inflation has terminated, the scalar field is expected to oscillate at the bottom of the po-

tential between the turning points where the velocity of the field vanishes. Let us focus on the domain where energy density of the scalar field is still dominant soon after inflation (*i.e.* when reheating is yet to set in, a period that is referred to as preheating). In such a situation, for the case of inflation and preheating driven by the conventional quadratic potential, the behavior of the background as well as the curvature perturbation associated with a typical large scale mode of cosmological interest can be solved for analytically (in this context, see, for instance, Ref. [125]). In figure B, we have plotted the evolution of the velocity $\dot{\phi}$ of the background scalar field and the curvature perturbation, say, \mathcal{R}_k , associated with a small scale mode obtained numerically, as a function of e-fold N during the epoch of preheating. In plotting the figure, for convenience, we have chosen to work with a small range of e-folds of inflation. Also, we have restricted our attention to the behavior of the velocity of the scalar field and the curvature perturbation during the epoch of preheating. It is clear from the figure that the curvature perturbation diverges exactly at the turning points when the scalar field oscillates at the bottom of the inflationary potential. The situation encountered in the cases of the bouncing scenarios we have considered in chapters 3 and 4 is exactly similar to the behavior during preheating. In fact, in both the situations, the divergences occur whenever $\dot{H} = 0$. Due to this reason, we believe that the divergent curvature and isocurvature perturbations which we encounter in the matter and near-matter bounces (we had considered in chapters 3 and 4) pose no cause for concern (for a discussion on this issue, also see Ref. [126]).

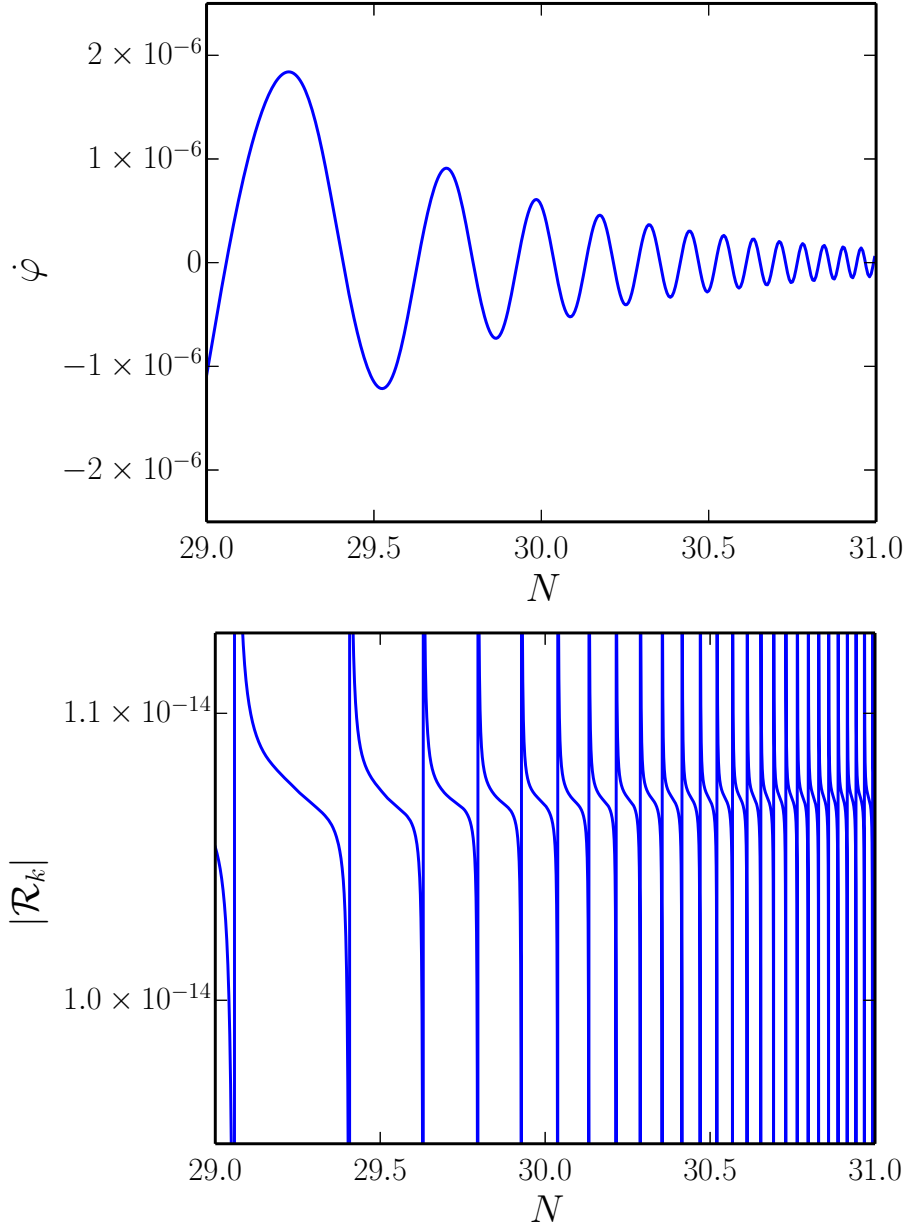


Figure B.1: The behavior of the velocity $\dot{\varphi}$ of the scalar field driving the background (on top) and the amplitude of the curvature perturbation \mathcal{R}_k (at the bottom), obtained numerically, has been plotted as a function of e-fold N during the epoch of preheating that succeeds inflation. For purposes of illustration, we have considered the simple case of the conventional quadratic potential to drive inflation and preheating. Also, for convenience, we have chosen to work with a small period of inflation and have highlighted the behavior of the velocity of the field and the amplitude of the curvature perturbation during the epoch of preheating (in this context, also see Ref. [125]). For our choice of the parameters and initial conditions, inflation ends at $N \simeq 28.3$ and the mode of interest leaves the Hubble scale during inflation at $N \simeq 26.2$. It is evident from the figures that the curvature perturbation diverges *exactly* at the points where $\dot{\varphi}$ and, hence, \dot{H} vanish.

Bibliography

- [1] E. W. Kolb and M. S. Turner, *The Early Universe* (Addison-Wesley, Redwood City, California, 1990); S. Dodelson, *Modern Cosmology* (Academic Press, San Diego, U.S.A., 2003); V. F. Mukhanov, *Physical Foundations of Cosmology* (Cambridge University Press, Cambridge, England, 2005); S. Weinberg, *Cosmology* (Oxford University Press, Oxford, England, 2008); R. Durrer, *The Cosmic Microwave Background* (Cambridge University Press, Cambridge, England, 2008); D. H. Lyth and A. R. Liddle, *The Primordial Density Perturbation* (Cambridge University Press, Cambridge, England, 2009); P. Peter and J-P. Uzan, *Primordial Cosmology* (Oxford University Press, Oxford, England, 2009); H. Mo, F. v. d. Bosch and S. White, *Galaxy Formation and Evolution* (Cambridge University Press, Cambridge, England, 2010); D. Baumann and L. McAllister, *Inflation and String Theory* (Cambridge University Press, Cambridge, England, 2015).
- [2] H. Kodama and M. Sasaki, *Prog. Theor. Phys. Suppl.* **78**, 1 (1984); V. F. Mukhanov, H. A. Feldman and R. H. Brandenberger, *Phys. Rep.* **215**, 203 (1992); J. E. Lidsey, A. Liddle, E. W. Kolb, E. J. Copeland, T. Barreiro and M. Abney, *Rev. Mod. Phys.* **69**, 373 (1997); A. Riotto, *ICTP Lect. Notes Ser.* **14**, 317 (2003); W. H. Kinney, *NATO Sci. Ser. II* **123**, 189 (2003); B. Bassett, S. Tsujikawa and D. Wands, *Rev. Mod. Phys.* **78**, 537 (2006); W. H. Kinney, arXiv:0902.1529 [astro-ph.CO]; D. Baumann, arXiv:0907.5424v1 [hep-

- th]; L. Sriramkumar, *Curr. Sci.* **97**, 868 (2009); L. Sriramkumar in *Vignettes in Gravitation and Cosmology*, Eds. L. Sriramkumar and T. R. Seshadri (World Scientific, Singapore, 2012), pp. 207–249; J. Martin, *Astrophys. Space Sci. Proc.* **45**, 41 (2016); J. Martin, arXiv:1807.11075 [astro-ph.CO].
- [3] D. Battfeld and P. Peter, *Phys. Rept.* **571**, 1 (2015); R. Brandenberger and P. Peter, *Found. Phys.* **47**, 797 (2017).
- [4] P. A. R. Ade *et al.* [Planck Collaboration], *Astron. Astrophys.* **571**, A15 (2014); N. Aghanim *et al.* [Planck Collaboration], *Astron. Astrophys.* **594**, A11 (2016).
- [5] Y. Akrami *et al.* [Planck Collaboration], arXiv:1807.06205 [astro-ph.CO].
- [6] P. A. R. Ade *et al.* [Planck Collaboration], *Astron. Astrophys.* **571**, A16 (2014); P. A. R. Ade *et al.* [Planck Collaboration], *Astron. Astrophys.* **594**, A13 (2016); N. Aghanim *et al.* [Planck Collaboration], arXiv:1807.06209 [astro-ph.CO].
- [7] P. A. R. Ade *et al.* [Planck Collaboration], *Astron. Astrophys.* **571**, A22 (2014); P. A. R. Ade *et al.* [Planck Collaboration], *Astron. Astrophys.* **594**, A20 (2016); Y. Akrami *et al.* [Planck Collaboration], arXiv:1807.06211 [astro-ph.CO].
- [8] J. Martin, C. Ringeval and V. Vennin, *Phys. Dark Univ.* **5-6**, 75 (2014).
- [9] D. Polarski, *Phys. Rev. D* **49**, 6319 (1994); D. Langlois, *Phys. Rev. D* **59**, 123512 (1999); N. Bartolo, S. Matarrese and A. Riotto, *Phys. Rev. D* **64**, 123504 (2001); C. T. Byrnes and D. Wands, *Phys. Rev. D* **74**, 043529 (2006); D. Langlois and S. Renaux-Petel, *JCAP* **0804**, 017 (2008).

- [10] C. Gordon, D. Wands, B. A. Bassett and R. Maartens, *Phys. Rev. D* **63**, 023506 (2001).
- [11] S. Tsujikawa, D. Parkinson and B. A. Bassett, *Phys. Rev. D* **67**, 083516 (2003); Z. Lalak, D. Langlois, S. Pokorski and K. Turzynski, *JCAP* **0707**, 014 (2007).
- [12] L. E. Allen and D. Wands, *Phys. Rev. D* **70**, 063515 (2004).
- [13] Y. F. Cai, D. A. Easson and R. Brandenberger, *JCAP* **1208**, 020 (2012).
- [14] F. Finelli, P. Peter and N. Pinto-Neto, *Phys. Rev. D* **77**, 103508 (2008).
- [15] D. A. Easson, I. Sawicki and A. Vikman, *JCAP* **1111**, 021 (2011).
- [16] D. Dobre, A. Frolov, J. Gherzi, S. Ramazanov and A. Vikman, *JCAP* **1803**, 020 (2018).
- [17] A. Ijjas and P. J. Steinhardt, *Phys. Rev. Lett.* **117**, 121304 (2016).
- [18] J. Chluba, J. Hamann and S. P. Patil, *Int. J. Mod. Phys. D* **24**, 1530023 (2015).
- [19] J. M. Cline, P. Crotty and J. Lesgourgues, *JCAP* **0309**, 010 (2003); C. R. Contaldi, M. Peloso, L. Kofman and A. Linde, *JCAP* **0307**, 002 (2003); B. A. Powell and W. H. Kinney, *Phys. Rev. D* **76**, 063512 (2007); R. K. Jain, P. Chingangbam, J.-O. Gong, L. Sriramkumar and T. Souradeep, *JCAP* **0901**, 009 (2009); R. K. Jain, P. Chingangbam, L. Sriramkumar and T. Souradeep, *Phys. Rev. D* **82**, 023509 (2010).
- [20] L. Covi, J. Hamann, A. Melchiorri, A. Slosar and I. Sorbera, *Phys. Rev. D* **74**, 083509 (2006); J. Hamann, L. Covi, A. Melchiorri and A. Slosar, *Phys. Rev. D* **76**, 023503 (2007); M. J. Mortonson, C. Dvorkin, H. V. Peiris and W. Hu, *Phys. Rev. D* **79**, 103519 (2009); D. K. Hazra, M. Aich, R. K. Jain, L. Sriramkumar and T. Souradeep, *JCAP* **1010**, 008 (2010); M. Benetti, M. Lattanzi,

- E. Calabrese and A. Melchiorri, *Phys. Rev. D* **84**, 063509 (2011); M. Benetti, *Phys. Rev. D* **88**, 087302 (2013).
- [21] M. Aich, D. K. Hazra, L. Sriramkumar and T. Souradeep, *Phys. Rev. D* **87**, 083526 (2013); C. Pahud, M. Kamionkowski and A. R. Liddle, *Phys. Rev. D* **79**, 083503 (2009); P. D. Meerburg, D. N. Spergel and B. D. Wandelt, *Phys. Rev. D* **89**, 063536 (2014); P. D. Meerburg and D. N. Spergel, *Phys. Rev. D* **89**, 063537 (2014).
- [22] D. K. Hazra, A. Shafieloo, G. F. Smoot and A. A. Starobinsky, *Phys. Rev. Lett.* **113**, 071301 (2014); D. K. Hazra, A. Shafieloo, G. F. Smoot and A. A. Starobinsky, *JCAP* **1408**, 048 (2014).
- [23] D. K. Hazra, A. Shafieloo and T. Souradeep, *JCAP* **1411**, 011 (2014); P. Hunt and S. Sarkar, *JCAP* **1401**, 025 (2014).
- [24] A. M. Levy, *Phys. Rev. D* **95**, 023522 (2017).
- [25] J. Khoury, B. A. Ovrut, P. J. Steinhardt and N. Turok, *Phys. Rev. D* **64**, 123522 (2001); E. I. Buchbinder, J. Khoury and B. A. Ovrut, *Phys. Rev. D* **76**, 123503 (2007).
- [26] M. Li, *Phys. Lett. B* **724**, 192 (2013); T. Qiu, X. Gao and E. N. Saridakis, *Phys. Rev. D* **88**, 043525 (2013); A. Fertig, J.-L. Lehners and E. Mallwitz, *Phys. Rev. D* **89**, 103537 (2014); A. Ijjas, J.-L. Lehners and P. J. Steinhardt, *Phys. Rev. D* **89**, 123520 (2014); A. M. Levy, A. Ijjas and P. J. Steinhardt, *Phys. Rev. D* **92**, 063524 (2015).
- [27] A. Ijjas and P. J. Steinhardt, *Class. Quant. Grav.* **33**, 044001 (2016).
- [28] A. Albrecht, P. Ferreira, M. Joyce and T. Prokopec, *Phys. Rev. D* **50**, 4807 (1994); D. Polarski and A. A. Starobinsky, *Class. Quant. Grav.* **13**, 377 (1996).

- [29] C. Kiefer, D. Polarski and A. A. Starobinsky, *Int. J. Mod. Phys. D* **7**, 455 (1998); C. Kiefer, I. Lohmar, D. Polarski and A. A. Starobinsky, *Class. Quant. Grav.* **24**, 1699 (2007); J. Martin, *Lect. Notes Phys.* **738**, 193 (2008); C. Kiefer and D. Polarski, *Adv. Sci. Lett.* **2**, 164 (2009); J. Martin, *J. Phys. Conf. Ser.* **405**, 012004 (2012); J. Martin, V. Vennin and P. Peter, *Phys. Rev. D* **86**, 103524 (2012); J. Martin and V. Vennin, *Phys. Rev. D* **93**, 023505 (2016).
- [30] T. Prokopec and G. I. Rigopoulos, *JCAP* **0711**, 029 (2007).
- [31] G. Leon, G. R. Bengochea and S. J. Landau, *Eur. Phys. J. C* **76**, 407 (2016).
- [32] L. Battarra and J. L. Lehnert, *Phys. Rev. D* **89**, 063516 (2014).
- [33] D. J. Stargen, V. Sreenath and L. Sriramkumar, arXiv:1605.07311v2 [gr-qc].
- [34] J. M. Maldacena, *JHEP* **0305**, 013 (2003).
- [35] D. Seery and J. E. Lidsey, *JCAP* **0506**, 003 (2005).
- [36] X. Chen, *Phys. Rev. D* **72**, 123518 (2005); X. Chen, M. x. Huang, S. Kachru and G. Shiu, *JCAP* **0701**, 002 (2007); D. Langlois, S. Renaux-Petel, D. A. Steer and T. Tanaka, *Phys. Rev. Lett.* **101**, 061301 (2008); D. Langlois, S. Renaux-Petel, D. A. Steer and T. Tanaka, *Phys. Rev. D* **78**, 063523 (2008); X. Chen, *Adv. Astron.* **2010**, 638979 (2010); Y. Wang, *Commun. Theor. Phys.* **62**, 109 (2014); E. Komatsu and D. N. Spergel, *Phys. Rev. D* **63**, 063002 (2001); E. Komatsu, D. N. Spergel and B. D. Wandelt, *Astrophys. J.* **634**, 14 (2005); D. Babich and M. Zaldarriaga, *Phys. Rev. D* **70**, 083005 (2004); M. Liguori, F. K. Hansen, E. Komatsu, S. Matarrese and A. Riotto, *Phys. Rev. D* **73**, 043505 (2006); C. Hikage, E. Komatsu and T. Matsubara, *Astrophys. J.* **653**, 11 (2006); J. R. Fergusson and E. P. S. Shellard, *Phys. Rev. D* **76**, 083523 (2007); A. P. S. Yadav, E. Komatsu and B. D. Wandelt, *Astrophys. J.* **664**, 680 (2007); P. Creminelli, L. Senatore and M. Zaldarriaga, *JCAP* **0703**, 019

- (2007); A. P. S. Yadav and B. D. Wandelt, *Phys. Rev. Lett.* **100**, 181301 (2008); C. Hikage, T. Matsubara, P. Coles, M. Liguori, F. K. Hansen and S. Matarrese, *Mon. Not. Roy. Astron. Soc.* **389**, 1439 (2008); O. Rudjord, F. K. Hansen, X. Lan, M. Liguori, D. Marinucci and S. Matarrese, *Astrophys. J.* **701**, 369 (2009); K. M. Smith, L. Senatore and M. Zaldarriaga, *JCAP* **0909**, 006 (2009); J. Smidt, A. Amblard, C. T. Byrnes, A. Cooray, A. Heavens and D. Munshi, *Phys. Rev. D* **81**, 123007 (2010); J. R. Fergusson, M. Liguori and E. P. S. Shellard, *JCAP* **1212**, 032 (2012).
- [37] P. A. R. Ade *et al.* [Planck Collaboration], *Astron. Astrophys.* **594**, A17 (2016).
- [38] D. Langlois, S. Renaux-Petel, D. A. Steer and T. Tanaka, *Phys. Rev. Lett.* **101**, 061301 (2008); D. Langlois, S. Renaux-Petel, D. A. Steer and T. Tanaka, *Phys. Rev. D* **78**, 063523 (2008).
- [39] J. M. Maldacena and G. L. Pimentel, *JHEP* **1109**, 045 (2011); X. Gao, T. Kobayashi, M. Yamaguchi and J. Yokoyama, *Phys. Rev. Lett.* **107**, 211301 (2011); X. Gao, T. Kobayashi, M. Shiraishi, M. Yamaguchi, J. Yokoyama and S. Yokoyama, *PTEP* **2013**, 053E03 (2013).
- [40] X. Chen, R. Easther and E. A. Lim, *JCAP* **0706**, 023 (2007).
- [41] X. Chen, R. Easther and E. A. Lim, *JCAP* **0804**, 010 (2008); D. K. Hazra, L. Sriramkumar and J. Martin, *JCAP* **1305**, 026 (2013).
- [42] P. Adshead, W. Hu, C. Dvorkin and H. V. Peiris, *Phys. Rev. D* **84** (2011) 043519 (2011).
- [43] V. Sreenath, R. Tibrewala and L. Sriramkumar, *JCAP* **1312**, 037 (2013).
- [44] M. Dias, J. Frazer, D. J. Mulryne and D. Seery, *JCAP* **1612**, 033 (2016);

- D. Seery, arXiv:1609.00380 [astro-ph.CO]; D. J. Mulryne, arXiv:1609.00381 [astro-ph.CO].
- [45] J. Khoury and P. J. Steinhardt, Phys. Rev. Lett. **104**, 091301 (2010); A. Linde, V. Mukhanov and A. Vikman, JCAP 1002, 006 (2010).
- [46] A. Fertig, J.-L. Lehners, E. Mallwitz and E. Wilson-Ewing, JCAP **1610**, 005 (2016).
- [47] A. Friedmann, Z. Phys. **10**, 377386 (1922).
- [48] G. Lemaitre, Annales Soc. Sci. Bruxelles A **47**, 49 (1927).
- [49] E. Hubble, Proc. Nat. Acad. Sci. **15**, 168173, (1929).
- [50] K. Abazajian *et al.*, Astrophys. J. Suppl. **182**, 543 (2009).
- [51] A. A. Penzias and R. W. Wilson, Astrophys. J. **142**, 419 (1965).
- [52] <https://map.gsfc.nasa.gov/media/060915/index.html>.
- [53] C. L. Bennet *et al.*, Astrophys. J. Suppl. **436**, 423 (1994); E. L. Wright *et al.*, Astrophys. J. Suppl. **436**, 443 (1994); K. M. Gorski, Astrophys. J. Suppl. **430**, L85 (1994); K. M. Gorski *et al.*, Astrophys. J. Suppl. **430**, L89 (1994).
- [54] C. L. Bennett *et al.*, Astrophys. J. Suppl. **208**, 20 (2013); G. Hinshaw *et al.*, Astrophys. J. Suppl. **208**, 19 (2013).
- [55] https://wiki.cosmos.esa.int/planck-legacy-archive/index.php/File:Cmb_inpaint_T_commander_v1.png
- [56] A. H. Guth, Phys. Rev. D **23**, 347 (1981).
- [57] F. Lucchin and S. Matarrese, Phys. Rev. D **32**, 1316 (1985).

- [58] A. D. Linde, *Phys. Rev. D* **49**, 748 (1994).
- [59] C. Long, L. McAllister and P. McGuirk, *Phys. Rev. D* **90**, 023501 (2014).
- [60] P. A. R. Ade *et al.* [BICEP2 Collaboration], *Phys. Rev. Lett.* **112**, 241101 (2014).
- [61] P. A. R. Ade *et al.* [BICEP2 and Planck Collaborations], *Phys. Rev. Lett.* **114**, 101301 (2015).
- [62] G. Gubitosi, M. Lagos, J. Magueijo and R. Allison, *JCAP* **1606**, 002 (2016).
- [63] V. A. Belinskii, I. M. Khalatnikov and E. M. Lifshitz, *Advances in Physics*, **19**, 525, (1970).
- [64] D. Wands, *Phys. Rev. D* **60**, 023507 (1999).
- [65] C. Lin, J. Quintin and R. H. Brandenberger, *JCAP* **1801**, 011 (2018).
- [66] M. J. Mortonson, H. V. Peiris and R. Easther, *Phys. Rev. D* **83**, 043505 (2011); R. Easther and H. V. Peiris, *Phys. Rev. D* **85**, 103533 (2012); J. Norena, C. Wagner, L. Verde, H. V. Peiris and R. Easther, *Phys. Rev. D* **86**, 023505 (2012).
- [67] J. Martin, C. Ringeval and R. Trotta, *Phys. Rev. D* **83**, 063524 (2011); J. Martin, C. Ringeval and V. Vennin, *Phys. Dark Univ.* **5-6**, 75 (2014); J. Martin, C. Ringeval, R. Trotta and V. Vennin, *JCAP* **1403**, 039 (2014); J. Martin, C. Ringeval, R. Trotta and V. Vennin, *Phys. Rev. D* **90**, 063501 (2014); J. Martin, C. Ringeval and V. Vennin, *JCAP* **1410**, 038 (2014); P. A. R. Ade *et al.* [Planck Collaboration], *Astron. Astrophys.* **594**, A20 (2016).
- [68] D. Parkinson, S. Tsujikawa, B. A. Bassett and L. Amendola, *Phys. Rev. D* **71**, 063524 (2005); R. Easther, J. Frazer, H. V. Peiris and L. C. Price, *Phys. Rev.*

- Lett. **112**, 161302 (2014).
- [69] D. Wands, Lect. Notes Phys. **738**, 275 (2008); D. Langlois, Lect. Notes Phys. **800**, 1 (2010); J. O. Gong, Int. J. Mod. Phys. D **26**, 1740003 (2016).
- [70] W. H. Press, S. A. Teukolsky, W. T. Vetterling, and B. P. Flannery, Cambridge University Press, New York, NY, USA, 3 ed., 2007.
- [71] V. Sreenath and L. Sriramkumar, JCAP **1410**, 021 (2014).
- [72] J. Silk and M. S. Turner, Phys. Rev. D **35**, 419 (1987); R. Holman, E. W. Kolb, S. L. Vadas and Y. Wang, Phys. Lett. B **269**, 252 (1991).
- [73] D. H. Lyth and E. D. Stewart, Phys. Rev. D **54**, 7186 (1996).
- [74] A. D. Linde, Phys. Rev. D **49**, 748 (1994); D. H. Lyth and E. D. Stewart, Phys. Rev. D **54**, 7186 (1996).
- [75] S. Clesse and J. Rocher, Phys. Rev. D **79**, 103507 (2009); S. Clesse, C. Ringeval and J. Rocher, Phys. Rev. D **80**, 123534 (2009).
- [76] R. Kappl, S. Krippendorff and H. P. Nilles, Phys. Lett. B **737**, 124 (2014); M. Peloso and C. Unal, JCAP **1506**, 040 (2015).
- [77] R. N. Raveendran and L. Sriramkumar, JCAP **1707**, 035 (2017)
- [78] M. Novello and S. E. P. Bergliaffa, Phys. Rept. **463**, 127 (2008).
- [79] Y. F. Cai, Sci. China Phys. Mech. Astron. **57**, 1414 (2014).
- [80] M. Lilley and P. Peter, Comptes Rendus Physique **16**, 1038 (2015).
- [81] S. D. P. Vitiello and N. Pinto-Neto, Phys. Rev. D **85**, 023524 (2012).
- [82] N. Pinto-Neto and S. D. P. Vitiello, Phys. Rev. D **89**, 028301 (2014).

- [83] D. A. Easson and A. Vikman, arXiv:1607.00996 [gr-qc].
- [84] T. J. Battefeld and R. Brandenberger, *Phys. Rev. D* **70**, 121302 (2004).
- [85] J. Martin, P. Peter, N. Pinto Neto and D. J. Schwarz, *Phys. Rev. D* **65**, 123513 (2002); S. Tsujikawa, R. Brandenberger and F. Finelli, *Phys. Rev. D* **66**, 083513 (2002); P. Peter and N. Pinto-Neto, *Phys. Rev. D* **66**, 063509 (2002); P. Peter, N. Pinto-Neto and D. A. Gonzalez, *JCAP* **0312**, 003 (2003); J. Martin and P. Peter, *Phys. Rev. D* **68**, 103517 (2003); V. Bozza and G. Veneziano, *Phys. Lett. B* **625**, 177 (2005); J. L. Lehners, *Phys. Rept.* **465**, 223 (2008); S. D. Odintsov and V. K. Oikonomou, *Phys. Rev. D* **90**, 124083 (2014); F. T. Falciiano, M. Lilley and P. Peter, *Phys. Rev. D* **77**, 083513 (2008); X. Gao, M. Lilley and P. Peter, *Phys. Rev. D* **91**, 023516 (2015); S. Nojiri, S. D. Odintsov and V. K. Oikonomou, *Phys. Rev. D* **93**, 084050 (2016).
- [86] Y. F. Cai, T. Qiu, Y. S. Piao, M. Li and X. Zhang, *JHEP* **0710**, 071 (2007); Y. F. Cai, T. Qiu, R. Brandenberger, Y. S. Piao and X. Zhang, *JCAP* **0803**, 013 (2008).
- [87] Y. F. Cai, T. t. Qiu, R. Brandenberger and X. m. Zhang, *Phys. Rev. D* **80**, 023511 (2009).
- [88] C. Lin, R. H. Brandenberger and L. P. Levasseur, *JCAP* **1104**, 019 (2011).
- [89] Y. F. Cai, R. Brandenberger and X. Zhang, *JCAP* **1103**, 003 (2011).
- [90] T. Qiu, J. Evslin, Y. F. Cai, M. Li and X. Zhang, *JCAP* **1110**, 036 (2011).
- [91] Y. F. Cai, D. A. Easson and R. Brandenberger, *JCAP* **1208**, 020 (2012).
- [92] Y. F. Cai, E. McDonough, F. Duplessis and R. H. Brandenberger, *JCAP* **1310**, 024 (2013).

- [93] Y. F. Cai, R. Brandenberger and P. Peter, *Class. Quant. Grav.* **30**, 075019 (2013).
- [94] Y. F. Cai, J. Quintin, E. N. Saridakis and E. Wilson-Ewing, *JCAP* **1407**, 033 (2014).
- [95] J. Quintin, Z. Sherkatghanad, Y. F. Cai and R. H. Brandenberger, *Phys. Rev. D* **92**, 063532 (2015).
- [96] J. Quintin and R. H. Brandenberger, *JCAP* **1611**, 029 (2016).
- [97] D. Wands, *Adv. Sci. Lett.* **2**, 194 (2009).
- [98] F. T. Falciiano, N. Pinto-Neto and E. S. Santini, *Phys. Rev. D* **76**, 083521 (2007); P. Peter and N. Pinto-Neto, *Phys. Rev. D* **78**, 063506 (2008).
- [99] J. M. Cline, S. Jeon and G. D. Moore, *Phys. Rev. D* **70**, 043543 (2004).
- [100] N. Arkani-Hamed, H. C. Cheng, M. A. Luty and S. Mukohyama, *JHEP* **0405**, 074 (2004).
- [101] D. Chowdhury, V. Sreenath and L. Sriramkumar, *JCAP* **1511**, 002 (2015).
- [102] L. Sriramkumar, K. Atmjeet and R. K. Jain, *JCAP* **1509**, 010 (2015).
- [103] D. Chowdhury, L. Sriramkumar and R. K. Jain, *Phys. Rev. D* **94**, 083512 (2016).
- [104] A. A. Starobinsky, *JETP Lett.* **30**, 682 (1979).
- [105] F. Finelli and R. Brandenberger, *Phys. Rev. D* **65**, 103522 (2002).
- [106] J. Garriga and V. F. Mukhanov, *Phys. Lett. B* **458**, 219 (1999); R. Akhoury, C. S. Gauthier and A. Vikman, *JHEP* **0903**, 082 (2009); S. Unnikrishnan and L. Sriramkumar, *Phys. Rev. D* **81**, 103511 (2010); O. Pujolas, I. Sawicki and

- A. Vikman, JHEP **1111**, 156 (2011); F. Arroja and M. Sasaki, Phys. Rev. D **81**, 107301 (2010).
- [107] K. A. Malik and D. Wands, JCAP **0502**, 007 (2005).
- [108] K. A. Malik and D. Wands, Phys. Rept. **475**, 1 (2009).
- [109] D. Langlois and S. Renaux-Petel, JCAP **0804**, 017 (2008).
- [110] T. J. Battefeld, S. P. Patil and R. Brandenberger, Phys. Rev. D **70**, 066006 (2004).
- [111] P. Peter, N. Pinto-Neto and S. D. P. Vitenti, Phys. Rev. D **93**, 023520 (2016).
- [112] E. F. Bunn, A. R. Liddle and M. J. White, Phys. Rev. D **54**, R5917 (1996).
- [113] Wolfram Research, Inc., *Mathematica, Version 11.0*, Champaign, IL (2018).
- [114] I. S. Gradshteyn and I. M. Ryzhik, *Table of Integrals, Series, and Products*, Seventh Edition (Academic Press, New York, 2007).
- [115] B. Xue, D. Garfinkle, F. Pretorius and P. J. Steinhardt, Phys. Rev. D **88**, 083509 (2013).
- [116] R. N. Raveendran, D. Chowdhury and L. Sriramkumar, JCAP **1801**, 030 (2018).
- [117] R. N. Raveendran and L. Sriramkumar, arXiv:1812.06803 [astro-ph.CO].
- [118] J. L. Lehnert, Adv. Astron. **2010**, 903907 (2010).
- [119] R. N. Raveendran and L. Sriramkumar, arXiv:1809.03229 [astro-ph.CO].
- [120] N. D. Birrell and P. C. W. Davies, *Quantum Fields in Curved Space* (Cambridge University Press, Cambridge, England, 1982); V. Mukhanov and

S. Winitzki, *Introduction to Quantum Effects in Gravity* (Cambridge University Press, Cambridge, England, 2007).

[121] G. Gubitosi and J. Magueijo, JCAP **1711**, 014 (2017).

[122] D. Langlois, S. Renaux-Petel and D. A. Steer, JCAP **0904**, 021 (2009);
J. E. Kim, H. P. Nilles and M. Peloso, JCAP **0501**, 005 (2005).

[123] A. Achúcarro, J. O. Gong, S. Hardeman, G. A. Palma and S. P. Patil, JCAP **1101**, 030 (2011).

[124] Y. B. Li, J. Quintin, D. G. Wang and Y. F. Cai, JCAP **1703**, 031 (2017).

[125] D. K. Hazra, J. Martin and L. Sriramkumar, Phys. Rev. D **86**, 063523 (2012).

[126] A. Ijjas, JCAP **1802**, 007 (2018).